# EFFECT OF IMPURITIES ON $CO_2$ STREAM PROPERTIES

by

**Ibrahim Al-Siyabi**

Submitted for the degree of Doctor of Philosophy

In

**Petroleum Engineering**

Heriot-Watt University

Institute of Petroleum Engineering

February 2013

# ABSTRACT

$CO_2$ obtained by capture process (such as post combustion, pre combustion and oxy-fuel combustion) is not 100% pure and may contain impurities such as $H_2$, Ar, CO, $H_2S$ and water. The presence of such impurities in $CO_2$ stream can lead to challenging flow assurance and processing issues. The gaseous $CO_2$-rich stream is generally compressed to be transported as liquid in order to avoid two-phase flow and increase the density of the system. One aim of this work is to evaluate the effect of impurities on the physical properties of $CO_2$ such as density, viscosity, speed of sound and on the phase behaviour of such systems. Speed of sound and isothermal compressibility of $CO_2$/impurities mixtures were measured at condition above the saturation curve and temperature from 268.15 to 301.15 K. A new volume correction was implemented to the Peng-Robinson equation of state in order to minimise the error associated with the isothermal compressibility prediction. Moreover, density and viscosity are two of the most important properties in transport properties. Therefore, the effect of impurities on density and viscosity were experimentally and theoretically investigated in liquid $CO_2$ and liquid $CO_2$/impurities systems. The viscosity measurements were performed using in-house capillary tube apparatus in the range from 280 to 343.15 K and pressure up to 40 MPa. Two viscosity models, LBC and Pedersen, were modified in order to predict the viscosity of both pure and impure $CO_2$. The density measurements were carried-out using an Anton Paar densitometer in both liquid and supercritical regions from 283.15 to 423.15 K. In order to improve the accuracy of EOSs in density of CO/impurities systems, a new modification was developed based on mixing the volume obtained from EOSs (SRK, PR and VPT) and the volume obtained from $CO_2$-MBWR.

The presence of water may result in ice and/or gas hydrate formation and cause blockage of pipelines. Several measurements were also conducted to evaluate the hydrate stability zone of pure and rich $CO_2$ systems in free water. A thermodynamic model based on the VPT EOS was adopted to predict the hydrate phase of the systems. In addition, few saturation measurements of synthetic alkane mixture plus pure or impure $CO_2$ were performed at 344.3 K in order to investigate the effect of impurities on the saturation pressure of $CO_2$/alkane system. IFT and swelling factor properties on $CO_2$/n-decane mixture were investigated at 310.95 K from ambient to near the minimum miscibility pressure of the mixture. The experiments were extended to cover the presence of impurities on the properties at the same range of pressure. Minimum

miscibility pressure of the systems was estimated by both Vanishing Interfacial Tension method and multiple-mixing-cell calculation.

# DEDICATION

This work is dedicated to my parents and my wife Maimoona.

# ACKNOWLEDGMENTS

**In the Name of Allah, the Most Gracious, the most Merciful**

This PhD thesis is submitted in partial fulfilment of the requirements for the degree at Heriot Watt University. The work has been conducted at the Institute of Petroleum Engineering (IPE) under the supervision of Prof. Bahman Tohidi and Dr. Antonin Chapoy.

I am deeply grateful to my advisor Prof. Bahman Tohidi for his guidance, his encouragement, and his resolute dedication. I would like express my appreciation to my second advisor Dr. Antonin Chapoy for his continuous support throughout my PhD studies, his prompt orienteering, saint like patience, encouragement in times of brainstorming and difficulties, as well as frequent opportunities for discussion of new ideas leading to key insight. I would also like to thank my external examiner Dr. Paolo STRINGARI and my internal examiner Dr. Asghar Shams for their time and suggestions.

I am also grateful to Mr. Rod Burgess and the late Mr. Keith Bell for their immense help with all the experimental work. I would like to thank Dr. Jinhai Yang for his inspiring discussions in all my work period. I would also like to thank my colleagues and friends in IPE and Edinburgh who make my stay pleasant and colourful.

The grants which financed my project from the Ministry of Higher Education of Oman were highly appreciated. Without their support, I would not have been able to complete this degree. Finally I would like to express my gratitude to the representatives of Total, Marathon Oil Corporation and Schlumberger in the Joint Industrial Project (JIP) in the Reservoir Fluid Study group for their comments and help during my study.

Ibrahim Al-Siyabi

ACADEMIC REGISTRY
**Research Thesis Submission**

| | | | |
|---|---|---|---|
| Name*:* | **IBRAHIM AL-SIYABI** | | |
| School/PGI: | **Institute of Petroleum Engineering** | | |
| Version: *(i.e. First, Resubmission, Final)* | **Final** | Degree Sought (Award **and** Subject area) | **PhD in Petroleum Engineering** |

## Declaration

In accordance with the appropriate regulations I hereby submit my thesis and I declare that:

1) the thesis embodies the results of my own work and has been composed by myself
2) where appropriate, I have made acknowledgement of the work of others and have made reference to work carried out in collaboration with other persons
3) the thesis is the correct version of the thesis for submission and is the same version as any electronic versions submitted*.
4) my thesis for the award referred to, deposited in the Heriot-Watt University Library, should be made available for loan or photocopying and be available via the Institutional Repository, subject to such conditions as the Librarian may require
5) I understand that as a student of the University I am required to abide by the Regulations of the University and to conform to its discipline.

* *Please note that it is the responsibility of the candidate to ensure that the correct version of the thesis is submitted.*

| | | | |
|---|---|---|---|
| Signature of Candidate*:* | | Date: | |

## Submission

| | |
|---|---|
| Submitted By *(name in capitals):* | **IBRAHIM AL-SIYABI** |
| Signature of Individual Submitting: | |
| Date Submitted: | |

## For Completion in the Student Service Centre (SSC)

| | | | |
|---|---|---|---|
| Received in the SSC by *(name in capitals):* | | | |
| *Method of Submission* *(Handed in to SSC; posted through internal/external mail):* | | | |
| *E-thesis Submitted* ***(mandatory for final theses)*** | | | |
| Signature: | | Date: | |

# TABLE OF CONTENTS

# LIST OF FIGURES

# LIST OF TABLES

# LIST OF MAIN SYMBOLS

| | |
|---|---|
| $x_{co_2}$ | Mole fraction of $CO_2$ in the mixture |
| $\tau$ | Period of oscillation |
| $\theta$ | Equilibrium contact angle in degrees |
| *AAD* | Average Absolute Deviation |
| *BWRS* | Benedict-Webb-Rubin-Starling EOS |
| *CCS* | Carbon Capture and Storage |
| *EOR* | Enhanced Oil Recovery |
| *EOS* | Equation of State |
| *g* | Acceleration due to gravity |
| *H* | Hydrate |
| *h* | Capillary rise |
| *IFT* | Interfacial Tension |
| $k_{ij}$ | Binary interaction parameter |
| $K_T$ | Isothermal compressibility |
| *LBC* | Lohrenz–Bray–Clark viscosity model |
| $L_{CO2}$ | Liquid $CO_2$ |
| *M* | Molecular weight |

| | |
|---|---|
| *MIX* | Mixture |
| *MMP* | Minimum Miscibility Pressure |
| *MOC* | Method of the Characteristics |
| *NDD* | Non density dependent mixing rules |
| *OF* | Objective function |
| *P* | Pressure |
| $P_c$ | Critical pressure |
| *PR* | Peng-Robinson EOS |
| $P_{sat}$ | Saturation pressure |
| *PT* | Patel-Teja EOS |
| *PV* | Pore Volume |
| *R* | Universal gas constant |
| *RF* | Recovery Factor |
| *SH* | Structure H |
| *SI* | Structure I |
| *SII* | Structure II |
| *SoS* | Speed of sound |
| *SRK* | Soave-Redlich-kwong EOS |
| *T* | Temperature |

| | |
|---|---|
| $T_c$ | Critical temperature |
| $V$ | Volume |
| *VIT* | Vanishing Interfacial Tension Approach |
| *VLE* | Vapour Liquid Equilibrium |
| *VPT* | Valderrama-Patel-Teja EOS |
| $Y_{CO2}$ | Vapour phase composition of $CO_2$ |
| $z$ | Piston displacement |
| $Z_{oil}$ | Oil height in the cell |
| $\alpha$ | Alpha function in EoS |
| $\eta$ | Viscosity |
| $\rho$ | Density |

# CHAPTER 1: **INTRODUCTION**

It is now widely accepted that anthropogenic $CO_2$ emissions from the burning of fossil fuels are largely responsible for the rapid rise in global temperatures recorded over the past century. Worldwide concerns over the threat of global warming have encouraged industrialised countries into working together to reduce carbon emissions, with specific targets being laid out in the 1997 Kyoto protocol agreement. To meet these goals, nations must increase investment in 'clean', renewable sources of energy, and develop solutions for reducing $CO_2$ (and other greenhouse gases) emissions from existing and new fossil fuel usage. With regard to carbon emissions, the most promising solution currently on the table is $CO_2$ capture and subsurface storage, primarily by injection into ageing oil reservoirs (where it can be used to improve oil recovery) or deep saline aquifers. A particularly promising fossil fuel technology, which can help addressing the above issues, is Integrated Gasification Combined Cycle (IGCC) reformation (e.g. White et al., 2000). In IGCC reformation, hydrocarbons (gas, coal, oil) are broken down to yield hydrogen and $CO_2$. The produced hydrogen can be used for electricity generation and/or as a clean fuel (e.g. to power motor vehicles), while the $CO_2$ is separated for subsurface disposal.

There are three capture processes: post-combustion, pre-combustion and oxy-fuel combustion. In a post-combustion, a solvent (mainly amines) process is required to capture $CO_2$ in flue gas of power plants. The process involves high energy to regenerate the solvent.

The pre-combustion process means that $CO_2$ is separated before the combustion process. The fuel is treated prior the combustion to produce $CO_2$ and $H_2$. The $H_2$ is used for generating power and the $CO_2$ is captured and stored. In oxy-fuel combustion process, oxygen is captured and removed from air to around 90% purity. Then $O_2$ is used to burn fuel instead of air to produce power. This process results in an exhaust stream consists of mainly pure $CO_2$ typically around 85 to 99%.

However $CO_2$ coming from the above capture processes is generally not pure and can contain impurities such as $N_2$, $H_2$,$O_2$, $H_2S$, $CH_4$, CO and water. Scenarii of excepted impurities on $CO_2$ are reported in Table 1.1 from [1], [2]. The type and amount of

impurities introduced in $CO_2$ depends on the type of capture process and the fuels beside the type of solvent used. The presence and type of other components may differ considerably between post-combustion, pre-combustion and oxy-fuel capture processes [3]. From Table 1.1, the non-condensable components $N_2$, Ar, $O_2$, CO and $N_2$ plus water are common impurities in all capture processes. The impurities fraction ranges from 15 volume% high to 0.05 volume% low. The removal of impurities is possible with further gas cleaning. However, $CO_2$ purification process is expensive, thus the overall cost will increase. The volume fraction of non-condensable gases such as $N_2$, $H_2$, $CH_4$, $O_2$ and Ar should be within 4% and $H_2$ should be removed as much as possible for its energy use [4].

*Table 1.1 Impurities expected in $CO_2$ stream from capture processes [1]*

| Components | Pre-combustion | | Post-combustion | | | Oxyfuel | | |
|---|---|---|---|---|---|---|---|---|
| | Selexol* | Rectisol* | Post-1* | Post-2* | Post-3* | Oxy-1* | Oxy-2* | Oxy-3* |
| $CO_2$(Volume%) | 97.95 | 99.7 | 99.93 | 99.92 | 99.81 | 85 | 98 | 99.94 |
| $N_2$(Volume%) | 0.9 | 0.21 | 0.045** | 0.045** | 0.09 | 5.8 | 0.71 | 0.01 |
| $O_2$(Volume%) | - | - | 0.015 | 0.015 | 0.03 | 4.7 | 0.67 | 0.01 |
| Ar(Volume%) | 0.03 | 0.15 | - | - | - | 4.47 | 0.59 | 0.01 |
| $H_2O$(ppm) | 600 | 10 | 100 | 100 | 600 | 100 | 100 | 100 |
| CO(ppm) | 400 | 400 | 10 | 10 | 20 | 50 | 50 | 50 |
| $H_2$(ppm) | 10000 | 20 | - | - | - | - | - | - |
| $CH_4$(ppm) | 100 | 100 | | | | | | |
| $SO_2$(ppm) | - | - | 10 | 10 | 20 | 50 | 50 | 50 |
| $H_2S$+COS(ppm) | 100 | 20 | - | - | - | - | - | - |

**More details about these processes see [2]*

***Concentration of Ar+$N_2$*

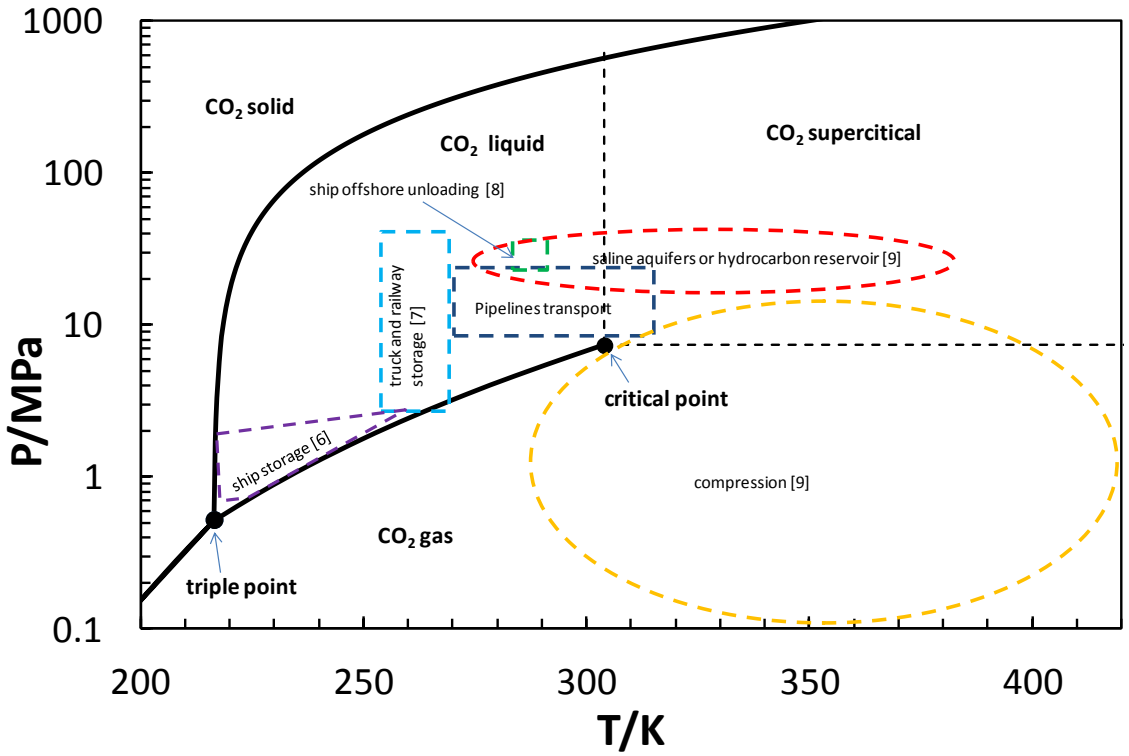


*Figure 1.1 Various operations involved in the $CO_2$ transport*

The intermediate step between $CO_2$ storage (or EOR) and capture is the transport. The most effective $CO_2$ transport options are either by pipeline or ship due to high bulk volume required for CCS. There are other $CO_2$ transport options such as railway or truck. Figure 1.1 shows the phase diagram of $CO_2$. The critical point of $CO_2$ [9] is (304.25 K and 7.3 MPa) and its triple point is (216.65 K and 0.51 MPa). $CO_2$ is compressed for transportation by ship, at a pressure of 0.6 to 1.7 MPa and cooled down to near the triple point. $CO_2$ is loaded to the ship tank at operating pressure and temperature while the unloading condition takes place at higher pressure and temperature (see example of offshore unloading Figure 1.1).

$CO_2$ is transported in long distance pipelines as a dense, gas or supercritical fluid or in the sub-cooled liquid state. The transport as a dense fluid seems to be the most economical among the others [5]. It is possible to transport $CO_2$ in gas phase; however this means lower density and high pressure drop per unit length i.e. lower capacity and higher costs [10]. The operating temperature of the pipelines is controlled by the underground soil temperature. $CO_2$ dense phase is the phase above the critical pressure of $CO_2$, 7.3 MPa. Above the critical pressure and temperature, $CO_2$ becomes supercritical. In this phase, $CO_2$ has high density as a liquid and low viscosity as gas.

However, in cold and moderate sites where the soil temperature is lower than 304.3 K, $CO_2$ is transported as liquid dense phase. The pipelines pressure for liquid dense phase should be kept above the critical pressure to avoid two phase flow. Geological and ocean storages are the two main possible methods to store the captured $CO_2$ [11]. Depleted oil and gas fields and deep saline formations are suitable for the geological storage of $CO_2$. Under high pressure (higher than 15 MPa), $CO_2$ is pumped into the depleted fields. The properties of $CO_2$, such as density and viscosity change as $CO_2$ is injected further deep underground. Knowing the properties will help to identify the capacity of the compressors required to compress $CO_2$ and hence minimizing the costs. As mentioned earlier, $CO_2$ can be used for EOR where $CO_2$ is injected into oil reservoirs to improve the flow of the remaining oil. The displacements range from viscosity reduction, oil swelling near the miscible pressure to completely miscible above the Minimum Miscible Pressure (MMP). The displacements depend on many factors under the same pressure and temperature such as VLE of $CO_2$ and oil and composition of both oil and $CO_2$ where impurities can strangely affect those factors.

The presence of the impurities combined with potentially long distance transportation of $CO_2$ could lead to challenging engineering and flow assurance issues. The presence of water may result in corrosion, ice and/or gas hydrate formation and pipeline blockage, so the fluid system should meet certain dehydration requirements. Furthermore, the gaseous $CO_2$ rich stream is generally compressed to be transported as liquid or dense-phase state in order to avoid two-phase flow and increase the density of the fluid system. The presence of the above impurities will also change the physical properties of the stream, i.e., the system's bubble point pressure and viscosity, hence affecting the compression requirement. Furthermore, in the majority of feasibility studies of $CO_2$ injection, the effects of these impurities have been overlooked or completely ignored.

The aim of this work is to investigate the effect of impurities such as $N_2$, $O_2$, $H_2$, $CH_4$, $SO_2$, CO, $H_2S$ and Ar on the phase behaviour, speed of sound, density, viscosity, and isothermal compressibility. The work is also extended to investigate the effect of impurities on the properties of $CO_2$/oil mixture. The properties include IFT, MMP, swelling factor and saturation pressure.

In Chapter 2 Vapour-Liquid Equilibria of $CO_2$ and $CO_2$/impurities systems have been evaluated using 3 cubic equations (SRK, PR and VPT) combined with the classical

mixing rules. To match the experimental data, the three equations have been tuned based on the VLE or saturation pressure of the binary $CO_2$/impurities mixtures. The critical point curves of the binary mixtures have been also estimated with the equation. In addition, the saturation pressure and speed of sound of a synthetic alkane mixture with $CO_2$ + impurity binary mixtures were measured at constant temperature, 344.3 K. The effect of four impurities, Ar, $H_2$, CO and $CH_4$, on the properties has been investigated.

Accurate measurements and prediction of speed of sound in $CO_2$-rich systems can have many applications, e.g., determining some thermodynamic properties, 4-D seismic, or monitoring compositional changes. In Chapter 3, speed of sound and isothermal compressibility in pure liquid $CO_2$ and $CO_2$ + impurities have been measured under pressure up to 50 MPa and temperature ranging from 268.15 to 301.15 K. The tested impurities were $N_2$, $CH_2$, CO, $O_2$, $H_2$ and Ar. Measurements have also been conducted on two multi-components $CO_2$-rich mixtures, i.e., $CO_2$-$CH_4$-$H_2$-$N_2$ and $CO_2$-Ar-CO. A new generalized correction based on the PR-model for specific volume of liquid $CO_2$ has been proposed. The model is tested with the measured isothermal compressibility for both $CO_2$ and $CO_2$/impurities system.

The aim of Chapter 4 is to evaluate the risk of hydrate formation in a rich carbon dioxide stream. The three phases HLV, HLL and HLLV equilibria of the ternary $CO_2$ + ($N_2$ or $CH_4$ or $O_2$ or Ar or $H_2$ or CO) + water systems have been determined at a constant composition (4.56% $N_2$, 7.09% $H_2$, 5.85% $CH_4$, 5.87% CO, 5.03% Ar, and 5.34% $O_2$ in dry basis). Measurements have been performed using a standard constant-volume equilibrium step-heating technique. A thermodynamic approach has been employed to model the phase equilibria. The thermodynamic model was used to predict the hydrate dissociation conditions of $CO_2$ and $CO_2$ rich streams in the presence of free water.

Effect of impurities on $CO_2$ density has been investigated and explained in Chapter 5. The density of $CO_2$ in the presence of several gaseous impurities was measured over a range of temperature from 283.15 K to 423.15 K and pressures up to 50 MPa in both liquid and supercritical phases. The measurements have been carried-out with an Anton Parr densitometer. Within 4 to 5 mole% of various impurities (i.e. $CH_4$, $N_2$, $O_2$, $H_2$, Ar and CO) in rich-$CO_2$ binary system have been tested in this study. The findings show a

significant reduction in the $CO_2$ + impurities systems density in presence of the above impurities. A new volume correction added to the EOSs was implemented to model the experimental data in both liquid and supercritical phases.

Viscosity is a key transport property for transport pipeline systems as well as sub-surface and process systems. In Chapter 6, the viscosity of $CO_2$ systems with impurities, such as methane, nitrogen, argon, carbon monoxide, oxygen and hydrogen, were measured using capillary viscosity measurement technique in an in-house designed and constructed set-up at pressures up to 5.5 MPa and temperatures of 280, 288.15, 300.15, 308.15, 323.15 and 343.15 K. The results show that all of the tested impurities caused a reduction of viscosity compared to pure $CO_2$. In addition, two models were modified in order to predict and estimate the viscosity of $CO_2$ systems. First, the predictive model of Pedersen was modified substituting $CO_2$ as a reference fluid to the original reference fluid. Second, the LBC correlation was used after tuning to match the obtained experimental data.

In Chapter 7:, the effect of impurities ($N_2$, $CH_4$, CO, $O_2$, $H_2$ and Ar) of $CO_2$/n-Decane system on the IFT (Interfacial Tension), the swelling factor and the MMP (Minimum Miscibility Pressure) have been investigated at 310.95 K. The impact of impurities in the injection gas was studied, four binary mixtures were investigated: $CO_2$-$CH_4$, $CO_2$-$N_2$, $CO_2$-$O_2$, $CO_2$-$H_2$ and two multi-components mixtures. A capillary rise apparatus was used to measure the IFTs and the swelling factors at the same pressure and temperature conditions and the VIT (Vanishing Interfacial Tension) approach was used to estimate the MMPs of the systems containing impurities. The experimental MMPs were compared with the predictions made by an in-house software developed based on the multiple-mixing cell approach. The above properties are compared between systems: $CO_2$/n-decane in the presence of impurities and the pure $CO_2$.

Chapter 8 presents the conclusions of this study and recommendations for future work.

**References**

[1] Kather, A., 2009, Presented at 2nd Working Group Meeting, *$CO_2$ Quality and Other Relevant Issues*, Cottbus, Germany.

[2] Rubin, E. S., Mantripragada, H., Marks, A., Versteeg, P., Kitchin, J., (2012), *The outlook for improved carbon capture technology Progress in Energy and Combustion*, Progress in Energy and Combustion Science, **38**, 630-671

[3] Anheden, M., Andersson A., Bernstone, C., Eriksson, S., Yan, J., Liljemark, S. and Wall, C., 2004, *$CO_2$ Quality Requirement for a System with $CO_2$ Capture, Transport and Storage*, The 7th International Conference on Greenhouse Gas Control Technologies (GHGT7), Vancouver, Canada.

[4] Visser, de, E., Hendriks, C., Barrio, M., Molnvik, M., de Koijer, G., Liljemark, S. and le Gallo, Y., 2008, *Dynamis $CO_2$ Quality Recommendations*, International journal of Greenhouse Gas Control, **2**, 478-484.

[5] Jäger, S. and Bosch, C., 2011, *Requirements for Safe and Reliable $CO_2$ Transportation Pipeline*, 6th Pipeline Technology Conference, Germany.

[6] Lee, U., Lim, Y., Lee, S, Jung, J. and Han, C., 2012, *$CO_2$ Storage Terminal for Ship Transportation*, Ind. Eng. Chem. Res., **51**, 389-397.

[7] Mohitpour, M., Seevam, P., Botros, K. K, Rothwell, B. and Ennis, C., *Pipelines Transportation of Carbon Dioxide Containing Impurities*, ASME.

[8] Aspelund, A., Molvnik, M. J. and de Koeijer, G., 2006, *Ship Transport of $CO_2$.Technical Solutions and Analysis of Costs, Energy Utilization, Exergy Efficiency and $CO_2$ Emissions*, Chemical Engineering Research and Design, **84**, 847-856.

[9] Paul, S., Shepherd, R., and Woollin, **,** P**.,** 2012, *Selection of Materials for High Pressure $CO_2$ transport*, Paper presented at Third International Forum on the Transportation of $CO_2$ by Pipeline, Newcastle.

[10] Sean, T. M, 2009, *The Economics of $CO_2$ Transport by Pipeline and Storage in Saline Aquifers and Oil Reservoirs*, Thesis, Carnegie Mellon University Pittsburgh, PA USA.

[11] Johnston, P. and Santillo, D. 2002. *Carbon Capture and Sequestration: Potential Environmental Impacts*, Proceedings of the IPCC workshop on carbon dioxide capture and storage, 18-21 November, 2002, Regina, Canada.

# CHAPTER 2: VLE OF $CO_2$/IMPURITIES+SATURATION PRESSURE AND SPEED OF SOUND OF $CO_2$/ALKANE MIXTURES

## 2.1 Introduction

$CO_2$ is transported under different pressure/temperature conditions, ranging from the triple point to near the critical point. Impurities can have high impacts on the thermodynamic properties of $CO_2$-rich systems that can further affect the design, transport cost and operation. In Enhanced Oil Recovery (EOR) process, laboratories studies showed that impurities can affect solubility, PVT properties and Minimum Miscible Pressure (MMP) behaviours. In addition, impurities affect thermodynamics and transport properties of $CO_2$ stream such as vapour liquid equilibrium (VLE), viscosity, density and hydrate stability. The need for a reliable model to predict the vapour liquid equilibrium is essential for $CO_2$ transport. Reliable VLE and physical properties data on $CO_2$ rich system are essential to design the necessary purification processes, compression and transportation of $CO_2$ for carbon capture and storage (CCS).

Accurate VLE models are important because the operation region for $CO_2$ should be within dense or supercritical area in which non-accurate prediction can lead to high risk or inefficient transport. In addition, two phase flow in a pipeline should be avoided due to the potential for damage to the pipelines [1]. The experimental data of $CO_2$ impurities on the phase behaviour properties are limited in the range of transport conditions and in some cases scattered. Therefore, the need of an accurate theoretical modelling approach to overcome this gap becomes potentially recommended in both industries and research studies.

Many papers are available about predicting pure $CO_2$ and impure $CO_2$ VLE using equation of states [2- 8]. For the design of $CO_2$ pipelines, no consensus has been achieved in which equations of state should be used for rich $CO_2$ mixtures. The EOSs used by authors ranged from specialized to complex equations such as Span and Wagner and Benedict-Webb-Rubin-Starling (BWRS) for pure $CO_2$, to general and

simplest ones such as Peng-Robinson (PR), Soave-Redlich-kwong (SRK) and Patel-Teja EOSs (PT). The term "complex" in equations of state comes from the parameters number and the structure of the equations. For example Span and Wagner EOS used around 51 terms (many of which include logarithms and exponentials) and BWRS with a minimum of 8 parameters (while the classic EOSs such as PR and SRK contain only two parameters). These equations may give better estimation of phase properties, however because of their complexity, Helmholtz and Gibbs free energy derivatives are more complicated to evaluate. $CO_2$ in the presence of impurities classified as mixtures, in which general EOSs interaction parameters are required. The EOSs should be tuned using experimental data to evaluate accuracy level achieved from their calculations. However, the non-ideal behaviour of mixture approaching the critical region is a challenge for the equations. In this work, three equations of state are used to predict the phase behaviour of $CO_2$/impurities system, PR, SRK and VPT (Valderrama-Patel-Teja equation of state) models. In addition, SRK is used to predict the critical locus curve of the binary $CO_2$/impurities mixture. The impurities that are covered in the work $H_2$, $N_2$, $CH_4$, $O_2$, Ar, CO, $H_2S$ and $SO_2$.

Vapour liquid equilibrium (VLE), volumetric properties, and solubility data of alkanes in supercritical carbon dioxide are important information in the petroleum process design area.VLE and volumetric properties in those binary and ternary mixtures have been studied both computationally and experimentally extensively in the last decade [9-14]. There is no data available for $CO_2$ containing impurities in the literature. In this work, a mixture of alkane (n-dodecane, n-tridecane and n-hexadecane) plus pure or impure $CO_2$ were prepared. The $CO_2$ gas mixture was prepared with 5 mole% of impurities ($H_2$, Ar, $CH_4$ and CO). The saturation pressure of the mixtures was measured at 344.3 K. The corresponding speed of sound property of the mixtures in the presence of impurities was measured above the mixture saturation pressure. The measurements are compared with those obtained for pure $CO_2$.

### 2.2 VLE of $CO_2$ and $CO_2$/Impurities System

The study of the phase behaviour of $CO_2$/impurities is essentially important for the operation and the design of all the processes of $CO_2$ transport (ship carriers, loading, un-loading) and capture (purification/liquefaction). Beside the experimental work, reliable empirical equations of state can play as a solution key in terms of cost and time. In this

study, in-house code is used to predict Vapour-Liquid Equilibrium of $CO_2$ and $CO_2$ binary systems by using Peng-Robinson (PR), Soave-Redlich-Kwong (SRK) and Valderrama-Patel-Teja (VPT) EOSs. Details of these equations are given below.

*Peng-Robinson EOS:*

$$P = \frac{RT}{V-b} - \frac{a}{V(V+b)+b(V-b)} \tag{2.1}$$

$$a = a_c(1+m(1-\sqrt{T_r}))^2 \tag{2.2}$$

$$a_c = \frac{0.45724R^2T_c^2}{P_c} \tag{2.3}$$

$$m = 0.37464 + 1.54226\omega - 0.26992\omega^{\ 2} \tag{2.4}$$

$$b = \frac{0.07780RT_c}{P_c} \tag{2.5}$$

*Soave-Redlich-Kwong EOS:*

$$P = \frac{RT}{V-b} - \frac{a}{V(V+b)} \tag{2.6}$$

$$a = a_c(1+m(1-\sqrt{T_r}))^2 \tag{2.7}$$

$$a_c = \frac{0.42748R^2T_c^2}{P_c} \tag{2.8}$$

$$m = 0.480 + 1.574\omega - 0.176\omega^{\ 2} \tag{2.9}$$

$$b = \frac{0.08664RT_c}{P_c} \tag{2.10}$$

*Valderrama-Patel-Teja EOS:*

$$P = \frac{RT}{V-b} - \frac{a}{V^2+V(b+c)-bc} \tag{2.11}$$

$$a = \Omega_a \frac{R^2T_c^2}{P_c}\left((1+m(1-T_r^{0.5}))^2\right) \tag{2.12}$$

$$b = \Omega_b \frac{RT_c}{P_c} \tag{2.13}$$

$$c = \Omega_c \frac{RT_c}{P_c} \tag{2.14}$$

$$\Omega_a = 0.66121 - 0.76105Z_c \tag{2.15}$$

$$\Omega_b = 0.02207 - 0.20868 Z_c \tag{2.16}$$

$$\Omega_c = 0.57765 - 1.87080 Z_c \tag{2.17}$$

$$m = 0.462823 + 3.5830 \omega Z_c + 8.117 (\omega Z_c)^2 \tag{2.18}$$

Where *P*, *V*, *T*, *R* are pressure, the molar volume, the temperature and the universal gas constant, respectively. The parameter *a* is a measure of the attractive forces between the molecules and the parameter *b* is a measure of the size of the molecules (intrinsic volume). ω and $Z_c$ are acentric factor and critical compressibility factor, respectively. The above equations are developed for pure components. The van der Waals conventional random mixing rules are used to determine, *b*, and, *c*, parameters for multi-components systems:

$$b = \sum_{i=1}^{N} x_i b_i \tag{2.19}$$

$$c = \sum_{i=1}^{N} x_i c_i \tag{2.20}$$

Non Density Dependent (NDD) mixing rule was used in this work to calculate the parameter, *a*. The attraction parameter, *a*, is divided into two parts, classical and asymmetric, $a^c$, and, $a^a$, as following:

$$a = a^c + a^a \tag{2.21}$$

$$a^c = \sum_{i=1}^{N} \sum_{j=1}^{N} x_i x_j (a_i a_j)^{0.5} (1 - k_{ij}) \tag{2.22}$$

$$a^a = \sum_{p} x_p^2 \sum_{i} x_i a_{pi} l_{pi} \tag{2.23}$$

$$a_{pi} = (a_p a_i)^{0.5} \tag{2.24}$$

$$l_{pi} = l_{pi}^0 - l_{pi}^1 (T - T_0) \tag{2.25}$$

Where $k_{ij}$ is the binary interaction parameter and $l_{pi}$ is the binary interaction parameter between polar component and other components. $l_{pi}$ is a function of temperature. It is calculated using Equation 2.25. $l_{pi}^0$ and $l_{pi}^l$ are the interaction parameters while $T_0$ is the freezing point in K. However, the asymmetric, $a^a$, is not calculated for $CO_2$ or $CO_2$ mixtures since $CO_2$ is classified as a non-polar component.

An extensive literature review was carried-out to obtain VLE data of the binary $CO_2$/mixtures. Eight binary $CO_2$/impurities mixtures are included: $H_2$, $N_2$, $CH_4$, $O_2$, Ar, CO, $H_2S$ and $SO_2$. The experimental data, listed in Table 2.1, were used for tuning the EOSs. Binary interaction parameters (BIPs) were tuned by minimizing either the experimental bubble point pressures or Vapour-Liquid Equilibrium data. VLE and bubble point data have been gathered for the various binary $CO_2$/impurities systems. The binary interaction parameters between $CO_2$ and the impurities were adjusted using the references mentioned in Table 2.1 through a Simplex algorithm using the Objective Function, OF, displayed in Equation 2.26.

$$OF = \left\{ \begin{array}{l} \dfrac{1}{N}\displaystyle\sum_{i=1}^{N}\left(\dfrac{P_{Exp}^{Bubble} - P_{Cal}^{Bubble}}{P_{Exp}^{Bubble}}\right) \\ \dfrac{1}{N}\displaystyle\sum_{i=1}^{N}\left[\left(\dfrac{y_{Exp} - y_{Cal}}{y_{Exp}}\right)^2 + \left(\dfrac{x_{Exp} - x_{Cal}}{x_{Exp}}\right)^2\right] \end{array} \right\} \tag{2.26}$$

The BIPs obtained for the binary mixtures are summarised in Table 2.2. According to the mixing rule used in EOSs, the BIP should be temperature independent and its value is between -1 to 1. The default value is zero for SRK and PR and 1 for VPT (i.e. (1 - $k_{ij}$) = 1). The change in BIPs can lead to high deviation, accordingly the need to choose the appropriate values. Figure 2.1 to Figure 2.3 show the average deviations in the saturation pressure ($P_{sat}$), vapour phase composition of $CO_2$ ($Y_{CO2}$) and ($P_{sat}$+$Y_{CO2}$) as a function of $k_{ij}$ in $CO_2$/$N_2$ mixture at 270 K. The plots show that the EOS BIPs for the mixture are very close to their default values (zero). The BIPs of $N_2$ regressed using the objective function for wide range of temperatures as listed in Table 2.2. The BIPs result for $CO_2$/$N_2$ using the three EOSs shown in Figure 2.1 to Figure 2.3 at 270 K are close to the general BIP for the same mixture. Our results are also matched the BIPs results generated by Li and Yan (2006) [7].

*Table 2.1 Literature data for the $CO_2$ + impurities systems*

| Mixtures | Source |
|---|---|
| $CO_2$/CO | [15-17] |
| $CO_2$/$N_2$ | [18-28] |
| $CO_2$/$O_2$ | [18,29] |
| $CO_2$/Ar | [30-31] |
| $CO_2$/$CH_4$ | [21],[25], [32-47] |
| $CO_2$/$SO_2$ | [48-50] |
| $CO_2$/$H_2$ | [39],[51,53] |
| $CO_2$/$H_2S$ | [54-56] |

*Table 2.2 BIPs for different binary $CO_2$/mixtures*

| | CO | $N_2$ | $O_2$ | Ar | $H_2$ | $CH_4$ | $SO_2$ | $H_2S$ |
|---|---|---|---|---|---|---|---|---|
| VPT | 0.005 | -0.014 | 0.111 | 0.129 | -0.387 | 0.099 | 0.02 | 0.082 |
| PR | -0.042 | -0.048 | 0.091 | 0.113 | 0.0202 | 0.092 | 0.02 | 0.090 |
| SRK | -0.022 | -0.046 | 0.106 | 0.123 | -0.142 | 0.100 | 0.02 | 0.096 |

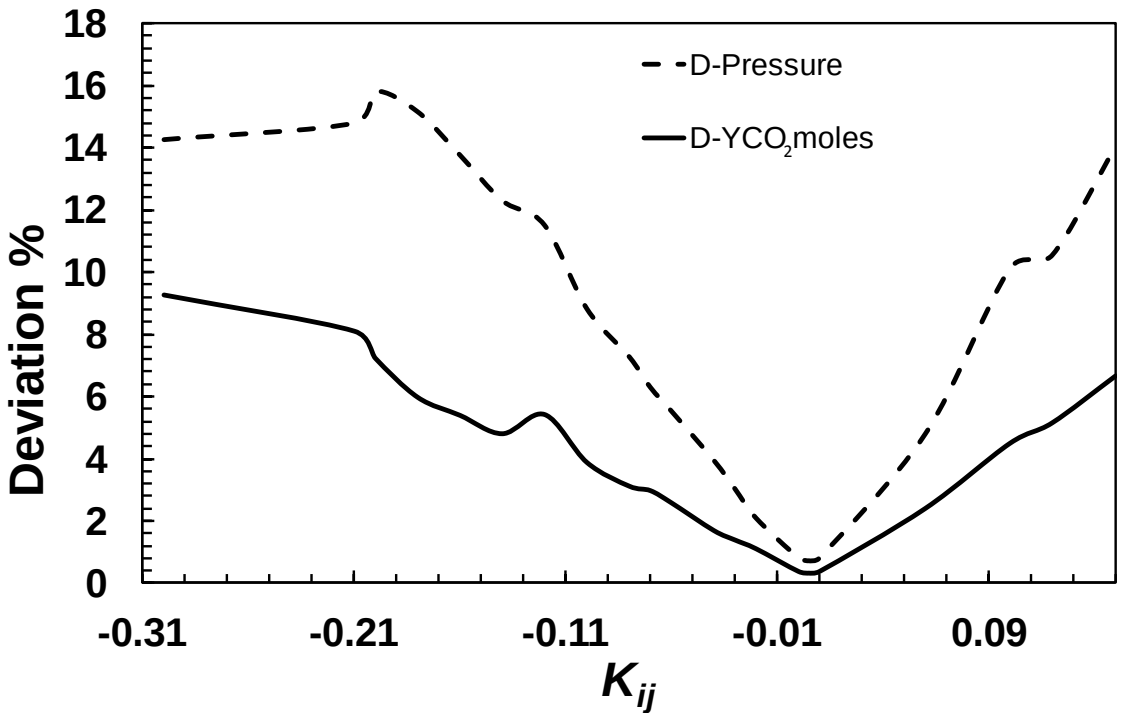


*Figure 2.1 AAD Deviations from PR EOS on $CO_2$/$N_2$ mixture at 270 K, data from [23]*

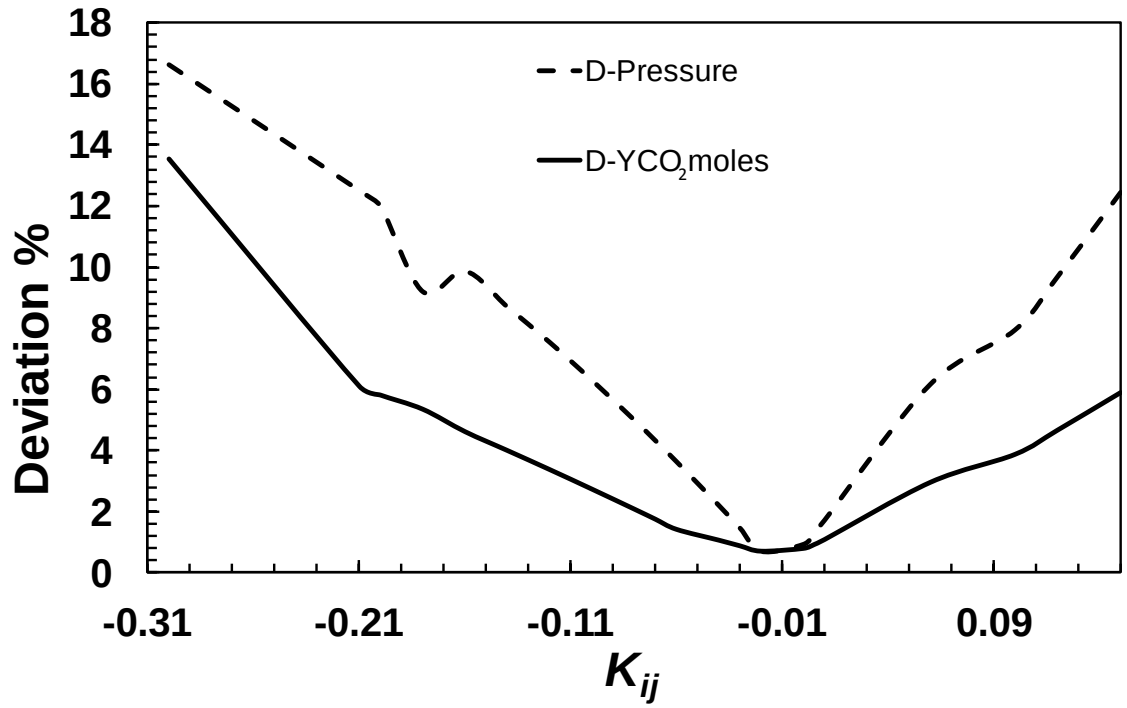


*Figure 2.2 AAD Deviations from SRK EOS on $CO_2/N_2$ mixture at 270 K, data from [23]*

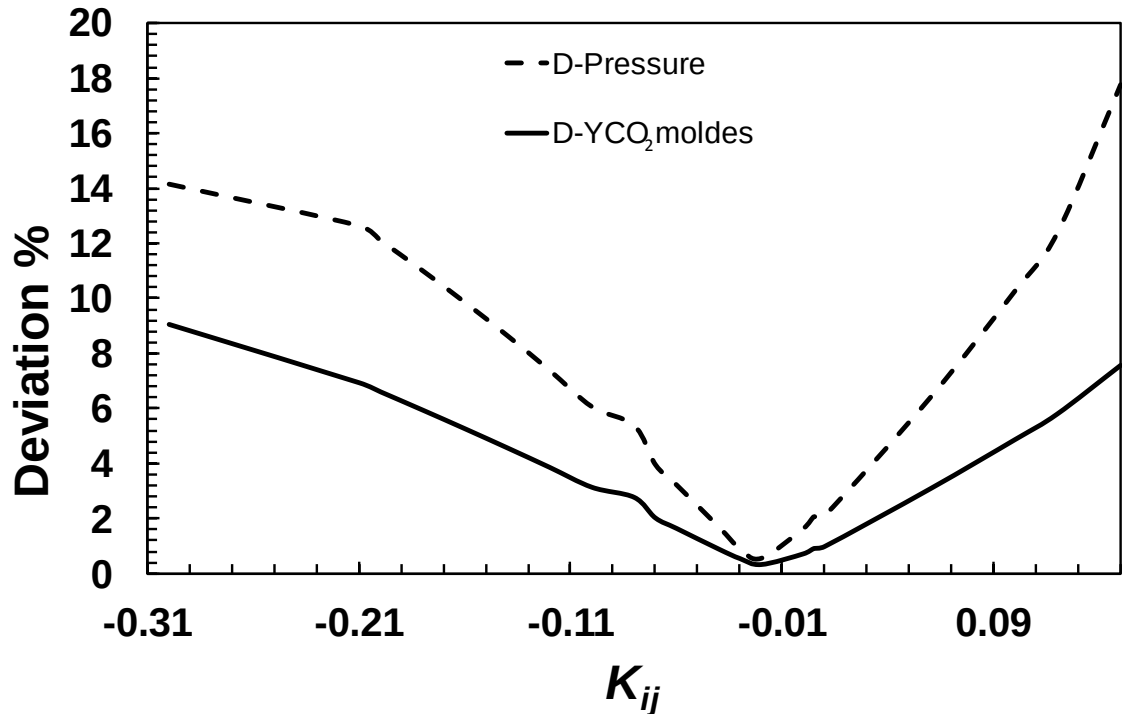


*Figure 2.3 AAD Deviations from VPT EOS on $CO_2/N_2$ mixture at 270 K, data from [23]*

*Table 2.3 AAD of EOSs on VLE data of binary $CO_2$ mixtures*

| Model | AAD % | $O_2$ | $CH_4$ | $H_2S$ | $H_2$ | $N_2$ | CO | $SO_2$ | Ar |
|---|---|---|---|---|---|---|---|---|---|
| SRK | $P_{sat}$ | 4.68 | 1.87 | 1.28 | 10.34 | 3.79 | 5.34 | 0.82 | 4.49 |
| | $Y_{CO2}$ | 3.99 | 2.69 | 4.19 | 11.48 | 2.41 | 4.12 | 0.76 | 4.02 |
| PR | $P_{sat}$ | 4.76 | 1.70 | 2.25 | 10.37 | 3.25 | 6.44 | 1.48 | 4.87 |
| | $Y_{CO2}$ | 3.17 | 2.32 | 5.09 | 10.37 | 1.99 | 2.92 | 0.60 | 2.76 |
| VPT | $P_{sat}$ | 4.64 | 1.70 | 1.73 | 9.92 | 3.46 | 5.03 | 1.39 | 4.62 |
| | $Y_{CO2}$ | 3.37 | 2.28 | 4.35 | 9.50 | 2.22 | 3.79 | 0.60 | 3.06 |

The experimental data (Table 2.1) of the binary $CO_2$ systems are used to tune the three EOSs models at different conditions. From Figure 2.4 (a-p), the models show a good agreement with experimental data However, they are weaker near the critical point for most of these binary mixtures. The models were tested in a wide range of pressure and temperature conditions. Table 2.3 lists the AADs of the EOSs on the saturated pressure ($P_{Sat}$) and vapour compositions ($Y_{CO2}$) for the systems studied here. Figure 2.4 (a-p) shows the calculated AAD as function of saturated pressure and temperature for the eight $CO_2$/impurities systems. From the tables and figures we can observe that the PR, SRK and VPT equations predict bubble pressure with about the same accuracy. The overall AAD on the saturation pressure for the eight binary systems are 4.08, 4.39 and 4.06% by using SRK, PR and VPT EOSs respectively. The overall AAD on vapour composition are 4.21, 3.65 and 3.64% by using SRK, PR and VPT EOSs respectively. This indicates that VPT is slightly superior to SRK and PR. The higher deviations found in the pressure predictions of the $CO_2$/impurities systems are due to higher errors near the critical region of the mixtures. The predictions in the vapour phase compositions are more accurate than the saturation pressure predictions in most of the tested impurities such as $O_2$, $N_2$, CO, Ar and $SO_2$. In terms of the impurities, the highest deviation is found for the binary $CO_2/H_2$ system. This is a more or less general behaviour of cubic equations of state when applied to $H_2$ containing mixtures. This is mainly because of the low critical temperature of $H_2$ compare to the other impurities and $CO_2$. The AAD on the $P_{sat}$ for the $CO_2/H_2$ mixture are 10.34, 10.37 and 9.92% by using SRK, PR and VPT respectively and the deviation can reach up to 55%. If the composition range for the mixture is restricted to a mixture up to 10% $CO_2$, the overall AAD on the $P_{sat}$ is significantly reduced to 2.80, 2.93 and 2.52% for SRK, PR and VPT, respectively. The

effect of modelling the previous impurities by using PR on the phase envelope of $CO_2$ is shown in Figure 2.5 (a-h) which also includes the saturation pressure for both pure carbon dioxide and 100% of the contaminants. The envelope size of the mixture is important in $CO_2$ transport and pipelines design and the two phase region should be avoided as possible. It is obvious from the figures that the envelope size depends on both the type of impurity and the composition of the impurity in the mixture. Each square dot along the critical locus curve represents 10% mole of impurity. It is also very clear that the size of phase envelope is increased as the impurity concentration is increased. Both mixture saturation and vapour lines of the tested mixtures (except for $SO_2$ and $H_2S$) tend to increase compared with the saturated line of pure $CO_2$. The figures indicate that the saturation pressures with $CO_2$ are increased greatly when the $CO_2$ rich stream contains $H_2$, $O_2$, Ar, CO, $CH_4$ and $N_2$. In the other hand, adding $SO_2$ and $H_2S$ reduces the saturation pressures. The effect of the tested impurities can be classified into four categories. The first includes $H_2$ which has the highest impact on VLE property. The second category is the impurities group (CO, Ar, $O_2$ and $N_2$). The third and fourth categories are $CH_4$ and the impurities group ($SO_2$ and $H_2S$) respectively. For instance at 290 K, 5% mole fraction of impurity, $H_2$ can raise the saturation pressure of pure $CO_2$ to 80%, the group (CO, Ar, $O_2$ and $N_2$) to 33 to 35% and $CH_4$ to 22%. However, at the same temperature and composition, the presence of $SO_2$ and $H_2S$ reduce the saturation pressure to 7% and 2%, respectively.

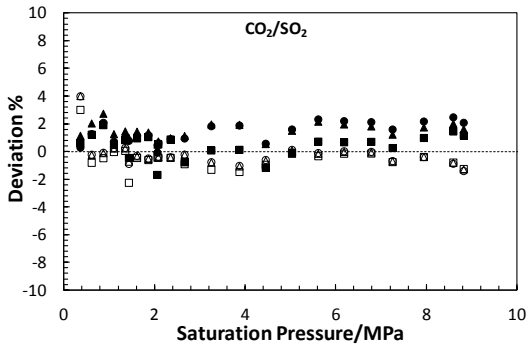
CO2/SO2
Deviation %
Saturation Pressure/MPa

a)

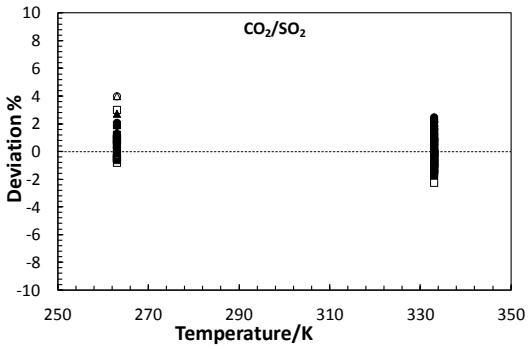
CO2/SO2
Deviation %
Temperature/K

b)

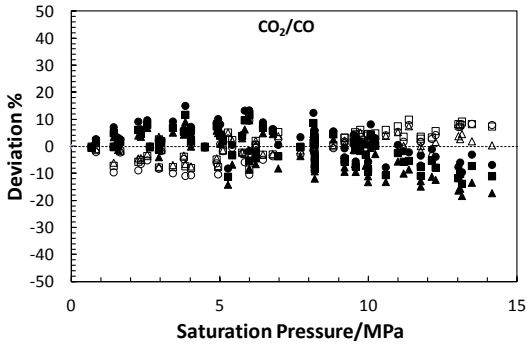
CO2/CO
Deviation %
Saturation Pressure/MPa

c)

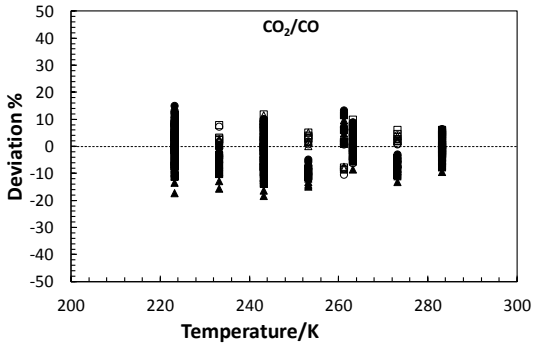
CO2/CO
Deviation %
Temperature/K

d)

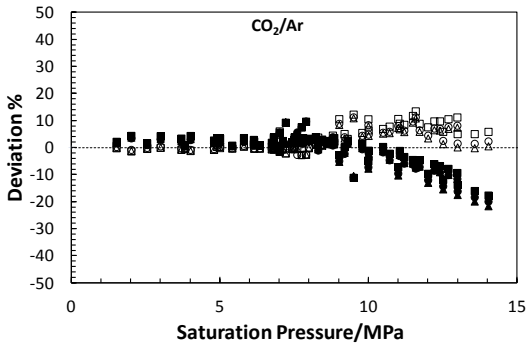
CO2/Ar
Deviation %
Saturation Pressure/MPa

e)

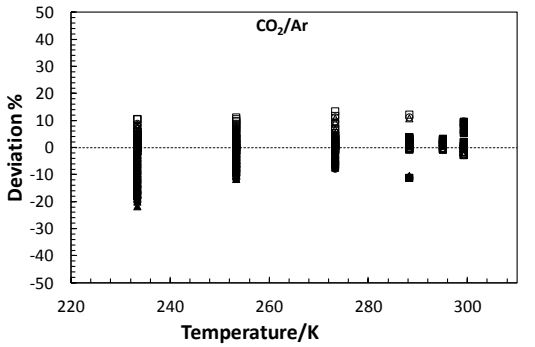
CO2/Ar
Deviation %
Temperature/K

f)

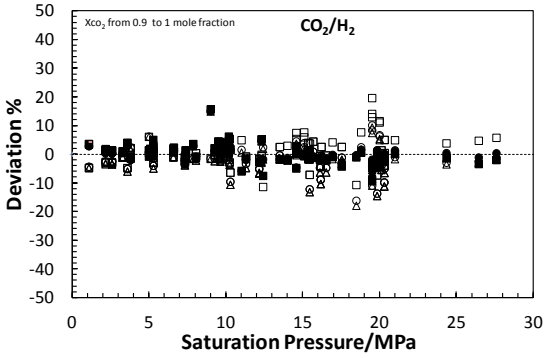
Xco2 from 0.9 to 1 mole fraction
CO2/H2
Deviation %
Saturation Pressure/MPa

g)

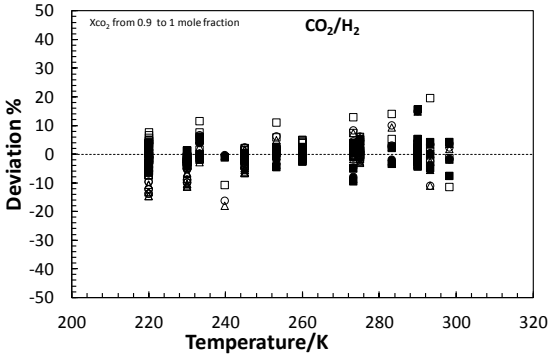
Xco2 from 0.9 to 1 mole fraction
CO2/H2
Deviation %
Temperature/K

h)

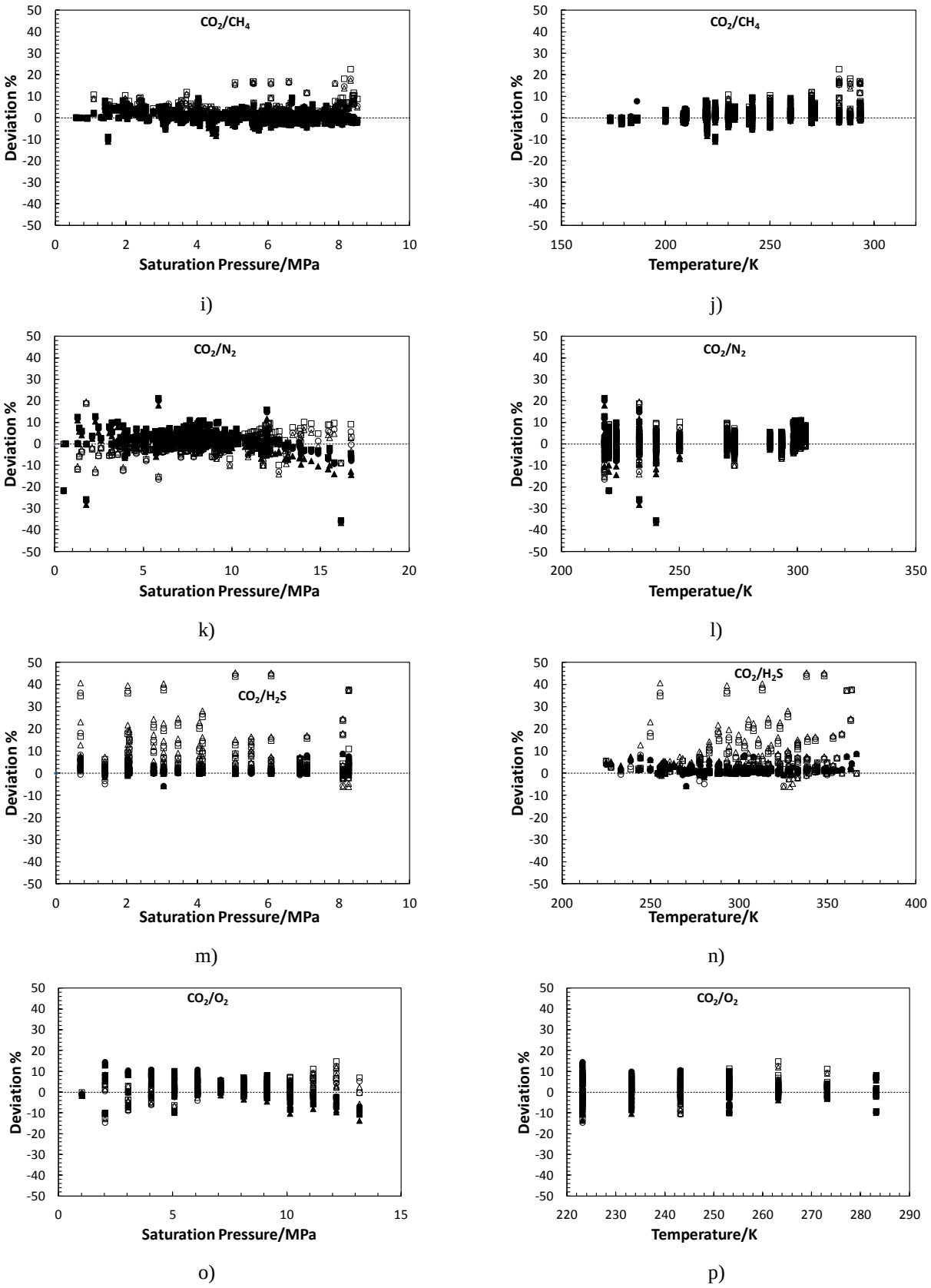


*Figure 2.4 (a-p) the deviation of PR (▲Δ), VPT (●○) and SRK (■□) EOSs on the calculated VLE properties of binary $CO_2$/mixtures; empty symbols represent AAD on vapour fraction of $CO_2$ ($Y_{CO2}$) and full symbols represent AAD on saturation pressure (Sources are listed in Table 2.1)*

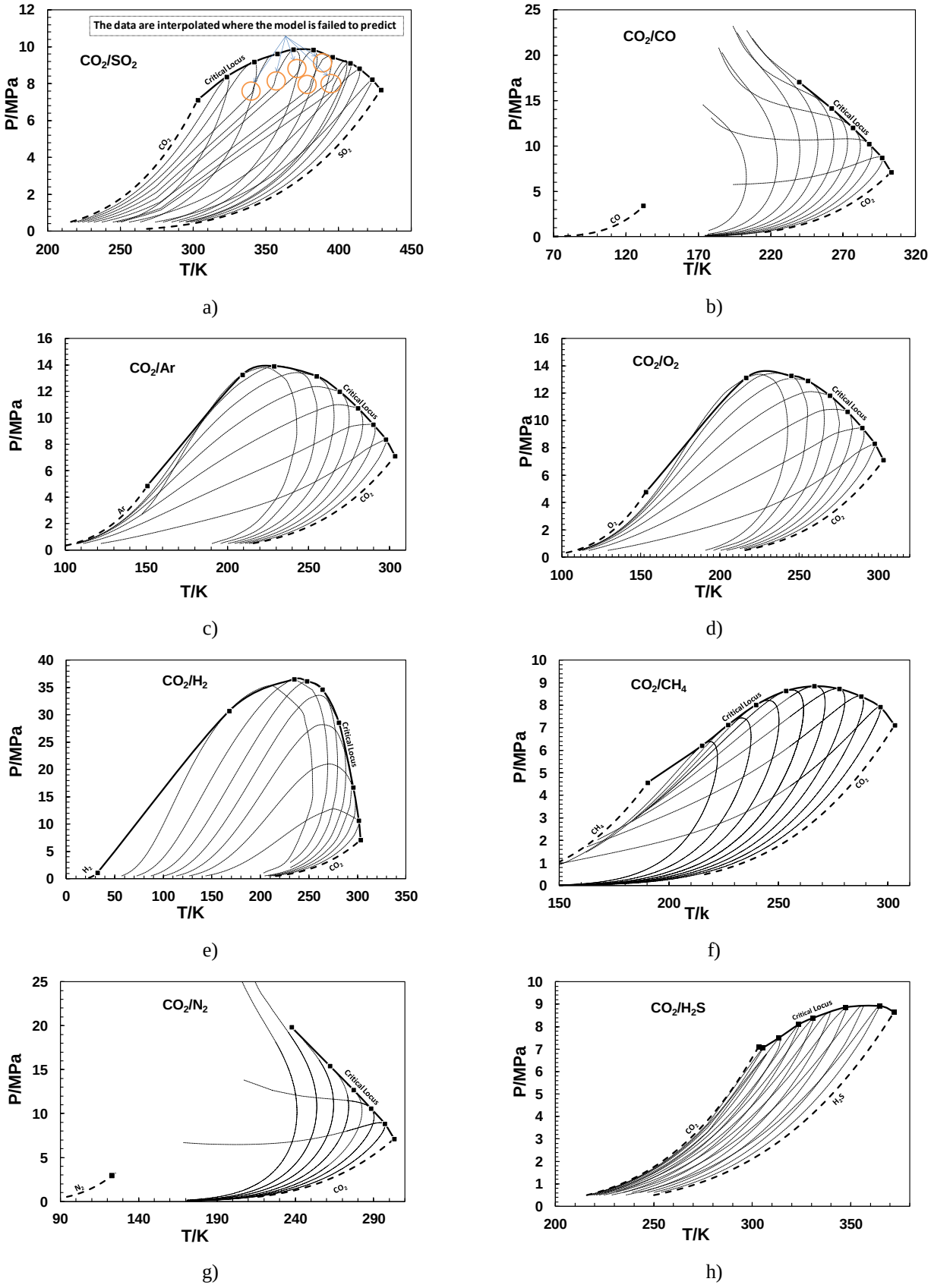


*Figure 2.5 (a-h) prediction results on VLE of $CO_2$ mixtures by PR EOS*

### *2.2.1 Critical Behaviour of $CO_2$ Rich Fluid*

For $CO_2$ to be transported in pipelines conditions (near or above supercritical phase), knowledge of the critical properties of the stream are essential. For economical and engineering reasons, it is better to have a high critical temperature and a low critical pressure; high critical temperature for reducing the cooling capacity (lower insulation cost and therefore lower maintenance cost) and low critical pressure for transportation at lower pressure [57]. Few critical points data were found in the literature for $CO_2$/impurities systems, such as $CO_2/N_2$, $CO_2/CH_4$ and $CO_2/H_2S$ and no critical data for the other impurities systems concern in this work. Figure 2.6 (a-f) shows the experimental and modelling critical locus curve for three binary mixtures, $CO_2/N_2$, $CO_2/CH_4$ and $CO_2/H_2S$. The data were calculated with the PR EOS. The experimental critical point data were not used for adjustment of the model but nevertheless reproduces the experimental results equally well as shown in the figures. For the binary $CO_2/CH_4$ (Figure 2.6-a and Figure 2.6-b), the model can predict well the critical pressure and temperature in high concentration $CO_2$ (up to 8% $CO_2$) and high concentration $CH_4$ (up to 20% $CH_4$). However, away from the above composition, the model cannot predict well the critical temperature or the critical pressure. The reason is probably that the source is from 1954 [42] and more reliable experimental data are required to test the reliability of the model. The critical curve of the binary $CO_2/H_2S$ is shown in Figure 2.6-c and Figure 2.6-d. From Figure 2.6-d, it is very clear that the experimental data of the critical temperature in rich $CO_2$ are in a good agreement with the model. However, the model is over-predicting compared to the measured values of the critical pressure. It is usually necessary to have more than one set of experimental data points from different sources in order to evaluate the model successfully. Figure 2.6-e and Figure 2.6-f show also plots for the critical properties of the system $CO_2/N_2$ system. The modelling results for the critical points in the system are in agreement with the measured values at high $CO_2$ mole fraction (above 80%). Then the model starts to deviate as more $N_2$ is added to the mixture.

The eight binary mixtures critical lines are shown in Figure 2.7 in the temperature range 243.3 K ($T_{Cm}/T_{C_{CO_2}} \approx 0.8$) to 365 K ($T_{Cm}/T_{C_{CO_2}} \approx 1.2$). Each dot on the critical locus curves represents 10 mole% of impurity in $CO_2$. In terms of the critical pressure, it is clear that the binary mixtures except for $H_2S$ tend to raise the critical

pressure of $CO_2$. For instance at 10 mole% of impurities, $H_2$ has the highest impact ( $P_{Cm}/P_{C_{CO_2}} \approx 1.4$) while $H_2S$ has the lowest ( $P_{Cm}/P_{C_{CO_2}} \approx 0.99$). The other impurities (CO, Ar, $O_2$, $N_2$, $SO_2$ and $CH_4$) impact varies in the range $1.1 \leq P_{Cm}/P_{C_{CO_2}} \leq 1.2$. In the other hand, the presence of $H_2S$ or $SO_2$ increases the critical temperatures of $CO_2$ by 0.7 % to 7% respectively while the other impurities (CO, Ar, $O_2$, $N_2$, and $CH_4$) decreases the critical temperature by an average of 2% and $H_2$ to less than 1%.

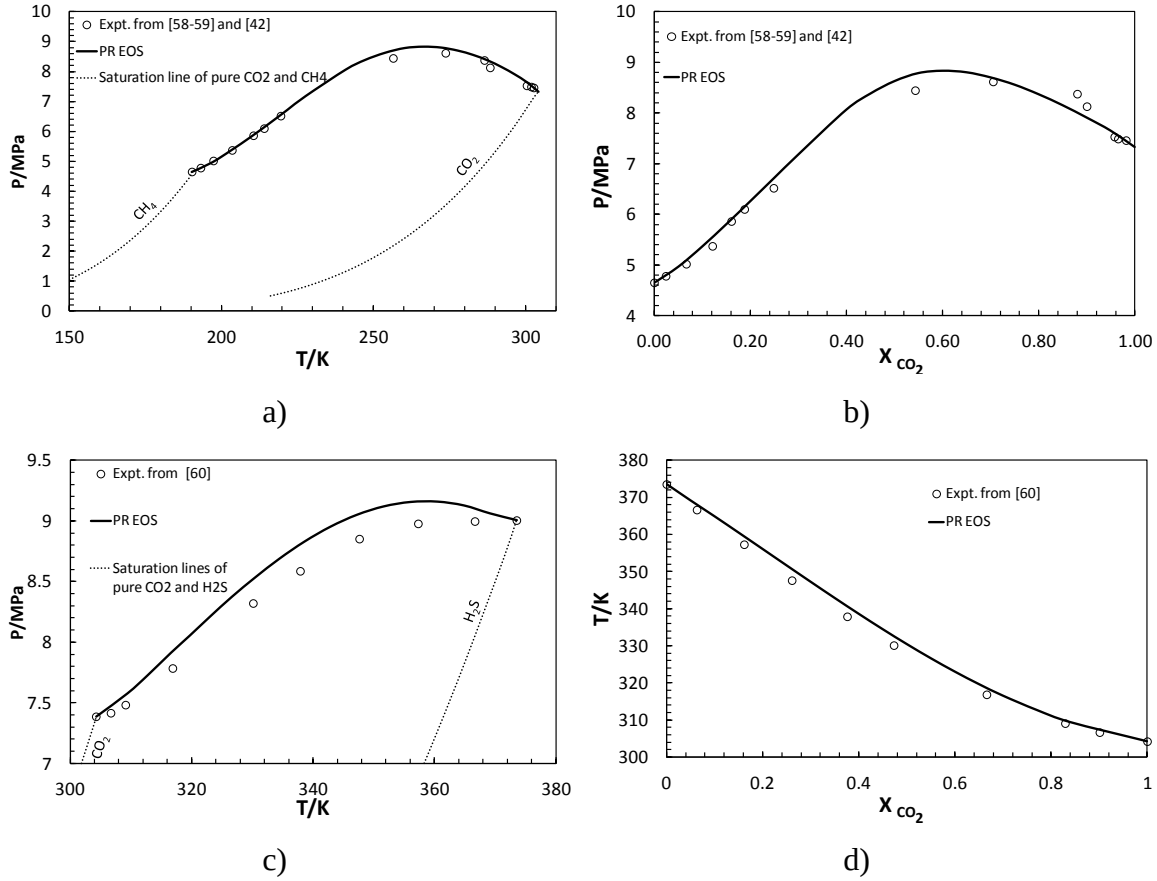

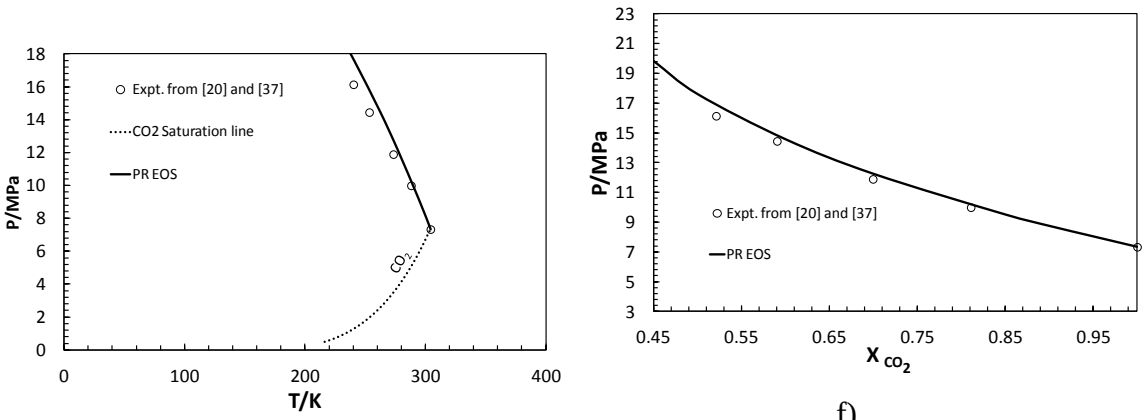


e) f)

*Figure 2.6 (a-f) critical properties of $CO_2/CH_4$ (a and b), $CO_2/H_2S$ (c and d), $CO_2/N_2$ (e and f); PR EOS is used for modelling*

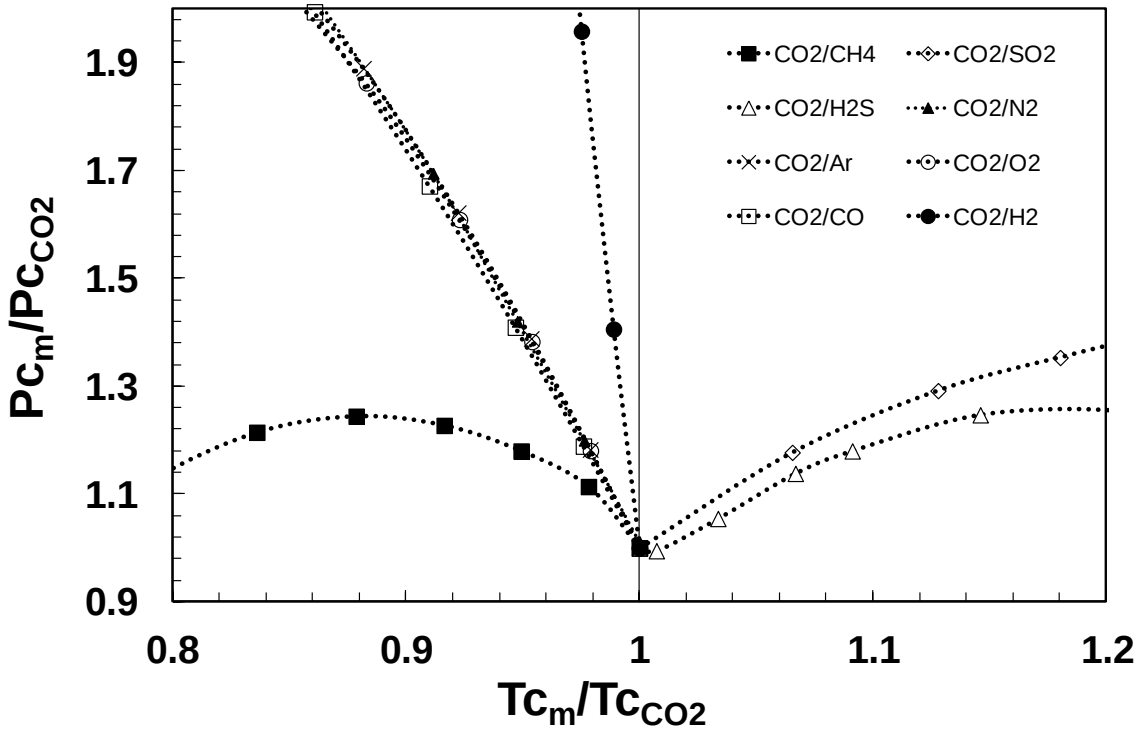


*Figure 2.7 Critical lines of the binary $CO_2$ mixtures. $Tc_m$ and $Pc_m$ are the critical temperature and pressure of mixtures, respectively. $Tc_{co2}$ and $Pc_{co2}$ are the critical temperature and pressure of $CO_2$ respectively*

### 2.3 Bubble Point and Speed of Sound Measurements of $CO_2$ and Alkanes System

The efficiency of oil displacement by $CO_2$ is related to the phase equilibrium since the process involves intimate contact of gases and liquids. Most studies on the phase behaviour of $CO_2$ with hydrocarbons have been limited to mixtures of pure $CO_2$ with hydrocarbons. These studies were usually made to obtain binary interaction parameters.

One of the aims of this study is to provide few experimental data on how impurities such as $N_2$, $CH_4$, CO, Ar etc. affect the phase behaviour of $CO_2$/crude oil mixtures.

*Materials*: n-decane ($C_{10}H_{22}$), n-tridecane ($C_{13}H_{28}$) and n-hexadecane ($C_{16}H_{34}$) of purity (weight) > 99 % were purchased from Fisher Scientific Co. and used without further purification. Carbon dioxide with a minimum purity of 99.9% (mole) was used in this work. Compositional details of the alkane oil used is given in Table 2.4.

*Table 2.4 Alkane mixture compositions*

| C. number | MW | Weight % (±0.03%) |
|---|---|---|
| C10 | 142.28 | 52.9 |
| C13 | 184.37 | 30.2 |
| C16 | 226.45 | 17.9 |
| Total | | 100 |

The equipment used to measure the speed of sound was specially designed for measuring acoustic properties of aqueous solutions. A schematic diagram of the ultrasonic set-up can be found in Chapter 3. All the mixtures were prepared gravimetrically using a digital balance (Sartorios) with a precision of ($10^{-2}$g). The maximum uncertainty of the sample preparation in mole fraction was ± 0.002. The system temperature is controlled by circulating coolant from a cryostat which is capable of maintaining the cell temperature stability to within better than 0.05 ºC. The piston displacement is measured by a digital piston displacement indicator attached to one end of the cell (accuracy $10^{-3}$ mm). The maximum length of the cell is 10 cm. The digital indicator measures the in-displacement of the piston into the cell. The liquid components of the sample were charged into the cell before the gas to avoid the possibility of backflush. The amounts of liquid and gas charged into the recombination cell were measured gravimetrically by weighing the containers before and after charging. In order to investigate the effects of $CO_2$ impurities on alkanes-$CO_2$ mixture, a mixture of three components were prepared n-decane ($C_{10}H_{22}$), n-tridecane ($C_{13}H_{28}$) and n-hexadecane ($C_{16}H_{34}$). The experiment was run with a constant weight composition of alkane mixture, given in Table 2.4. The total mixture composition was then recalculated after $CO_2$ or $CO_2$ with impurities injection. In this part of study, five tests

were carried-out in order to understand the effect of Ar, $H_2$, CO and $CH_4$ on $CO_2$ saturation pressure at 344.3 K. All tests were performed with 5 mole% of impurities.

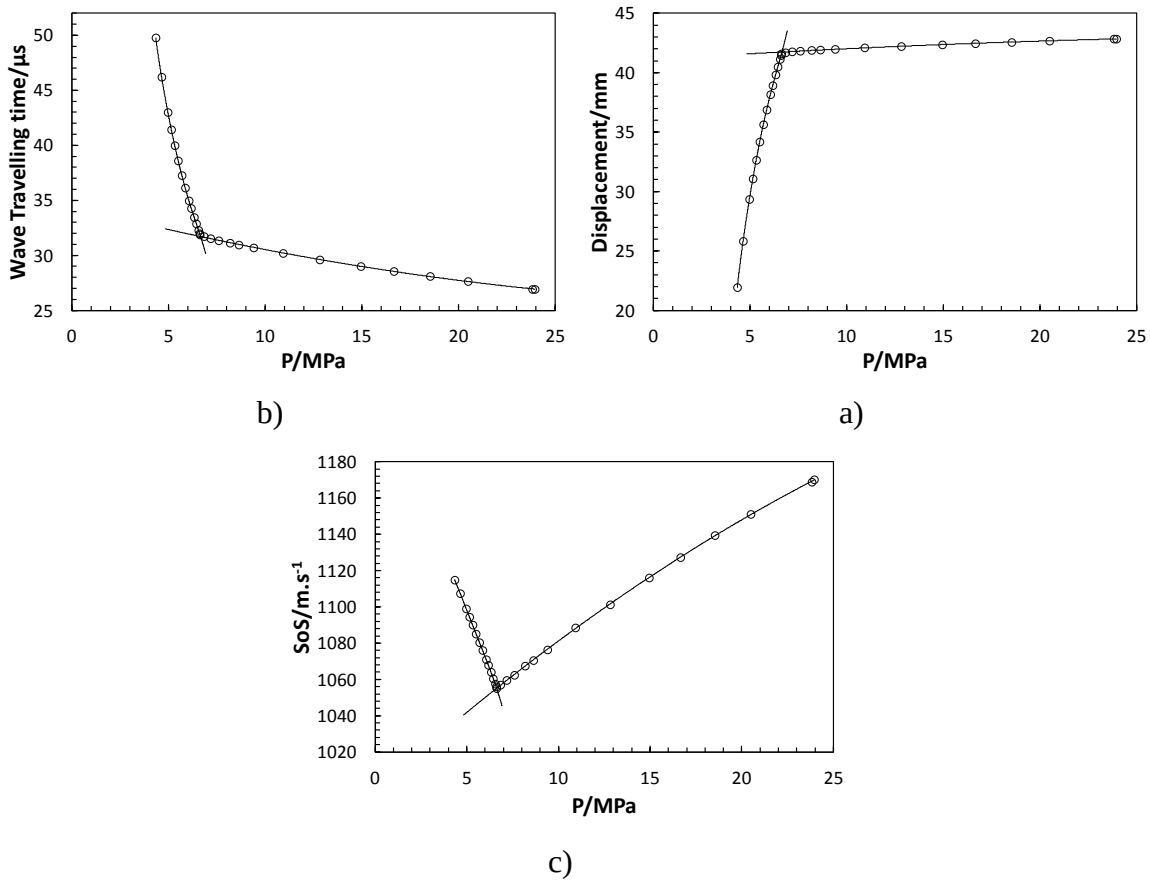


*Figure 2.8 (a-c) Plots showing an example of bubble point determination of pure $CO_2$ at 344.3 from plot of change in cell pressure versus (a) wave travelling time, (b) piston displacement and (c) speed of sound*

A typical test to determine the bubble of pure $CO_2$ (and impure $CO_2$) with /alkane mixture is as follow: the cell was charged with the test sample and set to the desired temperature for the measurement. The sample volume was then reduced by pumping a hydraulic fluid into the cell (behind the piston), at the opposite end to the sample. By this means the sample pressure was increased such that the sample was at a pressure significantly higher than the expected bubble point pressure. The cell was then rocked to mix the contents and ensure equilibrium. The sample volume was then increased step-wise by withdrawing liquid out of the cell. The piston displacement reading from the indicator is then taken at the corresponding pressure. At each step, mixing was continued until equilibrium was achieved, indicated by a constant pressure. The

stabilized equilibrium pressures and change in the displacement were plotted and the bubble point was indicated by a sharp change in the pressure. In addition, the bubble point was determined and confirmed from the break-point of the pressure versus travelling time and speed of sound plots as shown in Figure 2.8 (a-c). The plots show the bubble point estimation for pure $CO_2$ at 20.14 weight% in the alkane system. The calculated bubble point pressures of the mixture are 6.65, 6.66 and 6.63 MPa by using travelling distance, travelling wave time and speed of sound plots respectively. The values obtained from travelling wave time and the travelling distance are very close because they are based on the volume change. From Figure 2.8 (a-c), the speed of sound of the liquid mixture of $CO_2$/alkane starts to decrease as pressure decreases until the system reaches the bubble point pressure. This is mainly due to the reduction of the system bulk modulus. As the pressure decreases, below the bubble point, the dissolved $CO_2$ begins to escape from the alkane/$CO_2$ mixture. This dramatic phenomenon occurs because the compressibility decreases as $CO_2$ concentration decreases.

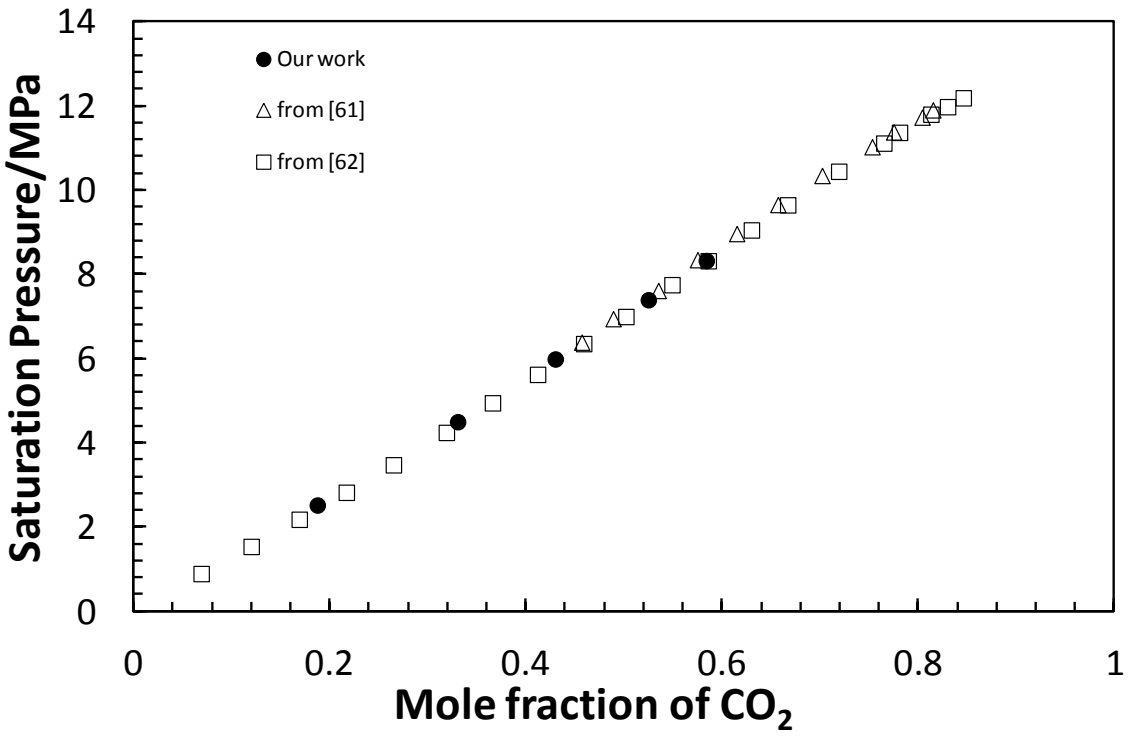


*Figure 2.9 Saturation pressure measurements of $CO_2$ and n-decane system at 344.3 K*

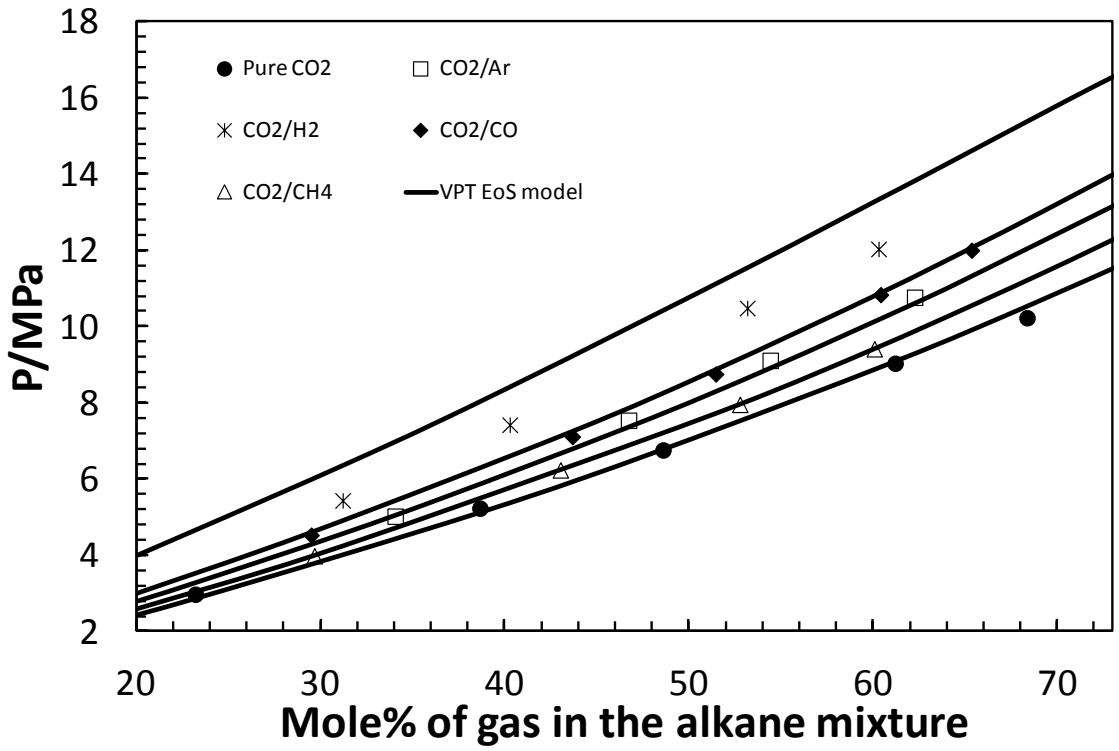


*Figure 2.10 Effect of 5 mole% impurities on the saturation pressure of $CO_2$/alkane mixture*

The experiment was first carried-out with $CO_2$ and n-decane system at 344.3 K for validation. Our results were in a good agreement with those performed by Nagarajan and Robinson [61] and Shaver et al. [62] as shown in Figure 2.9. Figure 2.10 shows the effect of 5 mole% impurity on the bubble point measurements of $CO_2$/alkane mixture. The increase in bubble pressure that is caused by additional mole percentage of gas is significantly greater in the presence of impurity than in pure $CO_2$. The change is as high as 1.2 MPa and 5.3 MPa at 30 mole% and 60 mole% respectively in the presence of hydrogen, while methane has the lowest impact to the $CO_2$/alkane saturation pressure (the saturation pressure of the mixture at 60 mole% $CO_2/CH_4$ gas is 2.4 MPa higher than in pure $CO_2$). The presence of argon and carbon monoxide in $CO_2$ stream can increase the saturation pressure of $CO_2$/alkane mixture to 4.1 MPa and 3.4 MPa. The VPT EOS to is used to predict the experimental data of $CO_2$/alkane (from 7.46 weight% to 36.57 weight% $CO_2$) and $CO_2$/alkane in the presence of impurities (from 9.83 weight% to 30.46 weight%) as shown in Figure 2.10.

Usually, equations of state (EOSs) are used to predict vapour liquid equilibrium of such mixtures and acceptable accuracy can be found with the VPT model as shown in Figure

2.10. To obtain better results with this EOS, binary interaction parameters, $k_{ij}$, are required. These parameters in such mixtures are temperature dependent and they are usually calculated from isothermal experimental VLE data [63]. The interaction parameters used in the VPT EOS for the binary $CO_2$/n-decane, $CO_2$/n-tridecane and $CO_2$/n-hexadecane are 0.104, 0.098 and 0.095 respectively. The other binary alkane/impurities systems are set to their default values. The deviation on the saturation pressure is less than 3% in all the mixture of alkane containing pure and impure $CO_2$ except for the one containing hydrogen where it may exceed 10%. This is mainly due the low critical temperature of hydrogen compare to other impurities.

*Table 2.5 SoS measurements of liquid alkane mixture in pure and impure $CO_2$*

| Pure $CO_2$ in alkane mixture | | | | | | | | | |
|---|---|---|---|---|---|---|---|---|---|
| 7.46 Weight% | | 14.39 weight % | | 20.14 weight % | | 29.61 weight % | | 36.57 weight % | |
| P/ MPa | SoS/ $m.s^{-1}$ | P/ MPa | SoS/ $m.s^{-1}$ | P/ MPa | SoS/ $m.s^{-1}$ | P/ MPa | SoS/ $m.s^{-1}$ | P/ MPa | SoS/ $m.s^{-1}$ |
| 23.02 | 1298 | 23.39 | 1229 | 23.95 | 1170 | 25.46 | 1089 | 28.33 | 1036 |
| 20.99 | 1291 | 21.30 | 1220 | 23.82 | 1169 | 22.86 | 1072 | 26.28 | 1022 |
| 20.09 | 1287 | 18.99 | 1208 | 20.49 | 1151 | 21.43 | 1062 | 23.32 | 999 |
| 18.68 | 1283 | 16.61 | 1195 | 18.53 | 1139 | 19.94 | 1051 | 21.78 | 987 |
| 16.50 | 1273 | 14.14 | 1181 | 16.66 | 1127 | 17.97 | 1036 | 19.11 | 965 |
| 14.19 | 1263 | 11.86 | 1167 | 14.94 | 1116 | 15.79 | 1020 | 17.11 | 949 |
| 12.28 | 1253 | 9.93 | 1155 | 12.82 | 1101 | 13.83 | 1005 | 14.85 | 930 |
| 9.15 | 1235 | 7.87 | 1140 | 10.92 | 1089 | 11.83 | 989 | 12.64 | 912 |
| 7.12 | 1223 | 6.01 | 1126 | 9.40 | 1076 | 9.97 | 974 | 11.80 | 906 |
| 5.88 | 1215 | 5.42 | 1122 | 8.63 | 1071 | 9.19 | 968 | 11.08 | 900 |
| 4.43 | 1205 | | | 8.18 | 1067 | | | | |
| 3.72 | 1200 | | | 7.59 | 1062 | | | | |
| 3.32 | 1198 | | | 7.17 | 1060 | | | | |
| | | | | 6.83 | 1057 | | | | |
| $CO/CO_2$ in alkane mixture | | | | | | | | | |
| 9.89 weight % | | 16.89 weight % | | 21.73 weight % | | 28.55 weight % | | 33.07 weight % | |

| P/ MPa | SoS/ $m.s^{-1}$ | P/ MPa | SoS/ $m.s^{-1}$ | P/ MPa | SoS/ $m.s^{-1}$ | P/ MPa | SoS/ $m.s^{-1}$ | P/ MPa | SoS/ $m.s^{-1}$ |
|---|---|---|---|---|---|---|---|---|---|
| 27.40 | 1274 | 39.76 | 1271 | 40.93 | 1234 | 39.29 | 1170 | 39.17 | 1134 |
| 22.14 | 1249 | 34.43 | 1248 | 35.61 | 1208 | 33.14 | 1136 | 30.30 | 1081 |
| 17.27 | 1224 | 28.88 | 1221 | 29.50 | 1176 | 27.74 | 1103 | 22.11 | 1022 |
| 13.57 | 1203 | 23.18 | 1190 | 24.51 | 1147 | 22.51 | 1067 | 16.35 | 971 |
| 8.19 | 1170 | 16.33 | 1148 | 18.72 | 1110 | 17.48 | 1028 | 11.84 | 923 |
| 5.83 | 1154 | 10.43 | 1107 | 14.30 | 1078 | 13.15 | 990 | | |
| | | 7.79 | 1087 | 10.43 | 1047 | 10.81 | 968 | | |

| $Ar/CO_2$ in alkane mixture | | | | | | | |
|---|---|---|---|---|---|---|---|
| 12.07 weight % | | 18.89 weight % | | 24.07 weight % | | 30.46 weight % | |
| P/ MPa | SoS/ $m.s^{-1}$ | P/ MPa | SoS/ $m.s^{-1}$ | P/ MPa | SoS/ $m.s^{-1}$ | P/ MPa | SoS/ $m.s^{-1}$ |
| 37.54 | 1294 | 41.33 | 1253 | 39.26 | 1197 | 36.68 | 1129 |
| 30.47 | 1263 | 34.05 | 1219 | 29.57 | 1134 | 32.10 | 1103 |
| 24.91 | 1237 | 27.49 | 1186 | 20.93 | 1092 | 25.04 | 1056 |
| 17.25 | 1196 | 20.74 | 1147 | 15.25 | 1051 | 16.45 | 988 |
| 13.01 | 1172 | 15.39 | 1113 | 10.60 | 1012 | 11.60 | 941 |
| 7.16 | 1134 | 10.57 | 1078 | | | | |
| 4.98 | 1119 | 7.44 | 1054 | | | | |

| $H_2/CO_2$ in alkane mixture | | | | | | | |
|---|---|---|---|---|---|---|---|
| 10.33 weight % | | 14.64 weight % | | 22.39 weight % | | 27.84 weight % | |
| P/ MPa | SoS/ $m.s^{-1}$ | P/ MPa | SoS/ $m.s^{-1}$ | P/ MPa | SoS/ $m.s^{-1}$ | P/ MPa | SoS/ $m.s^{-1}$ |
| 31.04 | 1284 | 28.20 | 1237 | 34.26 | 1188 | 34.18 | 1138 |
| 27.81 | 1270 | 23.05 | 1206 | 28.26 | 1157 | 30.29 | 1116 |
| 22.78 | 1247 | 19.32 | 1185 | 23.58 | 1128 | 24.71 | 1079 |
| 16.66 | 1214 | 15.75 | 1162 | 19.22 | 1098 | 19.91 | 1043 |
| 10.50 | 1178 | 10.15 | 1125 | 13.97 | 1059 | 14.34 | 995 |
| 6.79 | 1154 | 7.28 | 1105 | 10.35 | 1031 | 11.79 | 976 |
| 5.43 | 1144 | | | | | | |

| $CH_4/CO_2$ in alkane mixture | | | | | | | |
|---|---|---|---|---|---|---|---|
| 9.83 weight % | | 16.55 weight % | | 22.4 weight % | | 27.98 weight % | |
| P/ MPa | SoS/ $m.s^{-1}$ | P/ MPa | SoS/ $m.s^{-1}$ | P/ MPa | SoS/ $m.s^{-1}$ | P/ MPa | SoS/ $m.s^{-1}$ |
| 32.70 | 1300 | 36.32 | 1254 | 39.57 | 1221 | 44.62 | 1195 |
| 26.74 | 1273 | 27.98 | 1213 | 34.07 | 1193 | 36.70 | 1155 |
| 19.90 | 1238 | 20.66 | 1173 | 28.02 | 1160 | 28.79 | 1109 |
| 16.10 | 1219 | 14.65 | 1136 | 19.97 | 1109 | 22.05 | 1063 |
| 10.20 | 1185 | 9.74 | 1100 | 14.00 | 1066 | 15.43 | 1010 |
| 6.52 | 1161 | 6.64 | 1076 | 11.66 | 1047 | 11.36 | 972 |
| 4.59 | 1147 | | | 8.35 | 1019 | | |
| 4.22 | 1144 | | | | | | |

The injection of gas in a liquid reduces the sound speed in the liquid [64-67]. The speed of sound in an air water mixture can fall to 20 $m.s^{-1}$ while the speed of pure air and pure water are 1440 $m.s^{-1}$ and 340 $m.s^{-1}$ respectively [67]. This occurs because the mixture has the compressibility of gas and the density of a liquid [68]. The results of speed of sound under different pressures and mixture compositions are listed in Table 2.5. The results are given for $CO_2$/alkane mixture plus $CO_2$/alkane mixture containing impurities (CO, Ar, $H_2$ and $CH_4$). The mole percentage of impurities in the binary $CO_2$/impurities system is 5 mole%. The measurements were performed for a liquid single phase above the saturation line. The speed of sound measurements of $CO_2$/alkane are plotted in Figure 2.11. At a fixed mixture composition, the speed of sound increases as pressure increases. It is also clear that by increasing the concentration of $CO_2$ in the mixture, the SoS decreases. In order to investigate the effect of impurities on the SoS, a mathematical correlation was developed to match the data, taking the following form:

$$SoS_{co_2/alkane} = \frac{1282 - 1285x + 25.51P}{1 + 0.128x + 0.0154P} \tag{2.27}$$

P is the pressure in MPa, x is the weight fraction (0 to 1) and the calculated SoS is given in $m.s^{-1}$. The AAD and maximum deviation from the correlation are 0.17% and 0.53% respectively. The calculated reduction in the speed of sound is around 10 $m.s^{-1}$ per

adding 1 weight% of $CO_2$ at the same pressure and temperature condition. Figure 2.12-a and Figure 2.12-b show the effect of two impurities (Ar and $H_2$) on the speed of sound of the $CO_2$/alkane mixture. The presence of impurities on the $CO_2$ stream reduces slightly the speed of sound of the mixture. The effect is found in the range from 1 to 3% reduction. The reduction on the speed of sound increases as the pressure increases. The reduction on the property is not significantly affected by the type of impurities used.

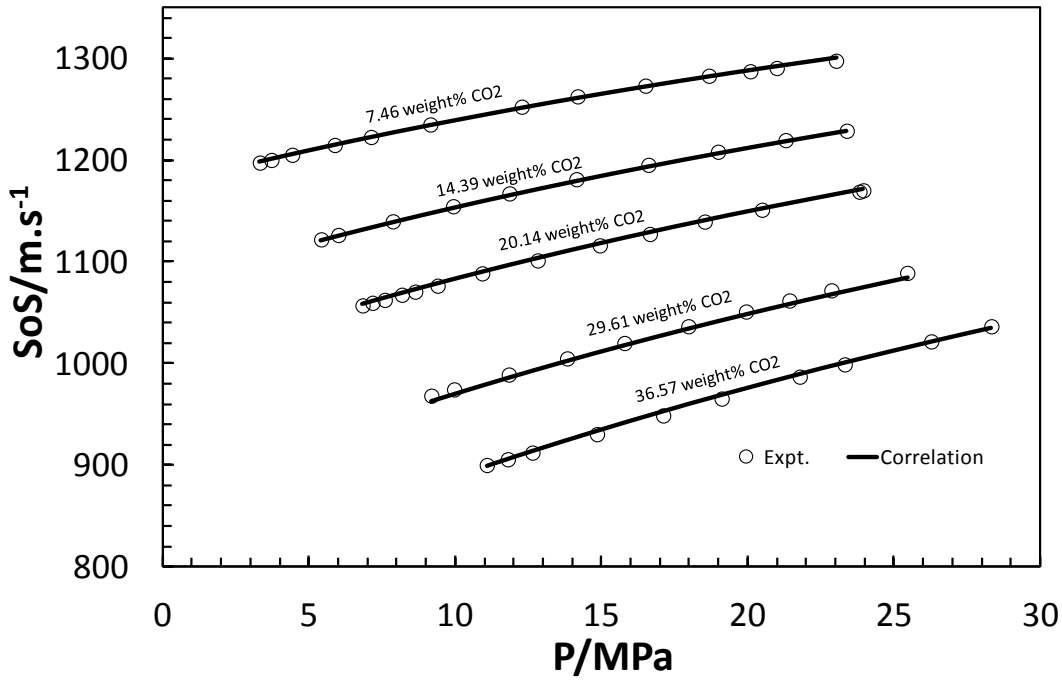


*Figure 2.11 The speed of sound of $CO_2$/alkane system at 344.3 K, data are correlated using Equation 2.27*

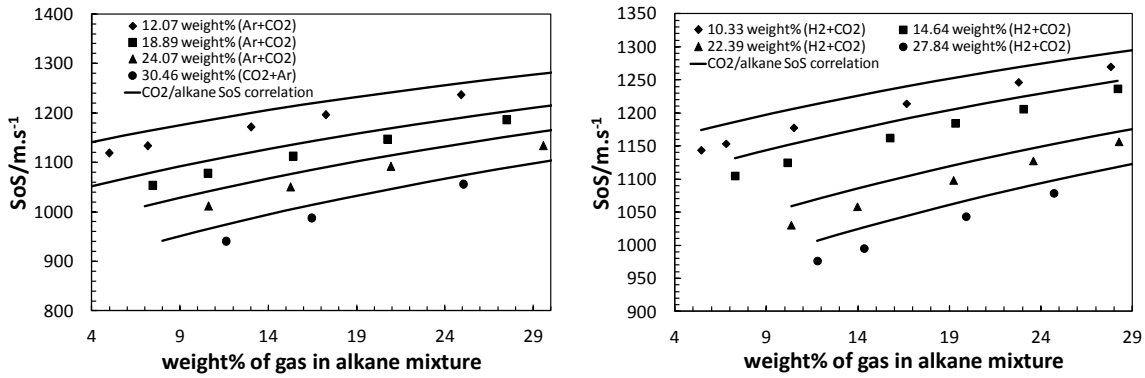


a) b)

*Figure 2.12 (a-b) Effect of impurities on speed of sound property of $CO_2$/alkane system at 344.3 K, the SoS of $CO_2$/alkane mixture is correlated using Equation 2.27 at the same condition of temperature and mixture composition.*

## 2.4 Conclusions

Extensive experimental data on VLE of $CO_2$/impurities system were collected in order to tune the three EOSs (PR, VPT, and SRK). The effects of impurities of $CO_2$ systems on the VLE and critical curve properties were investigated for eight binary mixtures (impurities: $H_2$, $CH_4$, CO, Ar, $O_2$, $N_2$, $SO_2$ and $H_2S$). The three EOSs predict the saturation pressure of binary mixtures with similar accuracy (4.06% to 4.39%) in all the tested impurities system. The average deviation is as high as 10% using the three EOSs in the binary $CO_2/H_2$ Because of the low critical temperature of hydrogen component. The prediction of VLE on the $CO_2/CH_4$ binary system has the lowest deviation, i.e., less than 2.8%. The presence of impurities in $CO_2$ rich system tends to raise the critical pressure of $CO_2$ except for $H_2S$. The impurities $H_2$, $CH_4$, CO, Ar, $O_2$ and $N_2$ have a negative impact by increasing the $CO_2$ critical temperature while $SO_2$ and $H_2S$ have a positive impact.

Few saturation pressure points were experimentally measured for $CO_2$/alkane mixture with pure and impure $CO_2$ at 344.3 K. The effect of four impurities were investigated, Ar, $H_2$, CO and $CH_4$. The increase on the saturation pressure of the mixture is ranged from the highest to the lowest impact as the following order: $H_2$, CO, Ar, and $CH_4$. In addition, the effects of impurities on the speed of sound of the previous mixtures were studied above the saturation line. Two key findings can be highlighted: 1) the impurities reduce approximately the speed of sound equally at the same conditions of pressure and temperature; 2) The speed of sound decreases as the amount of gas (pure or impure $CO_2$) increases.

**References**

[1] Mohitpour, M., Seevam P., Botros K. K., Rothwell B. and Claire E., 2012, *Pipeline Transportation of Carbon Dioxide Containing Impurities*, American Society of Mechanical Engineers.

[2] King, G. G., *Here Are Key Design Considerations for $CO_2$ Pipelines*, 1982, Oil and Gas Journal, **80,** 219-222.

[3] Farris, C. B., *Unusual Design Factors for Supercritical $CO_2$ Pipeline*, 1983, Energy Progress, **3,** 150-158.

[4] Oosterkamp, A. and Ramsen, J., 2008, *State-of-the-Art Overview of $CO_2$ Pipeline Transport with Relevance to Offshore Pipelines*, Polytec Report No. POL-O-2007-138-A.

[5] McCollough, D. E., 2003, *The Central Basin Pipeline: a $CO_2$ System in West Texas*, Energy Progress, **6**, 230-234.

[6] Zhang Z. X., Wang G. X., Massarotto P. and Rudolph V., 2006, *Optimization of Pipeline Transport for $CO_2$ Sequestration*, Energy Conversion And Management, **47**, 702-715.

[7] Li, H. and Yan, J., 2006, *Comparative study of Equations of State for Predicting Phase Equilibrium and Volume Properties of $CO_2$ and $CO_2$ Mixtures*, GHGT8, Trondheim.

[8] Kunz, O., Klimeck, R., Wagner, W. and Jaeschke, M., 2007, *The GERG-2004 Wide-Range Equation of State for Natural Gases and Other Mixtures*. GERG Technical Monograph.

[9] Camacho-Camacho, L. E., Galicia-Luna, L. A., Elizalde-Solis, O. and Martínez-Ramírez, Z., 2007, *New Isothermal Vapor-Liquid Equilibria for The $CO_2$+N-Nonane, and $CO_2$ + N-Undecane Systems*, Fluid Phase Equilib., **259**, 45-50.

[10] Camacho-Camacho, L. E. and Galicia-Luna, L. A., 2007, *Experimental Densities of Hexane + Benzothiophene Mixtures from 313 to 363 K and up to 20 MPa*, J. Chem. Eng. Data, **52**, 2455-2461.

[11] Camacho-Camacho, L. E., 2009, *Development of a Method to Measure Solid Solubilities and Solubilities of Solid + Liquid Mixtures in Supercritical Solvents or a Mixture of Liquid and Ionic Liquid up to 150 °C and 300 bar. PHD*. Thesis, SEPI-ESIQIE Instituto Politecnico Nacional, Mexico.

[12] Elizalde-Solis, O., Galicia-Luna, L. A. and Camacho-Camacho, L. E., 2007, *High-Pressure Vapor-Liquid Equilibria for $CO_2$ + Alkanol Systems and Densities of N-Dodecane and N-Tridecane*, Fluid Phase Equilib., **259**, 23-32.

[13] Elizalde-Solis, O. and Galicia-Luna, L. A., 2005, *Solubility of Thiophene + Pentane and Thiophene + Octane Binary Mixtures in Supercritical Carbon Dioxide at Temperatures from 333 to 383 K*, Ind. Eng. Chem. Res., **44**, 5757-5760.

[14] Camacho-Camacho L. E., Galicia-Luna L. A. and Elizalde-Solis O., 2011, *Vapor Liquid Equilibria of Binary and Ternary Systems Containing Carbon Dioxide, Alkane, And Benzothiophene*, J. Chem. Eng. Data, **56**, 4109-4115.

[15] Christiansen, L. J. and Fredenslund, A., 1974, *Gas-Liquid Equilibria of the $CO_2$-CO and $CO_2$-$CH_4$-CO Systems*, Adv. Cryog. Eng., **19**, 309-319.

[16] Kaminishi, G. I., Arai Y., Saito S. and Maeda S., 1968, *Vapor–Liquid Equilibriums for Binary and Ternary Systems Containing Carbon Dioxide*, J. Chem. Eng. Jpn., **1**, 109-116.

[17] Huamin S., 1991, *Solubility of Carbon Monoxide in Methanol and Carbon Dioxide under High Pressure*, Chem. Eng. (China), **19**, 61-69.

[18] Zenner, G. H. and Dana, L. I., 1963, *Liquid-Vapor Equilibrium Compositions of Carbon Dioxide-Oxygen-Nitrogen Mixtures*, Chem. Eng. Progr. Symp. Ser., **44**, 36-41.

[19] Yorizane, M., Yoshimura, S., Masuoka, H. and Nakamura, M., 1971, *Prediction of High Pressure Vapor-Liquid Equilibria for Multicomponent Systems by the BWR Equation of State*, J. Chem. Eng. Jpn., **4**, 10-16.

[20] Al-Sahhaf, T. A., Kidnay, A. J. and Sloan, E. D., 1983, *Liquid + Vapor Equilibria in the $N_2$ + $CO_2$ + $CH_4$ System*, Ind. Eng. Chem. Fundam., **22**, 372-380.

[21] Somait, F. A. and Kidnay, A. J., 1978, *Liquid-Vapor Equilibria at 270.00 K for Systems Containing Nitrogen, Methane, and Carbon Dioxide*, J. Chem. Eng. Data, **23**, 301-305.

[22] Yorizane, M., Yoshimura., S. and Masuoka, H., 1970, *Vapor Liquid Equilibrium at High Pressure ($N_2$-$CO_2$, $H_2$-$CO_2$ System)*, Kagaku Kogaku, **34**, 953-957.

[23] Brown, T. S., Niesen, V. G., Sloan, E. D. and Kidnay, A. J., 1989, *Vapor-Liquid Equilibria for the Binary Systems of Nitrogen, Carbon Dioxide, and N-Butane at Temperatures from 220 to 344 K*, Fluid Phase Equilib., **53**, 7-14.

[24] Yorizane, M., Yoshimura, S., Masuoka, H. and Miyano, Y., 1985), *New Procedure for Vapour-Liquid Equilibria. Nitrogen + Carbon Dioxide, Methane + Freon 22, and Methane +Freon 12*, J. Chem. Eng., **30**, 174-176.

[25] Xu, N., Dong, J., Wang, Y. and Shi, J., 1992, *High Pressure Vapor Liquid Equilibria at 293 K for Systems Containing Nitrogen, Methane And Carbon Dioxide*, Fluid Phase Equilib., **81**, 175-186.

[26] Bian B., 1992, *Measurement Of Phase Equilibria in the Critical Region and Study of Equation of State*, Thesis, University of Nanjing.

[27] Bian, B., Wang, Y. and Shi J., 1993, *Simulteanous Determination of Vapour-Liquid Equilibrium and Molar Volumes for Coexisting Phases up to Critical Temperature with a Static Method*, Fluid Phase Equilib., **90**, 177-187.

[28] Selleck, F. T., Reamer, H. H. and Sage, B. H., 1953, *Volumetric and Phase Behavior of Mixtures of Nitric Oxide and Nitrogen Dioxide*, Ind. Eng. Chem., **45**, 814-819.

[29] Fredenslund, A. A. and Sather, G. A., 1970, *Gas-Liquid Equilibrium of the Oxygen-Carbon Dioxide System*, J. Chem. Eng. Data, **15**, 17-22.

[30] Sarashina, E., Arai, Y. and Saito, S., 1971, *The P-V-T-x Relation for the Carbon Dioxide-Argon System, J. Chem. Eng. Jpn.*, **4**, 379-381.

[31] Coquelet, C., Valtz, A., Dieu, F., Richon, D., Arpentinier P. and Lockwood, F., 2008, *Isothermal P, x, y Data For The Argon + Carbon Dioxide System at Six Temperatures from 233.32 to 299.21 K and Pressures up to 14 MPa*, Fluid Phase Equilib., **273**, 38-43.

[32] Bian, B., Wang, Y., Shi, J., Zhao, E. and Lu, B. C.-Y., 1993, *Simultaneous Determination of Vapor-Liquid Equilibrium and Molar Volumes for Coexisting Phases up to the Critical Temperature with a Static Method*, Fluid Phase Equilib., **90**, 177-187.

[33] Al-Sahhaf, T. A., Kidnay, A. J. and Sloan, E. D., 1983, *Liquid + Vapor Equilibria in the $N_2$ + $CH_4$ System*, Ind. Eng. Chem. Fundam., **22**, 372-380.

[34] Knapp, H., Yang, X. and Zhang, Z., 1990, *Vapor-Liquid Equilibria in Ternary Mixtures Containing Nitrogen, Methane, Ethane and Carbon Dioxide at Low Temperatures and High Pressures*, Fluid Phase Equilib., **54**, 1-18.

[35] Wei, M. S.-W., Brown, T. S., Kidnay, A. J. and Sloan, E. D., 1995, *Vapor + Liquid Equilibria for the Ternary System Methane + Ethane + Carbon Dioxide*

*at 230 K and its Constituent Binaries at Temperatures from 207 to 270 K*, J. Chem. Eng. Data, **40**, 726-731.

[36] Shi, M., Wei, M., Zhang, J. and Wang, L., 1984 , *Simple and Speedy Measurement of Bubble Point and Dew Point for VLE Binary System under Pressure*, Chemical Engineering (China), **6**, 51-54.

[37] Arai, Y., Kaminishi, G. -I. and Saito, S., 1971, *The Experimental Determination of the P-V-T-X (Pressure-Volume-Temperature- Composition) Relations for the Carbon Dioxide - Nitrogen and the Carbon Dioxide – Methane Systems*, J. Chem. Eng. Jpn., **4**, 113-122.

[38] Davalos, J., Anderson, W. R., Phelps, R. E. and Kidnay, A. J., 1976, *Liquid-Vapor Equilibria at 150.00K for Systems Containing Methane, Ethane and Carbon Dioxide*, J. Chem. Eng. Data, **21**, 81-84.

[39] Freitag, N. P. and Robinson, D. B., 1986, *Equilibrium Phase Properties of the Hydrogen-Methane-Carbon Dioxide, Hydrogen-Carbon Dioxide-N-Pentane and Hydrogen-N-Pentane Systems*, Fluid Phase Equilib., **31**, 183-201.

[40] Webster, A. L., Kidnay, A. J., 2001, *Vapor-Liquid Equilibria for the Methane-Propane-Carbon Dioxide Systems at 230 K and 270 K*, J. Chem. Eng. Data, **46** 759-764.

[41] Mraw, S. C., Hwang, S. -C. and Kobayashi R., 1978, *Vapor-Liquid Equilibrium of the $CH_4$-$CO_2$ System at Low Temperatures*, J. Chem. Eng. Data, **23**, 135-139.

[42] Donnelly, H. G. and Katz, D. L., 1954, *Phase Equilibrium in the Carbon Dioxide-Methane System*, Ind. Eng. Chem., **46**, 511-517.

[43] Vetere, A., 1983, *Vapor—Liquid Equilibrium Calculations by Means of an Equation of State*, Chem. Eng. Sci., **38**, 1281-1291.

[44] Kaminishi, G. -I., Arai, Y., Saito, S. and Maeda, S., 1968, *Vapor-Liquid Equilibria for Binary and Ternary Systems Containing Carbon Dioxide*, J. Chem. Eng. Jpn., **1**,109-116.

[45] Neumann, A. and Walch, W., 1968, *Vapour-Liquid Equilibrium Carbon Dioxide + Methane at Low Temperatures and the Region of Low Carbon Dioxide Mole Fractions*, Chem.-Ing.-Tech., **40**, 241-244.

[46] Hensel, W. E. and Massoth, F. E., 1964, *Phase Equilibria for the Ternary System Methane + Carbon Dioxide + Hydrogen Sulfide*, J. Chem. Eng. Data, **9**, 352-356.

[47] Esper, G. J., Bailey, D. M., Holste, J.C. and Hall, K. R., 1989, *Volumetric Behavior of Near-Equimolar Mixtures for Carbon Dioxide + Methane and Carbon Dioxide + Nitrogen*, Fluid Phase Equilib., **49**, 35-47.

[48] Caubet F., 1901, Li*quéfaction Des Mélanges Gazeux* (France), Université de Bordeaux.

[49] Thiel, A. and Schulte, E., 1920, *Über Binäre Gleichgewitchtssysteme Mit Festem Kohlendioxyd*, Z. Phys. Chem., **96**, 312-342.

[50] Lachet, V., de Bruin, T., Ungerer, P., Coquelet, C., Valtz, A., Hasanov, V., Lockwood, F. and Richon, D., 2009, *Thermodynamic Behavior of the $CO_2$+$SO_2$ Mixture: Experimental and Monte Carlo Simulation Studies*, Energy Procedia, **1**, 1641-1647.

[51] Spano, J. O., Heck, C. K. and Barrick, P. L., 1968, *Liquid-Vapor Equilibria of the Hydrogen + Carbon Dioxide System*, J. Chem. Eng. Data, **13**,168-171.

[52] Bezanehtak, K., Combes, G. B., Dehghani, F., Foster, N. R. and Tomasko, D. L., 2002, *Vapor-Liquid Equilibrium for Binary Systems of Carbon Dioxide + Methanol, Hydrogen + Methanol, And Hydrogen + Carbon Dioxide at High Pressures*, J. Chem. Eng. Data, **47**,161-168.

[53] Tsang, C. Y. and Streett, W. B., 1981, *Phase Equilibria in The $H_2/CO_2$ System at Temperatures from 220 to 290 K and Pressures to 172 MPa*, Chem. Eng. Sci., **36,** 993-1000.

[54] Ferrell, J. K. and Rousseau, R. W., 1980, Matange, J. N., *Solubilities of Acid Gases and Nitrogen in Methanol*, Interagency Energy/Environment R&D Report, EPA-600/7-80-116, Environmental Protection Agency.

[55] Bierlein, J. A. and Kay, W. B., 1953, *Phase Equilibrium Properties of System Carbon Dioxide-Hydrogen Sulfide*, Ind. Eng. Chem., **45**,618-624.

[56] Sobocinski, D. P. and Kurata, F., 1959, *Heterogeneous Phase Equilibria of the Hydrogen Sulfide-Carbon Dioxide System*, AIChE J., **5**, 545-551.

[57] Li, H. and Yan, J., 2006, *Impacts of Impurities in $CO_2$-Fluids on $CO_2$ Transport Process*, Proceedings of GT2006, ASME Turbo Expo 2006: Power for Land, Sea and Air, Barcelona, Spain.

[58] Wu, D. and Cheng, Y., 2011, *The Experimental Study of the Impact on Supercritical $CO_2$ from $CH_4$ Composition in Coal*, 11th underground coal operators' conference, University of Wollongong & the Australasian Institute of Mining and Metallurgy, 277-284.

[59] Mraw, S. C., Hwang, S. C and Kobayashi, R., 1978, *Vapor-Liquid Equilibrium of the Methane-Carbon Dioxide System At Low Temperatures*, J. Chem. Eng. Data, **23** 135-139.

[60] Bierlein, J. A. and Kay, W. B., 1953, *Phase-Equilibrium Properties of System Carbon Dioxide-Hydrogen Sulfide*, Industrial Engineering & Chemistry, **45**, 618-624.

[61] NagaraJan, N. and Robinson Jr, R. L., 1986, *Equilibrium Phase Compositions, Phase Densities, and Interfacial Tensions for $CO_2$ + Hydrocarbon Systems. 2.*

*$CO_2$ + N Decane*, Journal of Chemical and Engineering Data, **3**, 168-171.

[62] Shaver, R. D, Robinson Jr, R. L. and Gasem K.A.M, 2001, *An Automated Apparatus for Equilibrium Phase Compositions, Densities, and Interfacial Tensions: Data For Carbon Dioxide + Decane*, Fluid Phase Equilibria, **179**, 43-66.

[63] Valderrama, J. O. and Obaid-Ur-Rehman, S., 1988, *Generalized Interaction Parameters in Cubic Equations of State for $CO_2$-N-Alkane Mixtures*, Fluid Phase Equilibria, **40**, 217-233.

[64] Barclay, F. J., Ledwedge, T. J. and Cornfield, G. C., 1969, *Some Experiments on Sonic Velocity in Two-Phase One-Component Mixtures and Some Thoughts on the Nature of Two-Phase Critical Flow*, Proc. InSt. Mech. Eng., **184**, 185-194.

[65] Mallock, A., *The Damping of Sound by Frothy Fluids*, 1910, Proc. Roy. Soc. London, Set. A, **84**, 391-395.

[66] Karplus, H. B., *Propagation of Pressure Waves in a Mixture of Water and Steam*, 1961, Res. Develop. Rep. ARF-4132-12, 58 pp., Atomic Energy Commission, Chicago, II1.

[67] McWilliam, D. and Duggins, R.K., 1969), *Speed of Sound in Bubbly Liquids*, Proc. Inst. Mech. Eng., **184**, 102-107.

[68] Kieffer, S. W., *Sound Speed in Liquid-Gas Mixtures' Water-Air And Water-Steam*, 1977, Journal of Geophysical Research, **82** 2895-2904.

# CHAPTER 3: SPEED OF SOUND AND ISOTHERMAL COMPRESSIBILITY OF $CO_2$-RICH SYSTEMS

## 3.1 Introduction

The speed of sound in $CO_2$ and $CO_2$-rich systems is an important physical property. It is required for the design of pulsation dampeners (natural frequency of the dampener is very much dependent on gas sound velocity) and/or the calculation of the velocities in throat in supersonic nozzles [1]. The sound speed is used to locate hydrate plugs and other obstructions in gas pipelines [2], and in testing pipelines for leaks [3]. It is required for the study of vibrations in high speed, high pressure gas compressors [4]. It also can have many applications, e.g., determining some thermodynamic properties, 4-D seismic, or monitoring compositional changes. The speed of sound is an important parameter in a depressurization case, because it determines how fast the pressure drop will propagate through the pipe [5]. Speed of sound is important for modelling and it is used to predict other fluid properties such as density and heat capacity ratio. Density and other thermodynamic properties that are predicted from the speed of sound data of liquids at high pressure can be found in literatures [6-10].

In this work, speed of sound and isothermal compressibility of $CO_2$ and $CO_2$/impurities system are investigated experimentally in the liquid region from 268.15 to 301.15 K and pressure up to 45 MPa. The isothermal compressibility of $CO_2$ and impure $CO_2$ is predicted by a proposed volume shift correction based on the general Peng Robinson model.

## 3.2 Experimental Section

### *3.2.1 Experimental Apparatus*

The equipment used to measure the speed of sound was specially designed for measuring acoustic properties of high pressure fluids. It has a maximum volume of 280 ml and a length of 10.05 cm which can be adjusted by a movable piston. The system temperature is controlled by circulating coolant from a cryostat which is capable to

maintaining the cell temperature stability to within better than 0.05 K. The equilibrium cell is well isolated from the outside temperature. The system pressure is regulated by a pump connected to the non-sample side of moveable piston. The piston displacement is measured by a digital piston displacement indicator attached to appropriate end of the cell (accuracy higher than $10^{-2}$ cm). The sample is introduced into the cell directly from a sampling cylinder connected to a cell valve as shown in the schematic diagram of the ultrasonic set-up, see Figure 3.1. An ultrasonic pulser/receiver is used to transmit ultrasonic signal and receive it after passing through the fluid sample in the cell. After pre-amplification, the pulser/receiver sends the signal to a digital oscilloscope for analyses of the received signals. The total distance travelled by the ultrasound pulse was calibrated by measuring the time of flight in deionised water. The speed of sound in water was taken from [11]. The distance calibration was confirmed by testing at different temperatures (278.15 K, 288.15 K and 298.15 K).

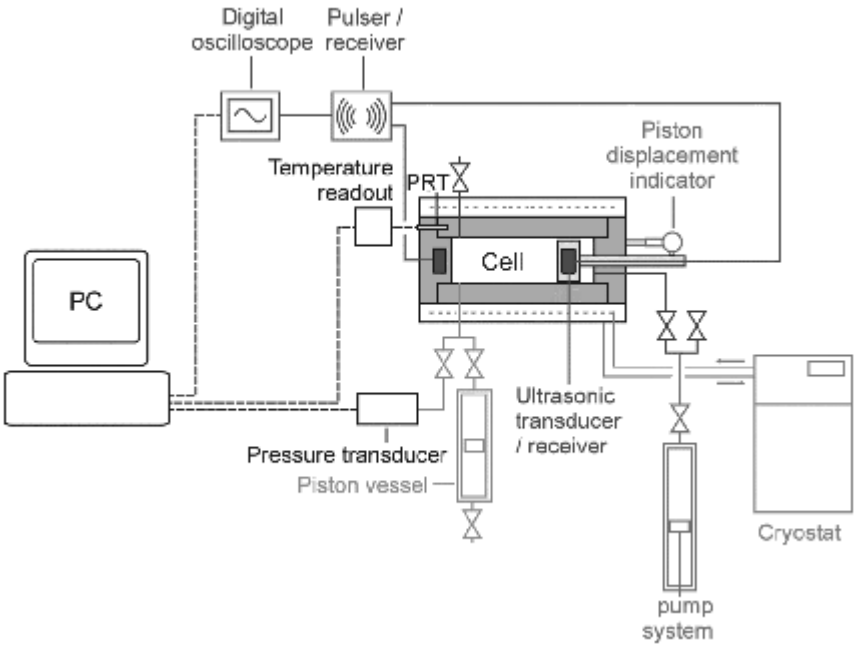


*Figure 3.1 Schematic diagram of the ultrasonic set-up*

### *3.2.2 Materials*

The following compounds were used to make the different synthetic mixtures studied in this work:

- Carbon Dioxide and methane supplied by Air Products, Research Grade

- Nitrogen, argon, oxygen, hydrogen and carbon monoxide supplied by BOC, Research Grade

Binary and multi-component mixtures of $CO_2$/impurities system are listed in Table 3.1. The mixtures were prepared gravimetrically (uncertainty ±0.3mole %)

*Table 3.1 Synthetic gas composition of $CO_2$/impurities mixtures*

| Mixture | $CO_2$ | $N_2$ | $CH_4$ | CO | $O_2$ | Ar | $H_2$ |
|---|---|---|---|---|---|---|---|
| $CO_2$+$N_2$ | Balance | 4.44 | --- | --- | --- | --- | --- |
| $CO_2$+$CH_4$ | | --- | 4.61 | --- | --- | --- | --- |
| $CO_2$+CO | | --- | --- | 4.31 | --- | --- | --- |
| $CO_2$+$O_2$ | | --- | --- | | 6.52 | --- | --- |
| $CO_2$+Ar | | --- | --- | --- | --- | 4.46 | --- |
| $CO_2$+$H_2$ | | --- | --- | --- | --- | --- | 4.53 |
| $CO_2$+Ar+CO (MIXa) | | --- | --- | 2.29 | --- | 1.16 | --- |
| $CO_2$+$CH_4$+$H_2$+$N_2$ (MIXb) | | 1.78 | 2.1 | --- | --- | --- | 0.8 |

### *3.2.3 Procedures*

The equilibrium cell and its loading lines were vacuumed prior to introducing $CO_2$ or $CO_2$ mixtures. The prepared sample was pressurised to 40 MPa in a sampling cylinder to ensure that the mixture is loaded into the cell as a single liquid phase. Then the system was pressurised by injecting hydraulic fluid into the non-sample side of the piston. The sample is given time to reach equilibrium. The equilibrium is confirmed by observing constant reading in both pressure and waveform signal. The mean wave travelling time and the corresponding displacement taken from the digital piston displacement indicator are recorded in a spreadsheet. The calibration equation obtained from the speed of sound in water is used for calculating the speed of sound in liquid $CO_2$ and $CO_2$ mixtures. The accuracy of the measurement is estimated within ±1 m/s.

## 3.3 Modelling Section

The Peng Robison-EoS is classified as a two-parameter cubic equation and has become one of the models of choice in the process modelling. The PR-EoS was chosen to model

the volumetric behaviour of $CO_2$ and $CO_2$/impurities mixtures with the quadratic van der Waals mixing rules and take the following form:

$$P = \frac{RT}{(V-b)} - \frac{a}{[V(V+b)+b(V-b)]} \tag{3.1}$$

Where,

$$a = a(T_c)\alpha(T_r,\omega) \tag{3.2}$$

$$\alpha(T_r,\omega) = [1+m(1-T_r^{0.5})]^2 \tag{3.3}$$

$$m = 0.37464 + 1.54226\omega - 0.26992\omega^2 \tag{3.4}$$

$$a(T_c) = 0.45724\frac{R^2T_c^2}{P_c} \tag{3.5}$$

$$b = 0.0778\frac{RT_c}{P_c} \tag{3.6}$$

In general an equation of state is developed first for pure compounds, and then extended to mixtures through the use of mixing rules for combining the parameters of pure compounds. For mixtures, the conventional van der Waals mixing rules were used in this work:

$$a_m = \sum_i^n \sum_j^n x_i x_j a_{ij} \tag{3.7}$$

$$b_m = \sum_i^n x_i b_i \tag{3.8}$$

$$a_{ij} = (1-k_{ij})\sqrt{a_i a_j} \tag{3.9}$$

Where, $a_i$, and, $b_i$, are calculated from Equations 3.2 and 3.6 using the critical pressure, *Pc*, critical temperature, $T_c$, and acentric factor, ω, for each component. In Equation 3.9, $k_{ij}$ is the binary interaction parameter.

The Mathias-Copeman [12] alpha function with three adjustable parameters is used to improve vapour pressure calculation of pure $CO_2$

$$if\ T < T_c \quad \alpha(T_r) = \left[1 + m_1\left(1 - \sqrt{T_r}\right) + m_2\left(1 - \sqrt{T_r}\right)^2 + m_3\left(1 - \sqrt{T_r}\right)^3\right]^2 \tag{3.10}$$

$$if\ T \geq T \quad \alpha(T_r) = \left[1 + m_1\left(1 - \sqrt{T_r}\right)\right]^2 \tag{3.11}$$

Where $m_1$, $m_2$ and $m_3$ are the three EoS-dependent adjustable parameters, the parameters where tuned for PR-EoS. Their values for carbon dioxide are 0.7138, -0.4422 and 2.4364, respectively.

Significant deviations can be observed (later in this chapter) in the prediction of liquid density compared to the experimental data. The liquid density of carbon dioxide predicted by the Peng Robinson (PR) equation of state is often off by 10% or more at temperature and pressure encountered in most of transport conditions. In this work, a volume shift is added to the PR model in order to improve liquid density of both pure and impure $CO_2$. The correction is defined as follow:

$$V_{corrected} = V_{EoS} + VC \tag{3.12}$$

where $V_{EoS}$ is the volume estimated from the PR equation of state and $VC$ is the volume-shift parameter, which in our calculation is defined as:

$$VC = s + \frac{a_c T_r}{b_c + T_r(304.2 + c_c P_r)} \tag{3.13}$$

Where $a_c$ = -0.001254, $b_c$ = -291.6, $c_c$ = -0.0655 and $s$ = -3.004

The modified volume correction is applied for $CO_2$ and $CO_2$/impurities system (The effect of adding the above correction to the other thermodynamic properties is not tested). The binary interaction parameters ($k_{ij}$) of $CO_2$ and its impurities can be found in Chapter 2. The molecular weight of the mixture is defined by:

$$M_{Mix} = M_{co_2} x_{co_2} + M_{impurity}(1 - x_{co_2}) \tag{3.14}$$

Where, $M_{co_2}$ and $M_{impurity}$ are the molecular weight of $CO_2$ and the impurity respectively. $x_{co_2}$ is the mole fraction of $CO_2$ in the mixture.

Span and Wagner [13] have the latest review of the thermodynamic properties of $CO_2$. Their work covered a wide range of pressure and temperature including the critical area based on large amount of experimental data. They generated highly accurate tables based on a complex equation of state. The tabulated data of their work is used in this work in order to compare our modified model of $CO_2$ liquid density. Figure 3.2 shows the liquid density of $CO_2$ from 228 through 301.15 K and pressure up to 50 MPa. Our modified PR-EoS model matches the results tabulated by Span and Wagner (1996) and the average deviation is less than 0.1%.

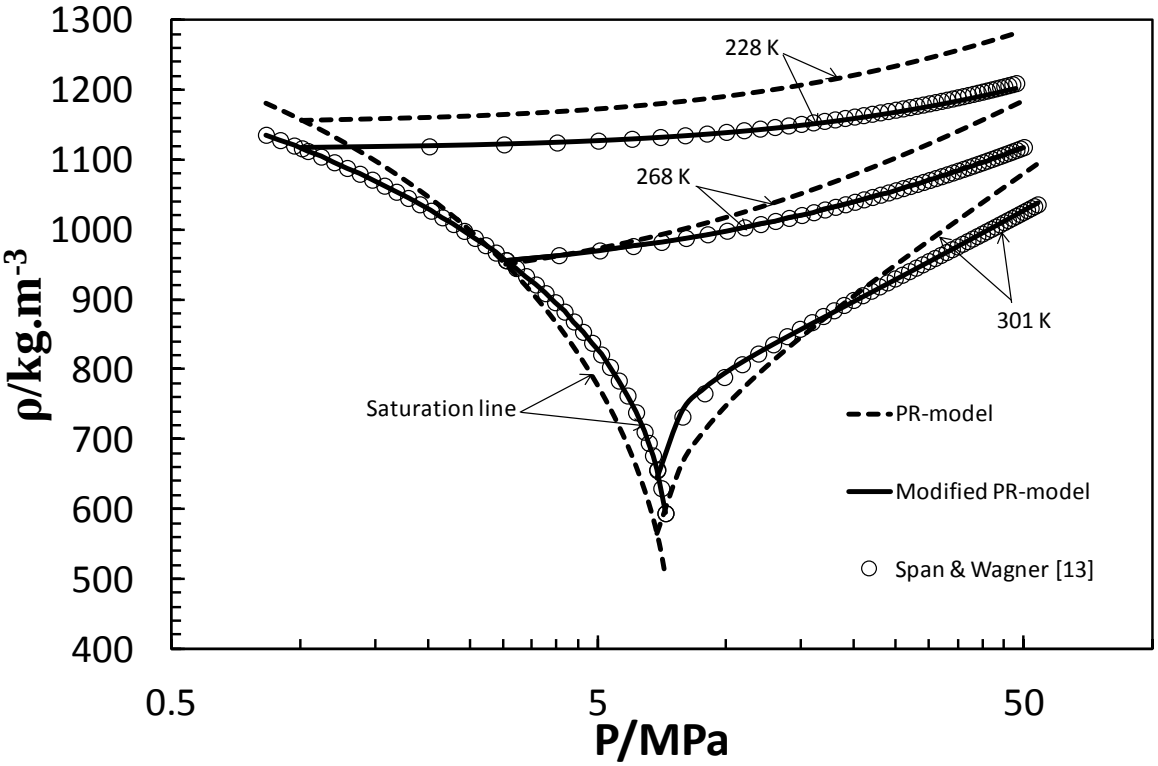


*Figure 3.2 Liquid and saturation liquid density of $CO_2$*

## 3.4 Results

### *3.4.1 Speed of Sound*

Six isothermal measurements of speed of sound were carried-out from 268.15 K to 301.15 K and pressure up to 45 MPa for pure $CO_2$ and the $CO_2$/impurities system. Speed of sound in liquid $CO_2$ as a function of pressure and temperature is shown in Figure 3.3 and listed in Table 3.2. The speed of sound of liquid $CO_2$ increases smoothly and monotonously at a constant temperature with increasing pressure, while at a similar

pressure away from the saturation pressure, it decreases slightly with increasing temperature. The reduction in the sound property becomes significant as it approaches the saturation line. The variation of the speed of sound with pressure is high compared to its temperature dependence.

*Table 3.2 Speed of sound and isothermal compressibility measurements of $CO_2$ and $CO_2$/impurities system*

| Pure $CO_2$ | | | | | | | | |
|---|---|---|---|---|---|---|---|---|
| 268.15 K | | | 278.15 K | | | 283.15 K | | |
| P /MPa | $K_T$ /MPa$^{-1}$ | SoS /m.s$^{-1}$ | P /MPa | $K_T$ /MPa$^{-1}$ | SoS /m.s$^{-1}$ | P /MPa | $K_T$ /MPa$^{-1}$ | SoS /m.s$^{-1}$ |
| 3.63 | 0.00721 | 594 | 6.89 | 0.00898 | 557 | 7.34 | 0.01100 | 519 |
| 7.37 | 0.00585 | 649 | 8.11 | 0.00817 | 577 | 8.34 | 0.01004 | 538 |
| 10.08 | 0.00509 | 682 | 10.34 | 0.00698 | 610 | 10.24 | 0.00854 | 570 |
| 14.00 | 0.00427 | 723 | 13.85 | 0.00569 | 654 | 13.41 | 0.00679 | 614 |
| 18.00 | 0.00369 | 760 | 17.40 | 0.00483 | 693 | 17.36 | 0.00545 | 661 |
| 21.93 | 0.00330 | 792 | 20.93 | 0.00421 | 726 | 20.71 | 0.00471 | 694 |
| 24.94 | 0.00306 | 814 | 24.10 | 0.00377 | 753 | 24.28 | 0.00413 | 727 |
| 28.35 | 0.00284 | 838 | 27.84 | 0.00336 | 782 | 27.25 | 0.00373 | 751 |
| 31.63 | 0.00264 | 861 | 30.82 | 0.00311 | 804 | 30.82 | 0.00337 | 779 |
| 35.36 | 0.00243 | 883 | 34.43 | 0.00290 | 829 | 34.56 | 0.00311 | 805 |
| 41.13 | 0.00216 | 916 | 37.45 | 0.00274 | 848 | 38.47 | 0.00286 | 831 |
| | | | 41.14 | 0.00240 | 870 | 41.22 | 0.00255 | 848 |
| 288.15 K | | | 293.15 K | | | 301.15 K | | |
| 6.93 | 0.01042 | 459 | 8.00 | 0.01837 | 434 | 9.43 | 0.02592 | 391 |
| 10.23 | 0.00926 | 528 | 10.41 | 0.01357 | 491 | 11.14 | 0.01952 | 438 |
| 14.35 | 0.00787 | 592 | 13.89 | 0.00941 | 551 | 14.51 | 0.01198 | 505 |
| 17.46 | 0.00690 | 630 | 16.89 | 0.00748 | 593 | 17.18 | 0.00917 | 546 |
| 20.64 | 0.00598 | 665 | 21.08 | 0.00597 | 641 | 21.74 | 0.00708 | 604 |
| 23.99 | 0.00513 | 697 | 24.08 | 0.00522 | 671 | 25.08 | 0.00606 | 640 |
| 28.23 | 0.00425 | 734 | 27.50 | 0.00450 | 703 | 27.43 | 0.00537 | 662 |
| 31.33 | 0.00376 | 757 | 31.23 | 0.00393 | 733 | 31.60 | 0.00442 | 699 |
| 34.65 | 0.00339 | 782 | 34.27 | 0.00368 | 757 | 34.63 | 0.00418 | 723 |
| 38.05 | 0.00318 | 805 | 37.96 | 0.00347 | 783 | 37.89 | 0.00406 | 748 |
| 41.64 | 0.00317 | 828 | 41.96 | 0.00250 | 809 | 41.38 | 0.00366 | 772 |
| $CO_2$+$N_2$ (4.44 % $N_2$) | | | | | | | | |
| 268.15 K | | | 278.15 K | | | 283.15 K | | |
| 9.45 | 0.00678 | 618 | 9.49 | 0.00954 | 534 | 10.51 | 0.01134 | 512 |
| 11.14 | 0.00626 | 640 | 11.08 | 0.00859 | 561 | 12.23 | 0.00977 | 542 |
| 13.10 | 0.00571 | 663 | 13.75 | 0.00722 | 600 | 14.20 | 0.00834 | 572 |
| 16.75 | 0.00481 | 702 | 16.91 | 0.00598 | 640 | 17.44 | 0.00669 | 615 |

| | | | | | | | | |
|---|---|---|---|---|---|---|---|---|
| 20.30 | 0.00413 | 735 | 20.51 | 0.00501 | 679 | 20.73 | 0.00562 | 653 |
| 24.52 | 0.00355 | 771 | 24.20 | 0.00436 | 714 | 24.31 | 0.00485 | 688 |
| 27.87 | 0.00323 | 797 | 27.51 | 0.00393 | 742 | 27.83 | 0.00428 | 720 |
| 31.39 | 0.00300 | 822 | 31.15 | 0.00352 | 771 | 31.16 | 0.00383 | 747 |
| 35.06 | 0.00276 | 847 | 34.86 | 0.00318 | 798 | 34.72 | 0.00345 | 774 |
| 38.19 | 0.00249 | 867 | 38.58 | 0.00312 | 823 | 38.30 | 0.00330 | 799 |
| 288.15 K | | | 293.15 K | | | 301.15 K | | |
| 13.29 | 0.01093 | 523 | 13.71 | 0.01282 | 495 | 15.03 | 0.01520 | 464 |
| 15.80 | 0.00875 | 562 | 15.76 | 0.01052 | 529 | 16.57 | 0.01303 | 491 |
| 18.31 | 0.00735 | 595 | 18.08 | 0.00868 | 562 | 18.62 | 0.01080 | 523 |
| 20.99 | 0.00634 | 627 | 21.17 | 0.00708 | 602 | 20.98 | 0.00896 | 555 |
| 23.92 | 0.00554 | 658 | 24.24 | 0.00605 | 635 | 24.12 | 0.00733 | 593 |
| 27.35 | 0.00480 | 691 | 27.92 | 0.00518 | 671 | 27.96 | 0.00606 | 634 |
| 30.97 | 0.00420 | 722 | 30.79 | 0.00465 | 697 | 30.95 | 0.00535 | 662 |
| 34.82 | 0.00378 | 752 | 34.00 | 0.00420 | 723 | 35.20 | 0.00456 | 698 |
| 37.51 | 0.00355 | 772 | 38.07 | 0.00383 | 749 | 38.45 | 0.00412 | 723 |
| 39.78 | 0.00323 | 787 | 41.64 | 0.00350 | 779 | 41.52 | 0.00382 | 745 |
| $CO_2$+$CH_4$ (4.61 % $CH_4$) | | | | | | | | |
| 268.15 K | | | 278.15 K | | | 283.15 K | | |
| 8.87 | 0.00681 | 614 | 7.43 | 0.01232 | 503 | 9.58 | 0.01251 | 502 |
| 11.09 | 0.00613 | 644 | 8.54 | 0.01099 | 526 | 10.99 | 0.01068 | 529 |
| 13.86 | 0.00531 | 678 | 10.54 | 0.00909 | 562 | 13.94 | 0.00837 | 576 |
| 17.20 | 0.00449 | 713 | 13.89 | 0.00702 | 610 | 16.95 | 0.00711 | 617 |
| 20.75 | 0.00388 | 746 | 17.68 | 0.00568 | 657 | 21.09 | 0.00584 | 663 |
| 24.41 | 0.00349 | 776 | 21.33 | 0.00486 | 695 | 24.71 | 0.00476 | 700 |
| 27.72 | 0.00325 | 802 | 24.43 | 0.00433 | 723 | 27.91 | 0.00402 | 728 |
| 31.29 | 0.00301 | 828 | 28.30 | 0.00380 | 756 | 31.21 | 0.00369 | 753 |
| 34.82 | 0.00273 | 852 | 31.41 | 0.00347 | 780 | 34.94 | 0.00366 | 782 |
| 38.05 | 0.00253 | 872 | 35.27 | 0.00316 | 808 | 37.37 | 0.00324 | 799 |
| | | | 38.00 | 0.00288 | 826 | | | |
| 288.15 K | | | 293.15 K | | | 301.15 K | | |
| 8.47 | 0.01957 | 429 | 9.26 | 0.02546 | 397 | 10.36 | 0.03579 | 354 |
| 10.77 | 0.01418 | 483 | 10.74 | 0.01968 | 439 | 12.27 | 0.02454 | 411 |
| 13.82 | 0.01007 | 538 | 12.96 | 0.01389 | 488 | 14.81 | 0.01571 | 467 |
| 16.95 | 0.00792 | 584 | 18.12 | 0.00837 | 570 | 17.98 | 0.01087 | 521 |
| 20.89 | 0.00639 | 632 | 20.76 | 0.00726 | 603 | 20.37 | 0.00923 | 555 |
| 24.46 | 0.00534 | 670 | 23.95 | 0.00619 | 639 | 24.26 | 0.00736 | 602 |
| 27.87 | 0.00458 | 701 | 27.74 | 0.00506 | 676 | 27.55 | 0.00595 | 637 |
| 31.22 | 0.00419 | 730 | 31.05 | 0.00451 | 705 | 30.81 | 0.00521 | 667 |
| 34.40 | 0.00399 | 755 | 34.60 | 0.00431 | 734 | 34.56 | 0.00515 | 700 |
| 37.82 | 0.00300 | 780 | 37.87 | 0.00320 | 759 | 38.22 | 0.00252 | 728 |
| $CO_2$+$H_2$ (4.53 % ) | | | | | | | | |
| 268.15 K | | | 278.15 K | | | 283.15 K | | |

| | | | | | | | | |
|---|---|---|---|---|---|---|---|---|
| 10.54 | 0.01004 | 620 | 10.77 | 0.01148 | 542 | 9.71 | 0.01851 | 492 |
| 13.02 | 0.00816 | 652 | 13.96 | 0.00850 | 592 | 12.73 | 0.01233 | 542 |
| 15.16 | 0.00687 | 677 | 17.29 | 0.00682 | 634 | 15.03 | 0.00962 | 574 |
| 17.52 | 0.00579 | 701 | 20.88 | 0.00575 | 673 | 17.58 | 0.00783 | 609 |
| 20.58 | 0.00485 | 725 | 24.48 | 0.00499 | 708 | 20.66 | 0.00656 | 646 |
| 25.39 | 0.00407 | 767 | 28.11 | 0.00437 | 739 | 24.11 | 0.00561 | 681 |
| 28.41 | 0.00376 | 790 | 31.33 | 0.00398 | 765 | 27.96 | 0.00479 | 716 |
| 31.38 | 0.00347 | 812 | 34.74 | 0.00369 | 790 | 31.35 | 0.00433 | 744 |
| 34.66 | 0.00317 | 834 | 38.33 | 0.00319 | 814 | 35.16 | 0.00401 | 773 |
| 38.07 | 0.00314 | 856 | | | | 38.27 | 0.00335 | 795 |
| 288.15 K | | | 293.15 K | | | 301.15 K | | |
| 9.78 | 0.02310 | 458 | 10.07 | 0.03112 | 418 | 13.34 | 0.02310 | 420 |
| 13.39 | 0.01339 | 521 | 13.88 | 0.01590 | 493 | 15.86 | 0.01667 | 472 |
| 17.23 | 0.00906 | 576 | 17.71 | 0.01023 | 553 | 18.21 | 0.01289 | 512 |
| 20.99 | 0.00731 | 622 | 21.28 | 0.00830 | 599 | 21.35 | 0.00997 | 556 |
| 24.55 | 0.00621 | 660 | 24.57 | 0.00708 | 635 | 24.31 | 0.00838 | 591 |
| 28.17 | 0.00527 | 694 | 28.25 | 0.00583 | 671 | 27.63 | 0.00713 | 627 |
| 31.48 | 0.00472 | 722 | 31.54 | 0.00520 | 700 | 31.02 | 0.00611 | 659 |
| 35.25 | 0.00442 | 751 | 34.96 | 0.00495 | 728 | 34.32 | 0.00539 | 688 |
| 38.38 | 0.00352 | 774 | 38.22 | 0.00336 | 752 | 37.76 | 0.00492 | 715 |
| | | | | | | 40.75 | 0.00435 | 737 |
| $CO_2$+$O_2$ (6.52 % ) | | | | | | | | |
| 268.15 K | | | 278.15 K | | | 283.15 K | | |
| 10.42 | 0.00665 | 599 | 11.46 | 0.00920 | 538 | 8.93 | 0.01809 | 444 |
| 13.18 | 0.00611 | 635 | 12.18 | 0.00883 | 550 | 11.54 | 0.01281 | 500 |
| 17.57 | 0.00502 | 686 | 14.55 | 0.00769 | 584 | 14.22 | 0.00951 | 546 |
| 21.09 | 0.00427 | 720 | 17.15 | 0.00658 | 618 | 17.26 | 0.00744 | 589 |
| 24.28 | 0.00378 | 749 | 20.36 | 0.00551 | 655 | 20.84 | 0.00613 | 632 |
| 28.27 | 0.00339 | 780 | 23.94 | 0.00470 | 691 | 24.10 | 0.00534 | 666 |
| 31.36 | 0.00316 | 803 | 28.01 | 0.00417 | 726 | 27.83 | 0.00456 | 700 |
| 34.54 | 0.00294 | 825 | 31.48 | 0.00388 | 754 | 31.16 | 0.00400 | 728 |
| 37.65 | 0.00272 | 845 | 34.82 | 0.00358 | 779 | 35.03 | 0.00361 | 758 |
| 40.84 | 0.00257 | 865 | 37.97 | 0.00318 | 801 | 38.35 | 0.00342 | 781 |
| | | | 40.52 | 0.00273 | 817 | 41.00 | 0.00303 | 799 |
| 288.15 K | | | 293.15 K | | | 301.15 K | | |
| 10.64 | 0.01809 | 438 | 12.92 | 0.01587 | 454 | 12.80 | 0.02219 | 391 |
| 13.87 | 0.01206 | 505 | 14.73 | 0.01301 | 489 | 13.98 | 0.01969 | 419 |
| 17.06 | 0.00885 | 555 | 17.26 | 0.01020 | 530 | 17.63 | 0.01354 | 488 |
| 20.79 | 0.00694 | 603 | 21.84 | 0.00734 | 590 | 21.39 | 0.00961 | 543 |
| 24.01 | 0.00596 | 638 | 24.28 | 0.00644 | 618 | 24.12 | 0.00793 | 577 |
| 28.33 | 0.00495 | 680 | 27.68 | 0.00552 | 652 | 27.35 | 0.00674 | 612 |
| 31.21 | 0.00441 | 705 | 31.09 | 0.00483 | 683 | 31.15 | 0.00580 | 648 |
| 34.67 | 0.00399 | 732 | 34.54 | 0.00432 | 712 | 34.59 | 0.00503 | 678 |

| | | | | | | | | |
|---|---|---|---|---|---|---|---|---|
| 38.15 | 0.00371 | 758 | 38.16 | 0.00389 | 739 | 37.91 | 0.00442 | 705 |
| 40.78 | 0.00326 | 777 | 40.82 | 0.00344 | 758 | 40.83 | 0.00444 | 727 |

$CO_2$+Ar (4.46 % )

| 268.15 K | | | 278.15 K | | | 283.15 K | | |
|---|---|---|---|---|---|---|---|---|
| 9.31 | 0.00636 | 607 | 10.26 | 0.00816 | 547 | 11.66 | 0.01064 | 531 |
| 11.15 | 0.00596 | 635 | 12.49 | 0.00745 | 581 | 14.38 | 0.00814 | 573 |
| 13.69 | 0.00536 | 665 | 16.35 | 0.00632 | 632 | 17.51 | 0.00661 | 613 |
| 17.15 | 0.00460 | 703 | 18.35 | 0.00579 | 654 | 20.95 | 0.00563 | 652 |
| 20.73 | 0.00400 | 736 | 21.70 | 0.00498 | 688 | 24.29 | 0.00491 | 685 |
| 23.86 | 0.00362 | 763 | 24.66 | 0.00438 | 715 | 28.01 | 0.00423 | 717 |
| 28.01 | 0.00325 | 795 | 28.23 | 0.00380 | 745 | 31.44 | 0.00381 | 745 |
| 31.57 | 0.00296 | 820 | 31.33 | 0.00344 | 769 | 34.86 | 0.00355 | 771 |
| 35.01 | 0.00272 | 843 | 35.31 | 0.00318 | 798 | 38.32 | 0.00295 | 795 |
| 38.32 | 0.00269 | 863 | 38.58 | 0.00315 | 819 | | | |
| 288.15 K | | | 293.15 K | | | 301.15 K | | |
| 12.38 | 0.01512 | 505 | 10.60 | 0.01778 | 421 | 11.75 | 0.02614 | 382 |
| 15.02 | 0.01205 | 548 | 15.04 | 0.01249 | 512 | 14.64 | 0.01756 | 451 |
| 16.80 | 0.01025 | 577 | 18.20 | 0.00925 | 559 | 17.06 | 0.01328 | 494 |
| 19.94 | 0.00767 | 612 | 21.15 | 0.00720 | 597 | 19.66 | 0.01045 | 534 |
| 22.39 | 0.00621 | 639 | 24.59 | 0.00592 | 634 | 22.11 | 0.00868 | 565 |
| 25.11 | 0.00510 | 667 | 28.08 | 0.00533 | 668 | 24.79 | 0.00725 | 596 |
| 28.13 | 0.00442 | 694 | 31.21 | 0.00492 | 695 | 28.08 | 0.00598 | 630 |
| 31.18 | 0.00413 | 720 | 34.56 | 0.00443 | 722 | 31.12 | 0.00531 | 658 |
| 34.91 | 0.00399 | 749 | 37.85 | 0.00440 | 747 | 34.82 | 0.00494 | 689 |
| 38.25 | 0.00364 | 773 | | | | 38.44 | 0.00349 | 718 |
| 41.75 | 0.00253 | 796 | | | | | | |

$CO_2$+CO (4.31 % )

| 268.15 K | | | 278.15 K | | | 283.15 K | | |
|---|---|---|---|---|---|---|---|---|
| 11.53 | 0.00641 | 622 | 11.98 | 0.00905 | 553 | 9.86 | 0.01469 | 475 |
| 14.38 | 0.00562 | 658 | 14.87 | 0.00754 | 597 | 14.47 | 0.00914 | 557 |
| 18.28 | 0.00481 | 700 | 17.75 | 0.00626 | 632 | 17.15 | 0.00745 | 595 |
| 20.27 | 0.00447 | 718 | 20.79 | 0.00531 | 666 | 20.91 | 0.00604 | 640 |
| 24.03 | 0.00389 | 752 | 24.04 | 0.00474 | 699 | 24.12 | 0.00524 | 673 |
| 27.65 | 0.00343 | 781 | 27.81 | 0.00437 | 731 | 27.90 | 0.00452 | 708 |
| 31.19 | 0.00311 | 808 | 30.72 | 0.00406 | 755 | 31.18 | 0.00404 | 735 |
| 34.59 | 0.00292 | 831 | 34.75 | 0.00342 | 785 | 34.73 | 0.00369 | 762 |
| 37.92 | 0.00274 | 852 | 38.18 | 0.00294 | 809 | 37.96 | 0.00342 | 786 |
| 40.77 | 0.00243 | 870 | 41.11 | 0.00323 | 829 | 40.91 | 0.00294 | 806 |
| 288.15 K | | | 293.15 K | | | 301.15 K | | |
| 10.31 | 0.01809 | 439 | 9.71 | 0.02832 | 376 | 10.37 | 0.04742 | 315 |
| 13.99 | 0.01159 | 515 | 13.52 | 0.01558 | 471 | 12.49 | 0.03008 | 386 |
| 16.89 | 0.00883 | 560 | 16.84 | 0.01039 | 529 | 15.08 | 0.01768 | 446 |
| 20.38 | 0.00700 | 605 | 20.50 | 0.00790 | 581 | 17.44 | 0.01245 | 489 |

| | | | | | | | | |
|---|---|---|---|---|---|---|---|---|
| 24.10 | 0.00583 | 646 | 23.99 | 0.00664 | 620 | 20.80 | 0.00979 | 539 |
| 27.93 | 0.00494 | 683 | 27.91 | 0.00548 | 660 | 24.08 | 0.00847 | 582 |
| 31.46 | 0.00431 | 714 | 31.21 | 0.00470 | 691 | 27.55 | 0.00668 | 618 |
| 34.94 | 0.00393 | 741 | 34.95 | 0.00426 | 722 | 31.21 | 0.00507 | 654 |
| 38.27 | 0.00364 | 766 | 37.99 | 0.00403 | 744 | 34.72 | 0.00495 | 684 |
| 40.93 | 0.00310 | 784 | 40.74 | 0.00314 | 764 | 38.20 | 0.00511 | 717 |
| | | | | | | 40.98 | 0.00154 | 733 |

$CO_2$+$CH_4$+$N_2$+$H_2$, MIXb,(2.10% $CH_4$ ,1.78 % $N_2$, 0.8 % $H_2$)

| 268.15 K | | | 278.15 K | | | 283.15 K | | |
|---|---|---|---|---|---|---|---|---|
| 7.57 | 0.01055 | 564 | 8.10 | 0.01411 | 488 | 7.54 | 0.02091 | 415 |
| 10.39 | 0.00718 | 609 | 10.67 | 0.01030 | 535 | 10.53 | 0.01335 | 491 |
| 14.02 | 0.00529 | 656 | 13.78 | 0.00771 | 585 | 13.89 | 0.00901 | 551 |
| 17.15 | 0.00465 | 691 | 17.02 | 0.00626 | 627 | 17.54 | 0.00691 | 602 |
| 20.96 | 0.00415 | 728 | 20.71 | 0.00523 | 668 | 21.24 | 0.00578 | 645 |
| 24.00 | 0.00373 | 754 | 24.24 | 0.00448 | 702 | 24.57 | 0.00496 | 679 |
| 28.13 | 0.00319 | 787 | 27.85 | 0.00394 | 734 | 27.97 | 0.00425 | 710 |
| 31.26 | 0.00297 | 810 | 31.48 | 0.00370 | 763 | 31.41 | 0.00383 | 739 |
| 35.25 | 0.00286 | 837 | 34.63 | 0.00355 | 786 | 34.99 | 0.00361 | 766 |
| 38.36 | 0.00238 | 857 | 38.26 | 0.00254 | 812 | 38.47 | 0.00276 | 791 |
| 288.15 K | | | 293.15 K | | | 301.15 K | | |
| 7.89 | 0.03562 | 374 | 8.55 | 0.03868 | 330 | 10.76 | 0.03822 | 342 |
| 10.38 | 0.02028 | 446 | 11.40 | 0.02119 | 427 | 14.11 | 0.02045 | 429 |
| 13.62 | 0.01091 | 512 | 14.09 | 0.01303 | 485 | 17.15 | 0.01281 | 487 |
| 17.15 | 0.00796 | 567 | 17.17 | 0.00939 | 536 | 20.67 | 0.00933 | 540 |
| 20.88 | 0.00697 | 614 | 21.64 | 0.00747 | 595 | 24.15 | 0.00775 | 583 |
| 24.30 | 0.00576 | 651 | 24.29 | 0.00639 | 625 | 27.57 | 0.00638 | 620 |
| 28.12 | 0.00438 | 688 | 27.70 | 0.00507 | 659 | 31.44 | 0.00513 | 657 |
| 31.41 | 0.00409 | 716 | 31.23 | 0.00455 | 691 | 34.89 | 0.00478 | 687 |
| 35.05 | 0.00442 | 745 | 34.73 | 0.00463 | 720 | 38.18 | 0.00453 | 713 |
| 38.70 | 0.00130 | 771 | 38.15 | 0.00179 | 746 | 40.55 | 0.00288 | 731 |

$CO_2$+Ar+CO, MIXa, (1.16% Ar,2.29% CO)

| 268.15 K | | | 278.15 K | | | 283.15 K | | |
|---|---|---|---|---|---|---|---|---|
| 13.19 | 0.00566 | 650 | 12.88 | 0.00827 | 580 | 11.33 | 0.01060 | 517 |
| 16.60 | 0.00469 | 690 | 16.31 | 0.00655 | 625 | 14.14 | 0.00845 | 563 |
| 20.24 | 0.00406 | 727 | 18.84 | 0.00567 | 654 | 17.34 | 0.00679 | 606 |
| 23.95 | 0.00359 | 759 | 21.68 | 0.00497 | 683 | 20.57 | 0.00567 | 643 |
| 27.92 | 0.00319 | 790 | 24.80 | 0.00440 | 712 | 24.11 | 0.00485 | 679 |
| 31.43 | 0.00292 | 815 | 28.19 | 0.00392 | 741 | 27.86 | 0.00428 | 713 |
| 34.99 | 0.00273 | 839 | 31.32 | 0.00352 | 765 | 31.37 | 0.00392 | 742 |
| 38.55 | 0.00254 | 861 | 34.66 | 0.00315 | 790 | 34.56 | 0.00366 | 766 |
| 40.99 | 0.00225 | 876 | 38.43 | 0.00292 | 816 | 38.25 | 0.00323 | 793 |
| | | | 40.80 | 0.00301 | 831 | 41.06 | 0.00255 | 811 |
| 288.15 K | | | 293.15 K | | | 301.15 K | | |

| | | | | | | | | |
|---|---|---|---|---|---|---|---|---|
| 10.25 | 0.01617 | 453 | 10.35 | 0.02073 | 410 | 14.28 | 0.01800 | 440 |
| 13.65 | 0.01084 | 520 | 13.95 | 0.01307 | 490 | 17.13 | 0.01255 | 493 |
| 17.36 | 0.00784 | 576 | 17.43 | 0.00917 | 546 | 20.70 | 0.00909 | 545 |
| 20.90 | 0.00635 | 619 | 20.95 | 0.00716 | 592 | 24.73 | 0.00715 | 594 |
| 24.71 | 0.00533 | 659 | 24.62 | 0.00595 | 634 | 28.39 | 0.00594 | 632 |
| 28.16 | 0.00461 | 691 | 28.02 | 0.00513 | 666 | 31.52 | 0.00512 | 662 |
| 31.48 | 0.00408 | 719 | 31.53 | 0.00445 | 697 | 34.97 | 0.00458 | 691 |
| 35.18 | 0.00371 | 748 | 34.98 | 0.00399 | 725 | 38.27 | 0.00426 | 717 |
| 38.44 | 0.00342 | 772 | 38.29 | 0.00369 | 750 | 41.22 | 0.00341 | 738 |
| 40.96 | 0.00289 | 789 | 40.97 | 0.00327 | 768 | | | |

In order to observe the effect of impurities, the speed of sound of six binary $CO_2$ mixtures and two multi-components $CO_2$/mixtures (Table 3.1) were measured in the same range of pressure and temperature. Figure 3.4 and Figure 3.5 show the experimental results of speed of sound property on both pure and impure $CO_2$ at 268.15 and 301.15 K respectively.

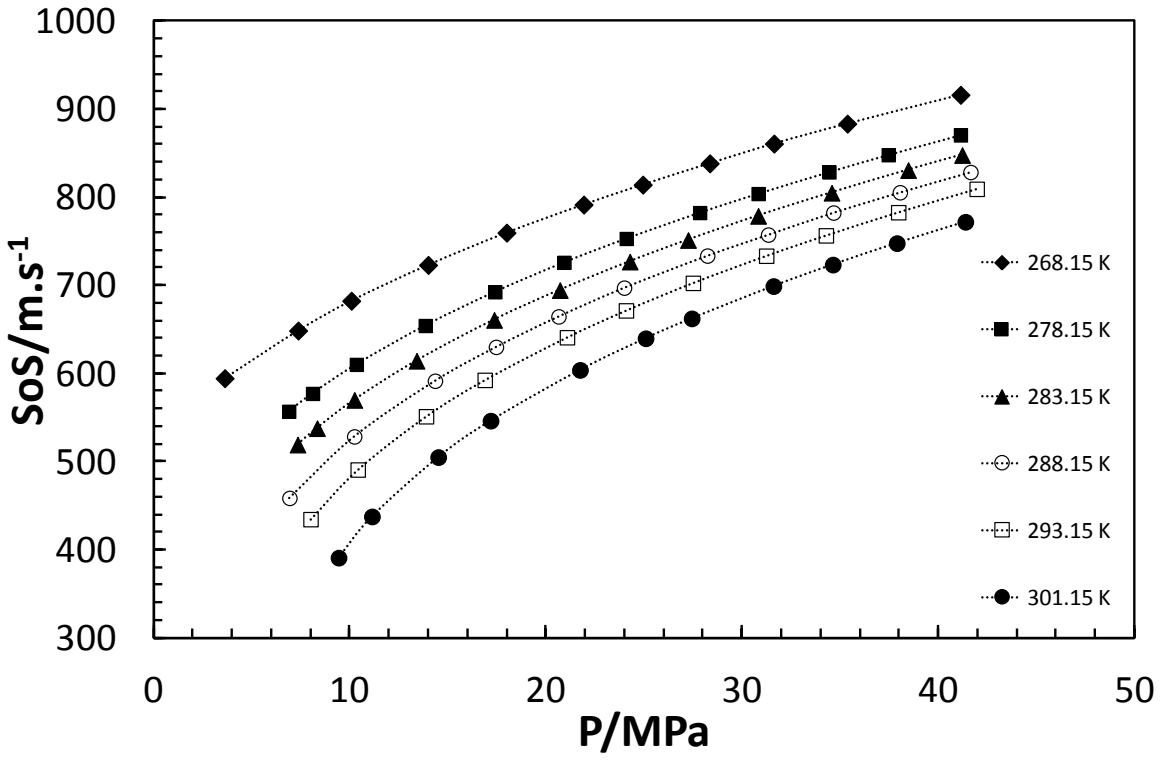


*Figure 3.3 Measurements in speed of sound of $CO_2$*

It can be seen that non-condensable impurities such as $O_2$, Ar, $N_2$, CO significantly reduce the speed of sound of $CO_2$ stream. The change is much higher as the temperature increases and it becomes more significant around the critical point of the mixture. The

binary $CO_2/O_2$ mixture (6.52% $O_2$) which contains the highest impurity concentration compared to the other investigated system has major effect on the property.

In order to analyse the effect of each impurity at different pressure and temperature conditions, the change in speed of sound (defined as $SoS_{pure CO_2} - SoS_{impure CO_2}$) is plotted at three different temperatures (268.15 , 278.15 and 293.15 K). Two $CO_2$/impurity systems were selected $CO_2/CH_4$ and MIXb $CO_2$+ ($CH_4$+$H_2$+$N_2$). Their effect on the $CO_2$ speed of sound is plotted in Figure 3.6 and Figure 3.7 respectively. The mole fraction of $CO_2$ in both systems is around 94.4%. The lines are plotted based on the experimental data (shown in Table 3.2) using cubic spline interpolation. The change is larger at pressures near the saturation line of the mixture and it becomes less significant as pressure increases. The change in speed of sound is strongly dependant on the pressure and the number of impurities present in $CO_2$ stream. In term of temperature dependency, the change is larger at higher temperatures near the saturation line. As the pressure increases the change reduces to a point where all the isothermal lines intersect. Beyond that point, the change in speed of sound becomes higher at low temperature and less significant at high temperature. This finding was observed in all the other tested $CO_2$ impurities systems. Speed of sound is a function of three properties: isothermal compressibility ($K_T$), density (ρ) and heat capacity (γ). The change of both density (see Chapter 4) and isothermal compressibility (see 3.4.2 in this chapter) of $CO_2$ in the presence of impurities is found to be consistent as pressure and temperature change. Therefore, more investigation is required to define the effect of heat capacity ratio on impure $CO_2$ stream and perhaps it can explain the above mentioned behaviour on speed of sound.

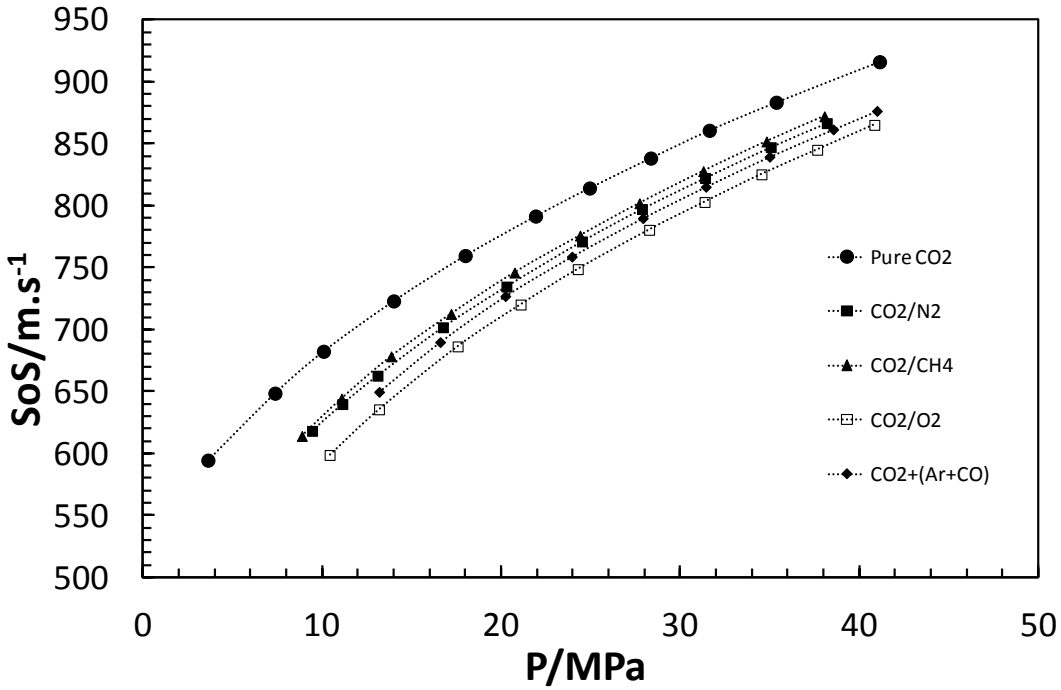


*Figure 3.4 Effect of $CO_2$ impurities on speed of sound property at 268.15 K*

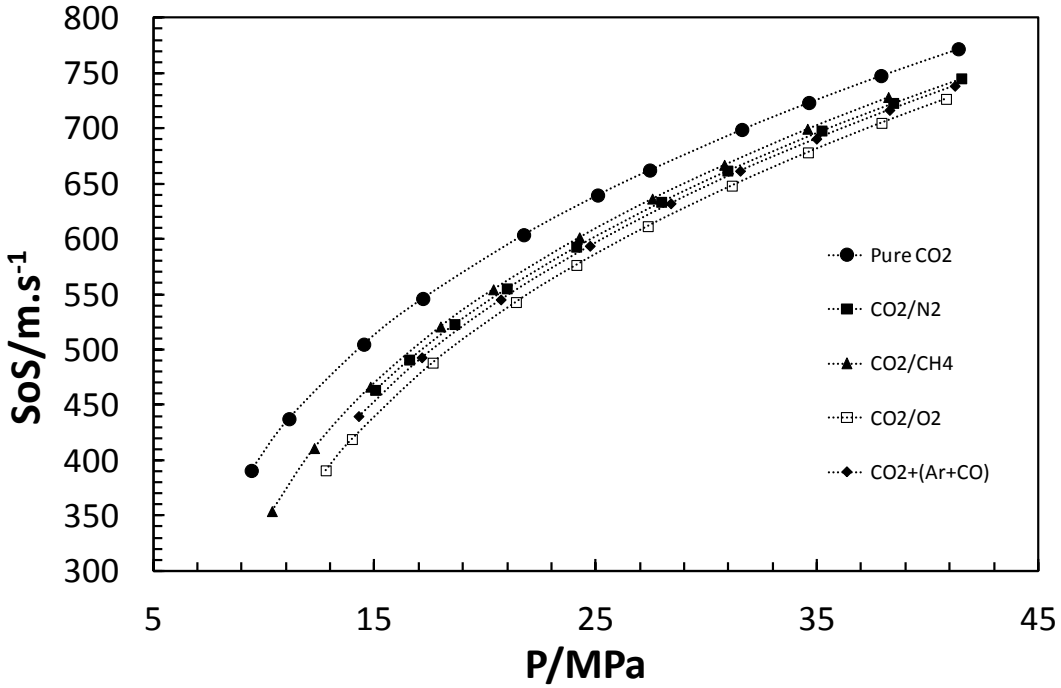


*Figure 3.5 Effect of $CO_2$ impurities on speed of sound property at 301.15 K*

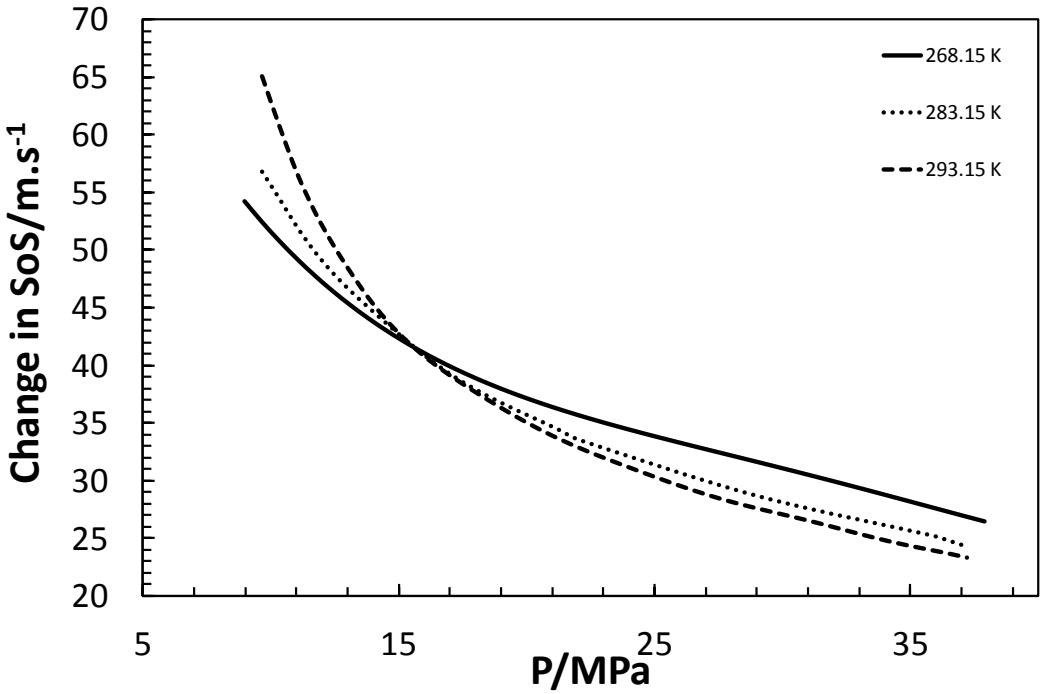


*Figure 3.6 Change in speed of sound (defined as $SoS_{pure CO_2} - SoS_{impure CO_2}$) as a function of pressure in $CO_2/CH_4$ mixture*

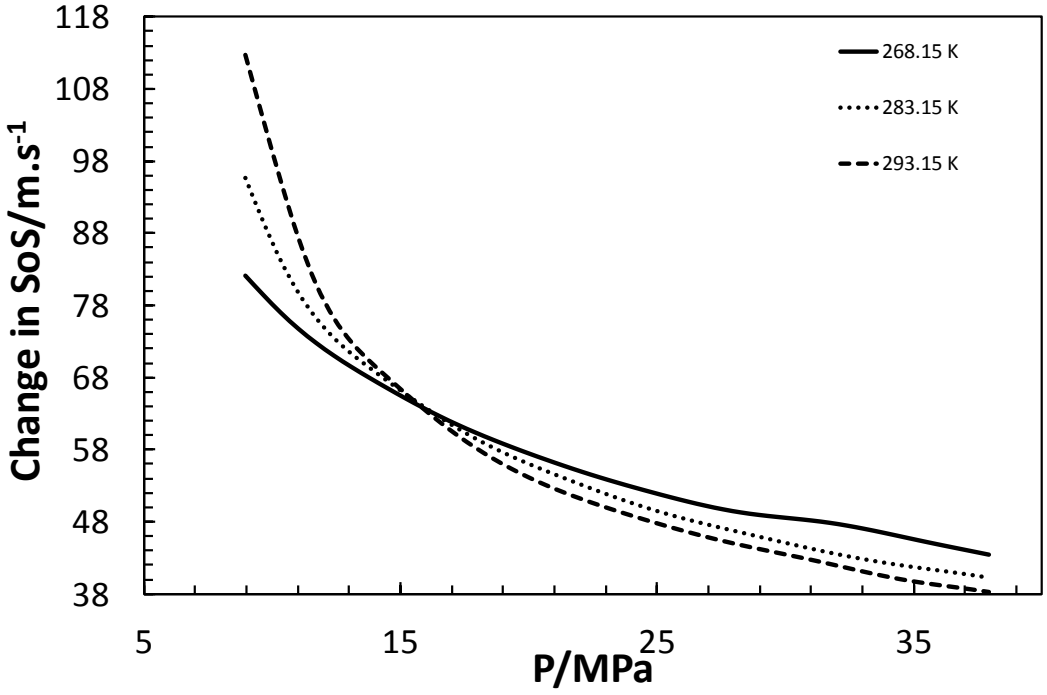


*Figure 3.7 Change in speed of sound (defined as $SoS_{pure CO_2} - SoS_{impure CO_2}$) as a function of pressure in MIXb ($CO_2$-$CH_4$-$H_2$-$N_2$)*

### *3.4.2 Isothermal Compressibility*

The isothermal compressibility coefficients are required in several reservoir engineering applications such as transient fluid flow problems and also in the determination of physical properties of crude oils. The isothermal compressibility coefficient ($K_T$) is defined as the rate of change in volume with pressure per unit volume of fluid at constant temperature. It is also defined as the quantitative expression of the sensitivity of density to pressure so it can be written in either of the following forms:

$$K_T = -\frac{1}{v}\left(\frac{\partial v}{\partial p}\right)_T \qquad or \qquad K_T = \rho\left(\frac{\partial \rho}{\partial p}\right)_T \tag{3.15}$$

Where $v$ is molar volume, $p$ is the pressure and $\rho$ is the density

In our study, the effect of the impurities on the isothermal compressibility of $CO_2$ and $CO_2$/impurities are experimentally estimated by calculating the effects on the derivative of the displacement with respect to the pressure (Under the assumption that the effective cross-section area is constant in all the tests).

$$K_T = -\frac{1}{z}\left(\frac{\partial z}{\partial p}\right) \tag{3.16}$$

where $z$ is the piston displacement

To calculate the isothermal compressibility ($K_T$), a cubic-spline method was used to smooth the measured displacement data, and $K_T$ was obtained by differentiate the displacement $z$ data with respect to pressure. It was estimated that the uncertainty of the $K_T$ data was better than 2% (The value is obtained by calculating the error of experimental data to the data obtained from spline interpolation). The isothermal compressibility results of pure and impure $CO_2$ systems are listed in Table 3.2. Figure 3.8 shows the isothermal compressibility of pure $CO_2$ at 268.15, 278.15 and 293.15 K. As can be seen from the figure, $K_T$ is sensitive to the pressure as the pressure approaches the critical point of $CO_2$. On the other hand, $K_T$ is non-sensitive to the pressure when the pressure is far enough from the saturation line. The figure also illustrates that $K_T$ is temperature dependent; its changes are limited as the temperature moves down away from the critical temperature of $CO_2$ even near the saturation line.

The proposed model in this work is tested to predict the measured isothermal compressibility of pure $CO_2$. The model predictions are in a good agreement with our experimental data and the average deviation was less than 3% which is comparable to the uncertainty estimated in the experimental measurements. The model was also used to predict the isothermal compressibility of $CO_2$/impurities systems. An example is given in Figure 3.9. This figure shows the isothermal compressibility of MIXa ($CO_2$+Ar+CO) at different temperatures. The results demonstrate the capability of the model to predict the compressibility of $CO_2$ mixtures. The calculated average deviation in these mixtures was reported less than 4%. The PR-model with the proposed shifting volume was not tested for higher impurity concentration in $CO_2$ mixture.

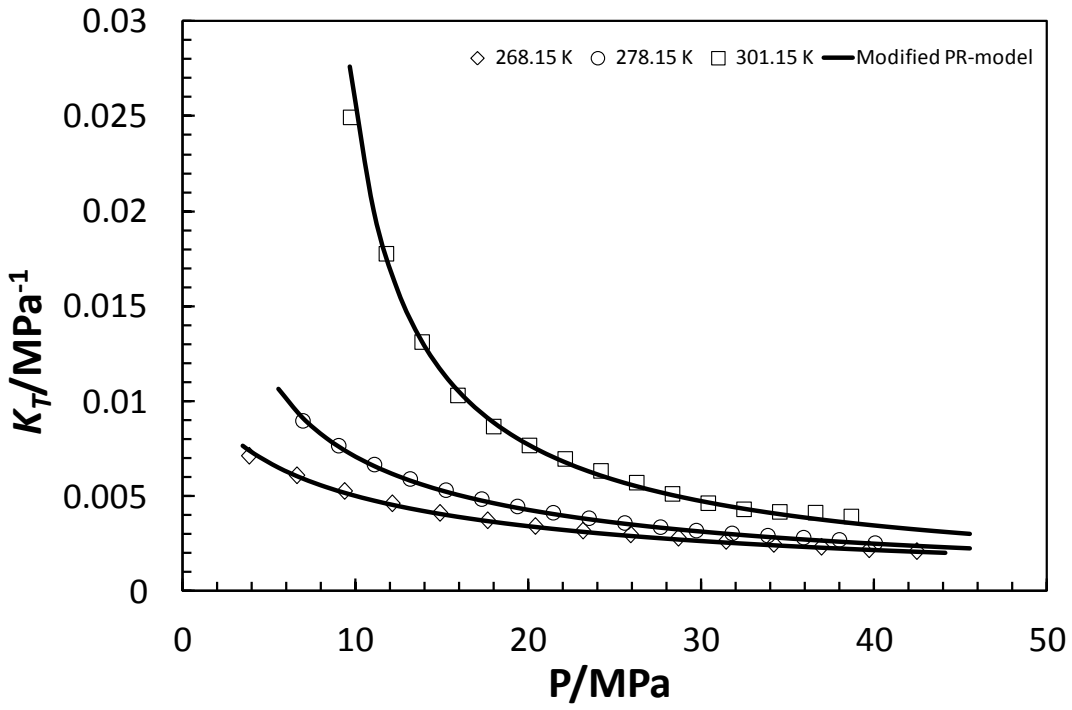


*Figure 3.8 Isothermal compressibility in pure $CO_2$ (measurements & modelling)*

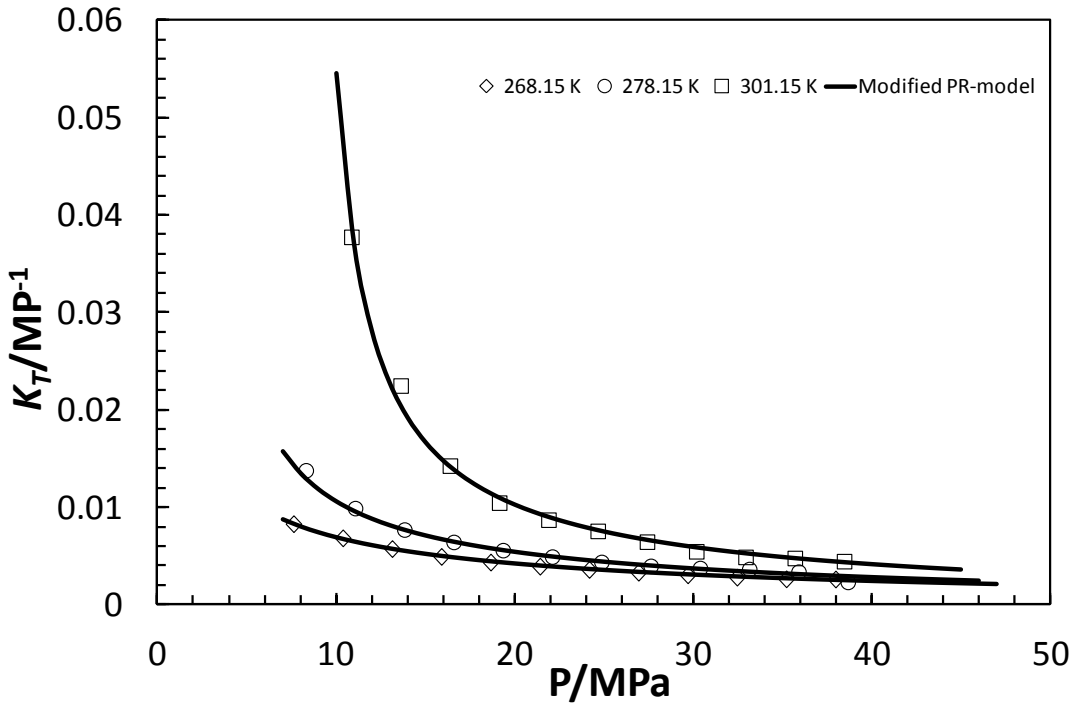


*Figure 3.9 Isothermal compressibility in MIXb ($CO_2$+Ar+CO) (measurements & modelling)*

Figure 3.10 and Figure 3.11 show the effect of three impurities systems at two different temperatures (268.15 and 301.15 K). In these systems, it is obvious that the presence of the impurities in $CO_2$ tends to increase the compressibility. The effect is higher at higher temperature and it is very significant as the pressure approaches the saturation line of the mixtures. This variation of $K_T$ with pressure and temperature of the mixtures are similar for all the investigated systems. In general, the effect in the compressibility also depends mainly on two factors: the concentration of the impurity in $CO_2$ mixture and the type of impurities present in the mixture.

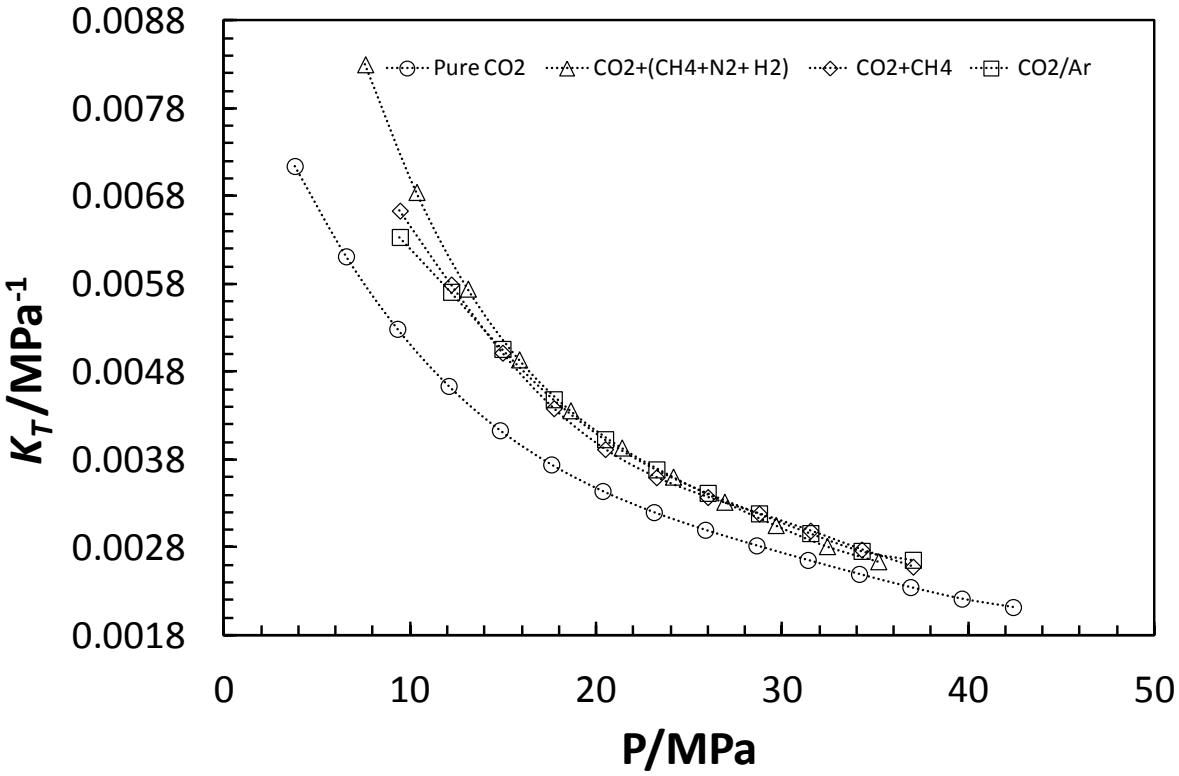


*Figure 3.10 Effect of three selected impurities systems on $CO_2$ stream at 268.15 K*

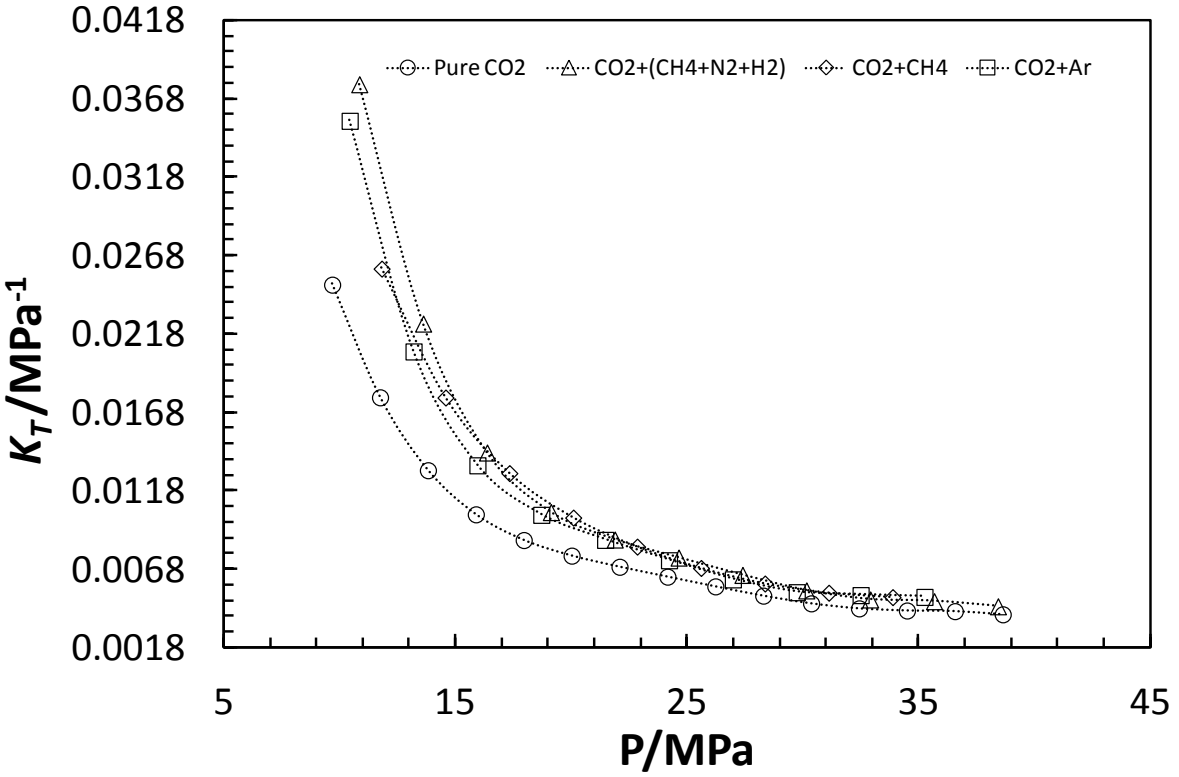


*Figure 3.11 Effect of three selected impurities systems on $CO_2$ stream at 301.15 K*

### 3.5 Conclusions

The presence of impurities tested in this work in $CO_2$ stream tends to reduce the speed of sound. The reduction depends more on pressure than temperature. The plot of ( $SoS_{pure CO_2} - SoS_{impure CO_2}$ ) versus pressure at different temperatures shows that this change is high at high temperature for a pressure near the saturation line. As the pressure increases, the isothermal lines of the change will intersect at a pressure $\approx$ 15 MPa. This finding was observed in all the investigated mixtures. Below that pressure, the change is higher at lower temperatures. Conversely, above that pressure the change is higher at higher temperatures. In the other hand, the presence of impurities increases the isothermal compressibility of $CO_2$ stream. The effect is much higher as the pressure approaches the critical temperature of the mixture.

**References**

[1] Sherwood, T. K., 1962, *Velocity of Sound in Compressed Gases*, J. Chem. Eng., Data, **7**, 47-50.

[2] Wallace, B.W. and Robert, C.A., 1978, *Prediction of Acoustic Velocities in Nonideal Gaseous Mixtures*, AIChE Journal, **24**, 341-343.

[3] Hough, J. E., 1988, *Leak Testing of Pipelines Uses Pressure and Acoustic Velocity*, Oil and Gas Journal86, **47**, 35-41.

[4] Dunskus, T., 1969, *Graphs Give Velocity of Sound in Ethylene*, Chem. Eng., 110-112.

[5] Halvor, L., Tore, F. and Svend, T.M., *Depressurization of Carbon Dioxide in Pipelines -Models and Methods*, SINTEF Energy Research, NO-7465 Trondheim, Norway.

[6] Petitet, J. P., Tufeu, R. and Neindre, B.,1983, *High-Pressure Vapour-Liquid Equilibrium in the Carbon Dioxide - A-Pinene System*, Int. J. Thermophys., **4**, 35-37.

[7] Fine, R. and Millero, F. J., 1973, *Compressibility of Water as a Function of Temperature and Pressure*, journal of chemical physics, **59**, 5529-5536.

[8] Kell, G. S. and Whalley, E., 1975, *Reanalysis of the Density of Liquid Water in the Range of 0-150 °C and 0 to 1 kbar*, J. Chem. Phys., **62**, 3496-3503.

[9] Chen, C. T., Fine, R. and Millero, F. J., 1977, *The Equation of State of Pure Water Determined from Sound Speeds*, J. Chem. Phys., **66**, 2142-2144.

[10] Chen, C. T. and Millero, F. J., 1976, *Sound-Speed Measurements for Pure Water*, J. Acoustic. Soc. Am., **60**, 1270-1273.

[11] Greenspan, M. and Tschiegg, C. E., 1959, *Tables of the Speed of Sound in Water*, J. Acoustic. Am., **31**, 75–76.

[12] Mathias, P. M. and Copeman, T. W., 1983, *Extension of the Peng-Robinson Equation Of State to Complex Mixtures: Evaluation of The Various Forms of the Local Composition Concept*, Fluid Phase Equilib., **13**, 91-108.

[13] Span, R. and Wagner, W., 1996, *A New Equation of State for Carbon Dioxide Covering the Fluid Region from the Triple Point Temperature to 1100 K at Pressures up to 800 MPa*, JPCRD, **25**, 1509-1596.

# CHAPTER 4: **DENSITY OF CARBON DIOXIDE RICH SYSTEMS**

## 4.1 Introduction

The density is important when calculating the flow in the pipeline. Knowledge of the inlet temperature, ambient temperature and heat transfer is needed to achieve a correct model of the flow. Maintaining a single phase and avoiding the abrupt pressure drops in $CO_2$ pipelines are an important issue for engineers where pipelines required boosting stations. The density also (as we can see later in the chapter) is very sensitive near the critical points, .i.e. a small change in both pressure or temperature results in a very large change in the density of $CO_2$ [1]. Properties of $CO_2$ stream are the temperature, pressure and density profile along the pipelines therefore, the effect of these parameters translates into recompression distances and compressor power requirements, which in turn would have cost implications [2].

PVTxy for $CO_2$/impurities system cited in the literature were collected recently by Li et al. [3]. Their conclusion was that the data for $CO_2$ in the presence of $H_2O$, $CH_4$, $N_2$ and $H_2S$ are available in a wide range of pressure and temperature. However, the other impurities associated with the pipelines transport are still limited. Beside the bibliographic references provided by Li et al. [3], Jiang et al. [4], provided volumetric properties for $CO_2/N_2$ binary system at 293 K and pressure from 0.60 to 5.18 MPa. Esper et al. [5] measured the density of the binary $CO_2/CH_4$ system at composition 0.48 $CO_2$, pressure from 0.08 to 48.3 MPa and temperature range 206 to 320 K. Seitz and Blencoe [6] extended their previous experimental work with the binary $CO_2/CH_4$ system [7] by covering temperature and pressure up to 673 K and 100 MPa respectively. Hwang et al. [8] reported experimental density measurements for $CO_2$ + $CH_4$ mixtures at temperatures from 225 K to 350 K and pressures up to 35 MPa (one isotherm up to 69 MPa). Additional PVT data for the binary mixture have been reported by Netherlandse Gasunie, and Ruhrgas as cited by Jaeschke and Humphreys [9]. Three references were found for the densities of the ternary $CO_2/N_2/CH_4$ system ([10], [11] and [7]). Bezanehtak et al. [12] contacted VLE and liquid density measurements for $CO_2/H_2$ binary system at temperatures from 278.15 K to 308.15 K and for pressures in the range 1.5 to 19.3 MPa. The authors compared their VLE results with those obtained

by Tsang and Streett [13], and the deviations for liquid and vapour phases were as high as 7.1% and 9.4%, respectively. Three PVT measurements in $CO_2$/Ar binary mixture were reported until 1977. Two isothermal data found in literature, at vapour and liquid regions, were measured by Altunin et al. [14] and Sarashina et al. [15] respectively. Kestin et al. [16] (cited from [3].) investigated the volumetric property for the binary mixture ranging from 293.15-303.15 K and pressure up to 2.58 MPa. A single PVT data was reported in the literature [17] for $CO_2$/CO mixture at a constant composition (0.5732 $CO_2$ mole%). The measurements were made in the temperature range 323 to 423 K and pressures up to 6.5 MPa. Recently, new supercritical volumetric measurements on three binary mixtures ($CO_2$/$N_2$, $CO_2$/$O_2$ and $CO_2$/Ar) were measured by Mantovani et al. [18]. Two different fractions in impurity mixture were prepared for each binary system ranging from 4.15 mole% to 16.94 mole%. The measurements were performed isothermally crossing vapour/supercritical boundary region, temperature range from 303 K to 383 K and in a pressure range from 1 MPa to 20 MPa.

The aim of this work is to investigate the effects of impurities on the $CO_2$ transport density. Six types of binary $CO_2$ rich systems were prepared plus a multi-components $CO_2$-rich mixture. The liquid $CO_2$ density measurements were carried-out from 283.15 K to 301.15 K and at a pressure up to 50 MPa. In addition, the densities of four binary mixtures of $CO_2$/Ar, $CO_2$/CO, $CO_2$/$H_2$ and $CO_2$/$O_2$, at constant fraction of impurities, were measured in the supercritical region. The measurements were carried-out isothermally at three temperatures, 323.15 K, 373.15 K and 423.15 K and at pressure up to 50 MPa.

### 4.2 Experimental Methods and Equipment Materials

The following compounds were used to make the different synthetic mixtures studied in this work:

- Carbon Dioxide, Supplied by Air Products, Research Grade
- Methane, Supplied by Air Products, Grade N4.5
- Nitrogen, Supplied by BOC, Research Grade
- Argon, Supplied by BOC, Research Grade
- Carbon Monoxide, Supplied by BOC, Research Grade
- Oxygen, Supplied by BOC, Research Grade

- Hydrogen, Supplied by BOC Gases, >= %99.995

The systems listed in Table 4.1 were prepared gravimetrically and used to conduct density tests. A multi component mixture, MIX1, (composition given in Table 4.2) supplied by BOC was also used to carry out the tests.

*Table 4.1 The Composition of mixtures used for the experiments*

| Liquid above the saturation line | | |
|---|---|---|
| Component | $CO_2$%mole (±0.3) | Impurity %mole (±0.3) |
| Pure $CO_2$ | 100 | 0.0 |
| $CO_2$+$CH_4$ | 94.1 | 5.9 |
| $CO_2$+$N_2$ | 95.4 | 4.6 |
| $CO_2$+Ar | 95.0 | 5.0 |
| $CO_2$+CO | 94.1 | 5.9 |
| $CO_2$+$O_2$ | 95.0 | 5.0 |
| $CO_2$+$H_2$ | 95.0 | 5.0 |
| $CO_2$+$H_2$ | 97.4 | 2.6 |
| MIX1 | 95.6 | See Table 4.2 |
| Supercritical above vapour/supercritical boundary line | | |
| Pure $CO_2$ | 100 | 0.0 |
| $CO_2$+Ar | 95 | 5.0 |
| $CO_2$+CO | 95 | 5.0 |
| $CO_2$+$O_2$ | 95 | 5.0 |
| $CO_2$+$H_2$ | 95 | 5.0 |
| MIX1 | 95.6 | See Table 4.2 |

*Table 4.2 Mixture composition (MIX1)*

| Mixture | % mole (±0.05) |
|---|---|
| Carbon Dioxide | Balance |
| Methane | 0.67 |
| Hydrogen | 0.82 |
| Nitrogen | 1.41 |
| Carbon Monoxide | 0.21 |
| Argon | 1.21 |
| Oxygen | 0.08 |
| Total | 100 |

### *4.2.1 Experimental Equipment*

The schematic diagram of the experimental system used in this work is shown in Figure 4.1. The compressed liquid and supercritical density data of $CO_2$ and $CO_2$/impurities systems were measured with a high temperature and pressure vibrating tube densitometer Anton Paar DMA-HPM which consists of a measuring cell and an interface module. The measuring cell contains a U-shaped Hastelloy C-276 tube that is being excited to vibrate at its characteristic frequency electronically and the interface module generates the period of oscillation and measures the period of oscillation. The DMA-HPM has been connected to a mPDS 2000V3 evaluation unit which indicates the vibration period with seven significant digits.

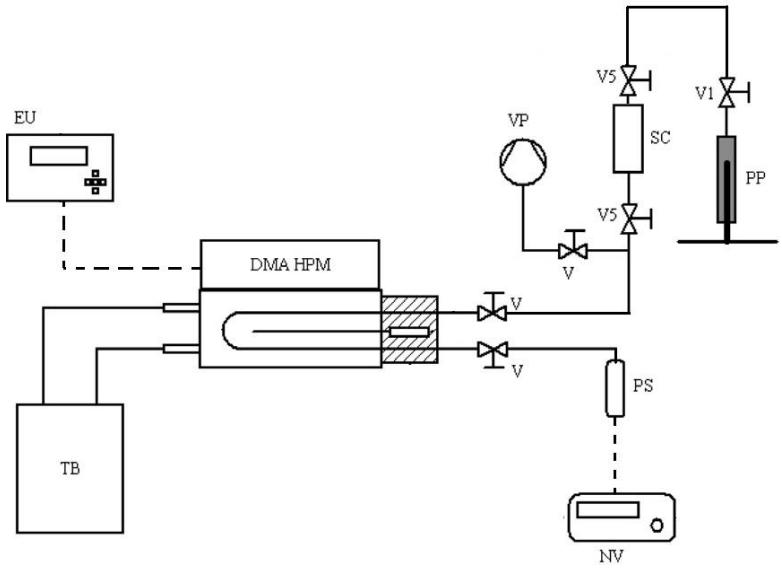


*Figure 4.1Schematic diagram of the compressed liquid densimeter apparatus. PP, Ruska motorized HP pump; PS, pressure sensor; SC, sample cylinder; VP, vacuum pump system; TB, thermostatic bath; EU, mPDS 2000V3 unit; NV, nanovolt meter; V, valves*

The vibrating tube is thermally controlled by a circulating coolant coming from an external thermostatic bath for liquid $CO_2$ mixture samples and by an oven for supercritical $CO_2$ samples. The measuring cell was insulated from the external environment and a maximum temperature fluctuation of ±0.01 K could be obtained all along the measurements. The temperature of the vibrating tube cell was measured by a built-in thermometer connected to the mPDS 2000V3 unit. The pressure of the system was applied with a Ruska motorised High Pressure Pump and measured by a pressure transducer (max 70 MPa); the pressure was kept constant to show significant digits in density do not change during the time of the measurement.

### *4.2.2 Experimental Calibration and Procedure*

After the entire circuit was purged, vacuum was applied to the system. Then the sample was introduced into the circuit by corresponding valves operation. When the temperature of the vibrating tube was stable, the vibration period of the U-tube was determined from the appropriate initial pressure to the maximum pressure. Then the temperature of the bath was changed and a new isotherm was repeated.

The measurement of density with a vibrating tube densitometer is not absolute, thus, the raw data (period of oscillation) should be further treated to obtain the densities. The relationship between them is [19]

$$\rho(T,P) = A(T,P)\tau^2(T,P) - B(T,P) \tag{4.1}$$

Where $\rho(T,P)$ is the sample density at temperature $T$ and pressure $P$, $\tau(T,P)$ is the period of oscillation at temperature and pressure, $A(T,P)$ and $B(T,P)$ are the apparatus parameters depending on temperature and pressure, and they must be determined from calibration measurements. In our calibration, $CO_2$ density is used as a reference substance at two different pressures (at a point just above the saturation point and a point at higher pressure both should be measured at the same temperature). The apparatus parameters were defined as follow:

$$A(T,P_1) = \frac{\rho(T,P_1) - \rho(T,P_2)}{\tau^2(T,P_1) - \tau^2(T,P_2)} \tag{4.2}$$

$$B(T,P_2)=\frac{\tau^2(T,P_2).\rho(T,P_1)-\tau^2(T,P_1).\rho(T,P_2)}{\tau^2(T,P_1)-\tau^2(T,P_2)} \quad (4.3)$$

### 4.3 Modelling

Many studies have been done to compare the abilities of various equations of state. Danesh et al. [20] compared 10 equations of state with classical mixing rules for predicting the phase behaviour and volumetric properties of hydrocarbon fluids. They concluded that the Valderrama modification of the Patel and Teja cubic equation of state [21] was superior to the other tested equations of state, particularly when the EOSs were compared without any use of binary interaction parameters. The other important equation of state is Peng Robinson EOS [22], which is classified as a two-parameter cubic equation and has become one of the models of choice in the process modelling. Span and Wagner [23] have the latest review of the thermodynamic properties of $CO_2$. Their work covered a wide range of pressure and temperature including the critical area based on large experimental data. They generated highly accurate tables based on a complex equation of state. Therefore, the tabulation data of their work is used to evaluate the absolute average deviation (ADD) for both PR and VPT EOS models. The deviations of the models from the experimental data were drawn for both liquid and supercritical $CO_2$ from 230 to 390 K and up to 50 MPa as shown in Figure 4.2 and Figure 4.3. The ADDs are 4.4 and 2.7% for PR and VPT EOSs respectively in liquid $CO_2$. In the supercritical region, the ADD is around 2.52% in both models. From the above figures, the maximum deviation can be as high as 10% in both cases. Hence, the use of those models without further modification for $CO_2$/impurities systems can definitely increase the deviation even with proper interaction parameters tuning.

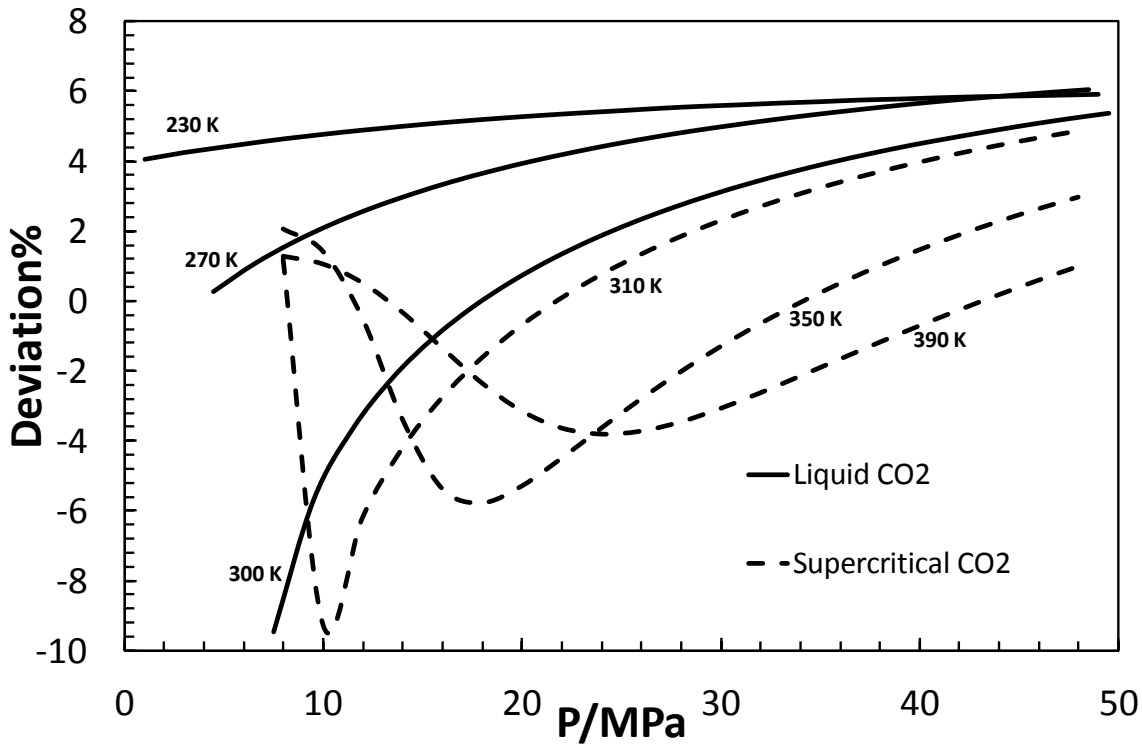


*Figure 4.2 Deviation between PR EOS and the data provided in [23] for pure $CO_2$*

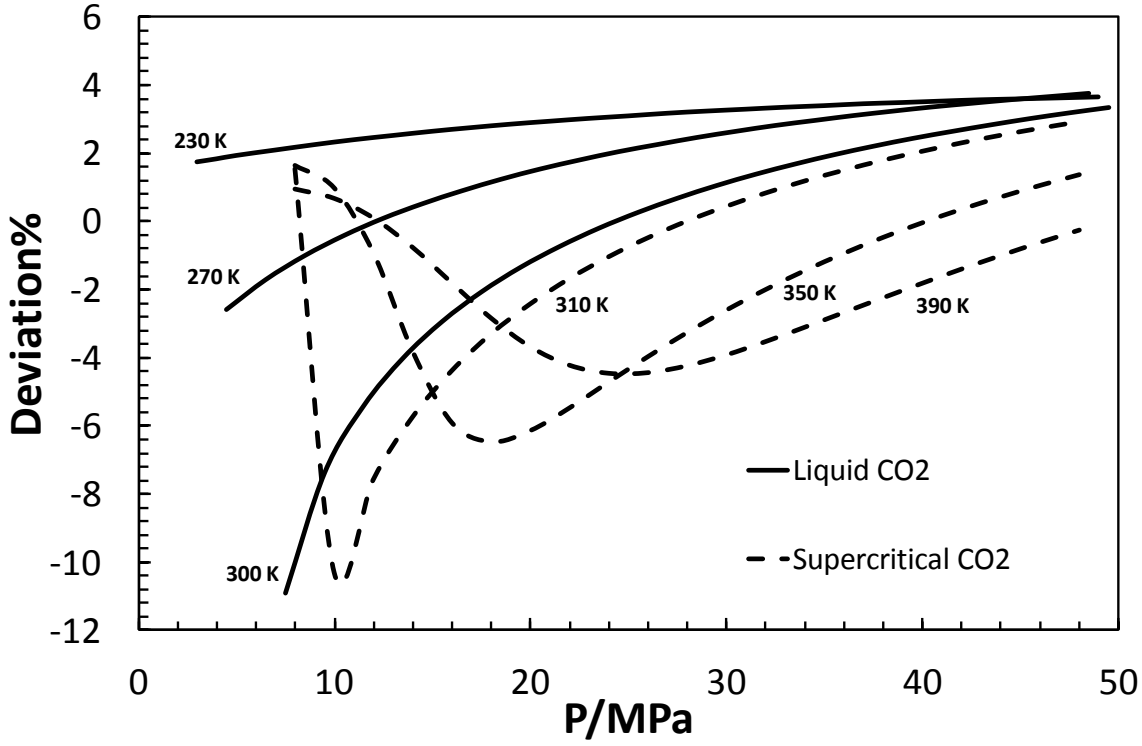


*Figure 4.3 Deviation between VPT EOS and the data provided in [23] for pure $CO_2$*

*Table 4.3 The interaction parameters of $CO_2$/binary system used in VPT EOS*

| Mixture | $k_{ij}$ |
|---|---|
| $CO_2$/Ar | 0.113 |
| $CO_2$/$O_2$ | 0.0909 |
| $CO_2$/$H_2$ | -0.386 |
| $CO_2$/CO | -0.0415 |
| $CO_2$/$N_2$ | -0.0607 |
| $CO_2$/$CH_4$ | 0.0915 |

In this work, the volume for $CO_2$ or a $CO_2$-rich mixture calculated by the EOS is corrected using the exact volume of $CO_2$ at the given T and P.

$$V^{new} = V^{EoS} - V^{c} \tag{4.4}$$

Where $V^{EoS}$ is the molar volume obtained from VPT EOS, the binary interaction parameters, $K_{ij}$ associated with the equation are tuned with independent experimental data and their values are given in

Table 4.3. The molar volume correction in the Equation 4.4, $V^{c}$, is defined as

$$V^{c} = \sum_{i}^{NComp} x_i V_i^{c} \tag{4.5}$$

$x_i$ is the composition of component *i* in the phase in which the volume is calculated. The volume calculated for impurities $V_i^{c}$ is set equal to 0 when there is no volume translation is used. For $CO_2$, $V_i^{c}$ is defined by

$$V^{c}{}_{CO_2} = V^{EoS}_{pure\,CO_2} - V^{MBWR} \tag{4.6}$$

The carbon dioxide density is computed from the MBWR equation in the form suggested by McCarty [24]

$$P = \sum_{n=1}^{9} a_n(T)\rho^n + \sum_{n=10}^{15} a_n(T)\rho^{2n-17} e^{-\gamma\rho^2} \tag{4.7}$$

## 4.4 Results & Discussion

### *4.4.1 Density of Liquid $CO_2$/Impurities System*

Liquid densities of $CO_2$ and six binary $CO_2$/impurities systems (see Table 4.1) were measured from (283.15 to 301.15) K, at pressures up to 50 MPa. Measurements were also conducted on a multi-components $CO_2$-rich mixture, MIX1, shown in Table 4.2. A total of 382 points were obtained in this test, as listed in Table 4.4. Our modified model prediction and its deviation with the experimental data are calculated and given in the table. The AAD of the modified and original models in pure $CO_2$ are 0.29% and 3.4% while the maximum deviation is 0.87% and 11.4% respectively. The modified model is found to be in a good agreement with our experimental data of impure $CO_2$ except near the critical point of the mixture. The actual critical temperature of the mixture tends to decrease in the presence of impurities (HydraFlash software). For example, at a composition fraction of 4.78% methane, the critical temperature of $CO_2$ is reduced from 304.2 K to 300.8 K. Therefore, the tested temperature, 301.15 K is even closer to the critical temperature of the mixture than of pure $CO_2$. Figure 4.4 and Figure 4.5 show the predictions of the proposed model correction at 283.15 and 301.15 K, respectively. The overall AAD for the tested impurities systems (excluding the binary $CO_2$/$H_2$ system) is 0.5%. The modified model deviates up to 5.57% and with AAD of 3.86% in $CO_2$/$H_2$ system below the critical temperature of the mixture. This is mainly due to the low molecular weight and critical temperature of $H_2$ comparing to the other impurities tested. From Table 4.4 some interesting observations can be made. The density of pure $CO_2$ and the $CO_2$/impurities mixtures have a stronger dependency on temperature compared to pressure at lower temperatures below their critical temperature. At condition very close to the critical point, a small change in temperature or pressure yields a very large change in the density of $CO_2$. In transport, this change could lead to a sudden change of phase and fluid velocity.

*Table 4.4 Experimental and modelling data for liquid $CO_2$ and liquid $CO_2$/impurities system*

| Pure $CO_2$ | | | | | |
|---|---|---|---|---|---|
| T = 283.15 K | | | T = 288.15 K | | |
| P/MPa | ρ/Kg.m$^{-3}$ | Dev% | P/MPa | ρ/Kg.m$^{-3}$ | Dev% |
| 42.95 | 1059.05 | 0.0 | 42.2 | 1041.95 | 0.02 |
| 39.49 | 1049.65 | 0.0 | 39.3 | 1033.55 | 0.02 |
| 36.03 | 1039.65 | 0.0 | 36.4 | 1024.65 | 0.02 |
| 32.58 | 1028.85 | 0.0 | 33.51 | 1015.15 | 0.02 |
| 29.12 | 1017.15 | 0.0 | 30.61 | 1004.85 | 0.03 |
| 25.66 | 1004.35 | 0.0 | 27.72 | 993.88 | 0.04 |
| 22.2 | 990.14 | 0.0 | 24.82 | 981.87 | 0.04 |
| 18.74 | 974.19 | 0.0 | 21.93 | 968.66 | 0.05 |
| 15.29 | 955.88 | 0.0 | 19.03 | 953.9 | 0.05 |
| 11.83 | 934.06 | 0.0 | 16.13 | 937.11 | 0.06 |
| 8.37 | 906.63 | 0.0 | 13.24 | 917.46 | 0.05 |
| | | | 10.34 | 893.41 | 0.03 |
| T = 293.15 K | | | T = 301.15 K | | |
| P/MPa | ρ/Kg.m$^{-3}$ | Dev% | P/MPa | ρ/Kg.m$^{-3}$ | Dev% |
| 44.41 | 1033.25 | 0.0 | 44.82 | 1010.45 | 0.04 |
| 40.89 | 1022.75 | 0.0 | 41.18 | 998.73 | 0.04 |
| 37.38 | 1011.55 | 0.0 | 37.54 | 986.01 | 0.05 |
| 33.86 | 999.43 | 0.0 | 33.9 | 972.08 | 0.06 |
| 30.34 | 986.14 | 0.1 | 30.25 | 956.63 | 0.07 |
| 26.83 | 971.42 | 0.1 | 26.61 | 939.24 | 0.07 |
| 23.31 | 954.89 | 0.1 | 22.97 | 919.22 | 0.08 |
| 19.8 | 935.9 | 0.1 | 19.33 | 895.45 | 0.08 |
| 16.28 | 913.4 | 0.1 | 15.69 | 865.75 | 0.08 |
| 12.76 | 885.34 | 0.1 | 12.05 | 824.86 | 0.08 |
| 9.25 | 846.64 | 0.0 | 8.41 | 751.38 | 0.09 |
| | | | 7.27 | 698.07 | 0.13 |
| $CO_2$/$CH_4$ | | | | | |
| T = 283.15 K | | | T = 288.15 K | | |
| P/MPa | ρ/Kg.m$^{-3}$ | Dev% | P/MPa | ρ/Kg.m$^{-3}$ | Dev% |
| 45.11 | 1015.73 | 0.1 | 44.55 | 999.77 | 0.13 |
| 41.23 | 1004.89 | 0.1 | 41.51 | 990.84 | 0.1 |
| 38.1 | 995.5 | 0.1 | 37.91 | 979.66 | 0.06 |
| 34.38 | 983.55 | 0.1 | 34.53 | 968.06 | 0.04 |
| 29.57 | 966.41 | 0.0 | 30.57 | 953.22 | 0.01 |

| | | | | | |
|---|---|---|---|---|---|
| 25.21 | 948.75 | 0.1 | 27.37 | 940.11 | 0.09 |
| 21.89 | 933.54 | 0.1 | 24.04 | 924.43 | 0.14 |
| 18.28 | 914.54 | 0.3 | 20.59 | 906.16 | 0.24 |
| 14.81 | 892.78 | 0.4 | 16.97 | 883.4 | 0.41 |
| 11.38 | 865.93 | 0.7 | 13.98 | 860.38 | 0.63 |
| 8.91 | 840.66 | 1.1 | 11.91 | 840.82 | 0.84 |
| 6.64 | 807.35 | 1.6 | 9.32 | 809.88 | 1.42 |
| T = 293.15 K | | | T = 301.15 K | | |
| P/MPa | ρ/Kg.m$^{-3}$ | Dev% | P/MPa | ρ/Kg.m$^{-3}$ | Dev% |
| 41.6 | 975.03 | 0.2 | 32.95 | 917.08 | 0.06 |
| 38.29 | 963.93 | 0.2 | 44.31 | 960.81 | 0.11 |
| 34.31 | 949.56 | 0.1 | 40.8 | 948.59 | 0.11 |
| 31.07 | 936.55 | 0.1 | 37.83 | 937.49 | 0.09 |
| 27.68 | 921.47 | 0.1 | 34.68 | 924.67 | 0.07 |
| 23.99 | 902.91 | 0.0 | 29.31 | 899.79 | 0.01 |
| 20.49 | 882.37 | 0.2 | 23.36 | 865.75 | 0.14 |
| 17.3 | 859.85 | 0.3 | 18.8 | 831.41 | 0.33 |
| 13.82 | 829.5 | 0.7 | 14.53 | 786.72 | 0.71 |
| 11.76 | 806.12 | 1.1 | 12.09 | 748.58 | 1.08 |
| 9.43 | 768.44 | 1.6 | 10.49 | 711.91 | 1.51 |
| 8.52 | 747.64 | 2.0 | 9.01 | 652.38 | 1.98 |
| 7.68 | 722.4 | 2.5 | 8.44 | 607.33 | 1.71 |
| $CO_2/N_2$ | | | | | |
| T = 283.15 K | | | T = 288.15 K | | |
| P/MPa | ρ/Kg.m$^{-3}$ | Dev% | P/MPa | ρ/Kg.m$^{-3}$ | Dev% |
| 37.93 | 1007.12 | 0.1 | 44.5 | 1012.84 | 0.1 |
| 32.47 | 988.25 | 0.1 | 44.05 | 1011.48 | 1.6 |
| 29.65 | 977.46 | 0.1 | 39.69 | 997.67 | 0.1 |
| 25.27 | 959 | 0.0 | 36.34 | 986.1 | 0.1 |
| 21.78 | 941.49 | 0.1 | 33.21 | 974.42 | 0.0 |
| 17.68 | 918.1 | 0.2 | 28.17 | 953.48 | 0.0 |
| 14.73 | 898.61 | 0.5 | 24.43 | 935.32 | 0.1 |
| 14.56 | 895.9 | 0.4 | 20.93 | 915.93 | 0.2 |
| 10.74 | 861.27 | 0.7 | 17.44 | 892.88 | 0.4 |
| 7.12 | 810.01 | 1.4 | 13.78 | 862.37 | 0.7 |
| | | | 9.96 | 810.54 | 0.5 |
| T = 293.15 K | | | T = 301.15 K | | |
| P/MPa | ρ/Kg.m$^{-3}$ | Dev% | P/MPa | ρ/Kg.m$^{-3}$ | Dev% |
| 44.36 | 996.98 | 0.1 | 45.17 | 976.41 | 0.0 |
| 40.98 | 985.87 | 0.1 | 41.04 | 961.61 | 0.0 |
| 38.27 | 976.3 | 0.1 | 37.91 | 949.35 | 0.0 |
| 34.72 | 962.81 | 0.1 | 34.78 | 936.03 | 0.0 |
| 33.72 | 959 | 0.0 | 31.15 | 918.91 | 0.0 |

| | | | | | |
|---|---|---|---|---|---|
| 30.95 | 947.25 | 0.0 | 26.21 | 892.55 | 0.2 |
| 27.72 | 932.09 | 0.1 | 22.22 | 865.74 | 0.4 |
| 24.28 | 913.9 | 0.2 | 18.34 | 832.64 | 0.5 |
| 21.02 | 893.9 | 0.3 | 15.09 | 793.4 | 0.5 |
| 17.42 | 867.25 | 0.5 | 12.14 | 744.13 | 1.1 |
| 14.57 | 840.14 | 0.7 | 10.34 | 691.48 | 1.2 |
| 12.25 | 812.02 | 1.0 | | | |
| 9.98 | 772.78 | 1.4 | | | |

$CO_2$/Ar

| T = 283.15 K | | | T = 288.15 K | | |
|---|---|---|---|---|---|
| P/MPa | ρ/Kg.m$^{-3}$ | Dev% | P/MPa | ρ/Kg.m$^{-3}$ | Dev% |
| 44.33 | 1051.57 | 0.0 | 44.45 | 1036.96 | 0.0 |
| 41.22 | 1042.52 | 0.0 | 40.92 | 1026 | 0.0 |
| 38.27 | 1033.37 | 0.0 | 37.74 | 1015.44 | 0.0 |
| 34.08 | 1019.35 | 0.0 | 33.45 | 999.6 | 0.0 |
| 28.83 | 999.63 | 0.1 | 28.72 | 980.73 | 0.1 |
| 24.92 | 982.98 | 0.2 | 24.67 | 961.69 | 0.2 |
| 21.68 | 967.32 | 0.2 | 20.56 | 939.53 | 0.3 |
| 17.67 | 944.95 | 0.4 | 17.84 | 921.84 | 0.4 |
| 14.28 | 922.11 | 0.6 | 14.26 | 894.11 | 0.7 |
| 10.91 | 893.38 | 0.9 | 10.93 | 859.96 | 1.1 |
| 7.8 | 856.93 | 1.5 | 8.76 | 828.81 | 1.6 |
| T = 293.15 K | | | T = 301.15 K | | |
| P/MPa | ρ/Kg.m$^{-3}$ | Dev% | P/MPa | ρ/Kg.m$^{-3}$ | Dev% |
| 44.34 | 1021.1 | 0.0 | 48.23 | 1008.44 | 0.1 |
| 40.62 | 1008.73 | 0.0 | 44.27 | 995.27 | 0.1 |
| 37.89 | 999.48 | 0.0 | 41.04 | 983.69 | 0.1 |
| 34.01 | 984.51 | 0.1 | 38.24 | 972.89 | 0.1 |
| 30.92 | 971.85 | 0.1 | 34.32 | 956.39 | 0.0 |
| 27.33 | 955.74 | 0.3 | 30.99 | 940.74 | 0.0 |
| 24.71 | 941.4 | 0.2 | 27.37 | 921.65 | 0.1 |
| 20.43 | 915.83 | 0.4 | 24.1 | 901.91 | 0.2 |
| 17.32 | 893.71 | 0.7 | 20.6 | 876.91 | 0.4 |
| 14.01 | 864.12 | 1.1 | 17.44 | 848.92 | 0.6 |
| 11.79 | 838.03 | 1.5 | 14.95 | 820.79 | 0.9 |
| 9.56 | 802.04 | 2.2 | 12.14 | 777.46 | 1.5 |
| | | | 9.7 | 709.31 | 2.5 |

$CO_2$/CO

| T = 283.15 K | | | T = 288.15 K | | |
|---|---|---|---|---|---|
| P/MPa | ρ/Kg.m$^{-3}$ | Dev% | P/MPa | ρ/Kg.m$^{-3}$ | Dev% |
| 47.04 | 1039.77 | 0.0 | 47.86 | 1027.62 | 0.0 |
| 42.94 | 1028.4 | 0.0 | 44.58 | 1018.26 | 0.0 |
| 38.14 | 1013.94 | 0.0 | 41.24 | 1008.15 | 0.1 |

| | | | | | |
|---|---|---|---|---|---|
| 33.36 | 997.9 | 0.1 | 38.14 | 998.12 | 0.1 |
| 28.65 | 980.27 | 0.2 | 34.21 | 984.13 | 0.1 |
| 24.54 | 962.69 | 0.2 | 30.81 | 970.99 | 0.2 |
| 20.66 | 943.7 | 0.3 | 27.36 | 956.24 | 0.2 |
| 17.04 | 922.87 | 0.5 | 23.63 | 938.51 | 0.3 |
| 13.72 | 899.91 | 0.7 | 20.44 | 920.47 | 0.4 |
| 10.83 | 874.68 | 1.0 | 17.23 | 899.7 | 0.6 |
| 8.74 | 851.51 | 1.4 | 13.57 | 870.16 | 0.9 |
| | | | 10.63 | 838.42 | 1.3 |
| | | | 9.56 | 825.54 | 1.7 |
| | | | 9.6 | 825.23 | 1.6 |

| T = 293.15 K | | | T = 301.15 K | | |
|---|---|---|---|---|---|
| P/MPa | ρ/Kg.m$^{-3}$ | Dev% | P/MPa | ρ/Kg.m$^{-3}$ | Dev% |
| 46.8 | 1009 | 0.1 | 48.55 | 992.07 | 0.1 |
| 42.49 | 995.59 | 0.0 | 44.56 | 979.01 | 0.1 |
| 38.12 | 980.18 | 0.1 | 40.76 | 965.5 | 0.1 |
| 33.74 | 964.13 | 0.0 | 40.75 | 965.4 | 0.1 |
| 29.19 | 944.65 | 0.1 | 37.97 | 954.72 | 0.1 |
| 24.23 | 919.6 | 0.2 | 34.21 | 938.95 | 0.1 |
| 20.91 | 899.76 | 0.3 | 30.63 | 922.08 | 0.2 |
| 17.21 | 873.13 | 0.6 | 27.35 | 904.68 | 0.2 |
| 13.71 | 840.4 | 0.9 | 24.17 | 885.41 | 0.3 |
| 10.7 | 800.61 | 1.5 | 20.49 | 858.88 | 0.5 |
| 9.27 | 773.67 | 2.0 | 17.35 | 830.68 | 0.7 |
| | | | 13.75 | 786.38 | 1.2 |
| | | | 10.67 | 723 | 1.9 |

$CO_2/O_2$

| T = 283.15 K | | | T = 288.15 K | | |
|---|---|---|---|---|---|
| P/MPa | ρ/Kg.m$^{-3}$ | Dev% | P/MPa | ρ/Kg.m$^{-3}$ | Dev% |
| 9.4 | 860.57 | 1.0 | 9.34 | 820.34 | 1.4 |
| 16.27 | 921.14 | 0.2 | 13.67 | 873.35 | 0.6 |
| 19.27 | 939.75 | 0.1 | 18.6 | 912.54 | 0.2 |
| 21.55 | 952.05 | 0.0 | 20.77 | 926.35 | 0.1 |
| 25.15 | 969.81 | 0.1 | 24.52 | 947.14 | 0 |
| 27.56 | 980.64 | 0.1 | 26.59 | 957.35 | 0.1 |
| 29.7 | 989.35 | 0.2 | 29.17 | 969.1 | 0.1 |
| 31.93 | 997.9 | 0.2 | 32.87 | 984.36 | 0.1 |
| 34.79 | 1008.26 | 0.2 | 35.36 | 993.76 | 0.2 |
| 38.29 | 1020.02 | 0.2 | 39.05 | 1006.66 | 0.2 |
| 42.53 | 1032.83 | 0.3 | 41.67 | 1015.22 | 0.2 |
| 46.85 | 1045.16 | 0.3 | 46.05 | 1028.49 | 0.3 |

| T = 293.15 K | | | T = 301.15 K | | |
|---|---|---|---|---|---|
| P/MPa | ρ/Kg.m$^{-3}$ | Dev% | P/MPa | ρ/Kg.m$^{-3}$ | Dev% |

| | | | | | |
|---|---|---|---|---|---|
| 8.93 | 761.88 | 1.9 | 9.34 | 623.5 | 3.9 |
| 12.85 | 832.34 | 0.9 | 13.73 | 770.65 | 1.1 |
| 17.57 | 879.81 | 0.4 | 18.46 | 834.87 | 0.7 |
| 21.67 | 909.48 | 0.2 | 22.59 | 871.08 | 0.7 |
| 25.4 | 931.49 | 0.0 | 25.59 | 896.57 | 0.2 |
| 28.66 | 948.12 | 0.0 | 30.04 | 915.82 | 0.9 |
| 32.33 | 964.76 | 0.1 | 33.54 | 934.97 | 0.7 |
| 36.17 | 980.31 | 0.1 | 36.77 | 952.29 | 0.4 |
| 39.84 | 993.76 | 0.1 | 40.2 | 967.15 | 0.3 |
| 43.75 | 1006.91 | 0.2 | 44.3 | 981.52 | 0.4 |
| 47.2 | 1017.63 | 0.2 | 47.79 | 993.19 | 0.4 |
| $CO_2/H_2$ (2.6%) | | | | | |
| T = 283.15 K | | | T = 288.15 K | | |
| P/MPa | ρ/Kg.m$^{-3}$ | Dev% | P/MPa | ρ/Kg.m$^{-3}$ | Dev% |
| 19.87 | 930.54 | 0.6 | - | - | - |
| 17.93 | 919 | 0.7 | - | - | - |
| 16.55 | 910.05 | 0.7 | - | - | - |
| 15 | 899.04 | 0.7 | - | - | - |
| 13.79 | 890.01 | 0.7 | - | - | - |
| 11.88 | 872.66 | 0.8 | - | - | - |
| 11.03 | 864.69 | 0.8 | - | - | - |
| 10.34 | 857.07 | 0.8 | - | - | - |
| 9.65 | 848.52 | 0.9 | - | - | - |
| 8.96 | 839.44 | 0.9 | - | - | - |
| 8.83 | 837.23 | 1.0 | - | - | - |
| T = 293.15 K | | | T = 301.15 K | | |
| P/MPa | ρ/Kg.m$^{-3}$ | Dev% | P/MPa | ρ/Kg.m$^{-3}$ | Dev% |
| 17.76 | 864.65 | 1.2 | 17.93 | 821.2 | 1.5 |
| 16.55 | 854.11 | 1.2 | 16.55 | 806.24 | 1.6 |
| 15 | 838.75 | 1.3 | 15 | 786.8 | 1.7 |
| 13.79 | 825.7 | 1.4 | 13.79 | 768.45 | 1.9 |
| 11.98 | 800.47 | 1.7 | 12.07 | 734.19 | 2.4 |
| 11.03 | 785.71 | 1.8 | 11.03 | 706.16 | 3.1 |
| 9.65 | 754.47 | 2.7 | 9.65 | 649.44 | 5 |
| 9.31 | 745.49 | 2.9 | 9.31 | 623.95 | 6.7 |
| 9.1 | 738.84 | 3.1 | 9.17 | 623.54 | 5.6 |
| 9.03 | 737.26 | 3.1 | | | |
| $CO_2/H_2$ (5%) | | | | | |
| T = 283.15 K | | | T = 288.15 K | | |
| P/MPa | ρ/Kg.m$^{-3}$ | Dev% | P/MPa | ρ/Kg.m$^{-3}$ | Dev% |
| 11.18 | 856.75 | 4.7 | 12.67 | 840.12 | 4.7 |
| 15.45 | 894.91 | 3.7 | 14.72 | 858.96 | 3.9 |

| | | | | | |
|---|---|---|---|---|---|
| 17.02 | 906.04 | 3.5 | 18.51 | 888.71 | 3.1 |
| 19.75 | 922.93 | 3.1 | 20.77 | 903.75 | 2.9 |
| 23.37 | 941.91 | 2.7 | 23.86 | 921.63 | 2.6 |
| 26.88 | 958.09 | 2.5 | 27.14 | 937.81 | 2.4 |
| 30.37 | 972.68 | 2.4 | 31.54 | 956.5 | 2.1 |
| 34.95 | 989.58 | 2.2 | 36.38 | 975.18 | 1.9 |
| 38.9 | 1000.5 | 1.9 | 40.4 | 991.03 | 2 |
| T = 293.15 K | | | T = 301.15 K | | |
| P/MPa | ρ/Kg.m$^{-3}$ | Dev% | P/MPa | ρ/Kg.m$^{-3}$ | Dev% |
| 10.27 | 761.44 | 6.6 | 11.26 | 740.19 | 12 |
| 16.35 | 845.21 | 3.8 | 13.1 | 776.35 | 9.2 |
| 16.38 | 845.44 | 3.8 | 15.89 | 814.62 | 7.1 |
| 21.22 | 899.62 | 4.7 | 18.49 | 842.86 | 6.3 |
| 27.5 | 934.14 | 3.9 | 22.66 | 874.23 | 5 |
| 35.07 | 966.59 | 3.4 | 25.28 | 888.7 | 4.3 |
| 42.97 | 994.11 | 3.0 | 27.6 | 900.8 | 3.9 |
| 49.24 | 1013.13 | 2.8 | 31.78 | 920.98 | 3.4 |
| | | | 36.92 | 945.2 | 3.2 |
| | | | 40.22 | 956.85 | 3 |
| | | | 42.3 | 964.16 | 2.8 |
| MIX1 | | | | | |
| T = 283.15 K | | | T = 288.15 K | | |
| P/MPa | ρ/Kg.m$^{-3}$ | Dev% | P/MPa | ρ/Kg.m$^{-3}$ | Dev% |
| 10.09 | 858 | 1.7 | 9.94 | 830.48 | 3.5 |
| 14.56 | 899.5 | 1.1 | 11.49 | 852.47 | 3.2 |
| 18.99 | 929.3 | 0.8 | 14.78 | 885.22 | 2.5 |
| 21.55 | 944.55 | 0.7 | 21.27 | 931.72 | 1.9 |
| 25.42 | 963.55 | 0.6 | 27.32 | 964.77 | 1.8 |
| 27.8 | 972.83 | 0.4 | 33.81 | 990.75 | 1.5 |
| 33.04 | 994.54 | 0.4 | 43.86 | 1026.12 | 1.5 |
| 37.83 | 1009.76 | 0.2 | | | |
| 41.89 | 1022.55 | 0.2 | | | |
| T = 293.15 K | | | T = 301.15 K | | |
| P/MPa | ρ/Kg.m$^{-3}$ | Dev% | P/MPa | ρ/Kg.m$^{-3}$ | Dev% |
| 41.99 | 988.96 | 0.0 | 11.79 | 734.75 | 1.9 |
| 37.31 | 972.51 | 0.0 | 13.42 | 767.83 | 1.4 |
| 33.32 | 956.91 | 0.1 | 15.93 | 805.27 | 1.1 |
| 27.35 | 929.73 | 0.2 | 20.5 | 851.65 | 0.7 |
| 23.9 | 911.16 | 0.3 | 24.46 | 881.58 | 0.6 |
| 19.75 | 884.31 | 0.5 | 29.31 | 910.8 | 0.5 |
| 16.64 | 859.67 | 0.8 | 34.25 | 935.48 | 0.4 |
| 13.32 | 825.01 | 1.2 | 37.92 | 951.41 | 0.4 |
| 11.12 | 793.31 | 1.7 | | | |

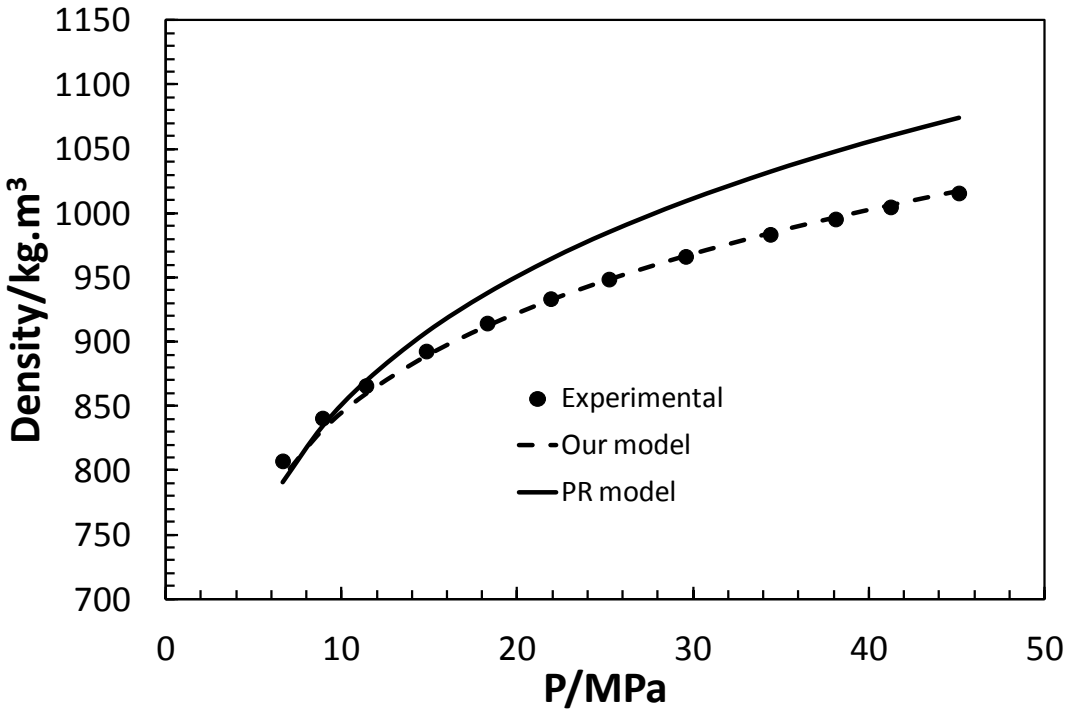


*Figure 4.4 Density of $CO_2$/$CH_4$ at 283.15 K*

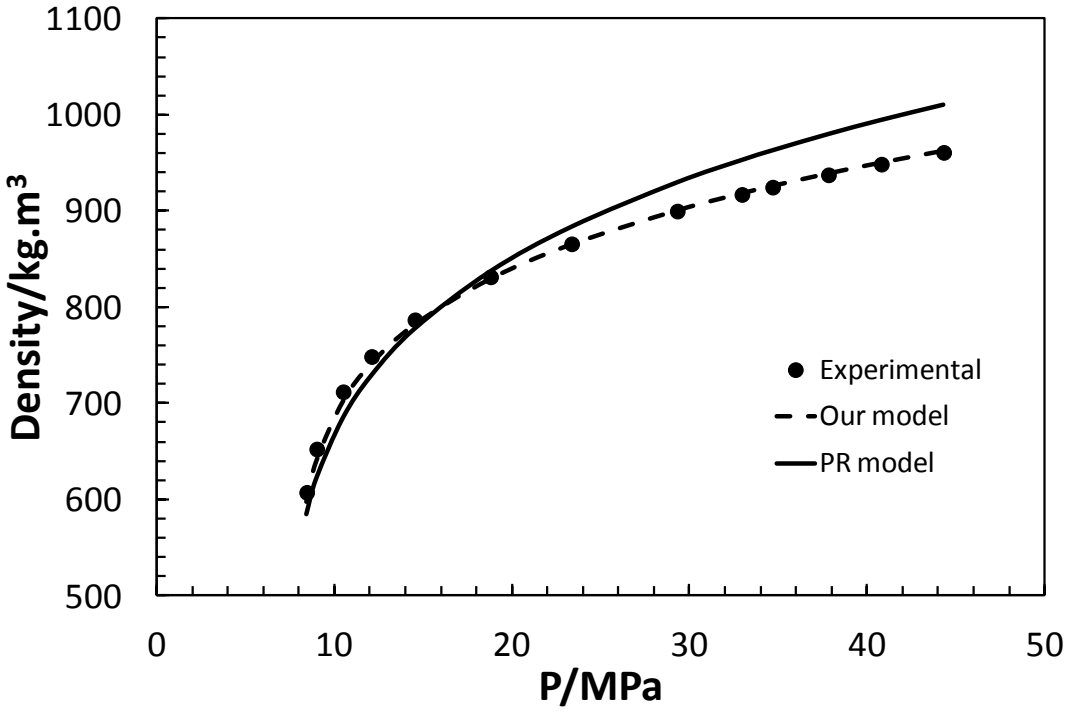


*Figure 4.5 Density of $CO_2$/$CH_4$ at 301.15 K*

Our modified model was used to evaluate the change in $CO_2$ density in the presence of impurities. An example of the change on the density when impurities are present can be seen in Figure 4.6. The change is plotted as a function of pressure at 283.15 K for four binary mixtures ($CO_2$/Ar, $CO_2/O_2$, $CO_2/H_2$ and $CO_2/CH_4$). $\Delta\rho$ is calculated by subtracting the density of the corresponding $CO_2$/impurities from the density of pure $CO_2$. In general, the impurities reduce $CO_2$ density over the range of pressure and temperature tested. The change is found to be higher near the critical points of the mixture. The reduction is higher in the presence of methane and it has a minimal effect in the presence of Argon. This is mainly due to the molecular weight ratio of impurity in the mixture to that of pure $CO_2$, i.e. as $\left(\frac{MW_{CO2}}{MW_{impurity}}\right)$ tends to 1, the density change becomes insignificant. This rule is obvious in all the tested mixture except for hydrogen binary mixture where the effect of smaller molecular weight is also significant. The reduced density is largely related to the increase volume of the mixture. This can be understood from the fact that non-condensable impurities are less dense than $CO_2$ and hence take greater volumes.

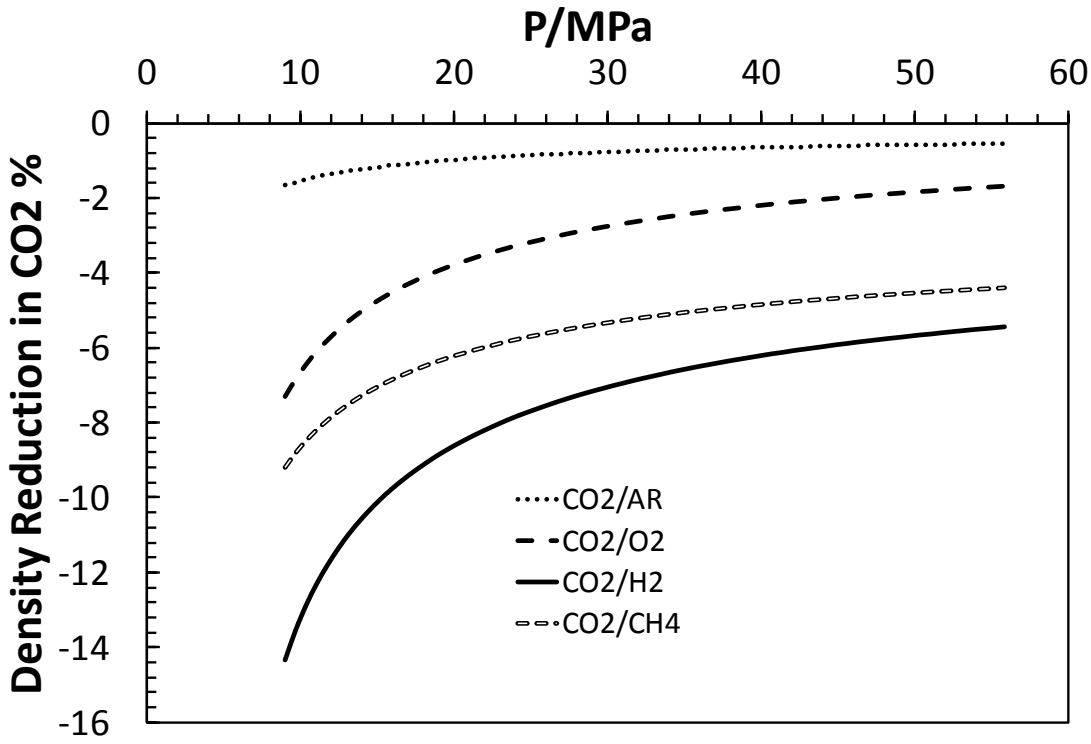


*Figure 4.6 Density reduction in liquid $CO_2$ in the presence of impurities at 283.15 K*

### 4.4.2 Density of Supercritical $CO_2$/Impurities System

In this part, five systems of $CO_2$/Ar, $CO_2$/CO, $CO_2$/$H_2$, $CO_2$/$O_2$ and MIX1 (composition given in Table 4.1 and Table 4.2) were measured at three different temperatures, 323.15 K, 373.15 K and 423.15 K. The experiment was carried-out at a pressure above the critical pressure of the mixture and up to 50 MPa. The results are listed in Table 4.5 with 160 measurement points. In supercritical region, the density of pure $CO_2$ is seen to be highly dependent on pressure compare to temperature. Near the critical pressure, a small change in pressure can have a large effect on the density. $CO_2$ fluids with high density will reduce the pipeline size and the running cost. This is not the case in the presence of impurities. In order to understand this effect, spline interpolation is implemented to the experimental data from 8.3 MPa to 41.3 MPa. Figure 4.7 shows the reduction on $CO_2$ density of three impurities, Ar, $H_2$ and $O_2$ at 323.15 K. A maximum reduction of the $CO_2$ density at a certain pressure under the given temperature is observed for the $CO_2$ mixtures. The reduction exceeds 25% in $CO_2$/$H_2$, 23% in $CO_2$/$O_2$ and 20% in $CO_2$/Ar mixtures. The maxima occur at a pressure equals to 11 MPa. A critical density change in the $CO_2$/impurities systems can be found from a pressure above the supercritical boundary to 20 MPa. The overall AAD% of the modified PR model is 1.67 in the tested systems listed in Table 4.5. The deviation increases as the impurities systems approach 11 MPa.

*Table 4.5 Experimental and modelling data for supercritical $CO_2$ and supercritical $CO_2$/impurities system*

| Pure $CO_2$ | | | | | | | | |
|---|---|---|---|---|---|---|---|---|
| T = 323.15 K | | | T = 373.15 K | | | T = 423.15 K | | |
| P/MPa | ρ/Kg.m$^{-3}$ | Dev% | P/MPa | ρ/Kg.m$^{-3}$ | Dev% | P/MPa | ρ/Kg.m$^{-3}$ | Dev% |
| 8.38 | 240.88 | 0.06 | 8.87 | 161.14 | 0.01 | 8.95 | 128.51 | 0.04 |
| 10.33 | 423.64 | 0.44 | 12.64 | 260.65 | 0.15 | 12.91 | 195.58 | 0.50 |
| 11.22 | 522.48 | 0.36 | 15.96 | 362.88 | 0.07 | 16.51 | 262.66 | 0.04 |
| 15.30 | 704.18 | 0.73 | 20.84 | 502.33 | 0.26 | 19.29 | 314.78 | 0.08 |
| 18.20 | 756.67 | 0.68 | 24.86 | 586.91 | 0.29 | 24.57 | 409.47 | 0.04 |
| 22.25 | 806.29 | 0.48 | 28.33 | 641.24 | 0.18 | 28.74 | 475.33 | 0.02 |
| 26.81 | 845.67 | 0.41 | 32.61 | 692.94 | 0.03 | 32.36 | 524.96 | 0.04 |
| 30.72 | 872.33 | 0.37 | 35.64 | 722.61 | 0.07 | 35.87 | 566.83 | 0.07 |

| | | | | | | | | |
|---|---|---|---|---|---|---|---|---|
| 35.33 | 898.54 | 0.33 | 39.62 | 755.54 | 0.17 | 40.13 | 610.35 | 0.13 |
| 42.72 | 933.02 | 0.26 | 42.83 | 778.45 | 0.22 | 45.49 | 656.46 | 0.20 |
| 46.25 | 947.16 | 0.23 | 47.37 | 806.56 | 0.27 | 49.15 | 683.56 | 0.26 |
| 54.48 | 976.12 | 0.16 | | | | | | |
| 58.54 | 988.78 | 0.13 | | | | | | |

$CO_2$/Ar

| T = 323.15 K | | | T = 373.15 K | | | T = 423.15 K | | |
|---|---|---|---|---|---|---|---|---|
| P/MPa | ρ/Kg.m$^{-3}$ | Dev% | P/MPa | ρ/Kg.m$^{-3}$ | Dev% | P/MPa | ρ/Kg.m$^{-3}$ | Dev% |
| 11.14 | 408.62 | 1.23 | 10.20 | 204.90 | 8.93 | 10.88 | 151.55 | 3.88 |
| 12.59 | 520.40 | 0.42 | 11.15 | 227.99 | 8.05 | 15.47 | 228.63 | 3.23 |
| 14.93 | 630.88 | 1.29 | 18.75 | 435.53 | 3.75 | 20.23 | 314.55 | 1.91 |
| 19.57 | 735.25 | 0.92 | 23.60 | 549.00 | 2.99 | 23.52 | 367.16 | 2.72 |
| 23.17 | 782.35 | 0.61 | 32.60 | 683.81 | 2.73 | 28.11 | 441.55 | 1.75 |
| 31.31 | 852.38 | 0.20 | 40.28 | 757.45 | 2.79 | 32.99 | 504.45 | 2.08 |
| 39.19 | 898.47 | 0.02 | 45.15 | 795.80 | 3.09 | 36.43 | 542.17 | 2.28 |
| 50.05 | 945.95 | 0.15 | | | | 41.77 | 596.54 | 1.78 |
| 57.77 | 973.03 | 0.20 | | | | | | |

$CO_2$/$O_2$

| T = 323.15 K | | | T = 373.15 K | | | T = 423.15 K | | |
|---|---|---|---|---|---|---|---|---|
| P/MPa | ρ/Kg.m$^{-3}$ | Dev% | P/MPa | ρ/Kg.m$^{-3}$ | Dev% | P/MPa | ρ/Kg.m$^{-3}$ | Dev% |
| 7.72 | 187.17 | 0.50 | 12.25 | 230.07 | 2.49 | 8.29 | 111.03 | 3.50 |
| 9.66 | 284.36 | 2.53 | 16.38 | 340.68 | 2.76 | 36.91 | 539.44 | 2.91 |
| 12.14 | 468.36 | 4.19 | 21.39 | 468.56 | 2.80 | 31.79 | 481.00 | 3.07 |
| 14.26 | 586.50 | 1.55 | 26.57 | 567.98 | 2.26 | 27.89 | 428.82 | 3.15 |
| 17.18 | 674.54 | 0.70 | 30.96 | 629.53 | 1.86 | 23.54 | 363.04 | 3.11 |
| 19.78 | 723.23 | 0.54 | 35.78 | 681.48 | 1.57 | 19.31 | 292.85 | 3.05 |
| 22.55 | 760.80 | 0.54 | 39.62 | 715.11 | 1.43 | 15.27 | 223.93 | 2.99 |
| 26.61 | 802.36 | 0.58 | | | | | | |
| 29.09 | 822.63 | 0.63 | | | | | | |
| 29.25 | 824.10 | 0.60 | | | | | | |
| 33.87 | 855.57 | 0.67 | | | | | | |
| 38.58 | 882.17 | 0.71 | | | | | | |

$CO_2$/$H_2$

| T = 323.15 K | | | T = 373.15 K | | | T = 423.15 K | | |
|---|---|---|---|---|---|---|---|---|
| P/MPa | ρ/Kg.m$^{-3}$ | Dev% | P/MPa | ρ/Kg.m$^{-3}$ | Dev% | P/MPa | ρ/Kg.m$^{-3}$ | Dev% |

| | | | | | | | | |
|---|---|---|---|---|---|---|---|---|
| 7.92 | 190.22 | 3.86 | 8.94 | 148.12 | 0.62 | 9.30 | 122.97 | 1.73 |
| 9.33 | 258.13 | 4.82 | 11.49 | 205.62 | 0.48 | 14.82 | 209.16 | 1.49 |
| 10.59 | 340.86 | 4.58 | 15.64 | 311.41 | 0.88 | 19.04 | 278.08 | 1.45 |
| 11.78 | 431.42 | 5.88 | 20.26 | 429.98 | 0.96 | 23.16 | 344.24 | 1.44 |
| 13.92 | 561.01 | 7.10 | 25.52 | 536.82 | 1.35 | 27.50 | 408.52 | 1.39 |
| 17.64 | 674.17 | 5.72 | 29.83 | 600.93 | 1.51 | 31.83 | 465.07 | 1.30 |
| 20.81 | 728.22 | 4.81 | 34.22 | 651.34 | 1.56 | 35.70 | 509.04 | 1.23 |
| 24.92 | 776.69 | 4.07 | 38.61 | 691.84 | 1.55 | 40.66 | 557.39 | 1.12 |
| 28.85 | 810.95 | 3.56 | 42.79 | 724.08 | 1.53 | 43.00 | 577.94 | 1.03 |
| 36.55 | 861.13 | 2.96 | 43.15 | 727.26 | 1.61 | | | |

MIX1

| T = 323.15 K | | | T = 373.15 K | | | T = 423.15 K | | |
|---|---|---|---|---|---|---|---|---|
| P/MPa | ρ/Kg.m$^{-3}$ | Dev% | P/MPa | ρ/Kg.m$^{-3}$ | Dev% | P/MPa | ρ/Kg.m$^{-3}$ | Dev% |
| 9.58 | 276.08 | 0.94 | 8.38 | 139.44 | 1.44 | 9.60 | 130.90 | 1.56 |
| 12.19 | 466.66 | 0.45 | 8.94 | 151.66 | 1.71 | 13.42 | 191.99 | 1.57 |
| 15.67 | 630.18 | 3.22 | 13.16 | 253.60 | 2.45 | 17.36 | 258.28 | 1.54 |
| 19.86 | 718.93 | 3.90 | 18.41 | 396.44 | 2.32 | 21.03 | 320.01 | 1.41 |
| 23.65 | 767.89 | 4.00 | 23.13 | 506.27 | 2.55 | 26.03 | 399.28 | 1.37 |
| 27.12 | 801.45 | 4.03 | 27.48 | 582.01 | 2.97 | 33.65 | 500.95 | 1.66 |
| 39.07 | 879.55 | 4.05 | 31.74 | 637.98 | 3.26 | 37.59 | 544.07 | 1.88 |
| | | | 36.25 | 684.48 | 3.46 | | | |

$CO_2$/CO

| T = 323.15 K | | | T = 373.15 K | | | T = 423.15 K | | |
|---|---|---|---|---|---|---|---|---|
| P/MPa | ρ/Kg.m$^{-3}$ | Dev% | P/MPa | ρ/Kg.m$^{-3}$ | Dev% | P/MPa | ρ/Kg.m$^{-3}$ | Dev% |
| 11.62 | 419.48 | 4.42 | 9.37 | 161.33 | 2.08 | 10.20 | 138.79 | 3.63 |
| 14.45 | 587.43 | 0.23 | 15.48 | 312.21 | 2.47 | 14.16 | 202.69 | 3.26 |
| 19.82 | 721.02 | 1.30 | 20.50 | 441.22 | 2.58 | 19.83 | 298.23 | 2.96 |
| 25.41 | 789.06 | 1.12 | 22.68 | 494.59 | 1.21 | 21.73 | 330.88 | 2.58 |
| 28.37 | 814.40 | 0.94 | 27.74 | 583.71 | 0.65 | 27.75 | 425.29 | 2.02 |
| 32.99 | 846.71 | 0.73 | 32.45 | 644.81 | 0.28 | 32.30 | 485.98 | 1.75 |
| 36.63 | 867.49 | 0.55 | 35.33 | 675.30 | 0.07 | 34.64 | 515.42 | 1.27 |
| 40.77 | 888.03 | 0.39 | 40.56 | 720.97 | 0.12 | 39.98 | 572.37 | 0.73 |
| 44.02 | 902.02 | 0.24 | 42.59 | 736.66 | 0.23 | 43.06 | 602.29 | 0.25 |
| 46.85 | 913.01 | 0.10 | 46.11 | 760.92 | 0.33 | 47.23 | 638.10 | 0.25 |

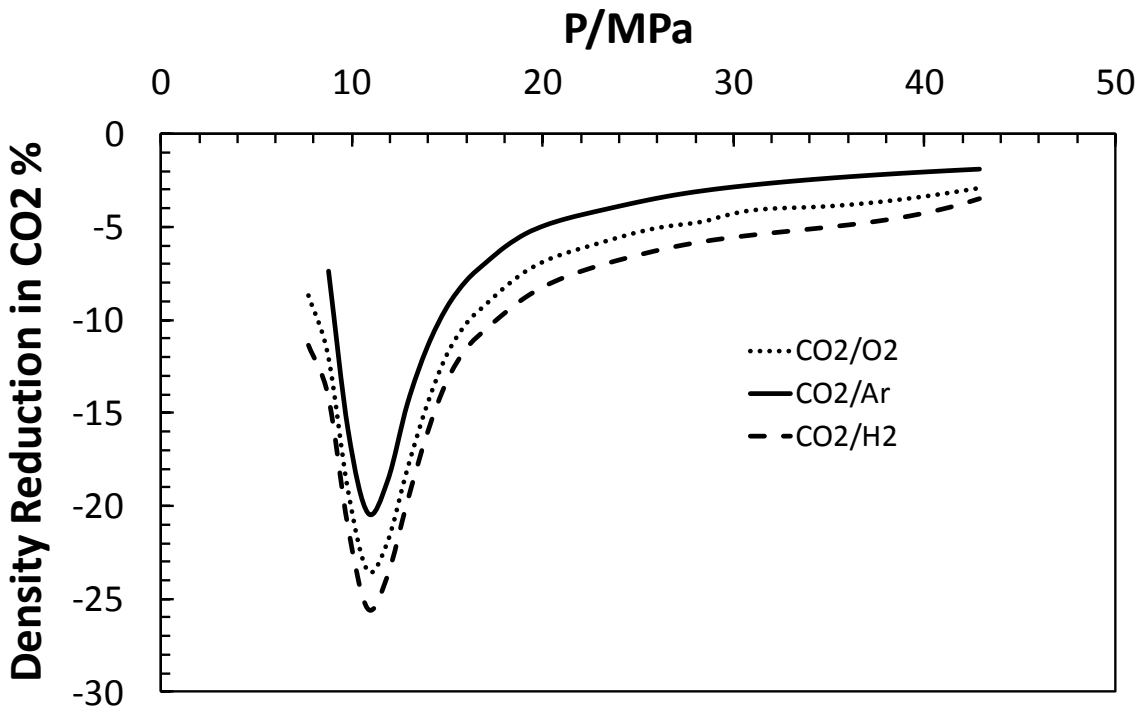


*Figure 4.7 Density reduction in supercritical $CO_2$ in the presence of impurities at 323.15*

### 4.5 Conclusions

The presence of impurities on $CO_2$ stream can potentially affect the density in both liquid and supercritical regions. Our model density calculations are in a good agreement with the experimental data for both pure and impure $CO_2$. The density of pure $CO_2$ and the $CO_2$/impurities mixtures have a stronger dependency on temperature compared to pressure at lower temperatures below the critical temperature. Above the critical temperature, a maximum reduction on the density at a certain pressure under a given temperature was found for each $CO_2$/impurity system. Overall, the light molecular weight impurities tend to reduce $CO_2$ density much more than those with molecular weight close to $CO_2$.

**References**

[1] Serpa, J., Morbee, J. and Tzimas, E., 2011, *Technical and Economic Characteristics of a $CO_2$ Transmission Pipeline Infrastructure*, EUR 24731 EN, P7.

[2] Seevam, P. N., Race, J. M. and Downie, M. J., (School of Marine Science and Technology, Newcastle University, UK), *Carbon Dioxide Impurities and Their Effects on $CO_2$ Pipelines*, The Australian Pipeliner-April 2008.

[3] Li, H., Jakobsen, J. P., Wilhelmsen, Ø. and Yan, J., 2011, *PVTxy Properties of $CO_2$ Mixtures Relevant for $CO_2$ Capture, Transport and Storage: Review of Available Experimental Data and Theoretical Models*, Appl. Energy, **88**, 3567-3579.

[4] Jiang, S., Wang, Y. and Shi, J., 1990, *Determination of Compressibility Factors and Virial Coefficients for the Systems Containing $N_2$, $CO_2$ and $Chclf_2$ by the Modified Burnett Method*, Fluid Phase Equil., **57**, 105-117.

[5] Esper, G. J., Bailey, J. C., Holste, D. M. and Hall, K. R., 1989, *Volumetric Behavior of Near-Equimolar Mixtures for Carbon Dioxide + Methane and Carbon Dioxide + Nitrogen*, Fluid Phase Equil., **49**, 35-47.

[6] Seitz, J. C. and Blencoe, J. G, 1996, *Volumetric Properties for $(1–X)CO_2$ + $XCH_4$,$(1-X)CO_2$ + $XN_2$, and $(1-X)CH_4$ + $XN_2$ at the Pressures 19.94, 29.94, 39.94, 59.93, 79.93, and 99.93 MPa and the Temperature 673.15 K*, J. Chem. Thermodyn., **28**, 1207-1213.

[7] Seitz, J. C., Blencoe, J. G. and Bodnar, R. J., 1996, *Volumetric Properties for $(1-x)CO_2+xCH_4$, $(1\ x)CO_2+xN_2$, and $(1-x)CH_4+xN_2$ at the Pressures 9.94, 19.94, 29.94, 39.94, 59.93, 79.93, and 99.93 MPa and Temperatures 323.15, 373.15, 473.15,and 573.15 K*, J. Chem. Thermodyn., **28**, 521-538.

[8] Hwang, C., Iglesias-Silva, G. A., Holste, J. C., Hall, K. R., Gammon, B. E. and Marsh, K. N., 1997, *Densities of Carbon Dioxide + Methane Mixtures from 225 K to 350 K at Pressures up to 35 MPa,* J. Chem. Eng. Data, **42**, 897-899.

**[9]** Jaeschke, M. and Humphreys, A. E., , 1990, *The GERG Databank of High Accuracy Compressibility Factor Measurements*, Verlag des Vereins Deutscher Ingenieure: Dusseldorf, GERG Technical Monograph 4, Germany

[10] Magee, J. W., Howley, J. and Ely, J. F., 1994, *A Predictive Model for the Thermophysical Properties of Carbon Dioxide Rich Mixtures*, RR-136. Tulsa: Gas Processors Association.

[11] Seitz, J. C., 1994, *Experimental Determination of the Volumetric Properties for the System $CO_2$ $CH_4$-$N_2$ at 100-1000 Bars and 50-300 °C*, Thesis , Virginia Polytechnic Institute and State University Dissertation.

[12] Bezanehtak, K., Combes, G. B., Dehghani, F. and Foster, NR., 2002, *Vapor–Liquid Equilibrium for Binary Systems of Carbon Dioxide + Methanol, Hydrogen + Methanol, and Hydrogen + Carbon Dioxide at High Pressures*, J Chem Eng Data, **47**, 161-8.

[13] Tsang, C. and Streett, W., 1981, *Phase Equilibria in the $H_2/CO_2$ System at Temperatures from 20 to 290 K and Pressures to 172 MPa*, Chem Eng Sci., **36**, 993-1000.

[14] Altunin, V. and Koposhilov, O., 1977, *An Experimental Study of Thermal Properties of Gaseous Mixtures of Carbon Dioxide with Argon*, Teploenergetika, **24**, 80-3.

[15] Sarashina, E., Arai, Y. and Saito, S., 1971, *The P-V-T-X Relation for the Carbon Dioxide-System*, J. Chem Eng Jap., **4**, 379-81.

[16] Kestin, J., Kobayashi, Y. and Wood, R., 1966, *The Viscosity of four Binary Gaseous Mixtures at 20 °C and 30 °C*, Phys Amsterdam, **32** ,1065-1089.

[17] Mallu, B., Natarajan, G. and Viswanath, D, 1987, *Compression Factors and Second Virial Coefficients of $CO_2$, $CO_2$ and {xCO + (1 - x) $CO_2$}*, J. Chem Thermodynamics, **19,** 549-54.

[18] Mantovani, M., Chiesa, P., Valenti, G., Gatti, M. and Consonni, S., 2012, *Supercritical Pressure- Density-Temperature Measurements on $CO_2$-$N_2$, $CO_2$-$O_2$ and $CO_2$-Ar Binary Mixtures*, J. Supercritical Fluids, **61**, 34-43.

[19] Kratky, O., Leopold, H. and Stabinger, H. H., 1969, *Dichtemessungen an Flüssigkeiten Und Gasen Auf $10^{-6}$ G/$Cm^3$ Bei 0.6 $Cm^3$ Präparatvolumen, Zeitschrift für Angewandte Physik*, **27**, 273-277.

[20] Danesh, A., Xu , D. -H. and Todd, A. C., 1991, *Comparative Study of Cubic Equations of State for Predicting Phase Behaviour and Volumetric Properties of Injection Gas-Reservoir Oil System*, Fluid Phase Equilib., **63**, 259-278.

[21] Valderrama, J. O., ,1990, *A Generalized Patel-Teja Equation of State for Polar and Non-Polar Fluids and Their Mixtures*J. Chem. Eng. Japan, **23**, 87-91.

[22] Peng, D. Y. and Robinson, D. B., 1976, *A New Two Constant Equation of State*, Industrial and Engineering Chemistry Fundamentals, **15**, 59-64.

[23] Span, R. and Wagner, W., 1996, *A New Equation of State for Carbon Dioxide Covering the Fluid Region from the Triple Point Temperature to 1100 K at Pressures up to 800 MPa*, J. Physical and Chemical Reference Data, **25**, 1509-1596.

[24] McCarty, R. D., 1974, *A Modified Benedict–Webb–Rubin Equation of State for Methane Using Recent Experimental Data*, Cryogenics, **14**, 276-280.

# CHAPTER 5: **HYDRATE STABILITY OF CARBON DIOXIDE RICH SYSTEM**

## 5.1 Introduction

Hydrate is a compound containing water discovered by Sir Humphrey Davey in 1811. Hydrate is ice-like solid component formed mainly from water and other small molecules. To form hydrate, three things are required: a sufficient amount of water (host), a former (guest) and right combination of pressure and temperature. Light gases such as $CH_4$, $N_2$, $O_2$, Ar, $H_2S$ and $CO_2$ can form hydrate in the presence of water. There are basically three common types of hydrate, structure I (SI), structure II (SII) and structure H (SH). Primary, the hydrate structure depends on the size of the gas molecules. The mixture of light gasses can result in a change on both the structure and the hydrate stability zone. Suitable thermodynamic conditions of forming hydrate can be found in pipelines; therefore both experimental and modelling works should be carried-out to define the fluid hydrate zone.

With regard to carbon emissions, the most promising solution currently on the table is $CO_2$ capture and subsurface storage, primarily by injection into ageing oil/gas reservoirs (where it can be used to improve oil/gas recovery) or deep saline aquifers. Conventionally, subsea pipelines are used to transport $CO_2$ in liquid or dense-phase state from the mainland for disposal. However $CO_2$ coming from capture processes is generally not pure and can contain impurities such as $N_2$, $H_2$, $O_2$, $H_2S$, $CH_4$, CO and water. The presence of these impurities combined with potentially long distance transportation of $CO_2$ could lead to challenging engineering and flow assurance issues. The presence of water may result in corrosion, ice and/or gas hydrate formation and pipeline blockage. Furthermore, the gaseous $CO_2$ rich stream is generally compressed to be transported as liquid or dense-phase state in order to avoid two-phase flow and increase the density of the fluid system. Scenario of excepted impurities on $CO_2$ is reported in [1] and [2], where $CO_2$ purity varies from 85 to 99.94% .The type and amount of impurities introduced in $CO_2$ depends on the type of capture process and the fuels beside the type of solvent used. The presence and type of other components may

differ considerably between post-combustion, pre-combustion and oxy-fuel capture processes [3].

Hydrate formation conditions of CCS streams is not as well known as for natural gas. Experience with pipeline transportation of $CO_2$ shows that $CO_2$ hydrates form up to temperatures of 283 K at some transportation pressures [4], [5]. Hydrates can form plugs in pipelines, either blocking valves, fouling up instrumentation or in the extreme case block the entire bore of the pipeline at a certain location. During depressurization the acceleration of a hydrate plug can cause structural damage to the pipeline wall in small radius bends [6]. Carbon dioxide is known to form structure I gas hydrates under the appropriate temperature and pressure conditions. As carbon dioxide is sub-critical at hydrate forming conditions and has a relatively low vapour pressure, different phases can be found in the hydrate-carbon dioxide-water system: a hydrate phase, a water rich liquid phase, an ice phase, a carbon dioxide rich vapour phase and a carbon dioxide rich liquid phase as well as two quadruple points. Experimental data for carbon dioxide hydrates have been measured and reported by various authors in the different hydrate regions. Data are widely available for the carbon dioxide/methane system. No experimental data were found in the open literature for $CO_2$ with oxygen, argon and $H_2S$. Data are available but limited to 1- 2 sources for $CO_2$ with nitrogen, hydrogen and carbon monoxide. Table 5.1 gives a list of these data, reporting temperature range and source of the experimental data. The aim of this study is to analyse the risk of hydrate formation in a rich carbon dioxide stream in a pipeline where the stream could be transported at a pressures up to 400 bars.

*Table 5.1 Literature data for hydrate equilibria of $CO_2$ and $CO_2$ mixtures*

| Comp. | Temperature Range | Type of equilibrium | $CO_2$/ mole fraction | Ref. |
|---|---|---|---|---|
| Pure $CO_2$ | 273.7 – 282.9 | V-L-H | | [7] |
| | 283.2 – 292.7 | $L_{CO2}$-V-H | | [8] |
| | 256.8 – 285 | I-V-H + V-L-H + $L_{CO2}$-V-H | | [9] |
| | 151.7– 192.5 | I-V-H | | [10] |
| | 194.5 – 217.8 | I-V-H | | [11] |
| | 277.2 – 283.1 | V-L-H | | [12] |
| | 273.9 – 283 .2 | V-L-H | | [13] |
| | 279.6 – 283.9 | V-L-H + $L_{CO2}$-V-H | | [14] |
| | 271.6 – 283.2 | V-L-H | | [15] |
| | 274.3 – 282.9 | V-L-H | | [16] |
| | 274.7 – 279.7 | V-L-H | | [17] |
| | 276.52 – 283.36 | V-L-H + $L_{CO2}$-V-H | | [18] |
| | 289.73 – 293.97 | $L_{CO2}$-V-H | | [19] |
| | 274.95 – 286.05 | V-L-H + $L_{CO2}$-V-H | | [20] |
| $CO_2/CH_4$ | 264.1 – 275.5 | V-L-H | ≈0.5 | [17] |
| | 275.5 – 285.7 | V-L-H | 0.274-0.824 | [21] |
| | 273.7– 287.6 | V-L-H | 0.08 to 0.85 | [22] |
| | 280.3 | V-L-H | 0 to 1 | [23] |
| | 273.5 – 283.1 | V-L-H | 0.13 - 0.53 | [24] |
| | 273.56 – 285.56 | V-L-H | 0 to 1 | [25] |
| | 272.66 – 285.76 | V-L-H | 0 to 1 | [26] |
| | 273.5 – 283.2 | V-L-H | 0.95 -0.9658 | [27] |
| | 275.9 – 277.7 | V-L-H | 0.06 – 0.25 | [28] |
| $CO_2/N_2$ | 273.1 – 280.2 | V-L-H | 0.91-0.97 | [17] |
| | 273.4 – 284.25 | V-L-H | 0 to 1 | [29] |
| | 272.85 – 284.25 | V-L-H | 0.07-0.97 | [30] |
| $CO_2/H_2$ | 274.15 – 283.23 | V-L-H | 0.5 | [31] |
| | 274.3 – 281.9 | V-L-H | 0.19-1 | [32] |
| | 273.9 – 281.9 | V-L-H | 0.4-0.83 | [33] |
| $CO_2/CO$ | 274.15 – 283.2 | V-L-H | 0.1 | [34] |

## 5.2 Experimental Section

### *5.2.1 Materials*

The following compounds were used to make the different synthetic mixtures studied in this work:

- Carbon Dioxide and Methane Supplied by Air Products, Research Grade
- Nitrogen, Argon, Oxygen, Hydrogen and Carbon monoxide Supplied by BOC, Research Grade.
- The water used was ultra pure water produced by an apparatus "PURELAB OPTION" made by ELGA and characterized up to 18.2 MΩ-cm resistance and a maximum organic carbon content of less than 10 ppb.

The binary mixtures of $CO_2$/impurities system are listed in Table 5.2. The mixtures were prepared gravimetrically (uncertainty ±0.3 mole %).

*Table 5.2 List of impurities composition used in the experiments*

| Impurity | $CO_2$ | Mole% |
|---|---|---|
| Nitrogen | Balance | 4.6% |
| Methane | | 5.9% |
| Carbon monoxide | | 5.9% |
| Oxygen | | 5.3% |
| Argon | | 5.0% |
| Hydrogen | | 7.1% |

### *5.2.2 Apparatus*

An autoclave rig with 300 $cm^3$ volume was used in this work. The basic rig design is comprised of a high pressure cell fitted with a magnetic mixer with a maximum rotation speed of 1,500 revolutions per minute giving good mixing to the cell contents. The rig is surrounded by a jacket through which coolant is circulated using a refrigerated circulator. The rig is well insulated and can be used at temperatures in the range of 233 to 333 K and at pressures up to 60 MPa. The pressure is measured using a strain gauge pressure transducer. The temperature is measured using a Platinum Resistance

Temperature (PRT) Probe. A schematic of the hydrate mixed autoclave rig is shown in Figure 5.1.

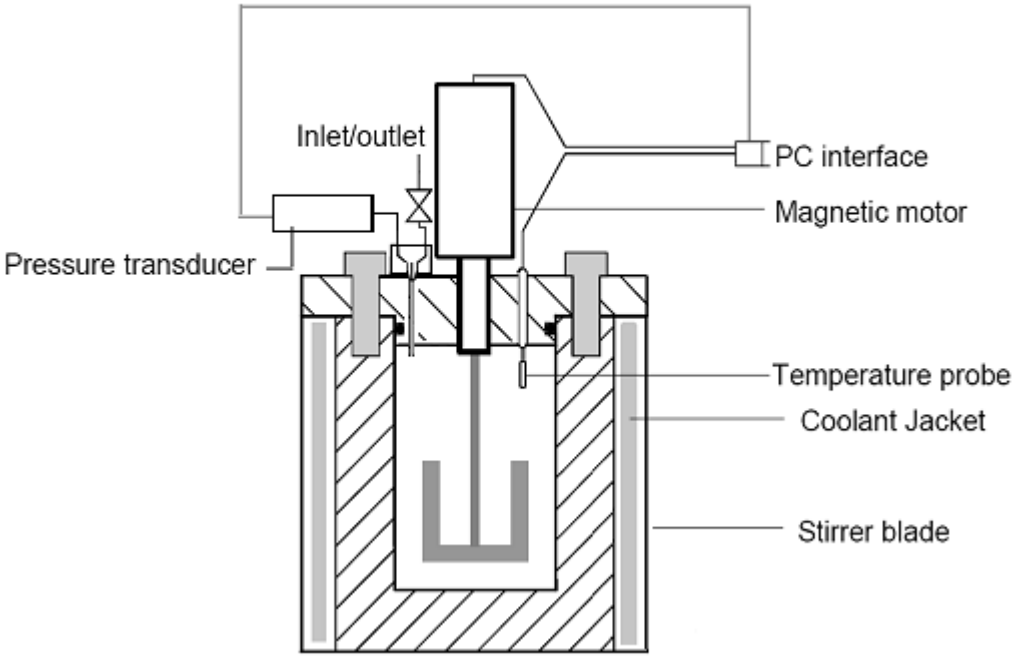


*Figure 5.1 Schematic of hydrate mixed autoclave rig*

### *5.2.3 Procedures*

The equilibrium cell and its loading lines are vacuumed prior to introduction of about 90 $cm^3$ deionised water. Then, $CO_2$ or $CO_2$ rich gas is introduced into the cell directly from a pressurized cylinder (through preliminary evacuated transfer lines) to a pressure corresponding to the pressure of the first measurement. Pressure and temperature are initially set to a point well outside the expected hydrate stability zone for the system under study. After introduction of the gas into the cell, stirring of the cell is started, to accelerate equilibrium in the system. The temperature is then lowered to form hydrates well inside the hydrate stability zone, i.e. ~-5 ºC. After the hydrate formation is observed (sudden pressure drop is observed in the system), the temperature is increased step-wise and the dissociation point is detected by the sudden change (break point) in pressure/temperature profile. The other dissociation points corresponding to the higher pressures were determined by injecting more gas and the above steps are repeated.

### 5.3 Modelling Section

A general phase equilibrium model based on the equality of component fugacities in all phases has been used to model the phase behaviour of the carbon-dioxide water system. A description of the thermodynamic model can be found elsewhere [35]. In summary, the statistical thermodynamics model uses the Valderrama modification of the Patel and Teja (*VPT-EoS*) equation of state [36] and non-density-dependent (*NDD*) mixing rules [37] for fugacity calculations in all fluid phases. A detail of the VPT EOS is given in Chapter 2. BIPS between $CO_2$ and $N_2$, $H_2$, CO, $O_2$ Ar and $CH_4$ were tuned using the data listed in Table 5.3. BIPS between $H_2$, $N_2$ and CO were set to zero. Binary interaction parameters (BIPS) between water and some of these components can be found elsewhere [38].

*Table 5.3 VLE and BP data for binary $CO_2$/impurities system*

| Mixtures | Source |
|---|---|
| $CO_2/N_2$ | [39]-[54] |
| $CO_2/CH_4$ | [42], [43], [46], [49], [52], [55]-[63] |
| $CO_2/O_2$ | [51], [64] |
| $CO_2/H_2$ | [41],[51], [65]- [68] |
| $CO_2$/Ar | [69], [70] |
| $CO_2$/CO | [71], [72] |

The hydrate phase is modelled using the solid solution theory of van der Waals and Platteeuw [73], as developed by Parrish and Prausnitz [74]. The equation recommended by Holder *et al.* [75] is used to calculate the heat capacity difference between the empty hydrate lattice and pure liquid water. The Kihara model for spherical molecules is applied to calculate the potential function for compounds forming hydrate phases [76].The fugacity of water in the hydrate phase is given by:

$$f_w^H = f_w^\beta \exp\left(-\frac{\Delta\mu_w^{\beta-H}}{RT}\right) \tag{5.1}$$

Where $H$, $\beta$ and $\mu$ refer to hydrate, empty hydrate lattice and chemical potential respectively. $\Delta\mu_w^{\beta-H}$ is the chemical potential difference of water between the empty hydrate lattice ( $\mu_w^{\beta}$ ) and the hydrate phase ( $\mu_w^{H}$ ). It is defined as following:

$$\Delta\mu_w^{\beta-H} = \mu_w^{\beta} - \mu_w^{H} = RT\sum_m \bar{v}_m \ln\left(1+\sum_j C_{mj} f_j\right) \tag{5.2}$$

Where $\bar{v}_m$ is the number of cavities of type $m$ per water molecule. $f_j$ is the fugacity of the gas component $j$. $C_{mj}$ is the Langmuir constant, which accounts for the gas-water interaction in the cavity. The relation for the Langmuir constant can be developed from the potential energy and numerical values for the Langmuir constant can be calculated by choosing a model for the guest-host interaction:

$$C_{mj}(T) = \frac{4\pi}{kT}\int_0^{\infty} \exp\left[-\frac{w(r)}{k^{'}T}\right] r^2 dr \tag{5.3}$$

Where $k$ and $w(r)$ are Boltzmann's constant and the spherically symmetric cell potential in the cavity with $r$ measured from the centre. Holder et al. [75] showed that the chemical potential difference of water between the empty hydrate lattice and the liquid phase can be defined as following:

$$\frac{\Delta\mu_w^{\beta-L}}{RT} = \frac{\Delta\mu_w^{0}}{RT_0} - \int_{T_0}^{T}\frac{\Delta h_w^{\beta-L}}{RT^2}dT + \int_{P_0}^{P}\frac{\Delta v_w^{\beta-L}}{RT}dP \tag{5.4}$$

Where 0 superscript stands for reference property. $v$ and $h$ refer to molar volume and enthalpy respectively. $\Delta\mu_w^0$ is the reference chemical potential difference between water in the empty hydrate lattice and pure water at 273.15 K.

### 5.4 Results & Discussion

The hydrate formation pressures of pure $CO_2$ in water were measured and compared with the data reported in the above literature (Table 5.1) in order to validate the

experimental apparatus and procedures. Figure 5.2 shows the experimental and predicted phase boundaries for carbon dioxide hydrates. As can be seen, the model predictions are in good agreement with our experimental data and the data collected from the open literature, demonstrating the validation to our experimental work and the reliability of the thermodynamic model. Our experimental data were found to be consistent with the data reported by Deaton and Frost [7] below the system saturation pressure and are also consistent with Ng and Robinson [14] data above the saturation pressure.

The three phases HLV equilibria of the ternary $CO_2$ + ($N_2$ or $CH_4$ or $O_2$ or Ar or $H_2$ or CO) + water systems were determined at a constant composition (4.56% $N_2$, 7.09% $H_2$, 5.85% $CH_4$, 5.87% CO, 5.03% Ar, and 5.34% $O_2$ in dry basis). The mixture hydrates formed over the wide temperature and pressure ranges of 276-288 K and 2-15 MPa.

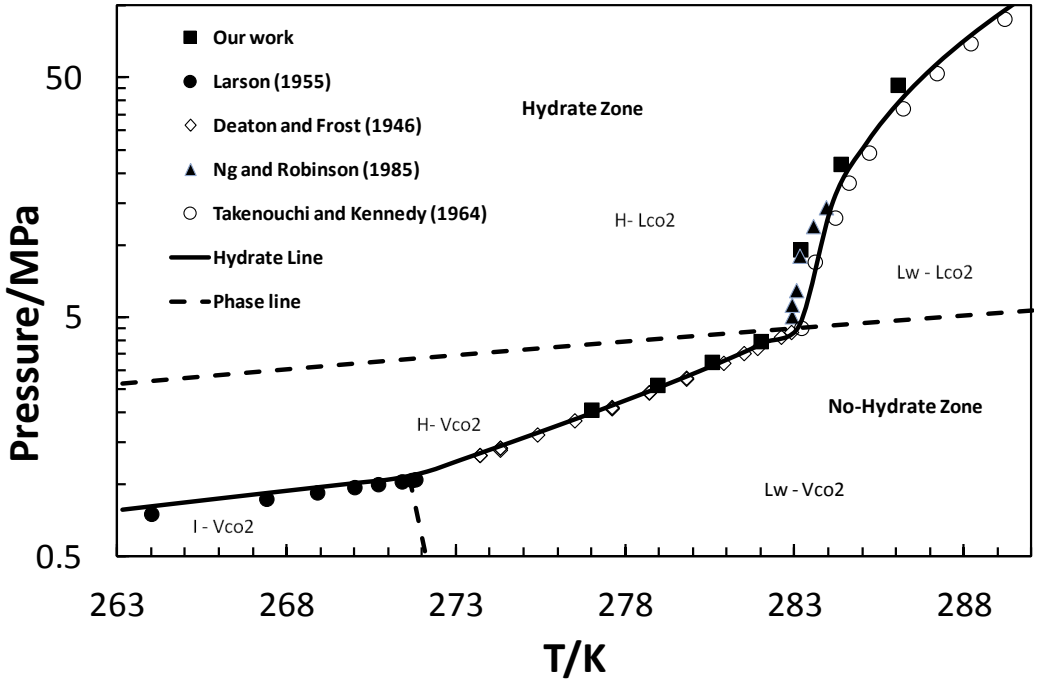


*Figure 5.2 Hydrate phase equilibria of the binary $CO_2$ + water mixtures*

*Table 5.4 Equilibrium hydrate dissociation pressure for the $CO_2$/impurities mixtures*

| Pure $CO_2$ | | | $CO_2/N_2$ | | | $CO_2/H_2$ | | |
|---|---|---|---|---|---|---|---|---|
| T/K | P/MPa | Aqueous Fraction | T/K | P/MPa | Aqueous fraction | T/K | P/MPa | Aqueous fraction |
| 278.95 | 2.60 | 0.94 | 276.91 | 2.05 | 0.96 | 274.45 | 1.64 | 0.97 |
| 277.00 | 2.05 | 0.96 | 279.65 | 2.82 | 0.94 | 275.45 | 1.85 | 0.96 |
| 280.56 | 3.24 | 0.93 | 281.23 | 3.66 | 0.92 | 280.55 | 3.33 | 0.93 |
| 282.00 | 3.96 | 0.91 | 283.64 | 5.72 | 0.86 | 284.05 | 6.83 | 0.85 |
| 283.17 | 9.58 | 0.53 | 287.40 | 40.82 | 0.51 | 285.65 | 12.69 | 0.56 |
| 284.36 | 21.79 | 0.52 | 288.55 | 55.11 | 0.50 | 286.75 | 16.51 | 0.55 |
| 286.05 | 46.65 | 0.50 | | | | | | |
| $CO_2/CH_4$ | | | $CO_2/CO$ | | | $CO_2/O_2$ | | |
| T/K | P/MPa | Aqueous Fraction | T/K | P/MPa | Aqueous Fraction | T/K | P/MPa | Aqueous Fraction |
| 276.00 | 1.82 | 0.96 | 273.15 | 1.38 | 0.97 | 276.75 | 2.05 | 0.96 |
| 279.20 | 2.68 | 0.94 | 278.35 | 2.63 | 0.94 | 278.85 | 2.68 | 0.94 |
| 281.35 | 3.61 | 0.92 | 280.75 | 3.64 | 0.92 | 281.75 | 4.05 | 0.91 |
| 284.15 | 5.81 | 0.57 | 283.85 | 6.69 | 0.83 | 284.01 | 7.04 | 0.56 |
| 285.75 | 12.25 | 0.54 | 284.75 | 11.63 | 0.55 | 285.25 | 13.19 | 0.54 |
| 286.95 | 19.97 | 0.53 | 285.85 | 21.30 | 0.53 | 285.75 | 18.33 | 0.53 |
| 285.75 | 12.25 | 0.54 | | | | | | |
| $CO_2$/Ar | | | | | | | | |
| T/K | P/MPa | Aqueous Fraction | | | | | | |
| 275.45 | 1.72 | 0.97 | | | | | | |
| 280.55 | 3.22 | 0.93 | | | | | | |
| 284.05 | 5.81 | 0.85 | | | | | | |
| 285.25 | 11.26 | 0.55 | | | | | | |
| 285.65 | 16.07 | 0.53 | | | | | | |

*The measured equilibrium data together with their predictions are plotted in Figure Figure 5.8. In the same plots, the vapour liquid equilibrium lines for all binary mixtures are plotted together with the HLV and HLL lines produced by VPT EOS model. The quadruple points where ice, liquid vapour, and hydrate (I + V + L + H) coexist for all*

*systems has been defined by the model. The quadruple point is noted by the phases that are in equilibrium and it has been evaluated by the model. The experimental results of the equilibrium hydrate dissociation pressure for the $CO_2$/impurities mixtures are also listed in Table 5.4*

Table 5.4. The aqueous fraction is the water ratio of water to the fluid mixture in the cell. As simple hydrates, $CO_2$ and $N_2$ form SI and SII, respectively [78]. The mixed hydrate structure is considered to be either SI or SII depending on the relative ratio of these two different gas molecules occupied in the small and large cavities. According to the literature [77], 15 mol% of $CO_2$ gaseous mixture was known as the boundary of coexisting SI and SII hydrate. For rich $N_2$, Seo and Lee [78] had the same conclusion where SI is crystallized at the gas mixture composition range of 3-20 mol % $CO_2$ and transformed to SII at 1 mol%. As generally expected, the hydrate formation line is located between two pure $CO_2$ and $N_2$ HLV lines, and the overall experimental data were well predicted by the thermodynamic model. The binary mixture containing 4.56 mol% $N_2$ is found slightly higher than that of pure $CO_2$ HLV phase. Phase equilibrium relations for the ternary system of $H_2$+$CO_2$+$H_2O$ in the presence of hydrate phase have been investigated. It is well known that $H_2$ is too small to stabilize cavities any hydrates by itself except for a high-pressure region of the GPa order where it can form SII clathrate hydrates [79-80], that is, $H_2$ almost never contribute to the stability of hydrate cage. The gas hydrate obtained from the $H_2$+$CO_2$ mixture has been analyzed previously [81] by use of Raman spectroscopy. The results reveal that $H_2$ is not enclathrated in the hydrate-cages at low pressure. That is, $H_2$ behaves only like a diluent gas toward the formation of $CO_2$ hydrate. The experimental results obtained in the current study (Table 5.4 and Figure 5.4) indicate that the hydrate dissociation pressures (HLV) from the $CO_2$/$H_2$ binary mixture are greater than those for pure $CO_2$. Kumar et al. [33] found that the increase of hydrogen in the gas mixture tends to shift the equilibrium to higher pressures at a given temperature. They reported that the mixture $CO_2$/$H_2$ forms SI like that formed by pure $CO_2$.

Both methane and carbon dioxide form SI hydrate. Phase diagram for $CH_4$/$CO_4$ hydrate is shown next to the previous mentioned mixtures in Figure 5.5. The HLV curve of the

mixture was found to locate between the carbon dioxide and methane hydrates curves. At a fixed temperature, the phase boundary (HLV) of $CO_2$ hydrate is shifted to higher pressures by adding 5.85% $CH_4$. Seo and Lee [25] indicated that in rich $CO_2$ mixture (above 60 mol% $CO_2$) the HLV curves of the mixed hydrates closely moved towards that of the simple carbon dioxide hydrate. Three HLV phase equilibrium data have been measured by Mohammadi et.al [34] for 10%$CO_2$+CO mixture. The mixture formed is SI and they plotted the data together with both pure $CO_2$ and pure CO. No literature was found for the other ternary $CO_2$/impurities (Ar, $O_2$)-water mixtures. According to [82], formation of SH is established for the argon-water system by using differential thermal analysis while $O_2$ forms SII [83, 84]. In our calculations, the rich $CO_2$-water mixture is assumed to be structure I under the temperature conditions investigated in this work.

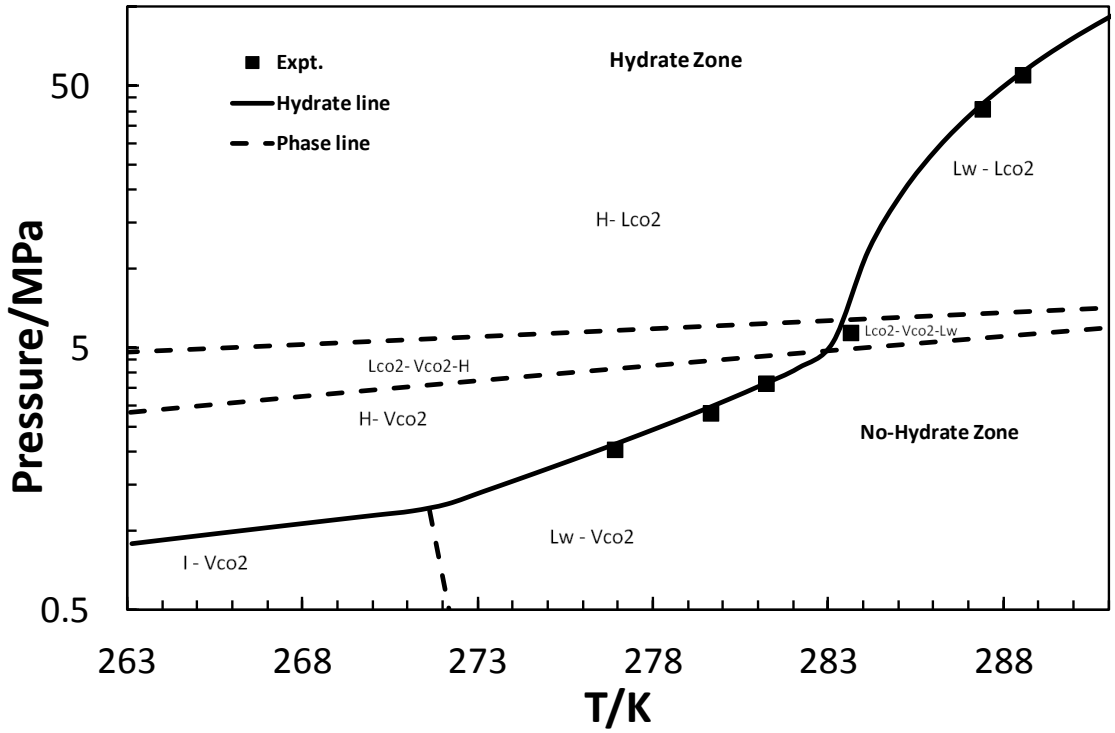


*Figure 5.3 Hydrate phase equilibria of the ternary $CO_2$ + $N_2$ + water mixtures*

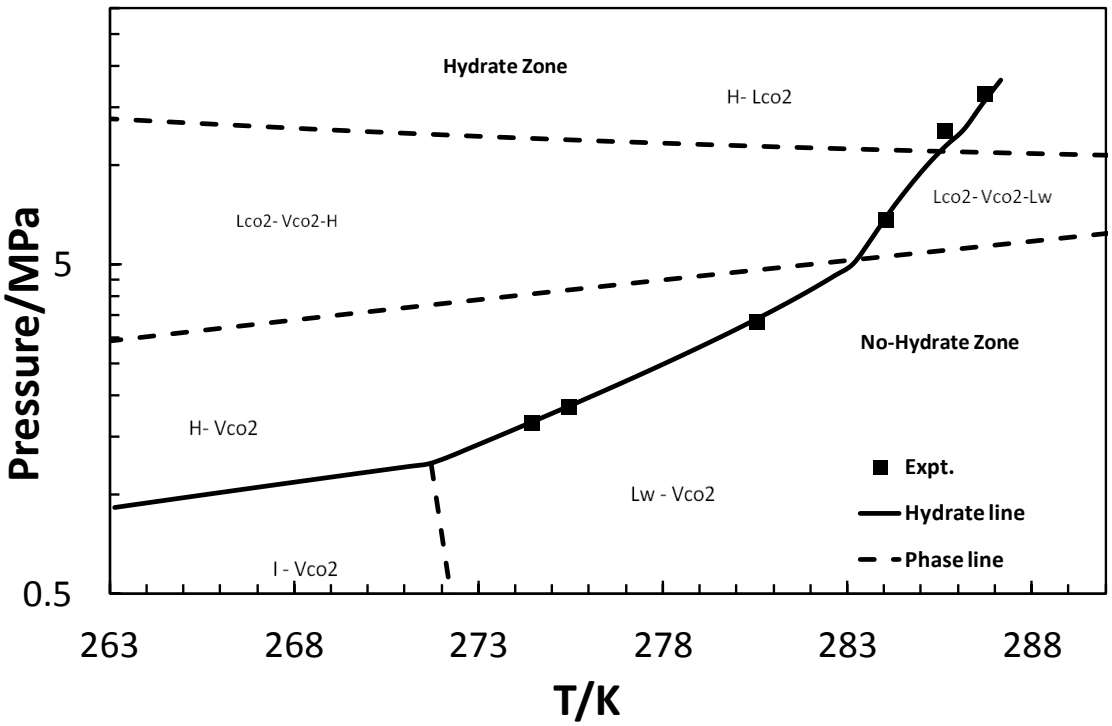


*Figure 5.4 Hydrate phase equilibria of the ternary $CO_2$ + $H_2$ + water mixtures*

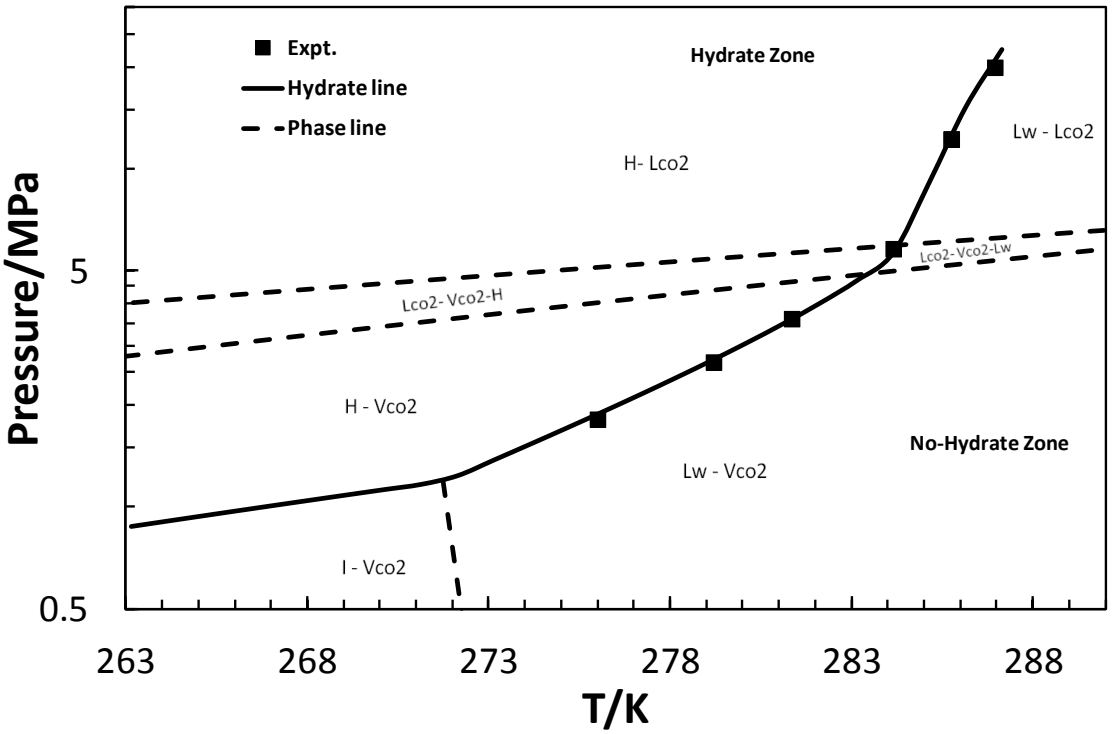


*Figure 5.5 Hydrate phase equilibria of the ternary $CO_2$ +$CH_4$ + water mixtures*

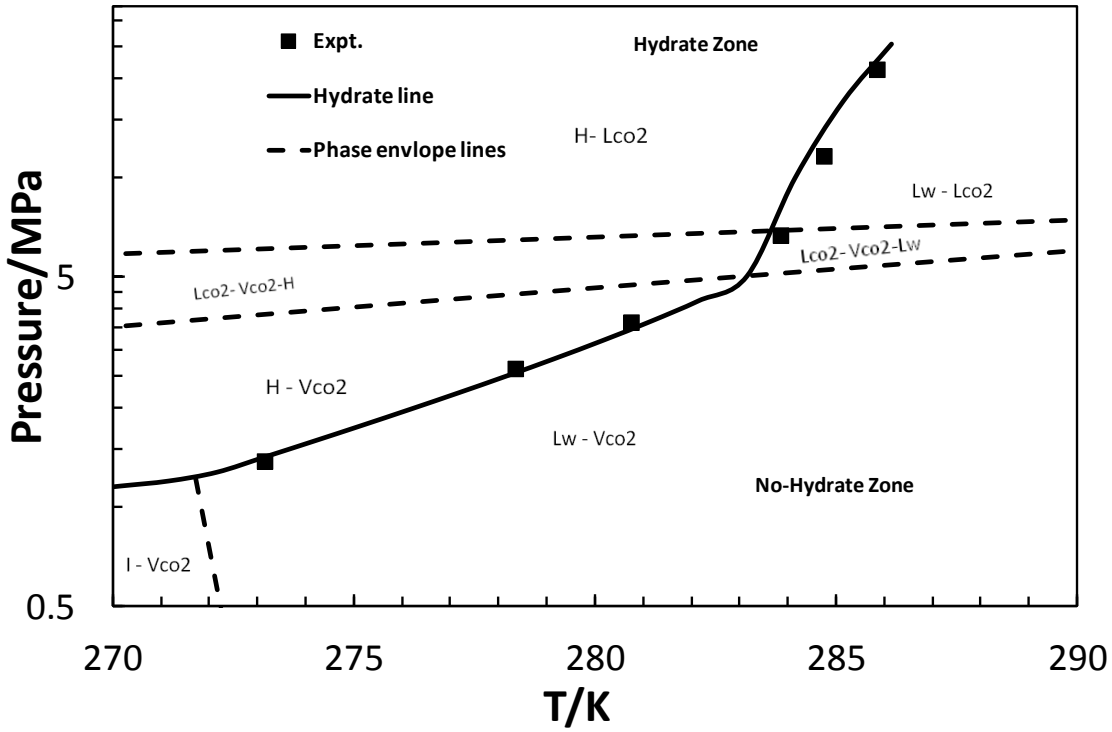


*Figure 5.6 Hydrate phase equilibria of the ternary $CO_2$ + CO + water mixtures*

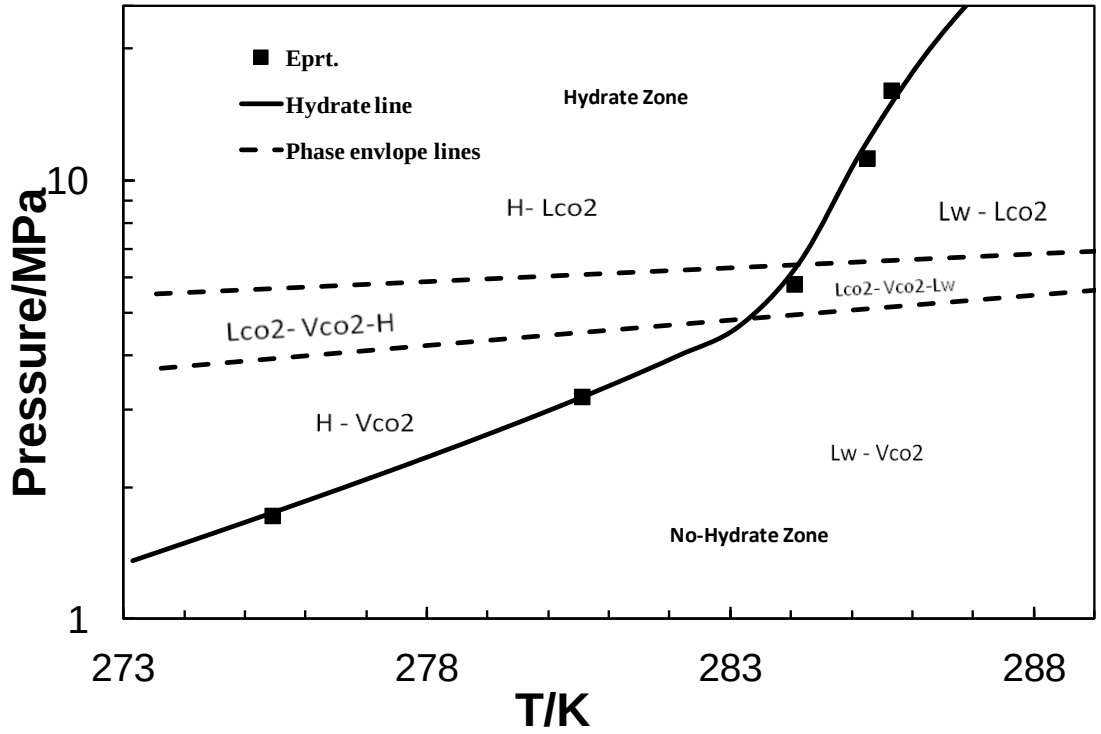


*Figure 5.7 Hydrate phase equilibria of the ternary $CO_2$ + Ar + water mixtures*

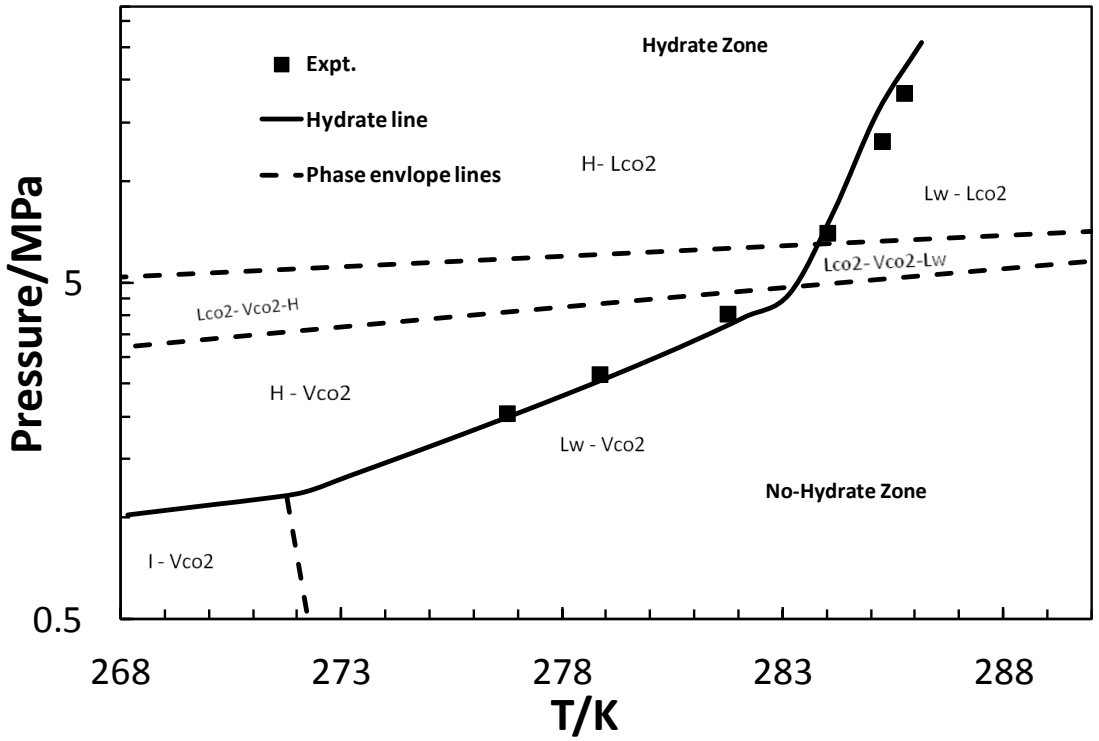


*Figure 5.8 Hydrate phase equilibria of the ternary $CO_2$ + $O_2$ + water mixtures*

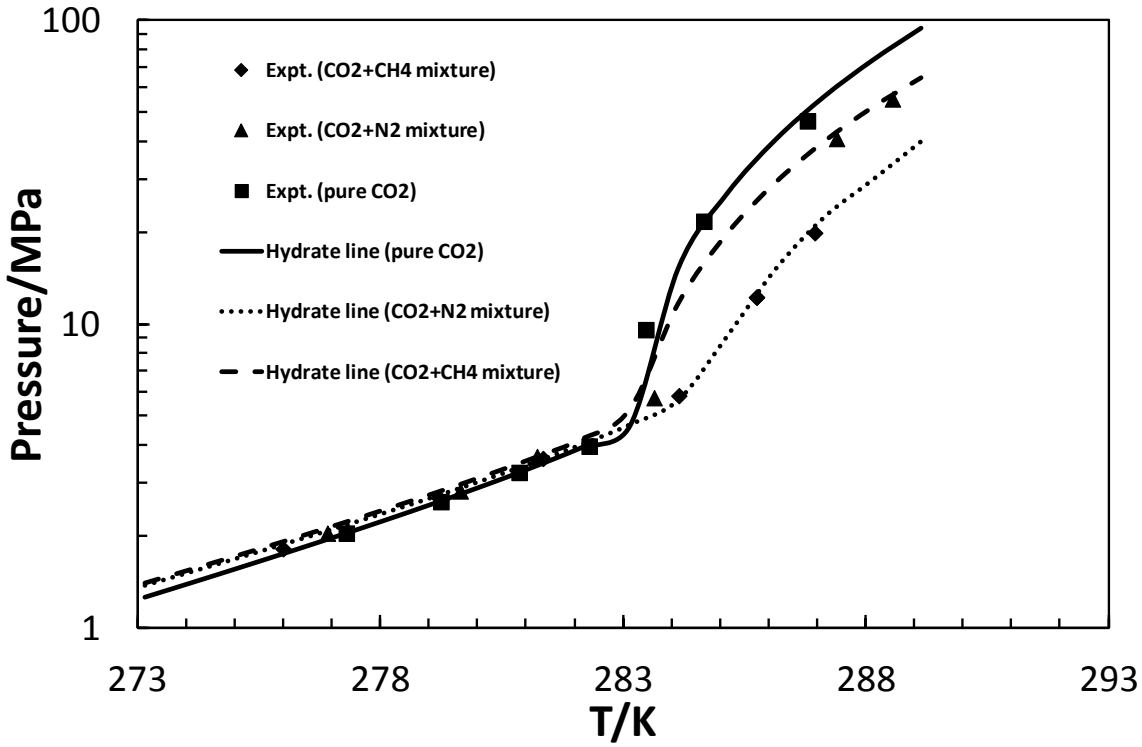


*Figure 5.9 Effects of impurities on the hydrate phase equilibria of $CO_2$*

At the composition of the gas mixtures systems, HLV equilibrium lines compared to the pure $CO_2$ were shifted slightly to higher pressure and lower temperature domain. In the other hand at higher pressure, above the bubble point of the systems, HLL equilibrium lines were shifted to lower pressure and higher temperature domain. The increase stability of the hydrate zone of $CO_2$ is higher in the presence of methane. The effect is less significant in the presence of nitrogen as shown in Figure 5.9. The other impurities (Ar, $O_2$, CO and $H_2$) seem to follow closely the hydrate phase path of the $CO_2/N_2$ system. In the vapour region the increase in the hydrate stability pressure of pure $CO_2$ is within 5%. In liquid region, at 288 K the reduction of the hydrate stability pressure can reach 60% in the $CO_2/CH_4$ mixture. At the same condition, the reduction in pressure of the hydrate stability zone for the other impurities excluding methane is between 28 to 35%.

## 5.5 Conclusions

In the work, the effects of impurities ($CH_4$, $N_2$, $O_2$, $H_2$, CO and Ar) on the hydrate stability conditions of $CO_2$ were determined. The hydrate equilibrium pressures were increased apparently with addition of the tested impurities in the vapour region. The effect of the tested impurities can be classified into two groups. Methane, as one group, tends to increase the hydrate pressure at constant temperature by double the increase achieved by the other impurities ($N_2$, $O_2$, $H_2$, CO and Ar) as second group. In the work, the VPT equation of state in conjunction with the van der Waals–Platteeuw model was used to predict successfully the hydrate dissociation conditions of $CO_2$ and six $CO_2$ binary mixtures. A good agreement between the predicted and experimental data was found.

**References**

[1] IEA Greenhouse Gas R&D Programme (IEAGHG), 2012, *Effects of Impurities on Geological Storage of $CO_2$*, Retrieved 03-26-2012.

[2] Kather, A., Presented at 2nd Working Group Meeting, 2009, *$CO_2$ Quality and Other Relevant Issues*, September 2009, Cottbus, Germany.

[3] Anheden M., Andersson A., Bernstone, C., Eriksson, S., Yan, J., Liljemark, S. and Wall, C., 2004, *$CO_2$ Quality Requirement for a System with $CO_2$ Capture, Transport and Storage*, The 7th International Conference on Greenhouse Gas Control Technologies (GHGT7), Vancouver, Canada.

[4] De Visser, E., Hendriks, C., Barrio, M., Mølnvik, M.J ., de Koeijer, G., Liljemark, S. and Le Gallo, Y., 2008, *Dynamis $CO_2$ Quality Recommendations*, International Journal of Greenhouse Gas Control 2., **4**, 478-484.

[5] Odru, P., Broutin, P., Fradet, A., Saysset, S., Ruer, J. and Girod, L., 2006, *Technical and Economic Assessment of $CO_2$ Transportation*, In: Institute France Petrole, Work Supported by the French Agency ADEME, Abstract Submitted to the GHGT-8 Conference in Trondheim, France

[6] Oosterkamp, A. and Ramsen, J., 2008, *State-of-the-Art Overview of $CO_2$ Pipeline Transport with Relevance to Offshore Pipelines*, Polytec Report No. POL-O-2007-138-A.

[7] Deaton, W. M. and Frost, Jr. E. M., 1946, *Gas Hydrate Composition and Equilibrium Data*, Oil & Gas J., **45**, 170-178.

[8] Takenouchi, S. and Kennedy, G. C., 1964, *The Binary System $H_2O$-$CO_2$ at High Temperatures and Pressures*, Am. J. Sci., 262, 1055-1074.

[9] Larson, S. D., 1955, *Phase Studies of the Two-Component Carbon Dioxide Water System Involving the Carbon Dioxide Hydrate*, PHD Thesis, U. Illinois.

[10] Miller, S. L., 1961, *The Occurrence of Gas Hydrates in the Solar System*, Proc. Natl. Acad. Sci., **47**, 1798-1808.

[11] Falabella, B.J., 1975, *.A Study of Natural Gas Hydrates, Dissertation*, U. Massachusetts.

[12] Unruh, C. H. and Katz, D. L., 1949, *Gas-Hydrate of Carbon Dioxide-Methane Mixtures*, J. Pet. Technol., **1**, 83-86.

[13] Robinson, D. B. and Mehta, B. R., 1971, *Hydrates in The Propane -Carbon Dioxide-Water System*, J. Can. Pet. Technol., **10**, 33-35.

[14] Ng, H. and J., Robinson, D. B., 1985, *Hydrate Formation in System Containing Methane, Ethane, Propane, Carbon Dioxide or Hydrogen Sulphide in the Presence of Methanol*, Fluid Phase Equilib., **21**, 145-155.

[15] Vlahakis, J. G., Chen, H. -S., Suwandi, M. S. and Bardhum, A. J., 1972, *The Growth Rate of Ice Crystals: Properties of Carbon Dioxide Hydrate, a Review of 51 Gas Hydrates,* Syracuse U. Research and Development Report 830, US Department of Interior.

[16] Adisasmito, S. and Sloan, Jr., E. D., 1992, *Hydrates of Hydrocarbon Gases Containing Carbon Dioxide*, J. Chem. Eng. Data., **37**, 343-349.

[17] Fan, S. S. and Guo, T. M., 1999, *Hydrate Formation of $CO_2$-Rich Binary and Quaternary Gas Mixtures in Aqueous Sodium Chloride Solutions*, J. Chem. Eng. Data, **44,** 829-832.

[18] Mooijer-van den Heuvel, M. M., Witteman, R. and Peters, C. J., 2001, *Phase Behaviour of Gas Hydrates of Carbon Dioxide in the Presence of Tetrahydropyran, Cyclobutanone, Cyclohexane and Methylcyclohexane*, Fluid Phase Equilib., **182**, 97-110.

[19] Nakano, S., Moritoki, M. and Ohgaki, K., 1998, *High-Pressure Phase Equilibrium and Raman Microprobe Spectroscopic Studies on the $CO_2$ Hydrate System*, J Chem. Eng. Data., **43**, 807-810.

[20] Chapoy, A., Burgass, R., Tohidi, B., Austell, J. M. and Eickhoff, C., 2009, *Effect of Common Impurities on the Phase Behaviour of Carbon Dioxide Rich Systems: Minimizing the Risk of Hydrate Formation and Two Phase Flow*, Offshore Europe, Aberdeen, Scotland.

[21] Unruh, C. H. and Katz, D. L., 1949, *Gas Hydrates of Carbon Dioxide-Methane Mixtures*, J. Petroleum Technology Transactions, **1**, 83-86.

[22] Adisasmito, S., Frank, R. J. and Sloan, E.D. J., 1991, *Hydrates of Carbon Dioxide and Methane Mixtures*, J. Chem. Eng. Data, **36**, 68-71.

[23] Ohgaki, K., Takano, K., Sangawa, H., Matsubara, T. and Nakano, S., 1996, *Methane Exploitation by Carbon Dioxide from Gas Hydrates: Phase Equilibria for $CO_2$-$CH_4$ Mixed Hydrate System*, J. Chem. Eng. Jpn., **29**, 478-483.

[24] Servio, P., Lagers, F., Peters, C. J. and Englezos, P., 1999, *Gas Hydrate Phase Equilibrium in the System Methane Carbon Dioxide Neohexane and Water*, Fluid Phase Equilib., **158**, 795-800.

[25] Seo, Y. -T, Lee, H. and Yoon, J. -H, 2001, *Hydrate Phase Equilibria of the Carbon Dioxide, Methane, and Water System*, J. Chem. Eng. Data, **46**, 381-384.

[26] Seo, Y. -T. and Lee, H., 2001, *Multiple-Phase Hydrate Equilibria of the Ternary Carbon Dioxide, Methane, and Water Mixtures*, J. Phys. Chem., **105**, 10084-10090.

[27] Dholabhai, P. D. and Bishnoi, P. R., 1994, *Hydrate Equilibrium Conditions in Aqueous Electrolyte Solutions: Mixtures of Methane and Carbon Dioxide*, J. Chem. Eng. Data, **39**, 191-194.

[28] D. G., Elliot, J. J., Chen, 1997,.*Process for Separating Selected Components from Multi-Component Natural Gas Streams*, United States of America Patent WO 97/09271, World International Property Organization.

[29] Olsen, B., Majumdar, A. J. and Bishnoi, P. R., 1999, *Experimental Studies on Hydrate Equilibrium Carbon Dioxide and its Systems*, Int. J. The Soc. of Mat. Eng. for Resources, **7**, 17-23.

[30] Kang, S. -P., Lee, H., Lee, C. -S. and Sung, W. -M., 2002, *Hydrate Phase Equilibria of the Guest Mixtures Containing $CO_2$, $N_2$ and Tetrahydrofuran*, Fluid Phase Equilib., **185**, 101-109.

[31] Ng., H. J. and Robinson, D. B., 1984, *Hydrate Formation Conditions in the Presence of Hydrogen*, Present at the AIChE Meeting, Atlanta, Georgia.

[32] Sugahara, T., Murayama, S., Hashimoto, S. and Ohgaki, K., 2005, *Phase Equilibria for $H_2$ +$CO_2$+$H_2O$ System Containing Gas Hydrates*, Fluid Phase Equilib., **233**, 193-196.

[33] Kumar, K., Wu, H -J. and Englezos, P., 2006, *Incipient Hydrate Phase Equilibrium for Gas Mixtures Containing Hydrogen, Carbon Dioxide and Propane*, Fluid Phase Equilib., **244**, 167-171.

[34] Mohammadi, A. H., Anderson, R. and Tohidi, B., 2005, *Carbon Monoxide Clathrate Hydrates: Experimental Equilibrium Data and Thermodynamic Modeling*, AICHE J. **51**, 2825-2833.

[35] Chapoy, A., Mohammadi A. H.,, Chareton, A., Richon, D., Tohidi, B., 2004), *Measurement and Modeling of Gas Solubility and Literature Review of the Properties for the Carbon Dioxide - Water System*, Ind. Eng. Chem., **43**, 1794-1802.

[36] Valderrama, J. O., 1990, *A Generalized Patel-Teja Equation of State for Polar and Non-Polar Fluids and Their Mixtures*, J. Chem. Engng Japan, **23**, 87-91.

[37] Avlonitis, D., Danesh, A. and Todd, A. C., 1994, *Prediction of VL and VLL Equilibria of Mixtures Containing Petroleum Reservoir Fluids and Methanol with a Cubic Eos*, Fluid Phase Equilib., **94**, 181-216.

[38] Chapoy, A., Haghighi, H. and Tohidi, B., 2008, *Development of a Henry's Constant Correlation and Solubility Measurements of N-Pentane, I-Pentane, Cyclopentane, N-Hexane and Toluene in Water*, Journal of Chemical Thermodynamics, **40**, 1030-1037.

[39] Yorizane, M., Yoshimura, S., Masuoka, H. and Miyano, Y., 1985, *New Procedure for Vapour-Liquid Equilibria. Nitrogen + Carbon Dioxide, Methane + Freon 22, and Methane +Freon 12*, J. Chem. Eng., **30**, 174-176.

[40] Yorizane, M., Yoshimura, S., Masuoka, H. and Nakamura, M., 1971, *Prediction of High Pressure Vapor-Liquid Equilibria for Multicomponent Systems by the BWR Equation of State*, J. Chem. Eng. Jpn., **4**, 10-16.

[41] Yorizane, M., 1971, *Determination of Vapor-Liquid Equilibrium Data at High Pressure and Low Temperature*, Kenkyu HokokusAsahi Garasu Kogyo Gijutsu Shoreikai, **18**, 61-76.

[42] Xu, N., Dong, J., Wang, Y. and Shi, J., 1992, *High Pressure Vapor Liquid Equilibria at 293 K for Systems Containing Nitrogen, Methane And Carbon Dioxide*, Fluid Phase Equilib., **81**, 175-186.

[43] Somait, F. A. and Kidnay, A. J., 1978, *Liquid-Vapor Equilibria at 270.00 K for Systems Containing Nitrogen, Methane, and Carbon Dioxide*, J. Chem. Eng. Data, **23**, 301-305.

[44] Muirbrook, N.K, Prausnitz, J.M., 1965, *Multicomponent Vapor-Liquid Equilibria at High Pressure*, AIChE J., **6**, 1092-1102.

[45] Zenner, G. H. and Dana, L. I., 1963, *Liquid-Vapor Equilibrium Compositions of Carbon Dioxide-Oxygen-Nitrogen Mixtures*, Chem. Eng. Progr. Symp. Ser., **44**, 36-41.

[46] Al-Sahhaf, T. A., Kidnay, A. J. and Sloan, E. D., 1983, *Liquid + Vapor Equilibria in the $N_2$ + $CO_2$ + $CH_4$ System*, Ind. Eng. Chem. Fundam., **22**, 372-380.

[47] Brown, T. S., Niesen, V. G., Sloan, E. D. and Kidnay, A. J., 1989, *Vapor-Liquid Equilibria for the Binary Systems of Nitrogen, Carbon Dioxide, and N-Butane at Temperatures from 220 to 344 K*, Fluid Phase Equilib., **53**, 7-14.

[48] Weber, W., Zeck, S. and Knapp, H., 1984**,** *Gas Solubilities in Liquid Solvents at High Pressures**:** Apparatus and Results for Binary and Ternary Systems of $N_2$**,** $CO_2$ and $CH_3OH$*, Fluid Phase Equilib., **18**, 253-278.

[49] Arai, Y., Kaminishi, G. -I. and Saito, S., 1971, *The Experimental Determination of the P-V-T-X (Pressure-Volume-Temperature- Composition) Relations for the Carbon Dioxide - Nitrogen and the Carbon Dioxide – Methane Systems*, J. Chem. Eng. Jpn., **4**, 113-122.

[50] Krichevskii, I. R. and Khazanova, N. E., 1962, *Liquid-Gas Equilibrium in the Nitrogen-Carbon Dioxide System under Elevated Pressures*, Khim. Promst.(Moscow), **7**, 169-171.

[51] Kaminishi, G. I. and Toriumi, T., 1966), *Vapor-Liquid Phase Equilibrium in the CO-$H_2$, $CO_2$-$N_2$, and $CO_2$-$O_2$ Systems*, Kogyo Kagaku Zasshi, **69**, 175-178.

[52] Bian, B., Wang, Y. and Shi J., 1993, *Simulteanous Determination of Vapour-Liquid Equilibrium and Molar Volumes for Coexisting Phases up to Critical Temperature with a Static Method*, Fluid Phase Equilib., **90**, 177-187.

[53] Wilson, G. M., Cunningham, J. R. and Nielsen, P. F., 1977, *Enthalpy and Phase Boundary Measurements on Mixtures of Nitrogen with Methane, Carbon*

*Dioxide and Hydrogen Sulfide*, Gas Processors Association, Research Report RR-24.

[54] Duarte-Garza, H. A., Holste, J. C., Hall, K. R. and Marsh, K. N, 1995, ***Isochoric*** *PVT and Phase Equilibria Measurements for Carbon Dioxide + Nitrogen*, J. Chem. Eng. Data, **40**, 704-711.

[55] Donnelly, H. G. and Katz, D. L., 1954, *Phase Equilibrium in the Carbon Dioxide-Methane System*, Ind. Eng. Chem., 46, 511-517.

[56] Pavlicek, J. and Richter, M., 1993, *High Pressure Vapour-Liquid Equilibrium in the Carbon Dioxide– A-Pinene System*, Fluid Phase Equilib., **90**, 125-133.

[57] Mraw, S. C., Hwang, S. C and Kobayashi, R., 1978, *Vapor-Liquid Equilibrium of the Methane-Carbon Dioxide System At Low Temperatures*, J. Chem. Eng. Data, **23** 135-139.

[58] Wei, M. S., Brown, T. S., Kidnay, A. J. and Sloan, E.D., 1995, *Vapor + Liquid Equilibria for the Ternary System Methane + Ethane + Carbon Dioxide at 230 K and its Constituent Binaries at Temperatures from 207 To 270 K*, J.Chem.Eng.Data, **40**, 726-731.

[59] Neumann, A. and Walch, W., 1968, *Vapour-Liquid Equilibrium Carbon Dioxide + Methane at Low Temperatures and the Region of Low Carbon Dioxide Mole Fractions*, Chem.-Ing.-Tech., **40**, 241-244.

[60] Davalos, J., Anderson, W. R., Phelps, R. E. and Kidnay, A. J., 1976, *Liquid-Vapor Equilibria at 150.00K for Systems Containing Methane, Ethane and Carbon Dioxide*, J. Chem. Eng. Data, **21**, 81-84.

[61] Hwang, S. C., Lin, H. M., Chappelear, P. S. and Kobayashi, R., 1976, *Dew Point Study in the Vapor-Liquid Region of the Methane-Carbon Dioxide System***,** J. Chem. Eng. Data, **22**, 493-497.

[62] Knapp, H., Yang, X. and Zhang, Z., 1990, *Vapor-Liquid Equilibria in Ternary Mixtures Containing Nitrogen, Methane, Ethane and Carbon Dioxide at Low Temperatures and High Pressures*, Fluid Phase Equilib., **54**, 1-18.

[63] Webster, A. L., Kidnay, A. J., Vapor-Liquid Equilibria for the Methane-Propane-Carbon Dioxide Systems at 230 K and 270 K, J. Chem. Eng. Data, 46 (2001) 759-764.

[64] Fredenslund, A. A. and Sather, G. A., 1970, *Gas-Liquid Equilibrium of the Oxygen-Carbon Dioxide System*, J. Chem. Eng. Data, **15**, 17-22.

[65] P.L., Barrick, C.K., Heck, J.O., Spano, Liquid-vapor equilibria of the hydrogen-carbon dioxide System, Tech.Rep. 66 (1966).

[66] Tsang, C. Y. and Streett, W. B., 1981, *Phase Equilibria in The $H_2/CO_2$ System at Temperatures from 220 to 290 K and Pressures to 172 MPa*, Chem. Eng. Sci., **36,** 993-1000.

[67] Augood, D. R., 1957, *The Separation of HD and $H_2$ by Absorptive Fraction*, Trans.Inst.Chem.Engr., **35**, 394-408.

[68] NagaraJan, N. and Robinson Jr, R. L., 1986, *Equilibrium Phase Compositions, Phase Densities, and Interfacial Tensions for $CO_2$ + Hydrocarbon Systems. 2. $CO_2$ + N Decane*, Journal of Chemical and Engineering Data, **3**, 168-171.

[69] Sarashina, E., Arai, Y. and Saito, S., 1971, *The P-V-T-x Relation for the Carbon Dioxide-Argon System, J. Chem. Eng. Jpn.*, **4**, 379-381.

[70] Coquelet, C., Valtz, A., Dieu, F., Richon, D., Arpentinier P. and Lockwood, F., 2008, *Isothermal P, x, y Data For The Argon + Carbon Dioxide System at Six Temperatures from 233.32 to 299.21 K and Pressures up to 14 MPa*, Fluid Phase Equilib., **273**, 38-43.

[71] Christiansen, L. J. and Fredenslund, A., 1974, *Gas-Liquid Equilibria of the $CO_2$-CO and $CO_2$-$CH_4$-CO Systems*, Adv. Cryog. Eng., **19**, 309-319.

[72] Huamin, S., 1991, *Solubility of Carbon Monoxide in Methanol and Carbon Dioxide under High Pressure*, Chem. Eng. (China), **19**, 61-70.

[73] Van der Waals, J. H., Platteeuw, J. C., 1959, *Clathrate Solutions*, Adv. Chem. Phys., **2**, 2-57.

[74] Parrish, W. R. and Prausnitz,. J. M., 1972, *Dissociation Pressures of Gas Hydrates Formed by Gas Mixtures*. Ind. Eng. Chem. Process Des, **11**, 26-35.

[75] Holder, G. D., Corbin, G., Papadopoulos, K. D., 1980, *Thermodynamic and Molecular Properties of Gas Hydrate from Mixtures Containing Methane, Argon and Krypton*, Ind. Eng. Chem. Fundam., **19**, 282-286.

[76] Kihara, T., *Virial Coefficient and Models of Molecules in Gases*, 1953, Reviews of modern physics, **25**, 831-843.

[77] Diamond, L. W., 1994, *Salinity of Multivolatile Fuid Inclusions Determined from Clathrate Hydrate Stability*, Geochim. Cosmochim. Acta, **58**, 19-41.

[78] Seo, Y-T. and Lee, H., 2004, *Structure and Guest Distribution of the Mixed Carbon Dioxide and Nitrogen Hydrates as Revealed by X-ray Diffraction and 13 C NMR Spectroscopy*, J. Phys. Chem. B, , **108**, 530-534.

[79] Mao, W. L., Mao, H. K., Goncharov, A. F., Struzhkin, V. V., Guo, Q. Z., Hu, J. Z., Shu, J. F., Hemley, R. J., Somayazulu, M. and Zhao, Y. S., *Hydrogen Clusters in Clathrate Hydrate*, Science 2002, ***297***, 2247-2249.

[80] Dyadin, Y. A., Larionov, E. G., Manakov, A. Y., Zhurko, F.V., Aladko, E. Y., Mikina, T. V. and Komarov, V. Y, 1999a, *Clathrate Hydrates of Hydrogen and Neon*, Mendelev Comm., **5**, 171-172.

[81] Sugahara, T., Murayama, S., Hashimoto, S. and Ohgaki, K., 2005, *Phase Equilibria for $H_2$ + $CO_2$ + $H_2O$ System Containing Gas Hydrates*, Fluid Phase Equilibria, **233**, 190-193.

[82] Dyadin, Y. A., Larionov, E. G., Mirinskij, D. S., Mikina, T. V. and Starostina, L. I., 1997, *Clathrate Formation in the Ar-$H_2O$ System Under Pressures up to 15,000 BAR* , Mendeleev Commun.,**1**, 32-33.

[83] Davidson, D. W., Handa, Y. P., Ratcliffe, C. I., Ripmeester, J. A., Tse, J. S., Dahn, J. R., Lee, F. and Calvert, L. D., 1986, *Crystallographic Studies of Clathrate Hydrates. Part I*, Mol. Cryst. Liq. Cryst., **141**, 141-149.

[84] Tse, J. S., Handa, Y. P. and Ratcliffe, C. I, 1986, *Structure of Oxygen Clathrate Hydrate by Neutron Powder Diffraction*, J. Inclusion Phenom., **4**, 235-240.

# CHAPTER 6: VISCOSITY OF CARBON DIOXIDE RICH SYSTEMS

## 6.1 Introduction

In many engineering processes, including transport phenomena, understanding viscosity of liquid and liquid mixtures is necessary. Transporting fluids including liquid $CO_2$ are subjected to various resistances due to friction. Fluid viscosity causes friction which causes pressure drop according to Darcy-Weisbach equation. Understanding the effect of impurities on $CO_2$ viscosity leads us defining the capacity of pumps and compressors and hence the cost.

Viscosity data of pure $CO_2$ gases and impure gases are readily available in literature. Li et al. [1], have published recently an extensive review of available experimental data and models for the transport properties of $CO_2$-mixtures relevant to $CO_2$ capture, transport and storage. They concluded that no data were available for $CO_2$ viscosity in the presence of impurities in the liquid and supercritical regions. A summary of the experimental data available in literature for $CO_2$/impurities systems is listed in Table 6.1. Several models [2-5] ranging from those based on kinetic theories to completely empirical have been proposed. Vesovic et al. (1990) [5] proposed a viscosity correlation that covered a wide range of pressure and temperature. They found that their model can predict liquid and supercritical $CO_2$ in the range from 5 to 7%. Fenghour et al. [6] extended Vesovic et al. [5] work to improve viscosity of liquid $CO_2$. The uncertainties associated with the proposed representation vary from 0.3% for dilute gas near room temperature to 5.0% at the highest pressures. It has a very good accuracy for pure $CO_2$. However, it cannot be applied for mixtures without modification. Quinones-Cisneros et al. [3] proposed what is called a “f-theory” model of viscosity for both pure components and their mixtures. The model is modified to be used in conjunction with the SRK, PR and PRSV cubic equations of state in order to develop three one parameter general models for viscosity prediction [7]. In a different approach, the Pedersen correlation which is a modified form of Ely and Hanley model [8] employed the corresponding states principle to predict the viscosity of pure components or their mixtures, knowing

the viscosity of a reference substance (methane). The method of Lohrenz–Bray–Clark (LBC), which relates the residual viscosity to the reduced density, is the most widely used engineering tool to predict the viscosity of reservoir fluids. It is a predictive model for gas or liquid viscosity. The LBC correlation is a modification of Jossi et al [9] correlation for pure components, and is suitable for gases and light oils. Pedersen, LBC and f-theory (general form of f-theory) models were tested by Al-Marri [10]. The author concluded that for supercritical $CO_2$ all models are very good to represent the viscosities when the pressure is less than 10.34 MPa. Above that pressure, CSP over predicts while the LBC underpreditc the viscosities but the f-theory and GF-f-theory are much better to predict the viscosities. The ADD% is 1.25 for f-theory, 1.39 for GF-f-theory, 15.15 for CSP (Pedersen model) and 6.38 for LBC. The f-theory model is rarely used in oil industries compare to the LBC and Pedersen models. However, the later models cannot be used to predict $CO_2$ and $CO_2$ mixtures without modification. Therefore, the viscosity models considered in this paper work are the Pedersen model (with $CO_2$ as a reference) and LBC (tuned) based on PR-EOS.

*Table 6.1 Source of viscosity data for $CO_2$/impurities system*

| System | T Range/K | P/MPa Range | Ref. |
|---|---|---|---|
| $CO_2 + CH_4$ | 298 | >0.1 | [11] |
| $CO_2 + CH_4$ | 323–473 | 3.4–68 | [12] |
| $CO_2 + CH_4$ | 293 –303 | 0.1–2.6 | [13] |
| | | | |
| $CO_2 + H_2$ | 300 –551 | 0.1 | [14] |
| $CO_2 + H_2$ | 291 | 0.1 | [15] |
| $CO_2 + H_2$ | 298 | 0.1 | [16] |
| $CO_2 + H_2$ | 295–303 | 0.098 | [17] |
| $CO_2 + H_2$ | 295–303 | 0.1 | [18] |
| $CO_2 + H_2$ | 500–1100 | 0.3 | [19] |
| | | | |
| $CO_2 + N_2$ | 293 | 0.1–2.14 | [20] |
| $CO_2 + N_2$ | 293 –303 | 0.1–2.6 | [21] |
| $CO_2 + N_2$ | 295–303 | 0.098 | [17] |
| $CO_2 + N_2$ | 289 | 2–12 | [22] |

| | | | |
|---|---|---|---|
| $CO_2 + N_2$ | 298–873 | 0.1 | [23] |
| $CO_2 + Ar$ | 293–303 | 0.1–2.6 | [21] |
| $CO_2 + Ar$ | 310–521 | 0.1 | [24] |
| $CO_2 + Ar$ | 298–873 | >0.1 | [23] |
| $CO_2 + CO$ | 298–473 | 0.1 | [25] |
| $CO_2 + O_2$ | 298–674 | 0.1 | [26] |
| $CO_2 + O_2$ | 295–303 | 0.098 | [17] |
| $CO_2 + O_2 + CO + H_2 + CH_4 + N_2$ | 293–1287 | 0.1 | [27] |
| $O_2 + N_2 + CO_2$ | 317–1161 | 0.1 | [28] |
| $CO_2 + O_2 + N_2$, $CO_2 + O_2 + H_2$ | 295–303 | 0.098 | [17] |
| $Ar + CO_2 + N_2$, $CH_4 + CO_2 + N_2$ | 298–873 | 0.1 | [23] |
| $Ar + N_2 + CO_2$, $CH_4 + N_2 + CO_2$ | 298–873 | 0.1 | [29] |
| $N_2 + O_2 + CO_2 + N_2O$ | 313–413 | >0.1 | [30] |

In this work, the viscosity of pure $CO_2$ and five binary $CO_2$/impurities mixtures were measured from 280 to 300.15 K in the liquid phase and from 308.15 to 343.15 K in the supercritical phase. Both measurements were run for pressure up to 41 MPa in liquid and supercritical regions. This work was essentially presented on a steering meeting held on 3rd May 2012 in Heriot-Watt University (Alsiyabi I. and Nazeri M.).

## 6.2 Experimental Methods and Equipment

### *6.2.1 Materials*

The following compounds were used to make the different synthetic mixtures studied in this work:

- Carbon dioxide, Supplied by Air Products, Research Grade
- Methane, Supplied by Air Products, Grade N4.5
- Nitrogen, Supplied by BOC, Research Grade
- Argon, Supplied by BOC, Research Grade
- Carbon monoxide, Supplied by BOC, Research Grade

- Oxygen, Supplied by BOC, Research Grade
- Hydrogen, Supplied by BOC Gases, >= %99.995

The systems listed in Table 6.2 were prepared gravimetrically and were used to conduct the viscosity tests. A multi component mixture, MIX1, (composition given in Table 6.3) supplied by BOC was also used to carry out the tests.

*Table 6.2 The Composition of mixtures used for the experiments*

| Component | $CO_2$ %mole | Impurity %mole (±0.3) |
|---|---|---|
| Pure $CO_2$ | 100 | 0 |
| $CO_2$ + methane | 95 | 5 |
| $CO_2$ + nitrogen | 95 | 5 |
| $CO_2$ + argon | 95 | 5 |
| $CO_2$ + carbon | 95 | 5 |
| $CO_2$ + oxygen | 95 | 5 |
| $CO_2$ + hydrogen | 95 | 5 |

*Table 6.3 The mixture composition (MIX1)*

| Mixture Components | % mole(±0.05) |
|---|---|
| Carbon Dioxide | Balance |
| Methane | 0.67 |
| Hydrogen | 0.82 |
| Nitrogen | 1.41 |
| Carbon m | 0.21 |
| Argon | 1.21 |
| Oxygen | 0.08 |
| Total | 100 |

### *6.2.2 Experimental Equipment*

All viscosity measurements were conducted in an in-house designed and constructed set-up. A schematic view of the setup is shown in Figure 6.1. This setup has been designed to have 200 MPa maximum working pressure and 520 K maximum working

temperature. The set-up is comprised of two small cylinders, with volumes of 100 and 25 $cm^3$, connected to each other through a capillary tube with a measured length of 14.781 metres and a calculated internal diameter of 0.296 mm. A three-way valve is installed on top of one of the cylinders to inject the sample inside the cylinders and tube system. All of the cylinders and tube are in a temperature controlled bath filled with water. The base side of the two cylinders are connected to the opposite sides of a push-pull, motor driven mercury pump. This pump can move the sample fluid forwards and backwards between the two cylinders. There is also a hand pump connected to the system to control the pressure of the entire fluid system by injection and withdrawal of mercury. Both the opposed piston pump and the hand pump are fitted with Mitutoyo linear transducers readable to 0.005 mm on Mitutoyo SD-D1E readouts. As a 1 mm movement represents 0.151 $cm^3$ displacement in both pumps, the readability is 0.000755 $cm^3$. The opposed piston pump has a variable control with which the speed can be adjusted to a maximum of 5$cm^3$/sec. The rate can be set with a margin of error of ±0.00003 $cm^3$/sec.

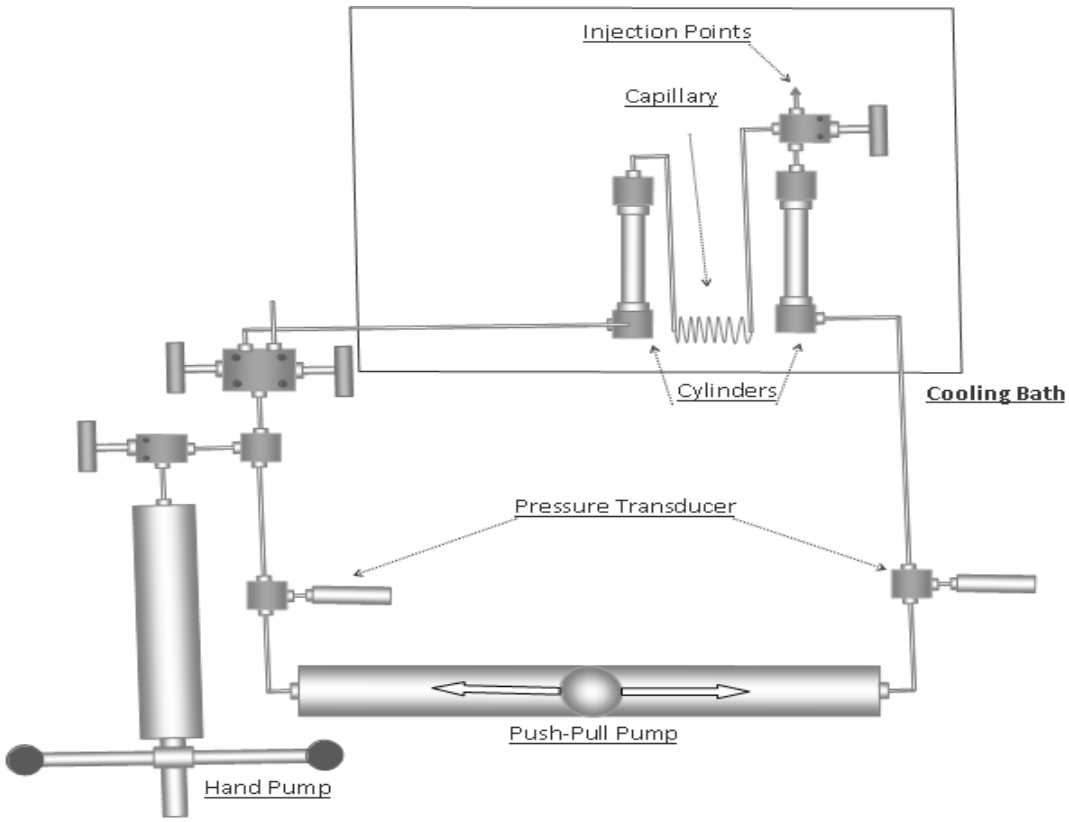


*Figure 6.1 schematic view of the viscosity experiments setup*

### *6.2.3 Experimental Procedure*

The capillary tube viscosity measurement method has been employed to measure the viscosity of $CO_2$ systems with impurities above the critical point. In each test, one of the cylinders was loaded with the prepared synthetic mixtures after vacuuming the entire system. Then after disconnecting the sample cylinder from the system, the sample fluid was pushed through the capillary tube into the other cylinder using the push-pull mercury pump. The temperature of the system was set to the desired condition and the desired pressure was set using the hand pump. Once conditions had stabilized the sample was pumped through the capillary tube at a set flow rate. Pumping the sample fluid through capillary tube by the piston pump results in a dynamic differential pressure that was monitored and recorded until stable. Then the pump was stopped to record the static differential pressure. The difference between the dynamic and static differential pressure was used as the pressure drop across the tube. To ensure laminar flow conditions, the Reynolds number was checked for the flow rates in which the measurements were performed. The Poiseuille equation, below, can relate the pressure drop across the capillary tube to the viscosity, tube characteristics and also flow rate for laminar flow:

$$\Delta P = \frac{128\ L\ Q\ \eta}{C\ \pi\ D^4} \tag{6.1}$$

Where, $\Delta P$ is differential pressure across the capillary tube viscometer in psi, Q represents flow rate in $cm^3$/sec, L is length of the capillary tube in cm, D refers to internal diameter of the capillary tube in cm equals 0.0296 cm, $\eta$ is the viscosity of the flown fluid in cP and C is a unit conversion factor equal to 6894757 if the above units are used. The internal diameter of the tube was calculated by knowing the length and volume of the tube. The tube length changes with temperature but this had no noticeable influence on the obtained viscosity. The set flow rate has no effect on the accuracy of the viscosity measurement. Only differential pressure is a variable in the above formulation and can cause error in the viscosity measurements. The usual uncertainty in differential pressure measurement is 0.01 psi and this leads to ±1% of error in the calculated viscosity for those measured in this study.

## 6.3 Modelling

Two models are suggested in this work to predict the viscosity of $CO_2$ dominated systems with impurities: $CO_2$-Pedersen and Lohrenz–Bray–Clark (LBC). The $CO_2$-Pedersen model predicts the viscosity using the corresponding states theory. The LBC correlation is a fourth-degree polynomial equation in the reduced density which can be tuned to match to experimental data.

### *6.3.1 $CO_2$-Pedersen Model*

The model has been described in Pedersen and Christensen [31]. According to the corresponding states principles applied to viscosity, the reduced viscosity, $\eta_r = \frac{\eta(P,T)}{\eta_c}$, for two components at the same reduced pressure, $P_r = \frac{P}{P_c}$, and reduced temperature, $T_r = \frac{T}{T_c}$, will be same.

$$\eta_r = f(P_r, T_r) \tag{6.2}$$

Based on the dilute gases considerations, viscosity at critical point can be approximated as:

$$\eta_c \approx \frac{P_c^{2/3} M^{1/2}}{T_c{}^{1/6}} \tag{6.3}$$

Where, M denotes the Molecular weight. Thus, the reduced viscosity can be expressed as:

$$\eta_r = \frac{\eta(P,T)}{\eta_c} = \frac{\eta(P,T)\, T_c{}^{1/6}}{P_c^{2/3} M^{1/2}} \tag{6.4}$$

For one component as a reference component if the function, *f*, in Equation 6.2 is known, it is possible to calculate the viscosity of any other components, such as component x, at any pressure and temperature. Thus,

$$\eta_x(P,T) = \frac{\left(\frac{P_{cx}}{P_{c0}}\right)^{\frac{2}{3}}\left(\frac{M_x}{M_0}\right)^{\frac{1}{2}}}{\left(\frac{T_{cx}}{T_{c0}}\right)^{\frac{1}{6}}}\eta_0\left(\frac{PP_{c0}}{P_{cx}}, \frac{T\,T_{c0}}{T_{cx}}\right) \tag{6.5}$$

Where, 0 refers to the reference component methane with the viscosity data published by Hanley et al. [32] has been selected as the reference fluid in the original Pedersen Model. In this work, carbon dioxide with the viscosity data published by Fenghour et al. [6] has been selected as the reference fluid for the $CO_2$ systems including impurities. The viscosity of $CO_2$ as a function of density and temperature can be calculated from the following equation:

$$\eta(\rho,T) = \eta_0(T) + \Delta\eta(\rho,T) \tag{6.6}$$

Where, $\eta_0(T)$ is the zero-density viscosity and can be obtained from the following equation:

$$\eta_0(T) = \frac{1.00697\,T^{1/2}}{\Psi^*_\eta(T^*)} \tag{6.7}$$

In this equation, the zero-density viscosity is in units of μPa.S and temperature, T, in K. The reduced effective cross section, $\Psi^*_\eta(T^*)$, is represented by the empirical equation.

$$\ln\Psi^*_\eta(T^*) = \sum_{i=0}^{4} a_i\,(\ln T^*)^i \tag{6.8}$$

Where the reduced temperature,$T^*$, is given by

$$T^* = kT/\varepsilon \tag{6.9}$$

And the energy scaling parameter, $\frac{\varepsilon}{k} = 251.196$ K. Where *k* is the Boltzmann's constant and ε is the minimum of the pair-potential energy. The coefficients, $a_i$, are listed in the

Table 6.4. The second contribution in Equation 6.6 is the excess viscosity, $\Delta\eta(\rho, T)$, which describes how the viscosity can change as a function of density outside of the critical region. The excess viscosity correlation can be correlated as follows:

$$\Delta\eta(\rho, T) = d_{11}\rho + d_{21}\rho^2 + \frac{d_{64}\rho^6}{T^{*3}} + d_{81}\rho^8 + \frac{d_{82}\rho^8}{T^*} \tag{6.10}$$

Where, the temperature is in Kelvin, the density in kg/m$^3$ and the excess viscosity in μPa.s. The coefficients are shown in Table 6.5.

*Table 6.4 Values of coefficients, $a_i$, in Equation 6.8 for $CO_2$*

| $i$ | $a_i$ |
|---|---|
| 0 | 0.235156 |
| 1 | -0.491266 |
| 2 | $5.211155 \times 10^{-2}$ |
| 3 | $5.347906 \times 10^{-2}$ |
| 4 | $-1.537102 \times 10^{-2}$ |

*Table 6.5 Values of coefficients, $d_{ij}$, in Equation 6.10*

| $d_{ij}$ | Value |
|---|---|
| $d_{11}$ | $0.4071119\times10^{-2}$ |
| $d_{21}$ | $0.7198037\times10^{-4}$ |
| $d_{64}$ | $0.2411697\times10^{-16}$ |
| $d_{81}$ | $0.2971072\times10^{-22}$ |
| $d_{82}$ | $-0.162788\times10^{-22}$ |

The corresponding states principle expressed in Equation 6.5 for the viscosity of pure components works well for mixtures. Pedersen et al. [4] have expressed the following expression to calculate the viscosity of mixtures at any pressure and temperature.

$$\eta_{mix}(P, T) = \frac{\left(\frac{P_{cmix}}{P_{c0}}\right)^{\frac{2}{3}}\left(\frac{M_{mix}}{M_0}\right)^{\frac{1}{2}}\left(\frac{\alpha_{mix}}{\alpha_0}\right)}{\left(\frac{T_{cmix}}{T_{c0}}\right)^{\frac{1}{6}}}\eta_0(P_0, T_0) \tag{6.11}$$

Where

$$P_0 = \frac{PP_{c0}}{P_{cmix}}\frac{\alpha_0}{\alpha_{mix}}; \quad T_0 = \frac{T\,T_{c0}}{T_{cmix}}\frac{\alpha_0}{\alpha_{mix}} \tag{6.12}$$

The critical temperature and pressure for mixtures, according to recommended mixing rules by Murad and Gubbins [33], can be found from

$$T_{cmix} = \frac{\sum_{i=1}^{N}\sum_{j=1}^{N} Z_i Z_j \left[\left(\frac{T_{ci}}{P_{ci}}\right)^{\frac{1}{3}} + \left(\frac{T_{cj}}{P_{cj}}\right)^{\frac{1}{3}}\right]^3 \sqrt{T_{ci}\,T_{cj}}}{\sum_{i=1}^{N}\sum_{j=1}^{N} Z_i Z_j \left[\left(\frac{T_{ci}}{P_{ci}}\right)^{\frac{1}{3}} + \left(\frac{T_{cj}}{P_{cj}}\right)^{\frac{1}{3}}\right]^3} \tag{6.13}$$

$$P_{cmix} = \frac{8\sum_{i=1}^{N}\sum_{j=1}^{N} Z_i Z_j \left[\left(\frac{T_{ci}}{P_{ci}}\right)^{\frac{1}{3}} + \left(\frac{T_{cj}}{P_{cj}}\right)^{\frac{1}{3}}\right]^3 \sqrt{T_{ci}\,T_{cj}}}{\left(\sum_{i=1}^{N}\sum_{j=1}^{N} Z_i Z_j \left[\left(\frac{T_{ci}}{P_{ci}}\right)^{\frac{1}{3}} + \left(\frac{T_{cj}}{P_{cj}}\right)^{\frac{1}{3}}\right]^3\right)^2} \tag{6.14}$$

The mixture molecular weight is found from

$$M_{mix} = 1.304 \text{ x } 10^{-4}\left(\bar{M}_w{}^{2.303} - \bar{M}_n{}^{2.303}\right) + \bar{M}_n \tag{6.15}$$

where $\bar{M}_w$ and $\bar{M}_n$ are the weight average and number average molecular weights, respectively.

$$\bar{M}_w = \frac{\sum_{i=1}^{N} Z_i M_i{}^2}{\sum_{i=1}^{N} Z_i M_i} \tag{6.16}$$

$$\bar{M}_n = \sum_{i=1}^{N} Z_i M_i \tag{6.17}$$

The parameter $\alpha$ for mixtures in Equation 6.11 can be found from

$$\alpha_{mix} = 1 + A\rho_r{}^B M_{mix}^C \tag{6.18}$$

*Table 6.6 The original Pedersen mixture tuning parameters*

| Parameters | Value |
|---|---|
| A | $7.378 \times 10^{-3}$ |
| B | 1.847 |
| C | 0.5173 |

The tuning parameters of A, B and C can be found from Table 6.6. α for the reference fluid can be found from the Equation 6.18 by replacing the molecular weight of the mixture with that of the reference fluid, carbon dioxide. The reduced density, $\rho_r$, defines as

$$\rho_r = \frac{\rho_0\left(\frac{PP_{c0}}{P_{cmix}}, \frac{T\,T_{c0}}{T_{cmix}}\right)}{\rho_{c0}} \tag{6.19}$$

The critical density of carbon dioxide, $\rho_{c0}$, is equal to 467.69 kg/m$^3$. The Modified Benedict–Webb–Rubin (MBWR) equation of state is used for computing the reference fluid density, $\rho_0$, at the desired pressure and temperature of $\frac{PP_{c0}}{P_{cmix}}, \frac{T\,T_{c0}}{T_{cmix}}$. The mathematical equation of the MBWR has been presented by Younglove et al. [4]. The procedure below should be followed to calculate the viscosity of $CO_2$ systems with impurities by the corresponding state principle of Pedersen Model:

1. Calculate the $T_{cmix}$, $P_{cmix}$ and $M_{mix}$ from Equations 6.13, 6.14 and 6.15 respectively.
2. Obtain the $CO_2$ density at $\frac{PP_{c0}}{P_{cmix}}, \frac{T\,T_{c0}}{T_{cmix}}$ from the MBWR EOS and calculate the reduced density from Equation 6.19
3. The mixture parameter, $\alpha_{mix}$, and $\alpha_0$ should be calculated from Equation 6.18

4. The reference pressure and temperature, $P_0$ and $T_0$, should be calculated from Equation 6.12
5. Calculate the $CO_2$ reference fluid, $\eta_0(P_0, T_0)$, in Equation 6.11 from Equation 6.6
6. Calculate the mixture viscosity from Equation 6.11

### *6.3.2 Lohrenz–Bray–Clark (LBC) model*

The LBC correlation is a fourth-degree polynomial equation in the reduced density, $\rho_r = \frac{\rho}{\rho_c}$, as presented in 1964. Lohrenz et al. [2] extended the JST method [9] for calculating the viscosity of mixtures of naturally occurring hydrocarbons. The equation is:

$$[(\eta - \eta^*)\xi + 10^{-4}]^{1/4} = a_1 + a_2\,\rho_r + a_3{\rho_r}^2 + a_4{\rho_r}^3 + a_5\,{\rho_r}^4 \tag{6.20}$$

where the constants $a_1$ to $a_5$ are listed in Table 6.7. These parameters can be tuned to match to the experimental data of $CO_2$ systems with impurities. In Equation 6.20, $\xi$ is the viscosity reducing parameter, which for a mixture is given by

$$\xi = \frac{\left[\sum_{i=1}^{N} Z_i T_{ci}\right]^{1/6}}{\left[\sum_{i=1}^{N} Z_i M_i\right]^{1/2}\left[\sum_{i=1}^{N} Z_i P_{ci}\right]^{2/3}} \tag{6.21}$$

*Table 6.7 Parameters in the original LBC Viscosity Correlation*

| LBC Parameters | Original Constants | New Constants |
|---|---|---|
| $a_1$ | 0.10230 | 0.07960 |
| $a_2$ | 0.023364 | 0.142735 |
| $a_3$ | 0.058533 | -0.113846 |
| $a_4$ | -0.040758 | 0.056084 |
| $a_5$ | 0.0093324 | -0.0090435 |

The critical density of mixtures can be determined from the critical molar volume.

$$\rho_c = \frac{1}{V_c} = \frac{1}{\sum_{i=1}^{N} Z_i V_{ci}} \tag{6.22}$$

The density of mixture for $CO_2$ systems with impurities can be calculated by Peng-Robinson equation of state. In this work, the density of the modified PR EOS demonstrated in Chapter 4 was used to calculate the mixture density. Therefore, a new set of parameters were obtained by minimizing the error with the experimental data of viscosity. The new parameters are listed together with the original ones in Table 6.7. Low pressure mixture viscosity, η*, can be determined from the following equation presented by Herning et al. [27].

$$\eta^* = \frac{\sum_{i=1}^{N} Z_i \eta_i^* \sqrt{M_i}}{\sum_{i=1}^{N} Z_i \sqrt{M_i}} \tag{6.23}$$

The dilute component viscosity,$\eta_i^*$, for each component has been expressed as a function of reduced temperature, $T_r$, by Stiel and Thodos [35] as follows:

$$\eta_i^* = 34 \text{ x } 10^{-5} \frac{1}{\xi_i} T_{ri}^{0.94} \quad ; \quad \text{for } T_{ri} < 1.5 \tag{6.24}$$

$$\eta_i^* = 17.78 \text{ x } 10^{-5} \frac{1}{\xi_i} (4.58 T_{ri} - 1.67)^{5/8} \quad ; \quad \text{for } T_{ri} > 1.5 \tag{6.25}$$

where,

$$\xi_i = \frac{T_{ci}^{1/6}}{M_i^{1/2} P_{ci}^{2/3}} \tag{6.26}$$

## 6.4 Results and Discussion

### *6.4.1 Experimental Results*

The viscosity of six binary $CO_2$ mixtures with 5% impurity ($H_2$, $CH_4$, $N_2$, $O_2$, CO and Ar) plus a multi-components mixture (MIX1) with 4.36% impurities are presented in this work. The measurements were performed at temperatures of 280, 288.15, 300.15, 308.15, 323.15 and 343.15 K. The experimental and modelling results for the viscosity of $CO_2$ and $CO_2$/impurities systems are given in Table 6.8 to Table 6.13 and Figure 6.2 to Figure 6.8. The experiments for each binary mixture were conducted in the single liquid phase region (above saturation) or in the supercritical region. In order to validate our experimental procedure and setup, the viscosity of $CO_2$ at 288 K obtained from Fenghour et al. [6] and at 323.15 K and 343.15 K from Pensado et al. [36] were compared to our experimental results. Figure 6.2 shows that our results are in a good agreement with these literature sources. The viscosity of carbon dioxide is a function of pressure and temperature; it increases as pressure increases and decreases as temperature increases. The viscosity of impure $CO_2$ was tested under the same condition of pressure and temperature of pure $CO_2$. The viscosity of liquid and supercritical $CO_2$ systems show an increase as pressure increases and the change becomes less significant as the system moves away from the saturation line. At constant pressure, the increase of temperature tends to reduce the viscosity of $CO_2$/impurities systems. As the system approaches the critical pressure and temperature, the viscosity change becomes significant. For example at the same pressure condition, 5% $N_2$ can reduce the viscosity of $CO_2$ up to 35% and 13% near the critical temperature (300.15 K) and at 288.15 K respectively.

The viscosity of $CO_2$ is highly reduced in the presence of $H_2$ compare to the other impurities tested. This is mainly due to the lower molecular weight of hydrogen, i.e. lower $CO_2$ mixture density. The other $CO_2$ systems are found to have a similar effect on the viscosity. Figure 6.2 to Figure 6.8 demonstrate the effect of Ar and $H_2$ on $CO_2$ viscosity at 280, 288.15, 300.15, 308.15, 323.15 and 343.15 K. The presence of $H_2$ and Ar strongly reduce the liquid $CO_2$ viscosity. The viscosity of $CO_2$/$H_2$ mixture is around 20% lower than those of pure $CO_2$ near the saturation at 288.15 K while the viscosity of $CO_2$/Ar mixture is lower by 10% at the same condition. In the supercritical region, the viscosity is much lower than in the liquid region of both pure and impure $CO_2$ systems.

For example, at 323.15 K, the viscosity of pure $CO_2$ drops as low as 30% and 22% in the presence of $H_2$ and Ar respectively. This reduction occurs at a pressure around 11 MPa for $CO_2$/Ar and $CO_2$/$H_2$ systems where their critical pressures are 7.96 and 8.93 MPa respectively (VPT EOS model). Therefore, the critical change in $CO_2$ viscosity seems to take place by 2 to 3 MPa above the supercritical boundary of the impurities system.

*Table 6.8 Experimental and modelling results of the 95% $CO_2$ + 5% $CH_4$ binary system*

| Temp. K (±0.01) | Pressure MPa (±0.05) | Exp.Visc. µPa.s (±1%) | Modified-Pedersen Dev% | Modified-LBC Dev% |
|---|---|---|---|---|
| 280 | 6.50 | 80.8 | 1.3 | 3.1 |
| 280 | 10.19 | 91.1 | 0.1 | 0.7 |
| 280 | 19.07 | 107.5 | 0.1 | 7.2 |
| 280 | 23.21 | 113.9 | 0.1 | 8.7 |
| 280 | 28.21 | 121.1 | 0.1 | 9.9 |
| 280 | 32.59 | 127.0 | 0.1 | 10.5 |
| 280 | 42.03 | 139.0 | 0.1 | 10.6 |
| 280 | 45.49 | 143.2 | 0.1 | 10.3 |
| 280 | 48.72 | 147.0 | 0.1 | 10.0 |
| 288.15 | 6.81 | 66.5 | 2.3 | 0.2 |
| 288.15 | 9.01 | 74.5 | 1.4 | 1.9 |
| 288.15 | 12.88 | 84.5 | 0.5 | 1.6 |
| 288.15 | 22.67 | 102.6 | 0.5 | 0.2 |
| 288.15 | 26.92 | 108.9 | 0.5 | 0.4 |
| 288.15 | 31.21 | 114.7 | 0.4 | 0.5 |
| 288.15 | 36.31 | 121.3 | 0.5 | 0.6 |
| 288.15 | 41.83 | 128.1 | 0.5 | 0.8 |
| 288.15 | 48.19 | 135.5 | 0.5 | 1.2 |
| 300.15 | 8.44 | 49.5 | 3.0 | 1.1 |
| 300.15 | 10.79 | 61.9 | 1.7 | 4.1 |
| 300.15 | 13.89 | 71.9 | 0.2 | 3.2 |
| 300.15 | 18.93 | 82.1 | 0.2 | 2.5 |
| 300.15 | 25.33 | 92.6 | 0.4 | 1.4 |

| | | | | |
|---|---|---|---|---|
| 300.15 | 29.01 | 98.3 | 0.9 | 0.7 |
| 300.15 | 34.43 | 105.3 | 0.8 | 0.8 |
| 300.15 | 39.13 | 110.9 | 0.7 | 1.0 |
| 300.15 | 45.75 | 118.4 | 0.5 | 1.2 |
| 308.15 | 9.16 | 35.8 | 2.5 | 5.9 |
| 308.15 | 12.50 | 57.3 | 1.0 | 4.6 |
| 308.15 | 16.58 | 68.8 | 0.0 | 3.5 |
| 308.15 | 19.69 | 75.6 | 0.8 | 2.4 |
| 308.15 | 24.66 | 84.3 | 1.4 | 2.1 |
| 308.15 | 36.70 | 100.8 | 1.6 | 2.2 |
| 308.15 | 36.93 | 101.0 | 1.5 | 2.2 |
| 308.15 | 42.37 | 108.0 | 2.1 | 1.6 |
| 308.15 | 46.50 | 112.8 | 2.2 | 1.2 |
| 323.15 | 10.71 | 30.0 | 6.6 | 1.0 |
| 323.15 | 14.95 | 48.9 | 0.4 | 0.5 |
| 323.15 | 20.13 | 62.2 | 0.1 | 1.0 |
| 323.15 | 27.95 | 76.1 | 1.3 | 1.2 |
| 323.15 | 32.46 | 81.8 | 0.9 | 2.4 |
| 323.15 | 37.44 | 88.1 | 1.1 | 2.7 |
| 323.15 | 43.62 | 95.1 | 1.1 | 3.1 |
| 323.15 | 48.66 | 100.1 | 0.8 | 3.5 |
| 343.15 | 50.10 | 88.8 | 2.3 | 1.7 |
| 343.15 | 45.03 | 83.4 | 2.0 | 1.5 |
| 343.15 | 34.46 | 71.5 | 1.8 | 0.1 |
| 343.15 | 31.60 | 67.7 | 1.6 | 0.5 |
| 343.15 | 28.10 | 62.4 | 0.9 | 0.7 |
| 343.15 | 23.90 | 55.7 | 0.8 | 1.6 |
| 343.15 | 19.62 | 47.0 | 0.7 | 1.6 |
| 343.15 | 13.95 | 31.1 | 1.8 | 2.9 |
| 343.15 | 9.24 | 21.0 | 0.9 | 2.0 |

*Table 6.9 Experimental and modelling results of the 95% $CO_2$ + 5% Ar binary system*

| Temp. K (±0.01) | Pressure MPa (±0.05) | Exp.Visc. µPa.s (±1%) | Modified-Pedersen Dev% | Modified-LBC Dev% |
|---|---|---|---|---|
| 280 | 7.75 | 87.1 | 2.9 | 3.6 |
| 280 | 10.34 | 93.3 | 2.4 | 2.9 |
| 280 | 13.86 | 100.7 | 2.4 | 3.0 |
| 280 | 24.14 | 118.0 | 2.1 | 3.5 |
| 280 | 28.68 | 124.9 | 2.3 | 3.9 |
| 280 | 33.41 | 131.3 | 2.1 | 3.9 |
| 280 | 41.75 | 142.3 | 2.2 | 4.5 |
| 280 | 47.90 | 150.4 | 2.4 | 5.4 |
| 288.15 | 8.80 | 74.5 | 0.7 | 0.9 |
| 288.15 | 11.55 | 82.2 | 0.8 | 0.1 |
| 288.15 | 15.01 | 90.2 | 1.3 | 0.7 |
| 288.15 | 19.83 | 99.9 | 2.2 | 2.0 |
| 288.15 | 24.33 | 107.1 | 2.1 | 2.2 |
| 288.15 | 29.97 | 115.2 | 2.0 | 2.2 |
| 288.15 | 34.17 | 120.9 | 2.0 | 2.2 |
| 288.15 | 41.35 | 130.0 | 1.9 | 2.3 |
| 288.15 | 46.46 | 136.2 | 1.9 | 2.6 |
| 300.15 | 9.15 | 54.9 | 2.8 | 3.0 |
| 300.15 | 13.63 | 73.0 | 3.5 | 0.7 |
| 300.15 | 17.03 | 81.6 | 4.2 | 1.7 |
| 300.15 | 32.65 | 105.2 | 2.5 | 1.2 |
| 300.15 | 38.15 | 112.0 | 2.3 | 0.9 |
| 300.15 | 45.08 | 120.9 | 2.7 | 1.2 |
| 300.15 | 49.34 | 126.2 | 3.0 | 1.6 |
| 308.15 | 8.93 | 29.0 | 4.0 | 1.2 |
| 308.15 | 10.63 | 48.2 | 2.5 | 1.4 |
| 308.15 | 11.82 | 54.0 | 0.4 | 2.4 |

| | | | | |
|---|---|---|---|---|
| 308.15 | 21.74 | 81.5 | 3.8 | 1.0 |
| 308.15 | 26.59 | 89.5 | 3.8 | 0.7 |
| 308.15 | 32.10 | 96.9 | 3.3 | 0.0 |
| 308.15 | 37.61 | 104.2 | 3.4 | 0.0 |
| 308.15 | 43.15 | 110.3 | 2.9 | 0.4 |
| 308.15 | 48.03 | 115.8 | 2.8 | 0.3 |
| 323.15 | 12.16 | 36.7 | 5.0 | 0.2 |
| 323.15 | 16.86 | 55.7 | 2.9 | 2.7 |
| 323.15 | 24.06 | 71.5 | 3.4 | 2.0 |
| 323.15 | 26.59 | 76.0 | 3.8 | 2.0 |
| 323.15 | 32.10 | 83.8 | 3.6 | 0.8 |
| 323.15 | 37.61 | 90.7 | 3.4 | 0.0 |
| 323.15 | 43.21 | 97.4 | 3.5 | 0.2 |
| 343.15 | 10.36 | 23.6 | 4.7 | 2.3 |
| 343.15 | 16.00 | 39.1 | 7.2 | 4.6 |
| 343.15 | 22.48 | 54.0 | 3.0 | 4.0 |
| 343.15 | 26.89 | 62.6 | 4.1 | 4.5 |
| 343.15 | 32.03 | 69.4 | 3.1 | 2.3 |
| 343.15 | 40.06 | 80.1 | 4.1 | 1.8 |
| 343.15 | 43.15 | 82.9 | 3.3 | 0.6 |
| 343.15 | 50.39 | 90.2 | 3.1 | 0.5 |

*Table 6.10 Experimental and modelling results of the 95% $CO_2$ + 5% CO binary system*

| Temp. K (±0.01) | Pressure MPa (±0.05) | Exp.Visc. μPa.s (±1%) | Modified-Pedersen Dev% | Modified-LBC Dev% |
|---|---|---|---|---|
| 280 | 8.90 | 85.4 | 2.4 | 0.9 |
| 280 | 10.07 | 88.3 | 2.4 | 0.8 |
| 280 | 14.39 | 97.7 | 2.5 | 1.3 |
| 280 | 18.45 | 104.9 | 2.3 | 1.5 |
| 280 | 25.36 | 115.4 | 1.9 | 1.4 |
| 280 | 29.39 | 121.8 | 2.4 | 2.1 |

| | | | | |
|---|---|---|---|---|
| 280 | 33.72 | 127.5 | 2.2 | 2.1 |
| 280 | 38.23 | 133.8 | 2.5 | 2.7 |
| 280 | 45.57 | 142.6 | 2.2 | 3.1 |
| 288.15 | 9.24 | 72.4 | 1.5 | 0.4 |
| 288.15 | 10.79 | 76.6 | 1.0 | 1.3 |
| 288.15 | 15.21 | 88.4 | 3.0 | 0.7 |
| 288.15 | 18.87 | 95.0 | 2.7 | 0.7 |
| 288.15 | 24.06 | 103.2 | 2.4 | 0.7 |
| 288.15 | 28.34 | 109.3 | 2.2 | 0.6 |
| 288.15 | 34.39 | 117.2 | 1.9 | 0.4 |
| 288.15 | 39.21 | 123.1 | 1.7 | 0.3 |
| 288.15 | 47.83 | 133.8 | 2.0 | 1.0 |
| 300.15 | 9.96 | 54.6 | 0.7 | 2.2 |
| 300.15 | 13.49 | 67.7 | 1.1 | 3.1 |
| 300.15 | 18.30 | 79.2 | 2.1 | 1.6 |
| 300.15 | 20.78 | 83.8 | 2.2 | 1.2 |
| 300.15 | 26.66 | 93.7 | 2.8 | 0.1 |
| 300.15 | 29.93 | 98.2 | 2.6 | 0.2 |
| 300.15 | 36.52 | 106.5 | 2.2 | 0.7 |
| 300.15 | 41.60 | 112.5 | 2.1 | 0.9 |
| 300.15 | 49.97 | 122.5 | 2.4 | 0.6 |
| 300.15 | 53.79 | 126.4 | 2.1 | 0.7 |
| 308.15 | 9.17 | 28.8 | 1.7 | 6.7 |
| 308.15 | 14.32 | 61.7 | 3.1 | 1.1 |
| 308.15 | 18.89 | 72.7 | 3.1 | 0.8 |
| 308.15 | 21.59 | 77.8 | 3.1 | 0.9 |
| 308.15 | 26.97 | 86.5 | 3.1 | 1.2 |
| 308.15 | 32.91 | 94.8 | 3.1 | 1.5 |
| 308.15 | 36.69 | 99.9 | 3.4 | 1.4 |
| 308.15 | 45.75 | 110.8 | 3.5 | 1.0 |
| 308.15 | 50.19 | 116.4 | 4.1 | 0.2 |
| 323.15 | 8.94 | 22.2 | 3.9 | 2.2 |
| 323.15 | 13.71 | 42.9 | 4.6 | 1.5 |
| 323.15 | 18.59 | 58.5 | 3.7 | 2.5 |

| | | | | |
|---|---|---|---|---|
| 323.15 | 22.95 | 67.5 | 3.7 | 1.8 |
| 323.15 | 26.17 | 73.0 | 3.9 | 1.3 |
| 323.15 | 31.43 | 80.7 | 3.9 | 0.4 |
| 323.15 | 35.85 | 86.7 | 4.2 | 0.0 |
| 323.15 | 40.21 | 91.7 | 3.9 | 0.7 |
| 323.15 | 46.35 | 98.2 | 3.5 | 1.4 |
| 343.15 | 9.19 | 21.8 | 4.4 | 6.1 |
| 343.15 | 13.26 | 28.8 | 3.6 | 2.4 |
| 343.15 | 19.21 | 44.9 | 2.4 | 2.2 |
| 343.15 | 23.07 | 54.1 | 4.0 | 4.5 |
| 343.15 | 26.28 | 59.6 | 3.7 | 3.8 |
| 343.15 | 31.04 | 66.5 | 3.5 | 2.5 |
| 343.15 | 36.01 | 72.7 | 3.3 | 1.1 |
| 343.15 | 40.70 | 77.9 | 3.0 | 0.0 |
| 343.15 | 45.52 | 82.8 | 2.8 | 1.1 |
| 343.15 | 49.35 | 86.5 | 2.6 | 1.7 |

*Table 6.11 Experimental and modelling results for the 95% $CO_2$ + 5% $O_2$ binary system*

| Temp. K (±0.01) | Pressure MPa (±0.05) | Exp.Visc. µPa.s (±1%) | Modified-Pedersen Dev% | Modified-LBC Dev% |
|---|---|---|---|---|
| 280 | 9.10 | 86.6 | 1.7 | 1.0 |
| 280 | 12.72 | 94.7 | 1.3 | 0.6 |
| 280 | 17.94 | 104.4 | 1.0 | 0.2 |
| 280 | 22.75 | 113.1 | 0.0 | 1.5 |
| 280 | 26.20 | 118.2 | 0.0 | 1.6 |
| 280 | 30.53 | 124.3 | 0.0 | 1.8 |
| 280 | 35.82 | 131.3 | 0.0 | 2.1 |
| 280 | 40.10 | 136.8 | 0.0 | 2.5 |
| 280 | 44.84 | 142.6 | 0.0 | 2.9 |
| 280 | 48.29 | 146.7 | 0.1 | 3.2 |
| 288.15 | 9.39 | 76.0 | 0.3 | 0.2 |
| 288.15 | 11.92 | 82.7 | 0.4 | 0.2 |

| | | | | |
|---|---|---|---|---|
| 288.15 | 17.86 | 94.6 | 0.4 | 0.2 |
| 288.15 | 21.30 | 100.4 | 0.5 | 0.5 |
| 288.15 | 25.17 | 106.3 | 0.4 | 0.7 |
| 288.15 | 29.56 | 112.6 | 0.5 | 0.8 |
| 288.15 | 34.56 | 119.2 | 0.4 | 0.8 |
| 288.15 | 39.84 | 125.8 | 0.4 | 0.9 |
| 288.15 | 44.13 | 131.0 | 0.4 | 1.1 |
| 288.15 | 47.77 | 135.2 | 0.3 | 1.3 |
| 300.15 | 8.75 | 49.7 | 1.5 | 0.4 |
| 300.15 | 11.53 | 64.9 | 0.8 | 1.3 |
| 300.15 | 16.92 | 78.6 | 1.0 | 1.4 |
| 300.15 | 21.66 | 87.2 | 0.9 | 0.7 |
| 300.15 | 24.21 | 91.3 | 1.0 | 0.5 |
| 300.15 | 29.65 | 99.1 | 0.8 | 0.3 |
| 300.15 | 35.19 | 106.4 | 0.8 | 0.4 |
| 300.15 | 39.05 | 111.1 | 0.8 | 0.5 |
| 300.15 | 42.92 | 115.7 | 0.8 | 0.5 |
| 300.15 | 47.10 | 120.4 | 0.7 | 0.6 |
| 308.15 | 10.60 | 47.3 | 0.7 | 0.0 |
| 308.15 | 13.35 | 60.4 | 1.3 | 1.7 |
| 308.15 | 16.52 | 69.1 | 1.4 | 1.3 |
| 308.15 | 20.70 | 77.5 | 1.4 | 1.3 |
| 308.15 | 25.72 | 85.7 | 1.3 | 1.6 |
| 308.15 | 28.35 | 89.5 | 1.2 | 1.8 |
| 308.15 | 32.79 | 95.5 | 1.2 | 2.1 |
| 308.15 | 38.12 | 102.1 | 1.1 | 2.2 |
| 308.15 | 41.62 | 106.2 | 1.1 | 2.2 |
| 308.15 | 47.47 | 112.7 | 0.9 | 2.0 |
| 323.15 | 9.15 | 22.3 | 1.3 | 5.8 |
| 323.15 | 14.63 | 46.3 | 1.2 | 1.5 |
| 323.15 | 18.17 | 58.6 | 2.0 | 1.9 |
| 323.15 | 19.92 | 62.6 | 2.0 | 1.6 |
| 323.15 | 26.72 | 74.6 | 2.0 | 0.2 |
| 323.15 | 28.46 | 77.1 | 1.9 | 0.2 |

| | | | | |
|---|---|---|---|---|
| 323.15 | 32.56 | 82.7 | 1.8 | 0.8 |
| 323.15 | 37.17 | 88.3 | 1.6 | 1.6 |
| 323.15 | 41.61 | 93.4 | 1.5 | 2.0 |
| 323.15 | 44.97 | 97.1 | 1.5 | 2.2 |
| 343.15 | 8.96 | 21.0 | 1.3 | 3.8 |
| 343.15 | 12.66 | 27.0 | 1.0 | 5.0 |
| 343.15 | 16.43 | 37.3 | 0.6 | 2.4 |
| 343.15 | 20.62 | 48.1 | 0.7 | 0.5 |
| 343.15 | 24.98 | 57.2 | 0.7 | 1.7 |
| 343.15 | 29.59 | 65.3 | 2.3 | 2.3 |
| 343.15 | 33.68 | 70.7 | 2.1 | 1.3 |
| 343.15 | 36.21 | 74.0 | 2.4 | 1.0 |
| 343.15 | 41.37 | 79.8 | 2.2 | 0.1 |
| 343.15 | 47.28 | 85.9 | 2.1 | 1.0 |

*Table 6.12 Experimental and modelling results of the 95% $CO_2$ + 5% $H_2$ binary system*

| Temp. K (±0.01) | Pressure MPa (±0.05) | Exp.Visc. µPa.s (±1%) | Modified-Pedersen Dev% | Modified-LBC Dev% |
|---|---|---|---|---|
| 280 | 8.73 | 86.0 | 16.3 | 10.7 |
| 280 | 13.10 | 93.5 | 11.3 | 6.4 |
| 280 | 18.47 | 102.3 | 9.1 | 5.0 |
| 280 | 20.79 | 106.0 | 8.7 | 4.8 |
| 280 | 24.75 | 112.0 | 8.3 | 4.7 |
| 280 | 28.35 | 117.2 | 8.0 | 4.6 |
| 280 | 33.00 | 123.5 | 7.7 | 4.6 |
| 280 | 37.00 | 128.7 | 7.6 | 4.7 |
| 280 | 40.53 | 133.0 | 7.3 | 4.7 |
| 280 | 48.26 | 141.7 | 6.6 | 4.9 |
| 288.15 | 12.57 | 77.6 | 8.8 | 2.4 |
| 288.15 | 17.20 | 87.4 | 7.7 | 2.3 |
| 288.15 | 21.75 | 96.1 | 7.9 | 3.1 |
| 288.15 | 26.85 | 104.8 | 8.3 | 3.9 |

| | | | | |
|---|---|---|---|---|
| 288.15 | 29.37 | 108.7 | 8.4 | 4.1 |
| 288.15 | 33.20 | 114.1 | 8.4 | 4.1 |
| 288.15 | 36.78 | 118.6 | 8.1 | 3.9 |
| 288.15 | 41.04 | 123.2 | 7.4 | 3.4 |
| 300.15 | 14.17 | 65.9 | 8.6 | 0.4 |
| 300.15 | 16.86 | 72.2 | 7.5 | 0.3 |
| 300.15 | 19.80 | 78.6 | 7.6 | 1.2 |
| 300.15 | 22.38 | 83.8 | 8.1 | 2.2 |
| 300.15 | 26.23 | 90.8 | 8.7 | 3.3 |
| 300.15 | 31.57 | 99.2 | 9.1 | 3.9 |
| 300.15 | 41.31 | 110.5 | 7.8 | 2.5 |
| 300.15 | 47.24 | 118.0 | 8.2 | 2.9 |
| 308.15 | 11.13 | 40.8 | 12.2 | 5.6 |
| 308.15 | 14.86 | 58.5 | 8.7 | 0.1 |
| 308.15 | 19.86 | 70.4 | 7.3 | 0.5 |
| 308.15 | 23.66 | 77.8 | 7.6 | 1.0 |
| 308.15 | 30.12 | 88.4 | 8.2 | 1.4 |
| 308.15 | 34.39 | 94.2 | 8.1 | 1.2 |
| 308.15 | 38.42 | 99.6 | 8.3 | 1.4 |
| 308.15 | 45.41 | 107.7 | 8.0 | 1.3 |
| 323.15 | 9.31 | 23.0 | 7.8 | 1.4 |
| 323.15 | 11.96 | 31.0 | 10.0 | 3.5 |
| 323.15 | 15.14 | 44.2 | 9.2 | 1.3 |
| 323.15 | 19.82 | 57.5 | 7.7 | 3.0 |
| 323.15 | 23.70 | 65.6 | 7.9 | 3.2 |
| 323.15 | 28.88 | 74.1 | 7.9 | 2.7 |
| 323.15 | 34.46 | 82.0 | 8.0 | 2.2 |
| 323.15 | 38.00 | 86.5 | 8.1 | 1.9 |
| 323.15 | 43.78 | 93.2 | 8.0 | 1.4 |
| 343.15 | 11.32 | 23.9 | 4.2 | 0.6 |
| 343.15 | 14.15 | 29.7 | 6.4 | 1.3 |
| 343.15 | 18.33 | 40.9 | 8.1 | 3.5 |
| 343.15 | 23.03 | 51.1 | 7.3 | 4.9 |
| 343.15 | 31.98 | 65.3 | 7.0 | 4.0 |

| | | | | |
|---|---|---|---|---|
| 343.15 | 36.19 | 71.1 | 7.6 | 3.8 |
| 343.15 | 40.77 | 77.2 | 8.5 | 4.0 |
| 343.15 | 44.73 | 82.1 | 9.1 | 4.1 |

*Table 6.13 Experimental and modelling results for MIX1*

| Temp. K (±0.01) | Pressure MPa (±0.05) | Exp.Visc. µPa.s (±1%) | Modified-Pedersen Dev% | Modified-LBC Dev% |
|---|---|---|---|---|
| 280 | 13.14 | 94.0 | 0.6 | 1.8 |
| 280 | 15.70 | 99.2 | 0.2 | 1.0 |
| 280 | 20.68 | 106.8 | 0.9 | 1.1 |
| 280 | 25.95 | 115.3 | 0.3 | 0.2 |
| 280 | 32.19 | 123.5 | 0.6 | 0.1 |
| 280 | 38.44 | 131.2 | 0.9 | 0.1 |
| 280 | 45.41 | 139.8 | 0.8 | 0.9 |
| 288.15 | 10.68 | 80.4 | 4.0 | 1.2 |
| 288.15 | 12.89 | 85.1 | 3.1 | 0.4 |
| 288.15 | 17.37 | 93.6 | 2.4 | 0.4 |
| 288.15 | 22.23 | 101.5 | 2.0 | 0.6 |
| 288.15 | 27.47 | 108.3 | 1.1 | 0.2 |
| 288.15 | 32.12 | 115.1 | 1.4 | 0.4 |
| 288.15 | 34.62 | 117.8 | 0.9 | 0.1 |
| 288.15 | 40.47 | 125.4 | 1.1 | 0.4 |
| 288.15 | 47.23 | 131.7 | 0.2 | 0.5 |
| 300.15 | 11.07 | 59.9 | 1.6 | 6.6 |
| 300.15 | 13.81 | 68.6 | 0.8 | 6.0 |
| 300.15 | 18.47 | 79.7 | 0.7 | 3.3 |
| 300.15 | 21.01 | 84.1 | 0.6 | 2.9 |
| 300.15 | 25.92 | 92.4 | 1.2 | 1.6 |
| 300.15 | 28.37 | 95.8 | 1.1 | 1.6 |
| 300.15 | 33.81 | 104.2 | 2.1 | 0.4 |
| 300.15 | 39.09 | 110.0 | 1.4 | 1.2 |
| 300.15 | 45.50 | 117.2 | 1.1 | 1.5 |

| | | | | |
|---|---|---|---|---|
| 308.15 | 12.26 | 55.3 | 2.3 | 3.7 |
| 308.15 | 14.95 | 64.8 | 3.1 | 2.0 |
| 308.15 | 18.52 | 72.1 | 1.7 | 2.8 |
| 308.15 | 20.12 | 74.8 | 1.2 | 3.3 |
| 308.15 | 23.75 | 82.3 | 2.7 | 1.7 |
| 308.15 | 27.23 | 88.2 | 3.3 | 1.1 |
| 308.15 | 31.63 | 93.3 | 2.1 | 2.5 |
| 308.15 | 33.88 | 96.6 | 2.5 | 2.1 |
| 308.15 | 40.67 | 104.1 | 1.7 | 2.8 |
| 308.15 | 45.16 | 110.1 | 2.4 | 1.8 |
| 308.15 | 50.66 | 115.2 | 1.5 | 2.3 |
| 323.15 | 12.24 | 35.9 | 4.1 | 3.2 |
| 323.15 | 14.79 | 45.8 | 1.0 | 3.8 |
| 323.15 | 17.60 | 56.2 | 2.4 | 0.4 |
| 323.15 | 21.49 | 63.6 | 0.6 | 1.8 |
| 323.15 | 29.00 | 76.3 | 1.5 | 2.1 |
| 323.15 | 32.55 | 81.6 | 2.1 | 1.9 |
| 323.15 | 36.06 | 86.4 | 2.5 | 1.8 |
| 323.15 | 44.19 | 95.7 | 2.4 | 2.4 |
| 323.15 | 51.21 | 103.5 | 2.7 | 2.1 |
| 343.15 | 50.32 | 88.1 | 2.4 | 2.0 |
| 343.15 | 42.52 | 80.2 | 2.5 | 1.1 |
| 343.15 | 34.15 | 70.6 | 2.6 | 0.4 |
| 343.15 | 30.22 | 65.6 | 2.8 | 1.5 |
| 343.15 | 26.03 | 58.8 | 2.0 | 1.5 |
| 343.15 | 22.49 | 52.4 | 1.8 | 1.7 |
| 343.15 | 18.47 | 43.6 | 2.5 | 1.3 |
| 343.15 | 14.26 | 31.0 | 1.2 | 4.8 |
| 343.15 | 12.33 | 26.6 | 3.2 | 3.2 |

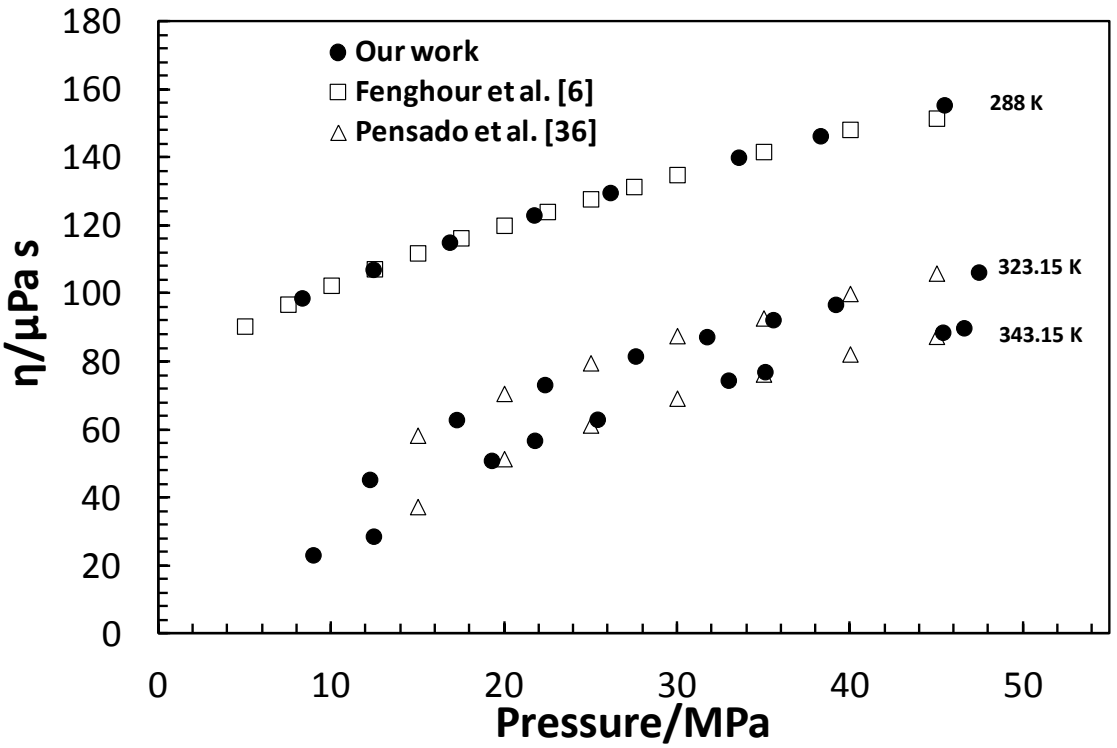


*Figure 6.2 Our viscosity data of pure $CO_2$ together with some literature data at three isothermal conditions*

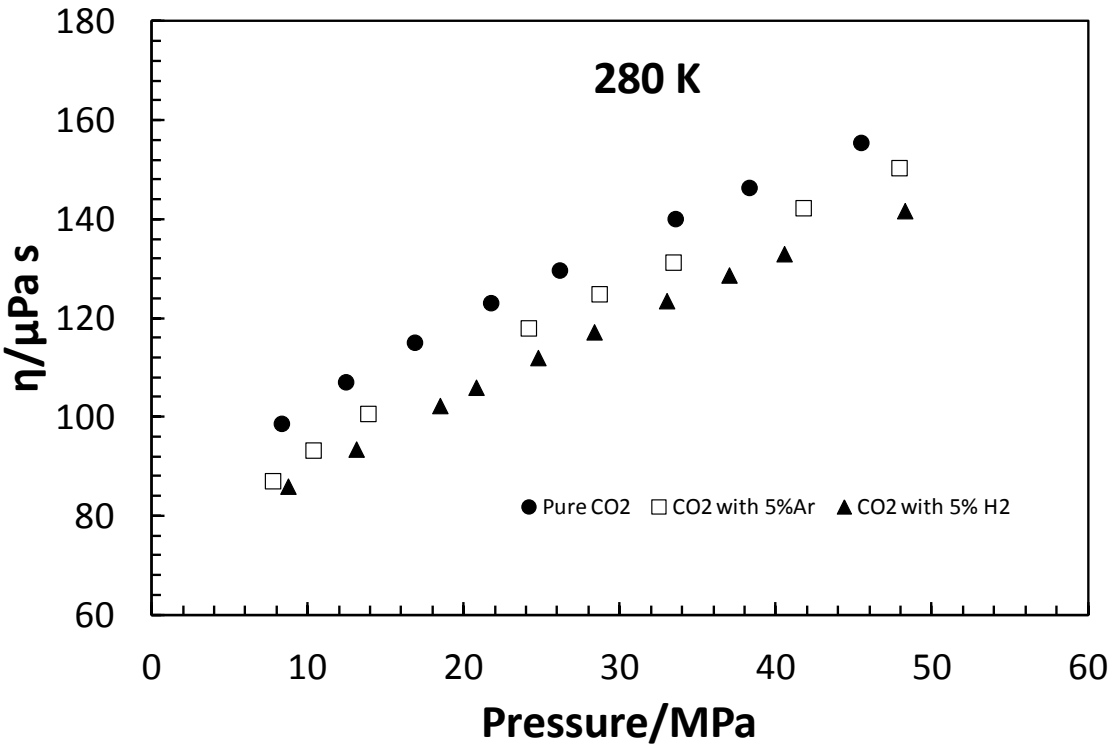


*Figure 6.3 The effect of Ar and $H_2$ on $CO_2$ viscosity at 280 K*

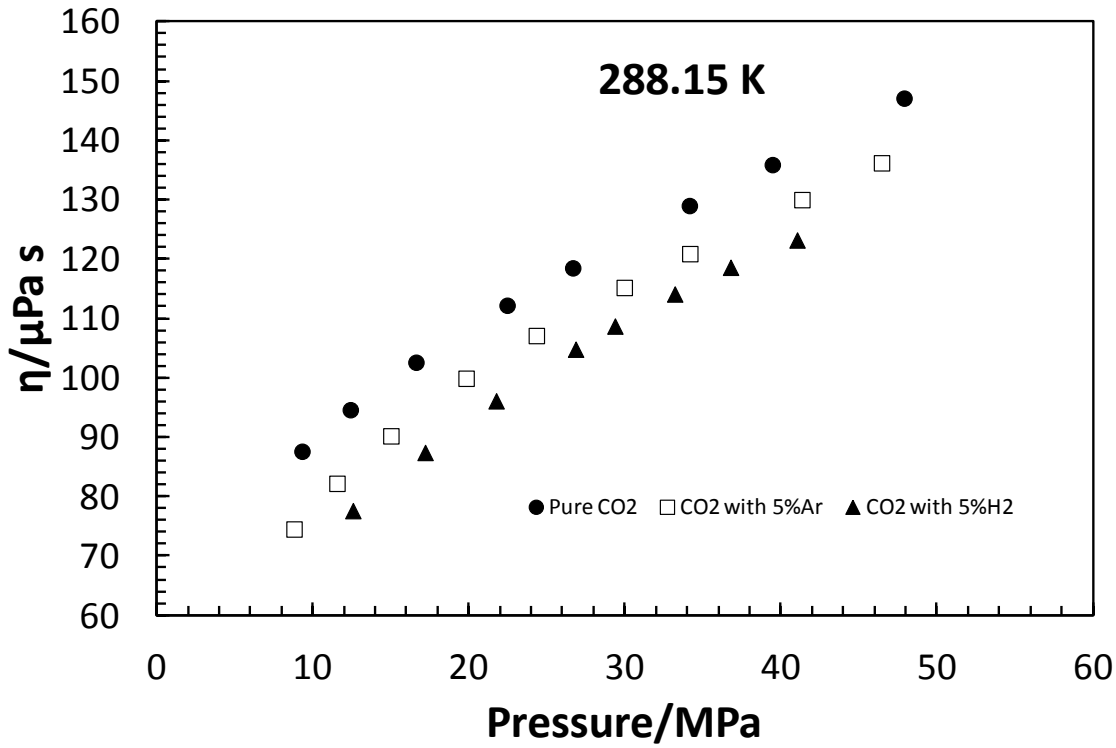


*Figure 6.4 The effect of Ar and $H_2$ on $CO_2$ viscosity at 288.15 K*

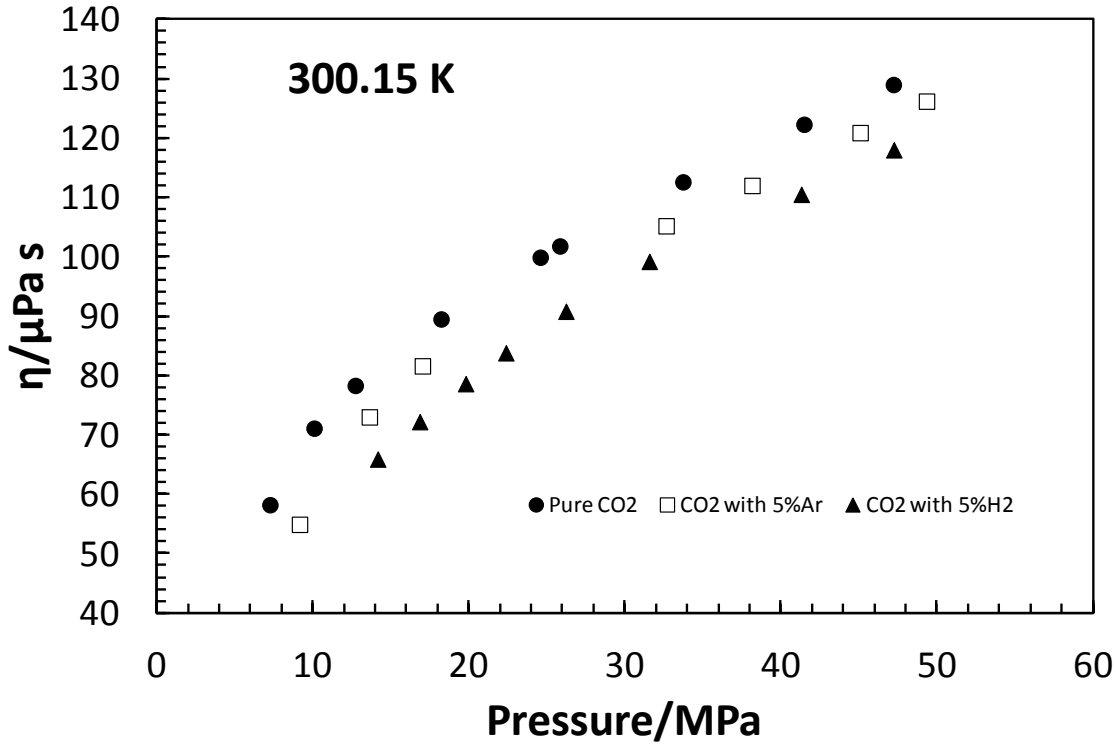


*Figure 6.5 The effect of Ar and $H_2$ on $CO_2$ viscosity at 300.15 K*

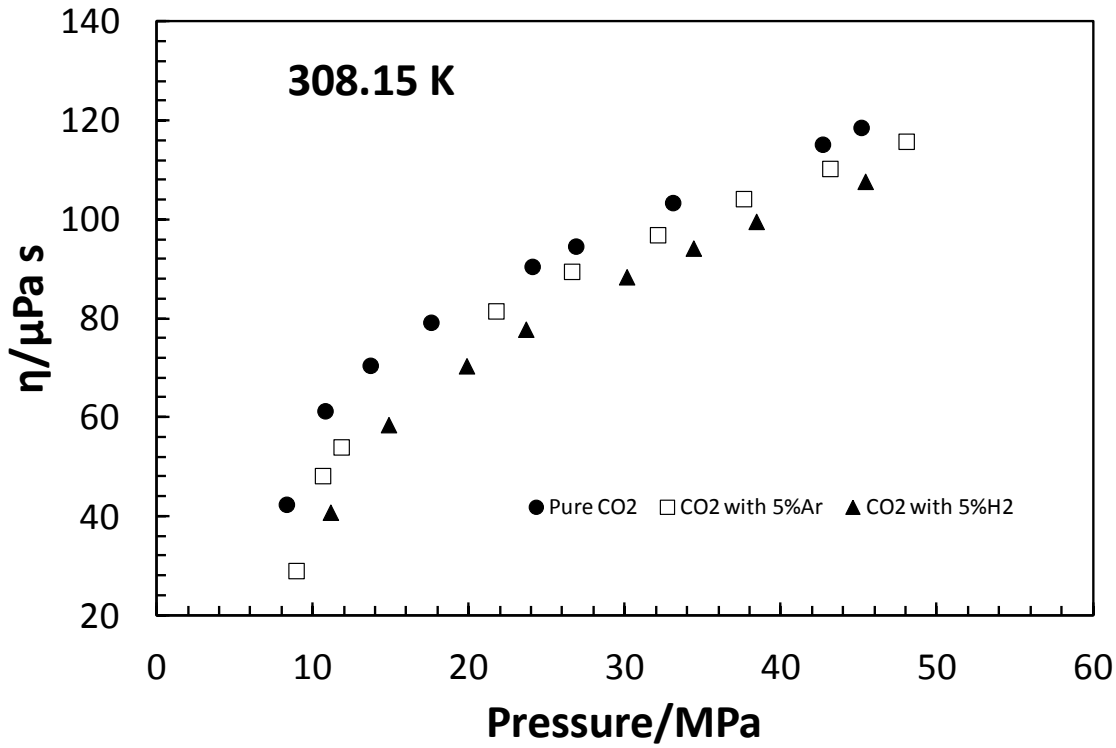


*Figure 6.6 The effect of Ar and $H_2$ on $CO_2$ viscosity at 308.15 K*

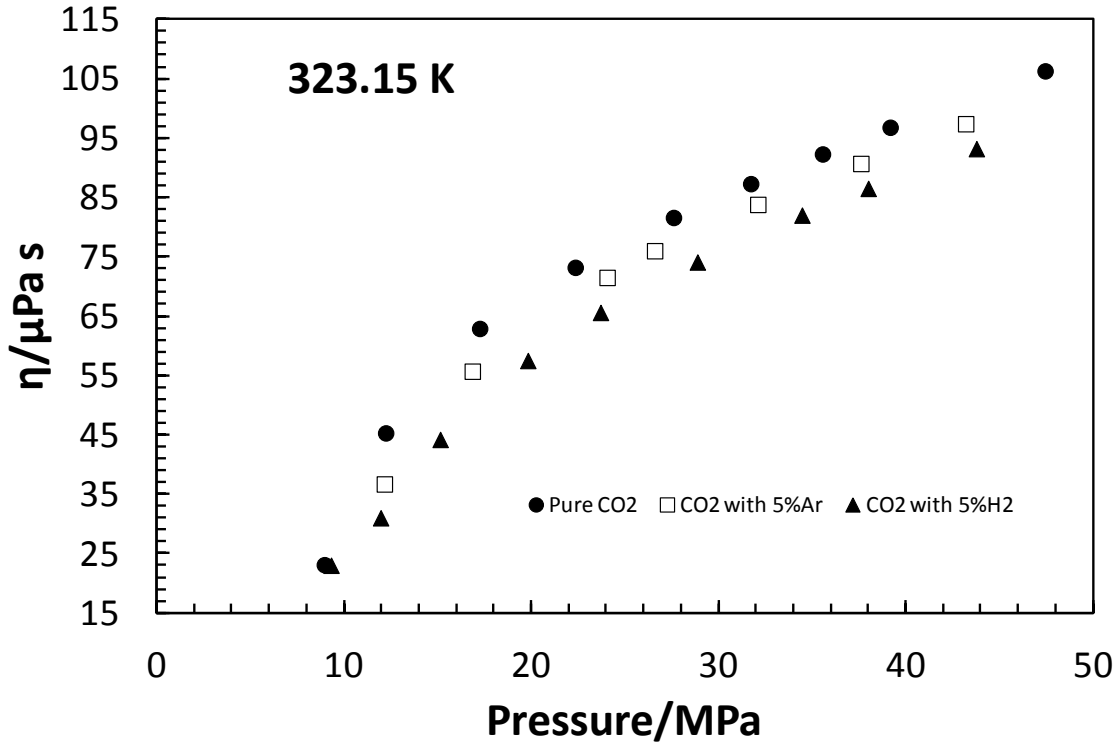


*Figure 6.7 The effect of Ar and $H_2$ on $CO_2$ viscosity at 323.15 K*

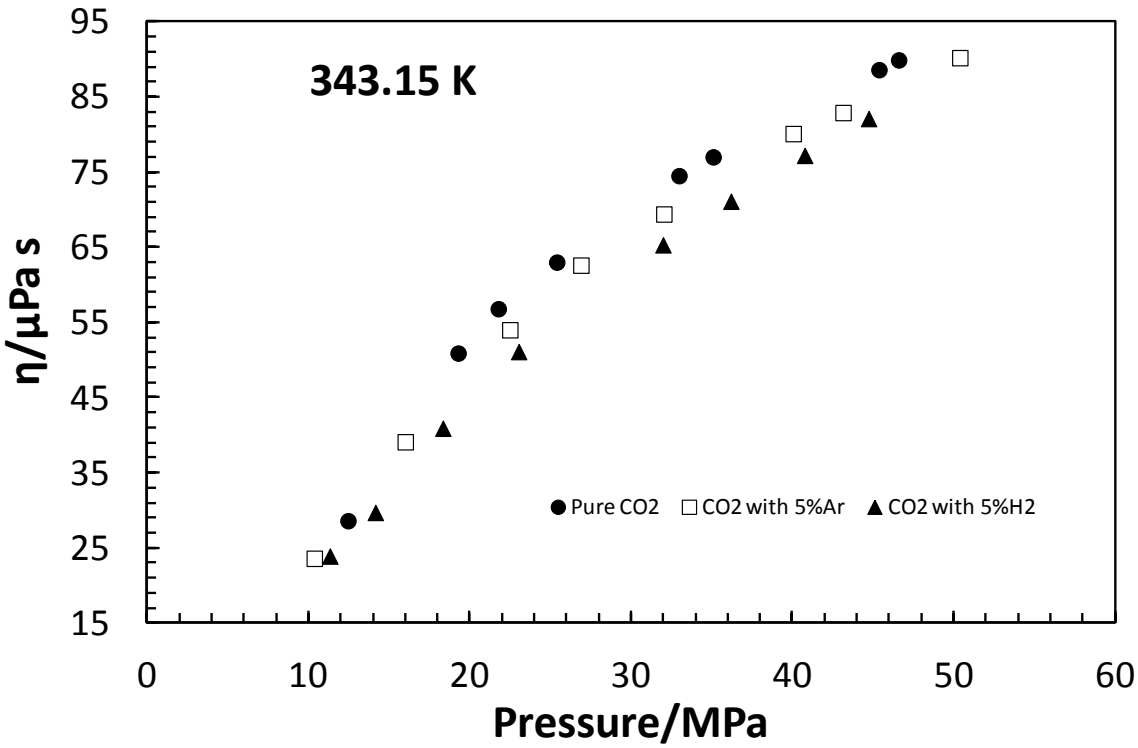


*Figure 6.8 The effect of Ar and $H_2$ on $CO_2$ viscosity at 343.15 K*

### *6.4.2 Modelling Results*

The procedures described in Section 6.3 for the LBC and $CO_2$-Pedersen models were used to predict the viscosity of a number of binary and multi-component mixtures ($CO_2$ and impurities) over wide ranges of temperature and pressure. The capability of the models was investigated in predicting the viscosity of pure $CO_2$ as shown in Figure 6.9 and Figure 6.10. The $CO_2$-Pedersen model gives accurate results with less than 1.3% maximum absolute deviation. In the other hand, the modified LBC is over predicting at low pressure near the saturated and supercritical boundaries. At low temperature and high pressure measurements, the model is under predicting and the deviation can reach 7%. The viscosity of each conducted test was calculated using these two models. The results are also shown in Table 6.8 to Table 6.13. The average absolute deviation associated with the models for each system can be found in Table 6.14. From the table, the $CO_2$-Pedersen model predicts the viscosity of pure $CO_2$, $CO_2/CH_4$ and $CO_2/O_2$ systems with greater accuracy than the LBC model. However, the overall predictions of the mixture viscosity shows that the modified LBC has lower deviation compare to the modified Pedersen model, i.e. AADs are 2.4% and 2.8% with the LBC and $CO_2$-Pedersen models respectively. The LBC correlation was tuned to match the

experimental data of $CO_2$ systems. The average absolute deviation for the LBC correlation before tuning was 9.3%, which reduced to 2.3% after tuning to the experimental data. To compare the original Pedersen model in which methane is the reference fluid, with the $CO_2$-Pedersen model, the viscosity data for a 0.95%$CO_2$ + 5% Ar has been compared. The results show that the $CO_2$-Pedersen model can predict the mixture viscosity with less than 1.9% deviation compare to 9.15% in the original Pedersen model.

*Table 6.14 Average Absolute Deviation (AAD) for the different studied systems*

| Component | CO2-Pedersen AAD% | CO2-LBC AAD% |
|---|---|---|
| Pure $CO_2$ | 0.3 | 3.2 |
| $CO_2$ + methane | 1 | 2.8 |
| $CO_2$ + nitrogen | 4.3 | 3.1 |
| $CO_2$ + argon | 2.9 | 1.9 |
| $CO_2$ + carbon monoxide | 2.8 | 1.5 |
| $CO_2$ + oxygen | 1 | 1.4 |
| $CO_2$ + hydrogen | 8.3 | 3.1 |
| MIX 1 | 1.8 | 1.8 |
| AAD% | 2.8 | 2.3 |

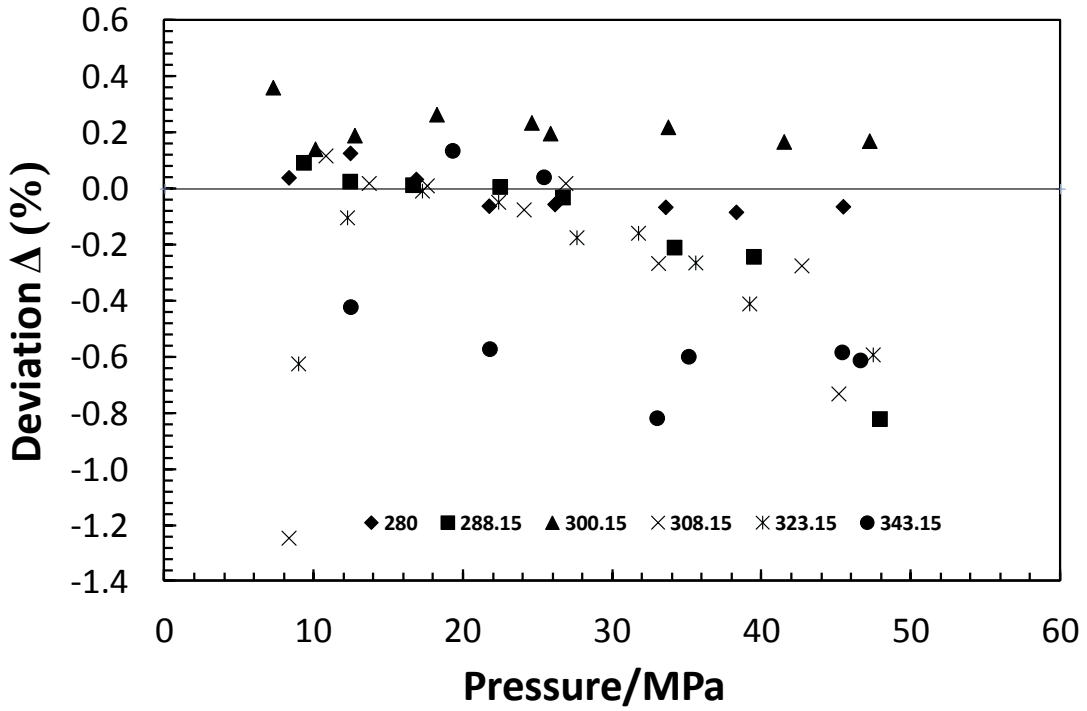


*Figure 6.9 Deviation of the $CO_2$-Pedersen model from the experimental results for pure $CO_2$*

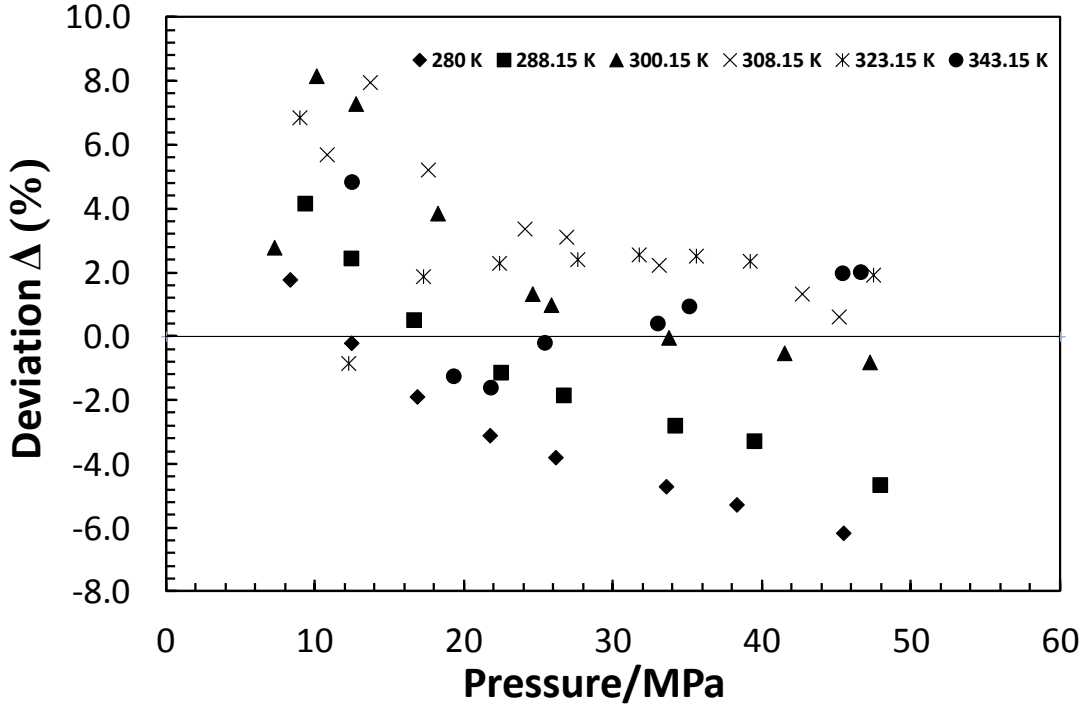


*Figure 6.10 Deviation of the LBC model from the experimental results for pure $CO_2$*

## 6.5 Conclusions

The capillary tube viscosity measurement method has been employed to measure the viscosity of $CO_2$ systems with impurities such as methane, nitrogen, argon, carbon monoxide, oxygen and hydrogen The experiments were conducted in an in-house designed and constructed set-up at pressures ranging from 7.4 to 50 MPa and at 280, 288.15, 300.15, 308.15, 323.15 and 343.15 K in the liquid and supercritical region. The results show that all of the tested impurities caused a reduction of viscosity compared to pure $CO_2$. In addition, two models were modified in order to predict the viscosity of pure and impure $CO_2$ systems. First, the predictive model of Pedersen was modified by substituting $CO_2$ as a reference fluid to the original reference fluid of methane. Then, the LBC correlation was tuned to match the obtained experimental data. The modelling results show that the models of $CO_2$-Pedersen and $CO_2$-LBC have an average absolute deviation (AAD) of 2.8% and 2.3%, respectively. However, more measurements on high pressure high temperature viscosity should be carried-out in order to compare the capability of the models in wide range of pressure and temperature.

**References**

[1] Li., H., Wilhelmsen, Ø., Yuexia, L., Wang, W. and Yan, J., , 2011, *Viscosities, Thermal Conductivities and Diffusion Coefficients of $CO_2$ Mixtures: Review of Experimental Data and Theoretical Model*International Journal of Greenhouse Gas Control, **5**, 1119-1139.

[2] Lohrenz, J., Bray, B. C. and Clark, C. R., 1964, *Calculating Viscosity of Reservoir Fluids from Their Composition*, J. Pet. Tech., **16**, 1171-1176.

[3] Quiñones-Cisneros, S. E., Zéberg-Mikkelsen, C. K. and Stenby, E. H., 2000, *The Friction Theory (F-Theory) for Viscosity Modeling*, Fluid Phase Equilib., **169**, 249-276.

[4] Pedersen, K. S., Fredenslund, A., Chirstensen, P. L. and Thomassen, P., 1984, *Viscosity of Crude Oils*, Chem. Eng. Sci., **39**, 1011-1016.

[5] Vesovic, V., Wakeham, W. A., Olchowy, G. A., Sengers, J. V., Watson, J.T. R. and Millat, J., 1990, *The Transport Properties of Carbon Dioxide*, J. Phys. Chem., **19**, 763-808.

[6] Fenghour, A., Wakeham, W. A. and Vesovic, V., 1998, *The Viscosity of Carbon Dioxide*, J. Phys. Chem. Ref. Data, **27**, 31-44.

[7] Cisneros, S., Zeberg, M., Claus, K, and Stenby, E. H., 2001, *One Parameter Friction Theory Models for Viscosity*, In: Fluid Phase Equilibria, **178**, 1-16.

[8] Ely, J. F. and Hanley, H.J. M., 1981, *Prediction of Transport Properties. 1. Viscosity of Fluids and Mixtures*, Ind & Engng Cheni Fundam, **20**. 323-331.

[9] Jossi, J. A., Steil, L. I. and Thodos, G., 1962, *The Viscosity of Pure Substances in the Dense Gaseous and Liquid Phases*, A/Ch.U, **8**, 59-63.

[10] Al-Marri, S. S, 2006, *PVT, Phase Behavior And Viscosity Measurements And Modeling Of The Ternary And Binary Systems Of Carbon Dioxide + Heavy*

*Hydrocarbon (N-Eicosane) + Light Gas (Ethane Or Propane)*, A dissertation presented to the faculty of the graduate school university of southern California .

[11] Jackson, W. M., 1956, *Viscosities of the Binary Gas Mixtures, Methane–Carbon Dioxide and Ethylene-Argon*, J. Phys. Chem., **60**, 789-791.

[12] DeWitt, K. J. and Thodos, G., 1966, *Viscosities of Binary Mixtures in Dense Gaseous State: the Methane–Carbon Dioxide System*, Can. J. Chem. Eng., **44**, 148-151.

[13] Kestin, J. and Yata, J., 1968, *Viscosity and Diffusion Coefficient of Six Binary Mixtures*, J. Chem. Phys., **49**, 80-91.

[14] Trautz, M. and Kurz, F., 1931, *The Viscosity, Thermal Conductivity and Diffusion in Gas Mixtures. XV. The Viscosity of $H_2$, $N_2O$, $CO_2$ and C3H8 and Their Binary Mixtures* (in German), Ann. Phys. (Leipzig), **9**, 981-1003.

[15] Heath, H. R., 1948, *The Viscosity of Gas Mixtures*, Proceedings of the Physical Society, Section B, London.

[16] Buddenberg, J. M. and Wilke, C. R., 1951, *Viscosities of Some Mixed Gases*, J. Phys. Coll. Chem., **55**, 1491-1498.

[17] Gururaja, G. J., Tirunarayanan , M. A. and Ramachandran, A., 1967, *Dynamic Viscosity of Gas Mixtures*, J. Chem. Eng. Data., **12**, 562–567.

[18] Kestin, J., Ro, S. T. and Wakeham, W. A., 1983, *The Transport Properties of Binary Mixtures of Hydrogen with CO, $CO_2$ and $CH_4$*, Physica, **119**, 615-638.

[19] Mal'tsev, V. A., Nerushev, O. A., Novopashin, S. A., Radchenko, V. V,. Licht, W. R., Miller, E. J and Parekh, V. S., 2004, *Viscosity of $H_2$-$CO_2$ Mixtures at (500, 800, and 1100) K*, J. Chem. Eng Data, 49, 684–687.

[20] Kestin, J. and Leidenfrost, W., 1959, *The Effect of Pressure on the Viscosity of $N_2$-$CO_2$ Mixtures*, Physica, **25**, 525-536.

[21] Kestin, J., Kobayashi, Y. and Wood, R. T., 1966, *The Viscosity of Four Binary Gaseous Mixtures at 20 And 30 °C*, Physica, **32**, 1065-108.

[22] Golubev, I. F., 1970, *Viscosity of Gases and Gas Mixtures*, Israel programme for scientific translations, Jerusalem.

[23] Kestin, J. and Ro, S. T., 1974, *The viscosity of nine binary and two ternary mixtures of gases at low density*, Ber. Bunsenges Phys. Chem., **78**, 20-24.

[24] Hobley, A., Matthews, G. P. and Townsend, A., 1989, *The Use of a Novel Capillary Flow Viscometer for the Study of the Argon-Carbon Dioxide System*, Int. J. Thermophys., **10**, 1165-1179.

[25] Kestin, J. and Ro, S. T., 1983, *The Viscosity of Carbon-Monoxide Mixtures with Four Gases in the Temperature Range 25-200 °C*. Ber. Bunsenges Phys. Chem., **87**, 600-602.

[26] Kestin, J., Khalifa, H. E., Ro, S. T. and Wakeham, W. A., 1977, *The Viscosity and Diffusion Coefficients of Eighteen Binary Gaseous Systems*, Physica, **88**, 242-260.

[27] Herning, F. and Zipperer, L., 1936, *Calculation of the Viscosity of Technical Gas Mixtures from the Viscosity of the Individual Gases*, GWF, das Gas-und Wasserfach, **79**, 69-73.

[28] Kenney, M. J., Sarjant, R. J. and Thring , M. W., 1956, *The Viscosity of Mixtures of Gases at High Temperatures*, Brit. J. Appl. Physics, **7**, 324-329.

[29] Kestin, J. and Ro, S. T., 1976, *Transport Properties of Nine Binary and Two Ternary Mixtures of Gases at Low Density*, Ber. Bunsenges. Phys. Chem., **80**, 619-624.

[30] Boushehrl, A. and Najafi, B.,1979, *Viscosity of Nonpolar Gases (Quaternary Mixtures)*, J. Chem. Eng. Data, **24**, 24-25.

[31] Pedersen, K. S. and Christensen, P. L., 2007, *Phase Behaviour of Petroleum Reservoir Fluids*, CRC Press, Taylor & Francis Group.

[32] Hanley, H.J. M., 1976, *Prediction of the Viscosity and Thermal Conductivity Coefficients of Mixtures*, Cryogenics, **16**, 643-651.

[33] Murad, S., and Gubbins, K. E., 1977, *Corresponding States Correlation for Thermal Conductivity of Dense Fluids*, Chem. Eng. Sci., **32**, 499-505.

[34] Younglove, B. A. and Ely, J. F., 1987, *Thermophysical Properties of Fluids. II. Methane, Ethane, Propane, Isobutane, and Normal Butane*, J. Phys. Chem. Ref. Data, **16**, 577-798.

[35] Stiel, L. I. and Thodos, G., 1961, *Viscosity of Nonpolar Gases at Normal Pressures*, AIChE J., **7**, 611-615.

[36] Pensado, A. S., Padua, A.A. H., Comunas, M.J. P. and Fernandez, J., 2008, *Viscosity and Density Measurements for Carbon Dioxide + Pentaerythritolester Lubricant Mixtures at Low Lubricant Concentration*, J. of Supercritical Fluids ,**44**, 172–185.

# CHAPTER 7: IFT, SWELLING FACTOR AND MMP OF $CO_2$/N-DECANE SYSTEM

## 7.1 Introduction

In order to minimize the emission of $CO_2$ to the atmosphere, $CO_2$ can potentially be either sequestrated into ground or utilized for enhanced oil recovery (EOR). The aim of $CO_2$-EOR process is to increase oil recovery by which $CO_2$ is injected into mature oil fields. Oil is recovered by $CO_2$ by either miscible or immiscible displacement processes, i.e. above or below the Minimum Miscibility Pressure (MMP) respectively. Above the MMP, the injected $CO_2$ completely mixes with the reservoir oil and the interfacial tension (IFT) between the $CO_2$ and the reservoir oil becomes zero. Both the density and viscosity are reduced and therefore the oil can be easily displaced. Below the MMP, where pressure is not enough to push IFT to zero, combination of viscosity reduction, oil swelling, and lowering of interfacial tension is enough to play a role in the $CO_2$/oil recovery process [1]. By dissolving $CO_2$ into oil, the IFT reduces [2]. This reduction significantly influences the relative permeability curves i.e. fluids act as single phase and trapping of fluids in pores is impossible [3]. Swelling (extraction) occurs when $CO_2$ dissolves into reservoir oil. It is a function of three parameters: pressure, temperature and oil composition when pure $CO_2$ is a solvent [2].

However $CO_2$ coming from capture processes is generally not pure and can contain impurities such as $N_2$, $H_2$, $O_2$, $H_2S$, $CH_4$, CO and water. Major properties in $CO_2$/oil fluid are influenced by the presence of impurities in the $CO_2$ stream. For instance, the MMP of $CO_2$ can increase in the presence of methane and nitrogen and decrease substantially in the presence of hydrogen sulphide and intermediate n-alkanes [4]. Metcalfe et al. [5] conducted slim tube experiments for $CO_2$ containing $H_2S$, methane and other hydrocarbons ($C_2$, $C_3$). The $CO_2$ streams containing $H_2S$ and/or LPG components have lower MMPs than those of pure $CO_2$ systems. Conversely, $C_1$ in the $CO_2$ stream raises the MMP. Their findings also stated that, $C_2$ is as effective in reducing MMP as $H_2S$ and ($C_3$, $C_4$) are even more effective. The effects of $CO_2$/impurities components on $CO_2$/oil MMP were also found by Shokir [6] in the

following order in terms of their impact: $N_2$, $C_1$, hydrocarbon components ($C_2$-$C_4$) and $H_2S$. $N_2$ and $C_1$ have a negative impact while the others have a positive impact. Nguyen et al. [7] covered the effect of nitrogen in different impurity range on the properties of $CO_2$/oil. They concluded that the presence of nitrogen in the $CO_2$ stream can potentially reduce diffusivity, swelling factor, solubility and oil recovery. Oil permeability and oil swelling are higher while IFT property of oil is lower in $CO_2$ injection compared to $N_2$ injection [4]. Effects on the solubility of $CO_2$/crude oil mixtures of adding $N_2$ contaminant was reported by Monger [8], Nguyen et al. [7] and Spivak and Chima [9]. The authors concluded that $N_2$ has an adverse effect on solubility and therefore on the immiscible carbon dioxide process mechanisms.

Several correlations were derived for predicting the Minimum Miscibility Pressure (MMP) pure $CO_2$ and $CO_2$ containing impurities with reservoir oil and reported in the literature [5, 10-17]. Some of those correlations require few input parameters (molecular weight of light components, $MC_5^+$, volatile oil fraction, intermediate oil fraction, °API gravity and oil weight) which are useful when detailed oil characterizations are not available, however they might lead to less accurate in predicting MMP. Computational methods to estimate the MMP for gas-oil systems comprise: Method of the Characteristics (MOC) [18, 19], 1D slim tube simulation [20, 21] and (one or multiple) mixing cell method (MCM) [22-25]. In this work, a modified version of the model proposed by Jaubert et al. [26] (which is based on Metcalfe et al. and Zick [24, 27] approaches) is used.

A wide range of IFT measurements methods are discussed by Rusanov and Prokhorov [28] and Drelich et al. [29]. These methods are capillary rise, pendant drop, drop weight, spinning drop, sessile drop and Wilhelmy plate methods. Two common IFT techniques are available for elevated pressure measurements, pendant drop and capillary rise methods. The later is rarely used in petroleum studies and it is not commercially available. However, it is one of the most and best accurate IFT methods [29, 30]. Ayirala [31] conducted IFT experiments on oil-$CO_2$ systems using the capillary rise method. He demonstrated that the technique can be easily adapted to high pressures and temperatures and is well suited to measure low interfacial tensions (0.044 dynes/cm).

In this work, an in-house experimental apparatus is adopted to measure the IFTs and swelling factors of pure and impure $CO_2$ gas with n-decane oil. Four $CO_2$ binary

mixtures ($CO_2/N_2$, $CO_2/O_2$, $CO_2/H_2$, and $CO_2/CH_4$) and two multi-components mixtures are investigated experimentally at 310.95 K. The MMPs of the systems are estimated experimentally using the Vanishing Interfacial Tension Approach (VIT) and predicted using a developed in-house modified algorithm based on the multiple-mixing cell approach.

## 7.2 Experimental Section

### *7.2.1 Materials*

The following compounds were used to make the different synthetic mixtures studied in this work:

- Carbon Dioxide, Supplied by Air Products, Research Grade
- Methane, Supplied by Air Products, Grade N4.5
- Nitrogen, Supplied by BOC, Research Grade
- Oxygen, Supplied by BOC, Research Grade
- Hydrogen, Supplied by BOC Gases, >= 99.995%
- N-decane, Supplied by ACROS-ORGANIC > 99%

The systems listed in Table 7.1 were prepared gravimetrically and used to conduct density tests. Multi component mixtures, MIX1 and MIX2 (compositions given in Table 7.2 supplied by BOC were also used to carry out the tests.

*Table 7.1 Injection gas compositions*

| Component | $CO_2$%mole | Impurity %mole (±0.3) |
|---|---|---|
| Pure $CO_2$ | 100 | 0 |
| $CO_2$+$CH_4$ | 95 | 5 |
| $CO_2$+$N_2$ | 95 | 5 |
| $CO_2$+$O_2$ | 95 | 5 |
| $CO_2$+$H_2$ | 95 | 5 |
| MIX1 | 95.64 | See Table.7.2 |
| MIX2 | 89.83 | See Table.7.2 |

*Table 7.2 Mixture compositions MIX1 and MIX2*

| Mixture Components | % mole (MIX1) | % mole (MIX2) |
|---|---|---|
| Carbon Dioxide | Balance | Balance |
| Methane | 0.6261 | - |
| Hydrogen | 0.8175 | - |
| Nitrogen | 1.41 | 5.05 |
| Carbon monoxide | 0.2127 | - |
| Argon | 1.21 | 2.05 |
| Oxygen | 0.08 | 3.07 |
| Total | 100 | 100 |

### *7.2.2 Equipment and procedures*

The basic theory for the capillary rise technique is to measure the meniscus height in a round glass tube with known inner radius. The equation governing the capillary rise in the tube is given by:

$$IFT = \frac{rh(\rho_{liquid} - \rho_{gas})g}{2\cos(\theta)} \tag{7.1}$$

Where:

*IFT* = interfacial tension in mN/m; *r* = pore throat radius in cm; *h* = capillary rise in cm

$\rho_{liquid}$ = density of liquid phase in g/cm$^3$; $\rho_{gas}$ = density of vapour phase in g/cm$^3$

$\theta$ = equilibrium contact angle in degrees (equals to zero, glass completely wet)

g = acceleration due to gravity (980 cm/s$^2$)

To achieve high accuracy, the tube must be absolutely vertical, its cross-section uniform and the liquid should be completely wetting the wall. In the presence of a vapour phase, the contact angle (θ) in the above equation can be set to zero for $CO_2$-oil systems, since liquids wet the glass surfaces completely [31]. The schematic diagram of the capillary rise technique used is shown in Figure 7.1. The relation between the tube radius, *r*, and the capillary rise, *h*, given in Equation 7.1 is inversely proportional to the interfacial surface tension i.e. as the radius becomes smaller the rise can be measured precisely,

especially at low IFT. Therefore, a radius of 0.2 mm tube was installed in this experiment, four and half times smaller than the tube radius used by Ayirala [31] work.

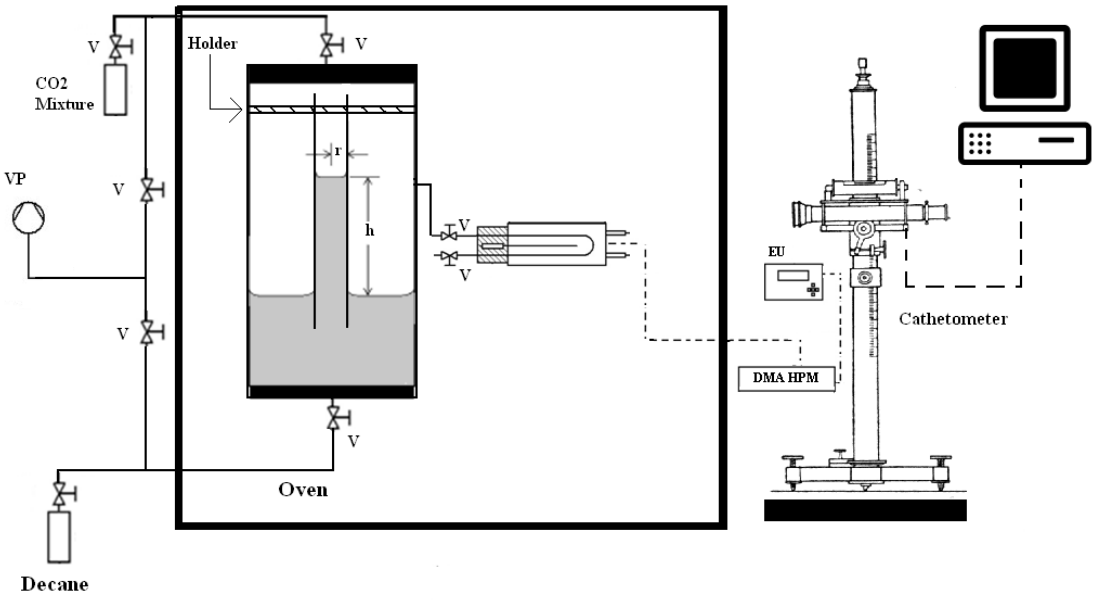


*Figure 7.1 Schematic of capillary rise technique used for $CO_2$/n-decane system*

At first, the capillary tube was carefully fitted into a special holder and is placed inside the equilibrium cell. The cell has a volume of 100 $cm^3$ fitted with a glass window and has a pressure limit up to 70 MPa. Since this test is very sensitive to trace contaminants, the cell should be cleaned. Heptane is introduced to the cell and followed by nitrogen purging. The cell and its loading lines are vacuumed prior to introduction of any fluid. The cell was then filled with pure $CO_2$ gas and was heated to 310.95 K using the oven. "n-decane" in a pressurized transfer vessel was injected into the cell so that the cell was filled with fluids at a fixed initial volumetric liquid oil ratio (80% $CO_2$ 20% n-decane). The cell pressure is regulated by injecting more $CO_2$ or $CO_2$/impurities. The compressed gas density data of $CO_2$ and $CO_2$/impurities systems were measured with a high temperature and pressure vibrating tube densitometer, Anton Paar DMA-HPM, which consists of a measuring cell and an interface module as shown in Figure 7.1. The liquid density was reported to increase slightly by increasing the pressure in n-decane/$CO_2$ system at different temperatures [32, 33]. For example at 344.3 K and pressure up to 12.4 MPa, the increase in the liquid phase density of n-decane/$CO_2$ system is about 1.4% compare to the density of pure n-decane. Therefore, the liquid phase density of $CO_2$/n-decane is measured at different pressures; however the liquid density of the

mixtures containing impurities is interpolated with data of $CO_2$/n-decane system. So the densitometer is only used to measure the density of vapour phase in the tested systems including impurities systems. The densitometer is calibrated with two fluids: pure $CO_2$ and water at 310.95 K. Two hours are given for the fluid phases to equilibrate in the cell. The capillary rise observed in the glass tube was then measured using the cathetometer. The height was measured precisely using the magnification system of the camera and a computer. The precision of the reading is better than 0.01 mm. Two heights, capillary rise and the oil level in the equilibrium cell, including the density are measured at each pressure. The above steps are repeated for the other systems containing impurities. Examples of images captured from the apparatus for pure $CO_2$ as injection gas are shown in Figure 7.2.

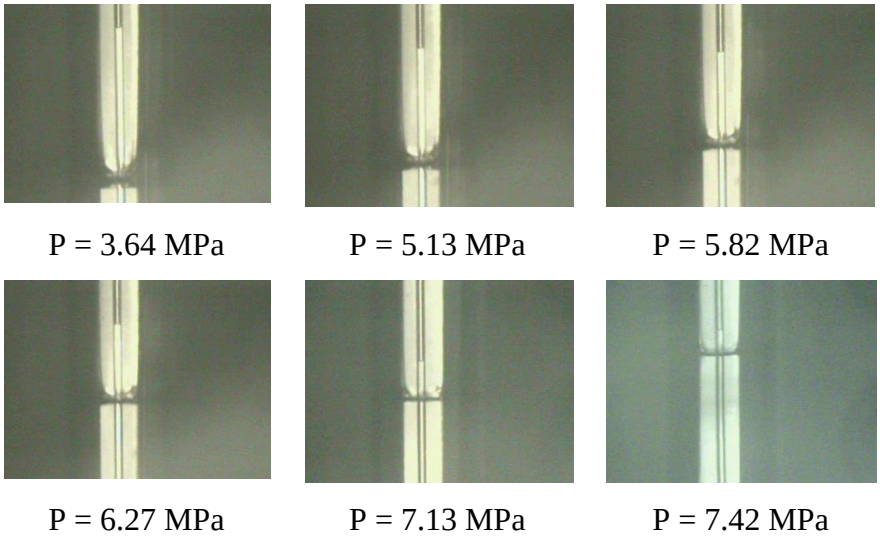


*Figure 7.2 Images of $CO_2$/n-decane at 310.95 K, shown that the capillary rise reduces as the system approaches the MMP by increasing the injection gas pressure*

## 7.3 Results and Discussion

### *7.3.1 IFT*

In order to validate the experimental setup, the IFTs results obtained by the capillary rise method are plotted together with the data available in literature. Figure 7.3 shows that the IFT measurements of $CO_2$/n-decane generated using the apparatus setup were in excellent agreement with literature data [31]. The Interfacial tension (IFT) between n-decane and $CO_2$ phase decreases as the pressure increases. The pendant drop results

show that the apparatus cannot measure IFT lower than 3.75 *mN/m*, making the capillary rise technique better suited for low IFT measurements.

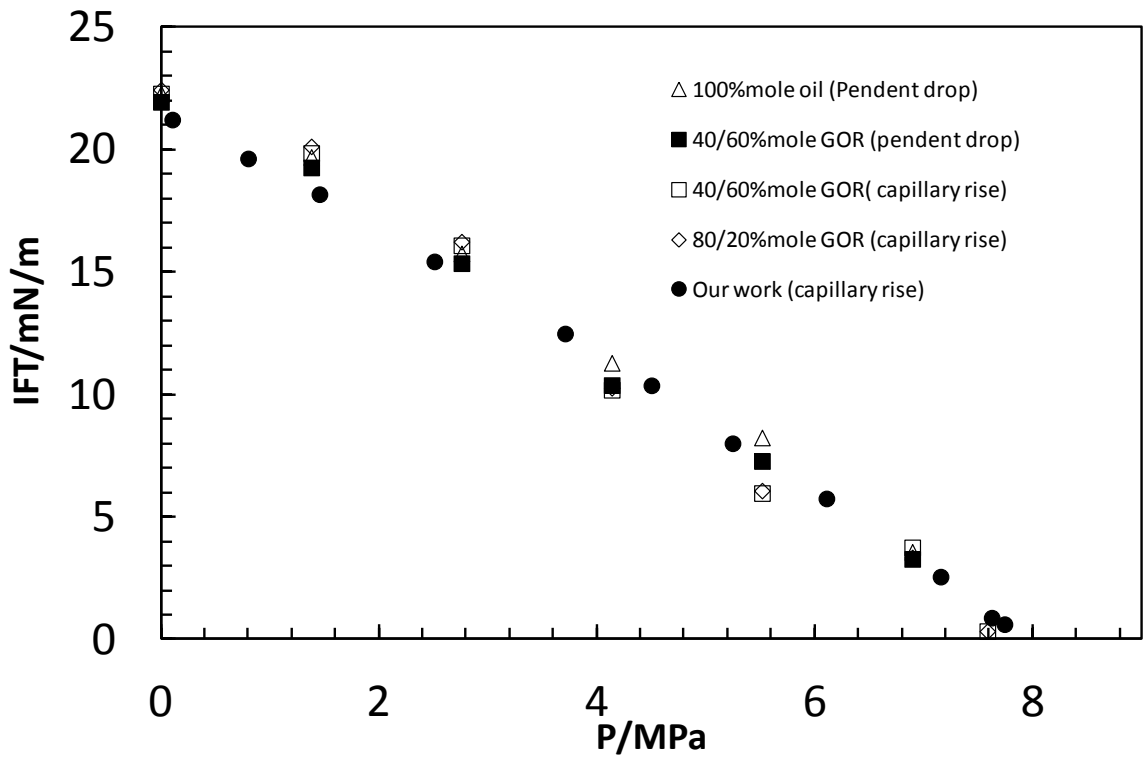


*Figure 7.3 Experimental data for $CO_2$/n-decane system at 310.95 K, literature data [31]*

The effect of impurities on this property is investigated and listed in Table 7.3. Four binary mixtures are used with 5% mole fraction of impurity, $CO_2/N_2$, $CO_2/H_2$, $CO_2/CH_4$, $CO_2/O_2$ and two multi-components mixtures MIX1 and MIX2 listed in Table 7.1 and Table7.2. The IFT values in $CO_2$/impurities systems are shifted to higher pressures making the displacement of n-decane less efficient. As the system pressure increased, the IFTs difference between pure and impure $CO_2$ in n-decane becomes higher. For the binary systems, hydrogen seems to have the highest impact of the four impurities and methane has the lowest impact. The vapour phase and organic phase (rich decane) IFTs with the three mixtures, $CO_2/H_2$, $CO_2/O_2$ and MIX1, almost behave in a similar manner as pressure increases while MIX2 with 10.17mole% impurity fraction has the highest impact compare to the tested systems. For example, the IFTs at around 2.7 *mN/m* occurs at pressure 7.2, 8.1, 8 and 9.2 MPa for pure $CO_2$, $CO_2/H_2$, MIX1 and MIX2 respectively. It means that, both mole fraction and the type of impurities affect the IFT for certain oil such as n-decane used in this work.

*Table 7.3 Equilibrated fluid densities, capillary rise heights and IFTs Measured in n-decane/$CO_2$ System and n-decane/impure $CO_2$ Systems at 310.95 K*

| Pure $CO_2$ | | | | |
|---|---|---|---|---|
| P/MPa (±0.1%) | $\rho_{liquid}$/g.cm$^{-3}$ (±0.0001) | $\rho_{gas}$/g.cm$^{-3}$ (±0.05) | Height/cm (±0.002) | IFT/mN.m$^{-1}$ (±0.05) |
| 0.10 | 0.7171 | 0.0018 | 3.028 | 21.23 |
| 0.80 | 0.7177 | 0.0141 | 2.848 | 19.64 |
| 1.45 | 0.7186 | 0.0265 | 2.68 | 18.18 |
| 2.51 | 0.7203 | 0.0491 | 2.346 | 15.43 |
| 3.71 | 0.7223 | 0.0778 | 1.977 | 12.49 |
| 4.50 | 0.7236 | 0.1 | 1.697 | 10.37 |
| 5.25 | 0.7247 | 0.1246 | 1.361 | 8 |
| 6.11 | 0.7258 | 0.1606 | 1.038 | 5.75 |
| 7.16 | 0.7262 | 0.2266 | 0.522 | 2.56 |
| 7.63 | 0.7258 | 0.2751 | 0.199 | 0.88 |
| 7.74 | 0.7257 | 0.2964 | 0.146 | 0.61 |
| $CO_2/N_2$ | | | | |
| P/MPa (±0.1%) | $\rho_{liquid}$/g.cm$^{-3}$ (±0.0001) | $\rho_{gas}$/g.cm$^{-3}$ (±0.05) | Height/cm (±0.002) | IFT/mN.m$^{-1}$ (±0.05) |
| 0.10 | 0.7171 | 0.0018 | 2.997 | 21.01 |
| 0.99 | 0.718 | 0.0173 | 2.789 | 19.15 |
| 2.82 | 0.7208 | 0.0537 | 2.329 | 15.23 |
| 4.47 | 0.7235 | 0.0954 | 1.836 | 11.3 |
| 5.27 | 0.7248 | 0.1184 | 1.543 | 9.17 |
| 6.71 | 0.7262 | 0.1715 | 1.098 | 5.97 |
| 7.37 | 0.7261 | 0.2041 | 0.696 | 3.56 |
| 7.82 | 0.7255 | 0.2322 | 0.486 | 2.35 |
| 8.22 | 0.7246 | 0.264 | 0.291 | 1.31 |
| $CO_2/CH_4$ | | | | |
| P/MPa (±0.1%) | $\rho_{liquid}$/g.cm$^{-3}$ (±0.0001) | $\rho_{gas}$/g.cm$^{-3}$ (±0.05) | Height/cm (±0.002) | IFT/mN.m$^{-1}$ (±0.05) |
| 0.10 | 0.7171 | 0.0023 | 3.043 | 21.32 |
| 0.81 | 0.7177 | 0.0137 | 2.847 | 19.64 |

| | | | | |
|---|---|---|---|---|
| 1.90 | 0.7193 | 0.0342 | 2.579 | 17.32 |
| 3.16 | 0.7214 | 0.0611 | 2.179 | 14.1 |
| 4.85 | 0.7241 | 0.1046 | 1.647 | 10 |
| 6.06 | 0.7257 | 0.1458 | 1.215 | 6.91 |
| 6.78 | 0.7262 | 0.1769 | 0.852 | 4.59 |
| 7.38 | 0.7261 | 0.21 | 0.614 | 3.11 |
| 7.80 | 0.7256 | 0.2408 | 0.478 | 2.27 |

$CO_2/H_2$

| P/MPa (±0.1%) | $\rho_{liquid}$/g.cm$^{-3}$ (±0.0001) | $\rho_{gas}$/g.cm$^{-3}$ (±0.05) | Height/cm (±0.002) | IFT/mN.m$^{-1}$ (±0.05) |
|---|---|---|---|---|
| 0.10 | 0.7171 | 0.0017 | 3.02 | 21.17 |
| 1.28 | 0.7184 | 0.0222 | 2.731 | 18.63 |
| 3.08 | 0.7213 | 0.0583 | 2.244 | 14.58 |
| 4.39 | 0.7234 | 0.0892 | 1.834 | 11.4 |
| 5.93 | 0.7256 | 0.1324 | 1.319 | 7.67 |
| 6.59 | 0.7261 | 0.1561 | 1.12 | 6.26 |
| 7.03 | 0.7262 | 0.1735 | 0.968 | 5.24 |
| 7.73 | 0.7257 | 0.202 | 0.671 | 3.44 |
| 8.13 | 0.7248 | 0.2247 | 0.549 | 2.69 |
| 8.54 | 0.7234 | 0.2515 | 0.396 | 1.83 |

$CO_2/O_2$

| P/MPa (±0.1%) | $\rho_{liquid}$/g.cm$^{-3}$ (±0.0001) | $\rho_{gas}$/g.cm$^{-3}$ (±0.05) | Height/cm (±0.002) | IFT/mN.m$^{-1}$ (±0.05) |
|---|---|---|---|---|
| 0.10 | 0.7171 | 0.0018 | 3.018 | 21.16 |
| 1.22 | 0.7183 | 0.0217 | 2.713 | 18.52 |
| 2.99 | 0.7211 | 0.0579 | 2.257 | 14.67 |
| 4.48 | 0.7236 | 0.0954 | 1.85 | 11.39 |
| 5.94 | 0.7256 | 0.1419 | 1.368 | 7.83 |
| 7.12 | 0.7262 | 0.1933 | 0.921 | 4.81 |
| 8.32 | 0.7242 | 0.282 | 0.492 | 2.13 |

MIX1

| P/MPa (±0.1%) | $\rho_{liquid}$/g.cm$^{-3}$ (±0.0001) | $\rho_{gas}$/g.cm$^{-3}$ (±0.05) | Height/cm (±0.002) | IFT/mN.m$^{-1}$ (±0.05) |
|---|---|---|---|---|

| | | | | |
|---|---|---|---|---|
| 0.10 | 0.7171 | 0.0017 | 3.022 | 21.19 |
| 1.27 | 0.7184 | 0.0221 | 2.733 | 18.65 |
| 3.17 | 0.7214 | 0.0614 | 2.232 | 14.44 |
| 5.38 | 0.7249 | 0.1198 | 1.544 | 9.16 |
| 6.98 | 0.7262 | 0.1811 | 0.981 | 5.24 |
| 8.01 | 0.7251 | 0.2417 | 0.578 | 2.74 |
| 8.54 | 0.7234 | 0.2918 | 0.369 | 1.56 |

MIX2

| P/MPa (±0.1%) | $\rho_{liquid}$/g.cm$^{-3}$ (±0.0001) | $\rho_{gas}$/g.cm$^{-3}$ (±0.05) | Height/cm (±0.002) | IFT/mN.m$^{-1}$ (±0.05) |
|---|---|---|---|---|
| 0.10 | 0.7171 | 0.0017 | 3.027 | 21.22 |
| 1.35 | 0.7185 | 0.0235 | 2.739 | 18.65 |
| 3.64 | 0.7222 | 0.0706 | 2.175 | 13.89 |
| 5.36 | 0.7249 | 0.114 | 1.703 | 10.2 |
| 7.06 | 0.7262 | 0.1708 | 1.231 | 6.7 |
| 8.39 | 0.724 | 0.2382 | 0.831 | 3.96 |
| 9.17 | 0.7198 | 0.289 | 0.645 | 2.72 |

### *7.3.2 Swelling factor*

When $CO_2$ comes into contact with oil, a process of dissolution occurs thereby causing swelling. The degree of swelling depends on pressure, temperature and oil composition [34]. Swelling is important for two reasons: firstly, the residual oil saturation is inversely proportional to the swelling factor. The residual oil saturation is an important point in relative permeability curves and determines the ultimate recovery. In addition, swollen oil droplets can push fluids out of the pores, creating a drainage process [35]. The oil swelling increases oil saturation therefore increases oil relative permeability too [3]. The governing equation used in oil and gas industries is defined as:

$$\text{swelling factor} = \frac{\text{oil volume at P and T}}{\text{oil volume at 1 atm and T}} \tag{7.2}$$

The relation between the volume is linearly proportional with distance, see Figure 7.4, (measured by cathetometer), i.e. the cross section of the cell can be assumed constant. In

this work, the volume of the cell was calibrated with distance. Therefore the swelling factor can be re-defined as:

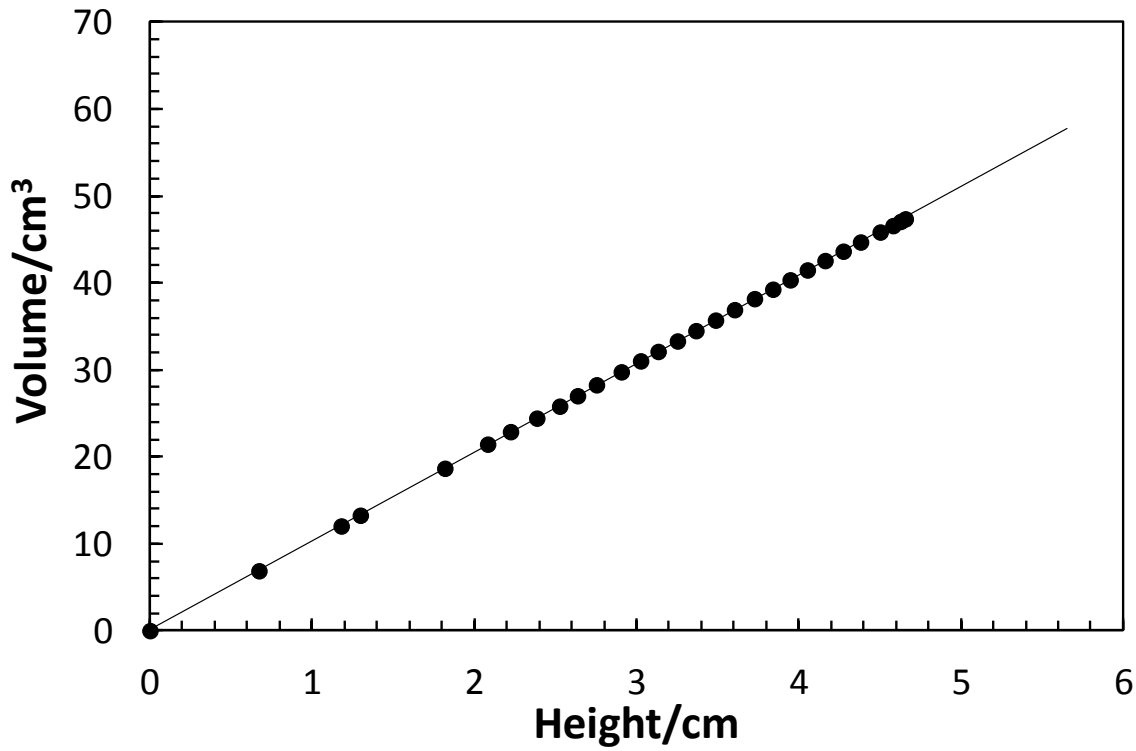


*Figure 7.4 The cell volume Calibration in terms of the vertical distance (height)*

$$\text{swelling factor} = \frac{Z_{oil} \text{ at P and T}}{Z_{oil} \text{ at 1 atm and T}} \text{ ; Where } Z_{oil} \text{ is oil height.} \quad (7.3)$$

The volume of oil in the liquid phase increases with pressure as $CO_2$ dissolves in and swells the oil. The isothermal measurements of the swelling factor for the pure and impure $CO_2$/n-decane systems at 310.95 K are shown in Figure 7.5. Swelling is temperature independent as was suggested previously [8] when a certain sample is used. Therefore, running swelling factor experiments at 310.95 K can give a good estimation for the effect of impure $CO_2$ in n-decane at different temperatures. Pure $CO_2$ swells n-decane to higher value compared to $CO_2$ containing impurities. For example, at pressure 7.3 MPa the swelling factors are 2.53, 1.73, 1.72 and 1.44 for pure $CO_2$, $CO_2/N_2$, MIX1 and MIX2 respectively. This means 10% mole fraction of impurities (as the case of MIX2) can potentially reduce swelling by 43% at the pressure given in the above

example. The effect of impurities on binary mixtures is insignificant below 6 MPa, and then the difference becomes wider as the pressure increases.

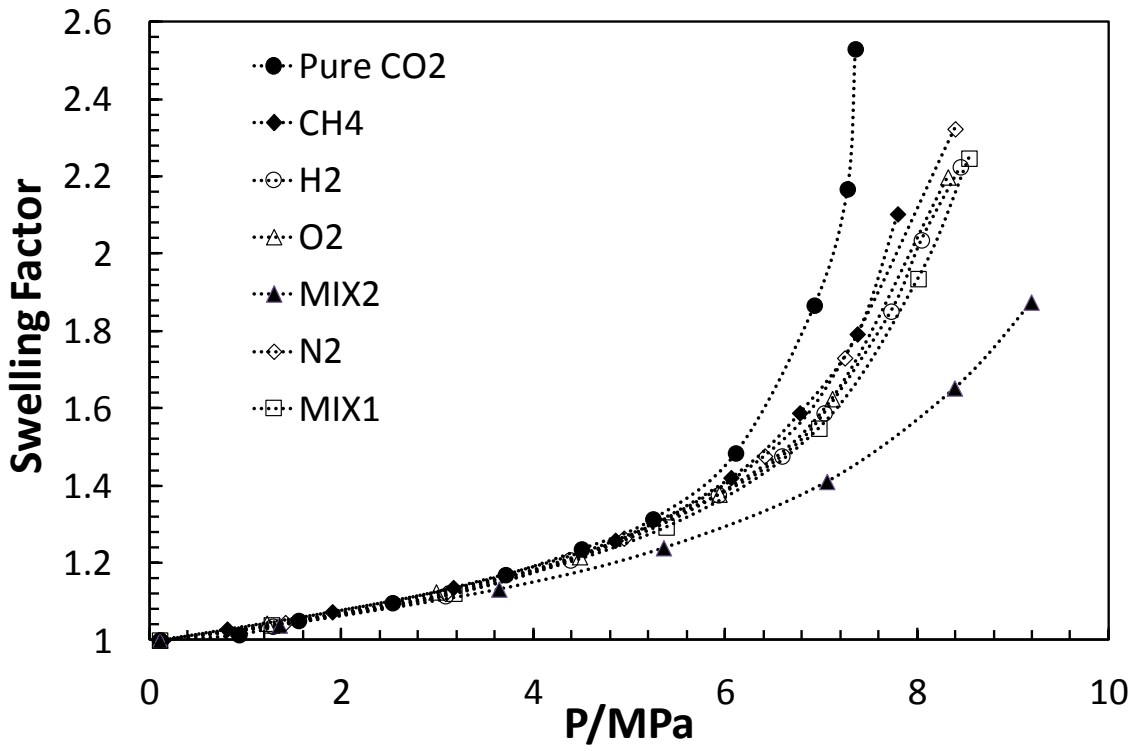


*Figure 7.5 Swelling factor measurements in $CO_2$ and $CO_2$/impurities systems with n-decane at 310.95 K*

### *7.3.3 MMP*

#### *7.3.3.1 Vanishing Interfacial Tension Approach (VIT)*

Recently [36] an experimental method, called the vanishing interfacial tension (VIT) technique, has been used to determine the miscibility conditions of different oil-$CO_2$ systems. The method is based on measuring the IFTs against one of the independent variables, pressure or enrichment levels of the gas phase. The MMP is determined by linearly extrapolating the measured equilibrium IFT versus equilibrium pressure data (in our case) to zero equilibrium IFT, i.e. the corresponding pressure at IFT = 0. The technique is based on the concept that the interfacial tension (IFT) between a crude oil and $CO_2$ becomes zero when they are miscible. Figure 7.6 demonstrates the VIT approach with pure and impure $CO_2$ at 310.95 K. The mixtures with their corresponding MMPs calculated by the method are given in Figure 7.7. This $CO_2$/n-decane system has

a reported slim-tube MMP of 8.2 MPa to 8.6 MPa a rising-bubble MMP of 8.8 MPa at 310.95 K [37]. A new method based on magnetic resonance imaging (MRI) [38] and VIT method [31] also provided MMP values of 7.8 and 7.79 MPa respectively for the same system. The MMPs values obtained with slim tube and rising-bubble apparatus are in good agreement with the MMP estimated in our work using the VIT approach (8.12 MPa). From Figure 7.7, the presence of impurities in $CO_2$ stream increase the MMP of $CO_2$/n-decane system to 8.93, 8.71, 9.28, 9.27, 9.23 and 10.36 MPa when the injection gas mixtures $CO_2/N_2$, $CO_2/CH_4$, $CO_2/H_2$, $CO_2/O_2$, MIX1 and MIX2 are used respectively.

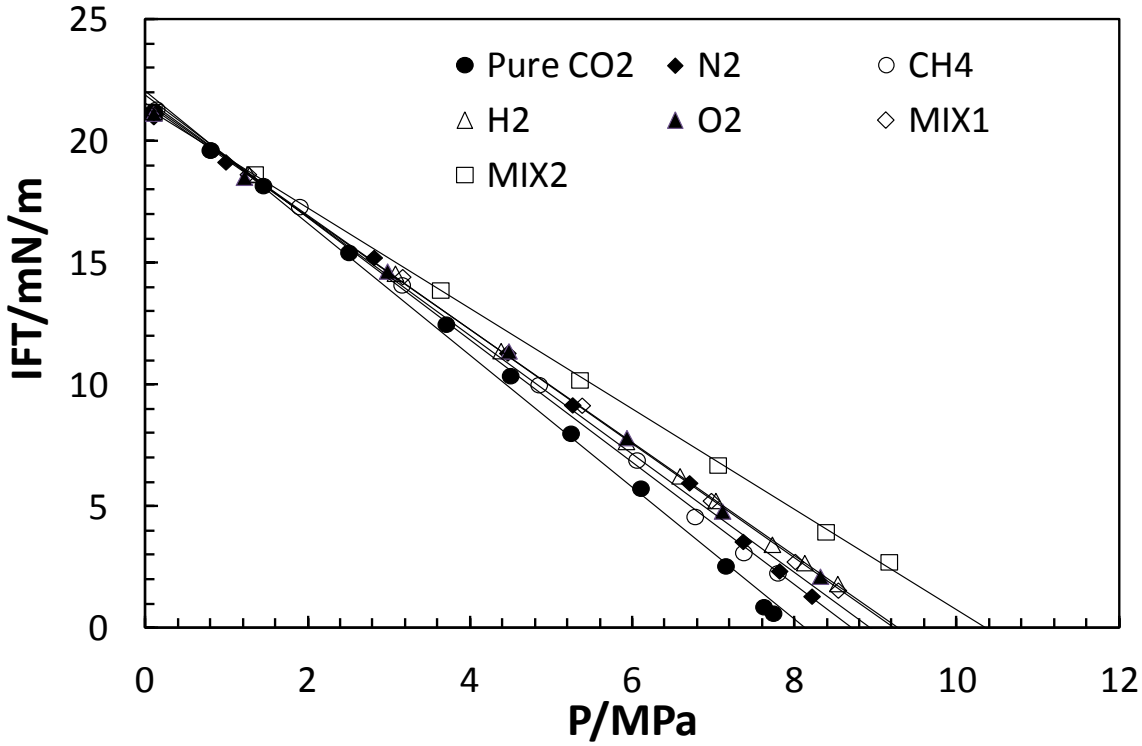


*Figure 7.6 Determination of VIT Miscibility in n-Decane-$CO_2$ System and n-Decane impure $CO_2$ System at 310.95 K*

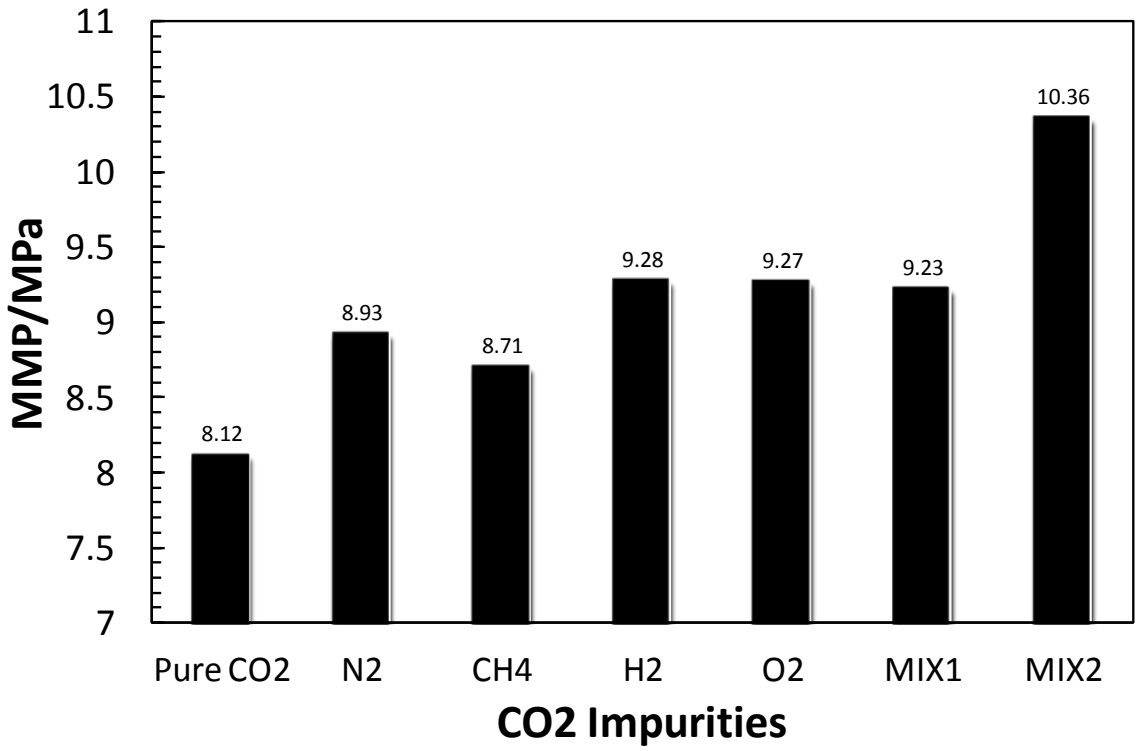


*Figure 7.7 The Effect of impurities on MMP of $CO_2$/n-decane system at 310.95 K*

### *7.3.3.2 Multiple Mixing Cell Algorithm for predicting the MMP*

The multiple mixing cell algorithm used in the developed in-house model, is a modification of the algorithm proposed by Jaubert [26] (which is based in the method used in [24] and [27]). The multicell method used is the same proposed by Metcalfe et al. [24] and described in Figure 7.8, where a Batch correspond to the multiple-contact achieved, by maintaining a constant volume after equilibrium (after every flash calculation), transferring the excess in volume from cell to cell, throughout all the cells from the first one to the last one, using 20% of the total amount of gas required for displacing totally the volume of one cell containing 1PV of initial oil (1.2PV of gas). Therefore, knowing that 6 injections (1.2PV/20%) of gas (batches) are required for displacing one cell of initial oil, 300 batches are required for displacing 50 cells, as in our case, (50*1.2PV/0.2=300). The equilibrium of each cell is obtained by flash calculation, using the parameters for Peng Robinson EOS given in Table 7.4 and 7.5.

*Table 7.4 Pure components properties*

| comp. | $T_c$ / K | $P_c$/MPa | ω | MW/g.mol$^{-1}$ |
|---|---|---|---|---|
| $CO_2$ | 304.20 | 7.38 | 0.23 | 44.01 |
| CO | 132.92 | 3.50 | 0.07 | 28.01 |
| $N_2$ | 126.05 | 3.39 | 0.04 | 28.01 |
| $O_2$ | 154.58 | 5.04 | 0.02 | 31.99 |
| Ar | 150.86 | 4.90 | 0.00 | 39.95 |
| $H_2$ | 33.18 | 1.33 | -0.22 | 2.02 |
| $CH_4$ | 190.58 | 4.60 | 0.01 | 16.04 |
| $nC_{10}$ | 617.70 | 2.11 | 0.49 | 142.29 |

*Table 7.5 Binary Interaction Parameters (BIPs) used in PR EOS*

| | Binary Interaction Parameters (BIPs) | | | | | | | |
|---|---|---|---|---|---|---|---|---|
| | $CO_2$ | CO | $N_2$ | $O_2$ | Ar | $H_2$ | $CH_4$ | $nC_{10}$ |
| $CO_2$ | - | 0.005 | -0.023 | 0.111 | 0.129 | 0.02 | 0.099 | 0.104 |
| CO | -0.042 | - | 0.005 | 0.000 | 0.007 | -0.016 | 0.022 | 0.000 |
| $N_2$ | -0.048 | 0.005 | - | -0.013 | -0.007 | -0.020 | 0.032 | 0.112 |
| $O_2$ | 0.091 | 0.000 | -0.013 | - | 0.000 | 0.000 | 0.000 | 0.000 |
| Ar | 0.113 | 0.007 | -0.007 | 0.000 | - | 0.000 | 0.026 | 0.000 |
| $H_2$ | 0.0202 | -0.016 | -0.02 | 0.000 | 0.000 | - | 0.000 | 0.000 |
| $CH_4$ | 0.092 | 0.022 | 0.032 | 0.000 | 0.026 | 0.000 | - | 0.041 |
| $nC_{10}$ | 0.104 | 0.000 | 0.112 | 0.000 | 0.000 | 0.000 | 0.041 | - |

In order to displace the oil of every cell (1 PV= 1 Pore Volume of 1 cell, in our case, each cell contains 1 bbl of initial oil), it is injected 1.2 PV of gas per cell of oil used in the simulation. This injection is made by batches of 20% of the gas (1.2PV/0.2 = 6 injections of gas (batch) per cell of oil to be displaced) as proposed by Metcalfe et al. [24], instead of using batches of 33% of gas (1.2PV/0.33≈ 4 injections) as used by Jaubert et al. [26]. This modification increases the amount of batch used, and therefore the total amount of flash calculations, which refined at every pressure, the recovery factor determined. As mentioned above, in the case of 50 cells, the total amount of batches is: 300 batches, and therefore the total amount of flash calculations: is 300 batch* 50 cells = 15000 flashes calculations, at each pressure supposed. The second modification used, corresponds to a more cautious procedure (more pressure steps at

high recovery factors values) required for generating the curve (Pressure vs Recovery Factor (RF)), in order to obtain the MMP at the value of 0.95% of recovery factor (RF). As it will be explained later, the experimental work is carried-out at low reservoir temperature; therefore drastic changes of the recovery factors with pressure are expected. Due to the higher amount of pressure steps required and the higher amount of flash calculation at every pressure step supposed, a compromise is required in order to calculate the MMP within a considerable computing time. Thus, in this work 50 cells have been used, showing a good accuracy for the prediction of MMP of $CO_2$/impurities systems.

The mobility method used in this algorithm, is the moving-excess-oil option proposed by Metcalfe et al.[24] in which the excess volume (either gas or liquid or both) is transferred from cell to cell, while the cell volume in each cell is kept constant. Figure 7.8 depicts clearly the multi-contact displacement method used. Before the first gas injection, all the cells contain the initial oil. During the every batch (gas injection), every transfer of excess volume from cell to cell, increases the concentration of volatile components (from the injection gas) in the residual oil. Nevertheless, the excess volume injected becomes heavier as the number of mobility steps (transfer from cell to cell) increases. Thus, on one hand, after reaching the equilibrium during the first batch, the residual oil in all cells becomes lighter than the initial oil and during the second batch, the residual oil in all cells becomes lighter than the residual oil in the first batch and so on, as the number of batches increases.

When the supposed pressure is near to the MMP, the residual fluid becomes more volatile with the increasing number of batches, until the oil in the initial cells is completely displaced (i.e.: the first cell is completely occupied by the injection gas) therefore, the excess volume of these cells is the same as the injection gas volume. On the other hand, during each batch, the initial gas injection is added uniquely to the first cell, and after reaching equilibrium, the excess volume, which is heavier than the initial injection gas, is injected to the second cell, which in turn, after reaching equilibrium, its excess volume is transferred to the third cell, making it heavier than the excess volume injected in the second cell, and so on, as the number of cells increase. In summary, the composition of residual oil becomes heavier with the number of cells, and becomes lighter with the number of batches, thus, the maximum volume of oil recovered (excess volume in the selected cell) is found in the last cell during the first batch.

The recovery factor is calculated in 5 selected cells, which amount to the total number of simulation cells (in our case, the cells: 10, 20, 30, 40 and 50), and is defined as the ratio between the sum of the excess volumes (at standard conditions) during the total number of batches in the given selected cell(i.e.: cell number 10), and the volume of initial oil (at standard conditions) in the number of cells selected to be displaced (i.e.: 10 cells). As it is depicted in Figure 7.8, only the first gas injection (first batch) will be in contact with the initial oil, and the following batches will be in contact with the residual oil obtained from the previous batch after removing the excess volume at equilibrium.

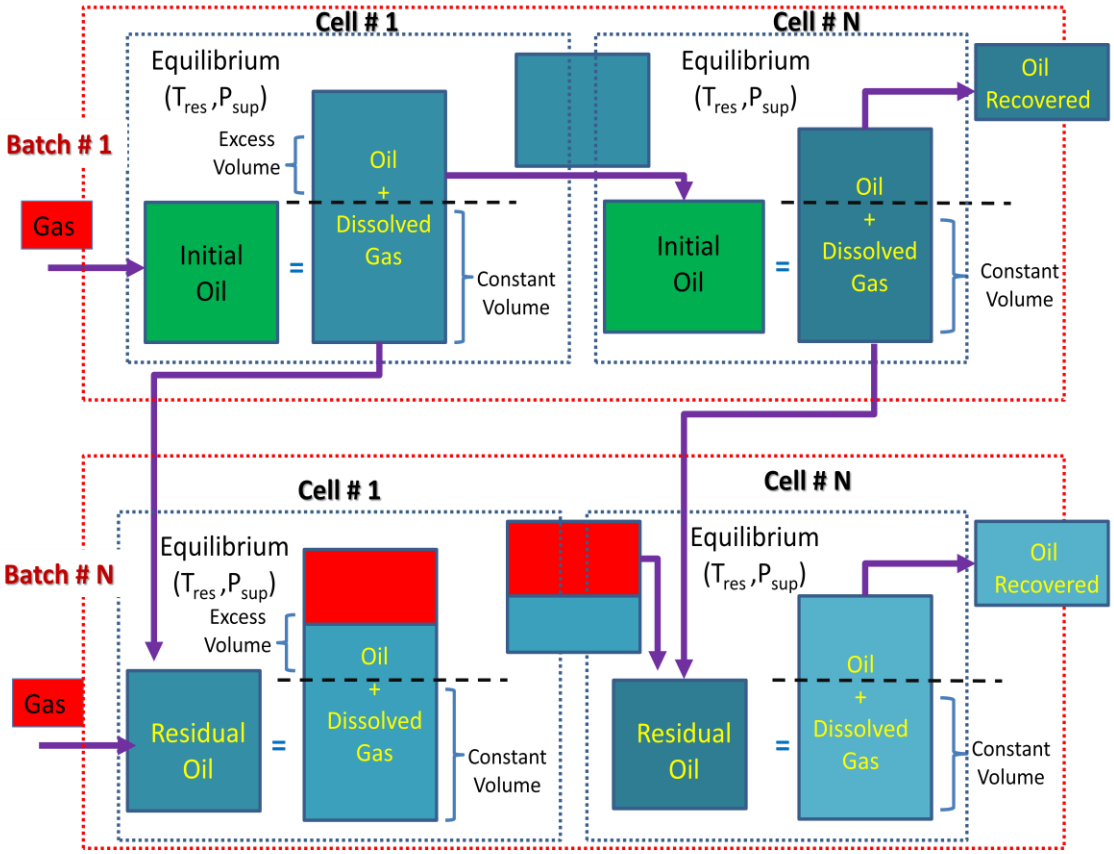


*Figure 7.8 Multiple-mixing cell mechanism (constant volume cells, moving-excess-oil option) proposed in [25]*

In order to eliminate the high dependence on the number of cells used in the simulation, generating either physical or numerical dispersion, Stalkup [39] proposed to extrapolate linearly the plot of ultimate recovery at 1.2 PV ($RF_{1.2}$) against ($1/\sqrt{N}$) where N is the number of cells. Thus, at a given supposed pressure the recovery factor is calculated for 5 cells (i.e.: 10, 20, 30, 40 and 50, in our case), and the plot of ultimate recovery against ($1/\sqrt{N}$) is elaborated, and finally, extrapolate to infinite number of cells, where ($1/\sqrt{N}$)

= 0, in order to obtain a recovery factor independent of the number of cells (RF infinite) at the supposed pressure.

Finally, using the previous data, a curve of recovery factor (RF) vs. Pressure can be generated and the MMP can be found by extrapolating at 95% of recovery factor. Jaubert et al. [26] proposed to use (3 to 5) supposed pressures in the range from 10% to 97% of oil recovery, reporting good results for the prediction of the MMP in several systems. This methods have been used by Hernandez et al. [41] validating the MMP predicted with literature data ([26, 42, 43 and 44]), obtaining a maximum relative error of 1.6%. It is important to note that all the previous cases used temperatures higher than 339.15 K, which is considered by Holm [40] as the range of high temperatures, where the recovery factor increase gradually with pressure. On the contrary, where the temperature is lower than 339.15 K, Holm [40] described a sharp reduction on oil recovery from pressures lower than the MMP.

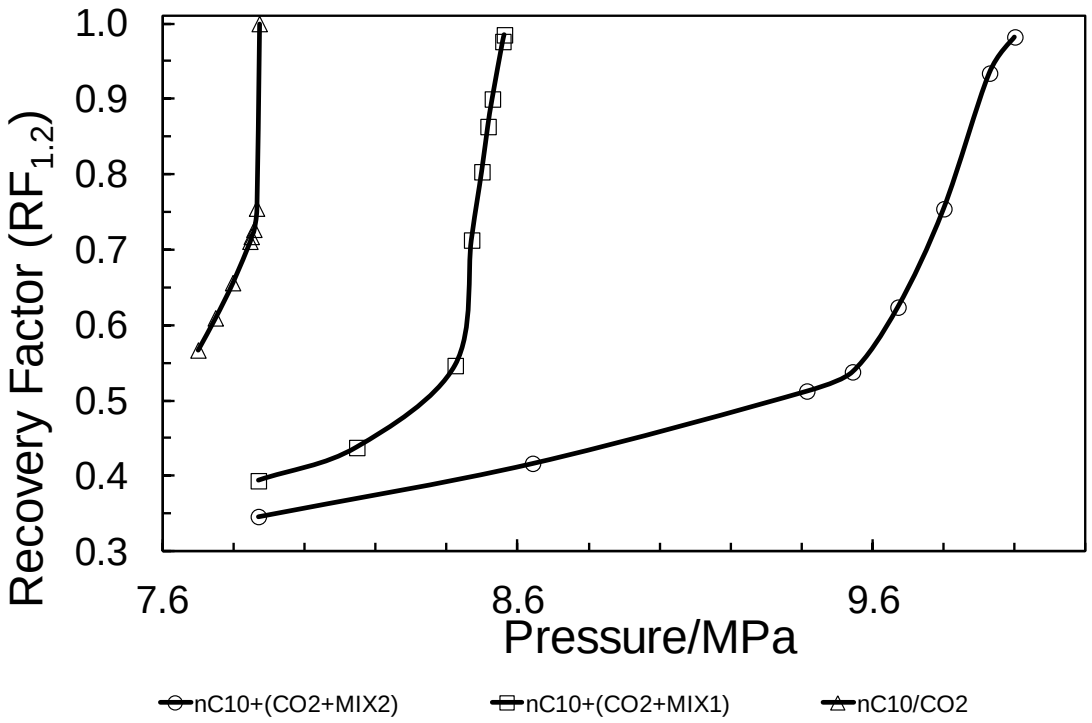


*Figure 7.9 Recovery factor vs. Pressure for $CO_2$ and $CO_2$+ impurities with n-decane at 310.95 K*

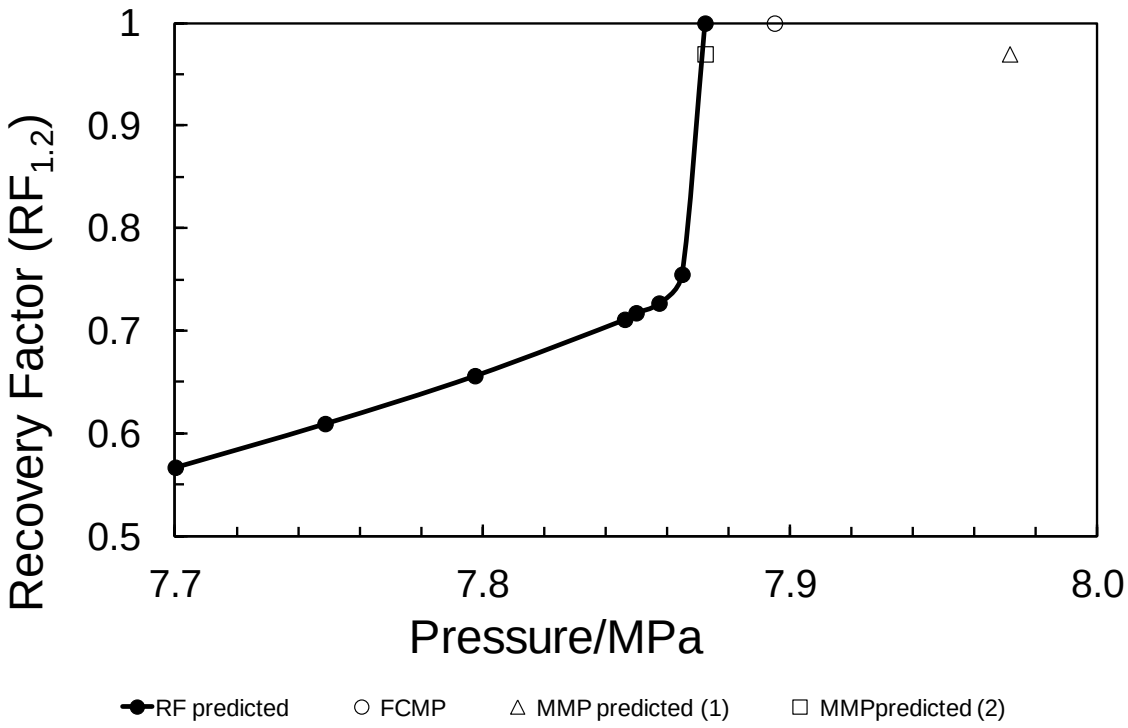


*Figure 7.10 Recovery Factor (RF) vs. pressure supposed, using 50 cells. MMP predicted (1): using the range of RF (0.1-0.95) and MMP predicted (2): using the range of RF (0.7:0.99), for $CO_2$+nC10 at 310.95 K*

This work uses a reservoir temperature of 310.95 K, which is considered as lower temperature, and which behavior described by Holm [40], can be confirmed on Figure 7.10, showing a drastically increase of Recovery Factor from ($RF_{1.2}$) greater than 75%. Consequently, using the method proposed by Jaubert et al. [26], for extrapolating $RF_{1.2}$ curves against pressure gives a far overestimated MMP, even greater than the FCMP as depicted in Figure 7.10. Therefore a more careful method for selecting the supposed pressures required for generating the curve of ultimate recovery vs. pressure is proposed in this work. A plot of $RF_{1.2}$ vs. Pressure is generated, and only the $RF_{1.2}$ in the range from 75% to 99% are used for interpolating (instead of extrapolating) the MMP to the value of 97% of $RF_{1.2}$.This modification requires a higher pressure supposed (more than 12) in order to avoid an inaccurate description of the curve of $RF_{1.2}$ vs. Pressure, and therefore a bad prediction of MMP. The sharp increase of recovery with pressure is shown in Figure 7.10 for pure $CO_2$ in n-decane at 310.95 K. It can be seen that extrapolating the curve in the range of (10 to 95)% will produce an MMP equal to 7.97 MPa which is not acceptable since it is greater than the FCMP, 7.90 MPa. However, using the method proposed in this work; interpolating in the range of (70-99) % of oil

recovery at the value of 97%, gives a good and logical result, MMP equal 7.87 MPa. Figure 7.9 shows the Recovery Factor for three gases with n-decane, pure $CO_2$, $CO_2$ + MIX1 and $CO_2$ + MIX2. The presence of MIX1 and MIX2 in the $CO_2$ stream can reduce the recovery by 45 and 51% respectively at 7.85 MPa. The effect of the $CO_2$/impurities near the miscibility displacement is obvious from the trend of the injection of the three gasses. By adding more impurities on $CO_2$, higher pressures are required in order to obtain similar recovery factor, and therefore higher MMPs are required with the presence of impurities on $CO_2$. Table 7.6, shows the comparison between the predicted and experimental MMP, obtained with the in-house multi-cell algorithm and the VIT experimental approach for the seven systems studied in this work. The average absolute deviation obtained is lower than 4.3%.

*Table 7.6 Comparison of experimental and predicted MMP for the studies systems in this work*

| Gas injected to $nC_{10}$ | MMP | | | |
|---|---|---|---|---|
| | FCMP | Predicted | Experimental | Dev% |
| $CO_2$ | 7.89 | 7.88 | 8.12 | 3.0 |
| $CO_2$+$N_2$ | 10.11 | 8.72 | 8.93 | 2.3 |
| $CO_2$+$CH_4$ | 8.85 | 8.41 | 8.71 | 3.4 |
| $CO_2$+$H_2$ | 10.90 | 8.86 | 9.28 | 4.5 |
| $CO_2$+$O_2$ | 9.31 | 8.65 | 9.27 | 6.7 |
| $CO_2$+MIX1 | 9.53 | 8.63 | 9.23 | 6.5 |
| $CO_2$+MIX2 | 12.50 | 9.99 | 10.36 | 3.5 |

The steps for evaluating the MMPs at low temperature (lower than 339.15 K) are described as follows:

1) Define the initial composition of oil in all cells.
2) Determine the volume of oil and gas at Standard conditions.
3) Determine the moles of gas injected; knowing that at each batch 20% of the 1.2 Pore Volume of Oil is injected.
4) Calculate the total moles in the cell.
5) Calculate the new composition of the cell.

6) Flash calculation at reservoir temperature, and pressure from $P_1$ to $P_6$ when 20% of PVI is proposed.
7) Calculate the new equilibrium volume of the cell.
8) Calculate the equilibrium excess volume of oil & gas, while the cell volume is kept constant.
9) Evaluate the recovery factor ($RF_{1.2}$) at the end of each set of cells, by dividing the excess oil volume exiting cell ($N_{10}$ to $N_{50}$) to the initial oil volume. The oil recovered is calculated at surface condition (15 °C, 1 atm).
10) To evaluate the $RF_{1.2}$ at infinite number of cells, a linear extrapolation is plotted for $RF_{1.2}$ against $1/\sqrt{}$ (Chosen cells).
11) The values of ln ($RF_{1.2}$ at infinity) are plotted with their corresponding pressures, in our calculation a perfect linear fitting is found for $RF_{1.2}$ at infinite from 0.7 to 0.99.
12) The MMP is interpolated for $RF_{1.2}$ at infinity equal to 0.97.

### 7.4 Conclusions

IFTs of $CO_2$ (pure and impure) in n-decane were measured with the capillary rise method. The method can be used to measure low IFTs (0.044 dynes/cm). The apparatus is also used to evaluate the swelling factors of the systems. The VIT approach can give a good estimation of the MMP of the tested systems when the IFTs measurements are fitted linearly. Overall, the effects of the tested impurities ($N_2$, $H_2$, $O_2$, $H_2S$, $CH_4$, CO) on $CO_2$ stream of injection of gas, for miscible displacement of n-decane are:

1) Shift the IFTs to higher values
2) Reduce the swelling factors
3) Increase the MMPs

Finally, a good agreement was obtained between the predicted MMPs using the proposed in-house model for low reservoir temperature, and the MMP obtained with VIT approach.

**References**

[1] Al-Abri, A. and Robert A., 2010, *Phase Behaviour, Fluid Properties and Recovery Efficiency of Immiscible and Miscible Condensate Displacements by $SCCO_2$ Injection: Experimental Investigation*, Transport in Porous Media. **85**, 743-756.

[2] Mangalsingh, D. and Jagai, T., 1996, *A Laboratory Investigation of the Carbon Dioxide Immiscible Process*, SPE 36134, Fourth Latin American and Caribbean Petroleum Engineering Conference. Trinidad and Tobago.

[3] Ghoodjani, E. and Bolouri, SH., 2011, *Experimental Study of $CO_2$-EOR and $N_2$-EOR with Focus on Relative Permeability Effect*, J Pet Environ Biotechnology, **2**, 106- 111.

[4] LAKE, L. W., 1989, *Enhanced Oil Recovery*, Prentice Hall, New Jersey.

[5] Metcalfe, R. S. and Amoco Production Co, 1982, *Effects of Impurities on Minimum Miscibility Pressures and Minimum Enrichment Levels for $CO_2$ and Rich-Gas Displacement*, Society of Petroleum Engineers Journal, **22**, 219-225.

[6] Shokir, E.M.E. -M., 2007, *$CO_2$-Oil Minimum Miscibility Pressure Model for Impure and Pure $CO_2$ Streams*, Journal of Petroleum Science and Engineering, **58**, 173-185.

[7] Nguyen, T. A., Farouq, A.S. M. and University Of Alberta, 1998, *Effect of Nitrogen on the Solubility and Diffusivity of Carbon Dioxide into Oil and Oil Recovery by the Immiscible WAG Process*, Society of Petroleum Engineers Journal, **37**, 24-31.

[8] Monger, T. G., 1987, *Measurement and Prediction of Swelling Factors and Bubble Points for Paraffinic Crude Oils in the Presence of Carbon Dioxide and Contaminant Gases*, Industrial Engineering Chemistry Research, **26:6**, 1147-1153.

[9] Spivak, A. and Chima, C. M., 1984, *Mechanisms of Immiscible $CO_2$ Injection in Heavy Oil Reservoirs*, Wilmington field, CA, SPE Paper 12667 presented at the 1984 California Regional Meeting Long Beach, CA 31-43.

[10] Holm, L. W. and Josendal, V. A., 1974, *Mechanisms of oil displacement by carbon dioxide*, Journal of Petroleum Technology, **26**, 1427-1438.

[11] Holm, L. W. and Josendal, V. A., 1980, *Discussion of Determination and Prediction of $CO_2$ Minimum Miscibility Pressures*, Journal of Petroleum Technology, **32**, 870-871.

[12] Mungan, N., 1981, *Carbon Dioxide Flooding Fundamentals*, Journal of Canadian Petroleum Technology, **20**, 87- 92.

[13] Johnson, J. P. and Pollin, J. S., 1981, *Measurement and Correlation of $CO_2$ Miscibility Pressures*, paper SPE 9790 presented at the SPE/DOE Enhanced Oil Recovery Symposium, Tulsa, OK, 5- 8.

[14] Holm, L. W., and Josendal, V. A., 1982, *Effect of Oil Composition on Miscible-Type Displacement by Carbon Dioxide*, Society of Petroleum Engineers, **22**, 87-98.

[15] Holm, L. W. and Josendal, V. A., 1984, *Effect of Volatility and Molecular Structure of Reservoir Oil on Oil Recovery Efficiency Using Carbon Dioxide*, paper presented at the AIChE National Meeting, Anaheim, CA, 20-23.

[16] Sebastian, H. M., Wenger, R. S. and Renner, T. A., 1984, *Correlation of Minimum Miscibility Pressure for Impure $CO_2$ Streams*; SPE Paper 12648 presented at the SPE/DOE Enhanced Oil Recovery Symposium, Tulsa, 15-18.

[17] Dong, M., Huang S., Srivastava, R. and Saskatchewan Research Council, 2000, *Effect of Solution Gas in Oil On $CO_2$ Minimum Miscibility Pressure*, Journal of Canadian Petroleum Technology, **39**, 54-61.

[18] Johns, R. T. and Orr, F. M., 1996, *Miscible Gas Displacement of Multicomponent Oils*, SPE Journal (30798-PA), **1**, 39-50.

[19] Wang, Y., and Orr, F. M., 1997, *Analytical Calculation of Minimum Miscibility Pressure*, Fluid Phase Equilib., **139**, 101-124.

[20] Jaubert, J. N., Arras, L., Neau, E., and Avaullee, L., 1998, *Properly Defining the Classical Vaporizing and Condensing Mechanisms when a Gas is Injected into a Crude Oil*, Ind. Eng. Chem. Res., **37**, 4860-4869.

[21] Yellig, W. F., and Metcalfe, R. S., 1980, *Determination and Prediction of $CO_2$ Minimum Miscibility Pressures*, J. Pet. Technol., **32**, 160-168.

[22] Cook, A. B., Walker, C. J., and Spencer, G. B., 1969, *Realistic K Values of C7+ Hydrocarbon for Calculating Oil Vaporization During Gas Cycle at High Pressures*, Journal of Petroleum Technology (SPE 2276-PA), **21**, 901-915.

[23] Jensen, F., and Michelsen, M. L. ,1990, *Calculation of First Contact and Multiple Contact Minimum Miscibility Pressures*, In Situ: Oil-Coal-Shale-MInerals, **14**, 1-17.

[24] Metcalfe, R. S., Fussell, D. D., and Shelton, J. L.,1973, *A Multicell Equilibrium Separation Model for the Study of Multiple Contact Miscibility in Rich-Gas Drives*, SPE Journal (3995-PA), **13**, 147-155.

[25] Pedersen, K. S., Fjellerup, J., Fredenslulnd, A., and Thomassen, P., 1986, *Studies of Gas Injection Into Oil Reservoirs by a Cell to Cell Simulation Model*, SPE Journal (13832-ms).

[26] Jaubert, J. N., Wolff, L., Neau, E., and Avaullee, L., 1998, *A very Simple Multiple Mixing Cell Calculation to Compute the Minimum Miscibility Pressure whatever the Displacement Mechanism*, Ind. Eng. Chem. Res., **37**, 4854-4859.

[27] Zick, A. A., 1986, *Combined Condensing/Vaporizing Mechanism in the Displacement of Oil by Enriched Gases*, SPE Journal (15493), 1-11.

[28] Rusanov, A. I. and Prokhorov, V. A., 1996, *Interfacial Tensiometry*, Elsevier, Amsterdam.

[29] Drelich, J., Fang, Ch. and White, C. L., 2002, *Measurement of Interfacial Tension in Fluid- Fluid Systems*, Encyclopedia of Surface and Colloid Science, Marcel Dekker, Inc. 3152-3166.

[30] Adamson, A.W., 1990, *Physical Chemistry of Surfaces*, John Wiley and Sons, Inc., New York.

[31] Ayirala, S. C., 2005, *Measurement and Modeling of Fluid-Fluid Miscibility in Multicomponent Hydrocarbon Systems*, doctor of philosophy dissertation LSU Department of Petroleum Engineering.

[32] Nagarajan, N. and Robinson Jr., R. L., 1986, *Equilibrium Phase Compositions, Phase Densities, and Interfacial Tensions for $Co_2$ + Hydrocarbon Systems. 2. $CO_2$+N-Decane*, J. Chem. Eng. Data, **31**, 168-171.

[33] Shaver, R. D., Robinson Jr., R. L. and Gasem, K.A. M., 2001, *An Automated Apparatus for Equilibrium Phase Compositions, Densities, and Interfacial Tensions: Data for Carbon Dioxide + Decane*, Fluid Phase Equilibria, **179**, 43-66.

[34] Simon, R., Graue, D. J. and California Research Corp., 1965, *Generalized Correlations for Predicting Solubility, Swelling and Viscosity Behavior of $CO_2$-Crude Oil Systems*, Journal of Petroleum Technology, **17**, 102-106.

[35] Srivastava, RK., Huang S., Dong M. and Saskatchewan Research Council, 1999, *Comparative Effectiveness of $CO_2$, Produced Gas, and Flue Gas for Enhanced Heavy Oil Recovery*, SPE Reservoir Evaluation & Engineering, **2**, 238-247.

[36] Rao, D. N., 1997, *New Technique of Vanishing Interfacial Tension for Miscibility Determination*, Fluid Phase Equilibria, **139**, 311-324.

[37] Elsharkawy, A.M., Suez Canal U., Poettmann, F.H., Christiansen, R.L. and Colorado School of Mines, 1992, *Measuring Minimum Miscibility Pressure: Slim-Tube or Rising-Bubble Method?*, paper presented at SPEIDOE Eighth Symposium on Enhanced Oil Recovery held in Tulsa, Oklahoma, 107-116.

[38] Song, Y-C., Zho, N-J., Liu, Y., Zhao, J. F., Liu, W. G, Zhang, Y., Zhao, Y. C., Yue, C. and Jiang, L-L., 2011, *Magnetic Resonance Imaging Study on the Miscibility of a $CO_2$/N-Decane System*, CHIN.PHYS.LETT., **28**, 096401(1-4).

[39] Stalkup, F. I., 1987, *Displacement Behavior of the Condensing/Vaporizing Gas Drive Process*, SPE 16715. Presented at the SPE Annual Technical Conference and Exhibition, Dallas, TX, 27-29.

[40] Holm, L. W., 1986, *Miscibility and Miscible Displacement*, Society of Petroleum Engineers, 15794-PA, Technology Today Series, **38**, 817-818.

[41] Hernandez-Baez, D. M., and Martinez-Cruz, F. L., 2006, *Desarrollo de un Algoritmo numerico para la Prediccion de la Minima Presion de Miscibilidad (MMP) en un Yacimiento de Petroleo y su Validacion con Datos Experimentales del Equipo de Miscibilidad Slim Tube*, (Universidad Industrial de Santander (UIS), Bucaramanga.

[42] Jessen, K., Michelsen, M. L., and Stenby, E. H., 1998, 1998, *Effective Algorithm for Calculation of Minimum Miscibility Pressure*, Society of Petroleum Engineers,50632-MS, European Petroleum Conference, The Hague, Netherlands.

[43] Hearn, C. L. and Whitson, C. H., 1995, *Evaluating Miscible and Immiscible Gas Injection in the Safah Field, Oman*, Society of Petroleum Engineers (29115-MS), SPE Reservoir Simulation Symposium, San Antonio, Texas.

[44] Hua, Y. and Russell, T. J., 2002, *Simplified Method for Calculation of Minimum Miscibility Pressure or Enrichment*, SPE Journal, (77381-MS), 10(4)

# CHAPTER 8: CONCLUSIONS AND RECOMMENDATIONS FOR FUTURE WORK

## 8.1 Introduction

1) $CO_2$ could potentially be captured from flue gasses power plants and other large industrial stations and then transported for either sequestration or EOR purpose. The purified $CO_2$ would not be pure and may contain some impurities which potentially could affect the behaviour of the $CO_2$ stream. In this work, several transport and physical properties of $CO_2$ in the presence of impurities were investigated. The properties that were covered are VLE, critical data, density, speed of sound, isothermal compressibility and hydrate formation. In addition the effect of impurities on other properties such as interfacial tension, swelling factor, MMP, saturation pressure and speed of sound in $CO_2$/alkane mixture were also investigated. The present research is aimed to evaluate both experimental and modelling aspects of the above mentioned properties on $CO_2$ and $CO_2$/impurities mixtures. A summary of the main outcomes of the work are highlighted below.
2) A large experimental database from literature of VLE of $CO_2$ and binary $CO_2$ rich mixtures was gathered. Three EOSs, PR, SRK and VPT, were tuned in a wide range of pressure and temperature (Chapter 2). The binary interaction parameters of the equations were evaluated for the binary $CO_2$/impurities systems. Eight impurities were investigated in this work, $H_2$, Ar, CO, $SO_2$, $H_2S$, $O_2$, $N_2$ and $CH_4$. Both maximum and average deviations in the saturated pressure and vapour composition were plotted for the $CO_2$/impurities mixture. The work in Chapter 2 also includes the evaluation of the critical data of the $CO_2$/impurities mixtures.
3) Saturated pressures were measured experimentally for pure and impure $CO_2$ in a synthetic alkane mixture at 344.3 K (Chapter 2). The alkane mixture contains C10, C13 and C16 while the $CO_2$ impurities used were Ar, $H_2$, CO and $CH_4$. The VPT EOS was used to predict the measured data.
4) A series of new isothermal compressibility and speed of sound data of $CO_2$ and $CO_2$/impurities systems were generated above the saturation pressure from 268.15 to

301.15 K (Chapter 3). A new modified volume correction is presented in this work based on the PR EOS for $CO_2$ and $CO_2$/impurities in order to get better prediction of liquid isothermal compressibility in $CO_2$ and $CO_2$ rich systems. The speed of sound in liquid alkane/$CO_2$ mixture (Chapter 2) was measured. The sound property in pure $CO_2$ mixture was fitted with a new correlation to match the experimental data in order to compare with the mixture contains impurities.

5) Seven new isothermal density measurements were generated for $CO_2$ and $CO_2$ rich systems from 393.15 to 423.15 K. The measurements were carried-out with an Anton Paar densitometer in both liquid and supercritical $CO_2$ regions. A new modelling approach is adopted in the study based on mixing volume obtained from simple EOSs such as PR and SRK with the $CO_2$-MBWR in order to predict the density of both pure and impure CO2 mixtures (Chapter 4).
6) Experimental and calculated phase equilibrium conditions of pure and impure $CO_2$ hydrate with water were measured in a wide range of pressure and temperature (Chapter 5Chapter 5:). An in-house code based on the VPT EOS and the solid theory of van der Waals and Platteeuw was used to predict the hydrate stability of $CO_2$ and $CO_2$ rich mixtures in both gas and liquid regions. The impurities covered in the work were $N_2$, $CH_4$, CO, $O_2$, Ar and $H_2$.
7) Viscosity tests to study the impact of impurities on $CO_2$ liquid viscosity were conducted from 280 to 343.15 K (Chapter 6). The measurements were generated using an in-house capillary tube viscometer. Two viscosity models LBC and Pedersen were modified in order to minimize their errors with the generated experimental data.
8) A new IFT apparatus was developed in this work based on the capillary rise method (Chapter 7). The apparatus was used to quantify IFT of $CO_2$ and n-decane system at 310.95 K. The measurements were extended to cover systems that contain impurities in $CO_2$ stream. In this work, the systems investigated were binary $CO_2$ rich mixtures containing $CH_4$, $N_2$, $O_2$ and $H_2$ and two multi-components mixtures. The apparatus was also used to determine the swelling factor property simultaneously with IFT measurements. The Vanishing Interfacial Tension (VIT) approach was used to estimate the Minimum Miscibility Pressure (MMP) of the above mentioned systems. In addition, a Multiple Mixing Cell (MMC) was employed for computing the MMP of the investigated systems.

A number of important conclusions and recommendations are outlined in this chapter from the preceding chapters of this thesis. This includes the experimental and modelling works plus a summary of the impact of impurities on various properties of $CO_2$ stream mentioned in details previously (Chapter 1 to Chapter 7). In the light of this work, these conclusions and recommendations are stated below:

### 8.2 Conclusions from Literature Survey

Literature review is included previously in each chapter. In reviewing the literature, no or very little data were found on some $CO_2$/impurities properties. Whereas the effect of some impurities were covered widely, for others no data were found. A literature survey on $CO_2$ rich mixtures was generated by Li et al. [1], associated with the transport properties such as viscosity and thermal conductivity. One main conclusion was that no data were available for transport properties in the liquid phase. In this work, eight components were considered, $H_2$, Ar, $CH_4$, $N_2$, $O_2$, CO, $SO_2$ and $H_2S$. The main points regarding the literature review are summarized below

- ***VLE***

Experimental data are available in the literature for the binary systems of $CO_2/H_2S$, $CO_2/H_2$, $CO_2/CH_4$ and $CO_2/N_2$. However, there were still some gaps in the literature for experimental data in the other impurities. $CO_2$/Ar and $CO_2/SO_2$ have very little information in VLE, therefore the interaction parameters generated for the EOSs may not sufficient accurate in wide range of pressure and temperature. Limited data regarding ternary and multi-components VLE data are available except for the $N_2/CH_4/CO_2$ system. Critical data of rich $CO_2$ mixtures are limited in literature for $CO_2/N_2$, $CO_2/H_2S$ and $CO_2/CH_4$; and none for the other impurities systems.

- ***Density***

Limited density measurements are available for $CO_2$ + ($O_2$, $N_2$, $CH_4$, $SO_2$) and other impurities. Recently, one experimental work on supercritical density [2] was aimed to analysis the effect of three binary $CO_2$/impurities includes $O_2$, Ar and $N_2$.

- ***Viscosity***

No viscosity data are available for $CO_2$/impurities in both the liquid and supercritical regions. Limited data are available in the gas phase for systems containing $SO_2$ or CO compare to the other impurities. However no research work has deeply looked at the effect of impurities in rich $CO_2$ system on viscosity.

- ***Speed of Sound & Isothermal Compressibility***

No experimental data for speed of sound and isothermal compressibility properties for $CO_2$/impurities was found in the literature in the liquid and supercritical phases. Few data points were published on gas phase.

- ***Hydrate***

Data are widely available for pure $CO_2$ and the $CO_2/CH_4$ systems. Few data are available for $CO_2$ with $N_2$, $H_2$ and CO. No experimental data were found in the open literature for $CO_2$ with $O_2$, Ar and $H_2S$.

As mentioned in the previous chapters, $CO_2$ is used for Enhanced Oil Recovery (EOR), where $CO_2$/oil properties such as Minimum Miscibility Pressure (MMP), VLE, IFT and swelling factors are important. The literature collected for those properties is stated below.

- ***MMP ,IFT and Swelling Factor***

Few experimental data were available on the impact of impurities $CH_4$, $N_2$ and $H_2S$ on MMP and swelling factor measurements. However no data was found for the other impurities effect.

- ***VLE of Impure $CO_2$/Oil Mixture***

No data are available regarding the effect of impurities on VLE of impure $CO_2$/oil.

## 8.3 Experimental Apparatus

In the event that no data are available in the open literature, few measurements were carried to define the effect of impurities on $CO_2$ properties such as speed of sound, density, viscosity and IFT. Several apparatus were used in this study for measuring $CO_2$

and $CO_2$/impurities properties includes an in-house acoustic apparatus (Chapter 2 and Chapter 3 Anton Paar densitometer (Chapter 4) hydrate mixed autoclave rig (Chapter 5), in-house capillary tube viscometer (Chapter 6) and in-house IFT capillary rise apparatus (Chapter 7). The acoustic apparatus can be used effectively to measure the liquid speed of sound of $CO_2$ systems within less than 2 $m/s^{-1}$ in accuracy. The travelling time versus pressure generated from the setup can be used successfully to quantify the saturation pressure of the $CO_2$ systems. The calibration method based on one substance ($CO_2$ in this work) at two different pressure conditions (see Chapter 4) proposed in the work for Anton Paar densitometer is suitable and more reliable when impurities are considered. Slim tube viscometer operated by mercury pump is based on the fundamental Poiseuille's law mercury, therefore the viscosity measurements are found in a good agreement with other published data. However, a caution should be taken at high temperature where the system pressure may not be stable. The capillary rise setup is a new in-house setup added to this work to measure the IFT between oil and gas. This work is a complement of previous work by Ayirala [2]. Moreover, in order to achieve more accurate measurements, a tube with 4½ times smaller than his work was used. The apparatus can be suited to measure low interfacial tensions (0.044 $mNm^{-1}$). The apparatus has been successfully used to measure swelling factor.

### 8.4 Modelling Results

A number of models were implemented to the research to improve the prediction of $CO_2$/impurities properties. This includes a volume correction based on PR EOS for isothermal compressibility, a $CO_2$-MBWR and general EOS mixing volume approach for density, a thermodynamic approach was employed to model the phase equilibria, VIT and MOC approaches for MMP and modified LBC and Pedersen models for viscosity. The volume correction used in Chapter 3 is very accurate (less than 0.1% in AAD) prediction for $CO_2$ liquid density from 228 K to the critical temperature and pressure up to 50 MPa. The modified model results are also in a good agreement with the generated isothermal compressibility results of both pure and impure $CO_2$. The hydrate model was used to predict the hydrate stability zones of the $CO_2$/impurities systems in the presence of free water. Good agreement between predicted values and experimental data was found. For viscosity calculations, two models, LBC and Pedersen, were modified and their results show better prediction compare to the original

form of the equations.The results show that the $CO_2$-Pedersen model can predict the mixture viscosity with less than 2% deviation compare to 9 % in the original Pedersen model and from 9% to 2% in the LBC model. For MMP, the Multiply Mixing Cell model is within 4% of the experimental data at the temperature studied in this work. The tuned results of the EOSs on VLE of $CO_2$ impurities show that the three EOSs predict the VLE of binary mixtures with the same range of accuracy (3.85% to 4.14%) for all the tested impurities systems. However, the presence of $H_2$ in $CO_2$ stream makes the EOSs reduces the accuracy compare to the other impurities. The phase behaviours of the $CO_2$/ impurities are well described by the EOSs in a wide range of pressure and temperature; however the models failed in accuracy as the system approaches the critical point.

## 8.5 The Effect of Impurities on $CO_2$ Properties & Future Work Recommendations

The overall conclusions on the effect of the studied impurities on $CO_2$ properties can be summarized as following:

- ***Critical Data***

The presence of impurities in $CO_2$ rich system tends to raise the critical pressure of $CO_2$ except for $H_2S$. The impurities $H_2$, $CH_4$, CO, Ar, $O_2$ and $N_2$ have a negative impact as the $CO_2$ critical temperature is increased while $SO_2$ and $H_2S$ have a positive impact. Few experimental data on critical points of $CO_2$/impurities were found in the literature; therefore more VLE and critical data of the systems are required. Moreover, the prediction of the VLE from the cubic EOSs with the classic mixing rules is still weak especially near the critical points thus testing other mixing rules is recommended for any future work. Another option is to modify the mixing rule in the EOSs in order to improve the prediction of $CO_2$ mixtures critical data.

- ***Speed of Sound & Isothermal Compressibility***

The presence of impurities tested in this work tends to reduce the speed of sound. The reduction in the property strongly depends on pressure compared to temperature variation. As the pressure increases, the isothermal lines of the change will intersect at a pressure $\approx$ 15 MPa. This finding was observed in all the investigated mixtures. In the

other hand, the presence of impurities increases the isothermal compressibility of $CO_2$ stream. The effect is much higher as the pressure approaches the critical temperature of the mixture.

- ***Density***

The density of pure $CO_2$ and the $CO_2$/impurities mixtures have a stronger dependency on temperature compared to pressure at lower temperatures below the critical temperature. Above the critical temperature, a maximum reduction on the density capacity at a certain pressure under a given temperature was found for each $CO_2$/impurity system. Overall, the light MW impurities tend to reduce $CO_2$ density much more than those with MW close to $CO_2$. Other impurities such as $NO_x$, $SO_x$ and $H_2S$ must be investigated for future work. The pressure and temperature range might be extended to cover higher pressure and lower temperature conditions.

- ***Hydrate***

The hydrate equilibrium pressures were decreased apparently with addition of the tested impurities in the HLL phase. Methane tends to increase the hydrate zone by twice as much as the other impurities ($N_2$, $O_2$, $H_2$, CO and Ar). Investigation other impurities such as $H_2S$ and $SO_2$ plus increasing the fraction of impurities are recommended for future work in this part.

- ***Viscosity***

The viscosity of $CO_2$ and $CO_2$/impurities is a function of pressure and temperature; it increases as pressure increases and decreases as temperature increases. The experimental results show that all of the tested impurities caused a reduction of viscosity compared to pure $CO_2$. The reduction was found high for light impurities such as $H_2$ and low as with Ar. As the system approaches the critical pressure and temperature, the viscosity change becomes significant.

- ***Conclusions on $CO_2$/oil mixture***

The investigated impurities shift the $CO_2$ IFTs to higher values. Impurities such as $H_2$ have high impact on the IFT compare to the others. Higher concentrations of impurities

on the mixture increase the IFT. The investigated non-condensable impurities reduce the swelling factor and increase the Minimum Miscibility Pressure of $CO_2$.

**References**

[1] Li., H., Wilhelmsen, Ø., Yuexia, L., Wang, W. and Yan, J., *Viscosities, Thermal Conductivities and Diffusion Coefficients of $CO_2$ Mixtures: Review of Experimental Data and Theoretical Model*, 2011, International Journal of Greenhouse Gas Control, **5**, 1119-1139.

[2] Ayirala, S. C., 2005, *Measurement and Modeling of Fluid-Fluid Miscibility in Multicomponent Hydrocarbon Systems*, Doctor of philosophy dissertation LSU Department of Petroleum Engineering.